

AD-A061 378

AIR FORCE FLIGHT DYNAMICS LAB WRIGHT-PATTERSON AFB OHIO F/G 20/4
MASS INJECTION AND JET FLOW SIMULATION EFFECTS ON TRANSONIC AFT--ETC(U)
JUN 78 W CALARESE, R E WALTERICK
AFFDL-TR-78-57

UNCLASSIFIED

NL

1 OF 2
AD
A061378



AFFDL-TR-78-57

LEVEL II

(12)

AD A061378

MASS INJECTION AND JET FLOW SIMULATION EFFECTS ON TRANSONIC AFTERBODY DRAG

Aerodynamics and Airframe Branch
Aeromechanics Division

June 1978

TECHNICAL REPORT AFFDL-TR-78-57

Final Report for Period February 1977 - September 1977



DDC FILE COPY

Approved for public release; distribution unlimited.

AIR FORCE FLIGHT DYNAMICS LABORATORY
AIR FORCE WRIGHT AERONAUTICAL LABORATORIES
AIR FORCE SYSTEMS COMMAND
WRIGHT-PATTERSON AIR FORCE BASE, OHIO 45433

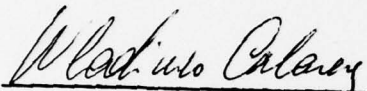
78 11 15 159

NOTICE

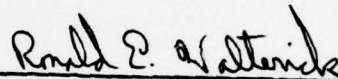
When Government drawings, specifications, or other data are used for any purpose other than in connection with a definitely related Government procurement operation, the United States Government thereby incurs no responsibility nor any obligation whatsoever; and the fact that the government may have formulated, furnished, or in any way supplied the said drawings, specifications, or other data, is not to be regarded by implication or otherwise as in any manner licensing the holder or any other person or corporation, or conveying any rights or permission to manufacture, use, or sell any patented invention that may in any way be related thereto.

This report has been reviewed by the Information Office (OI) and is releasable to the National Technical Information Service (NTIS). At NTIS, it will be available to the general public, including foreign nations.

This technical report has been reviewed and is approved for publication.

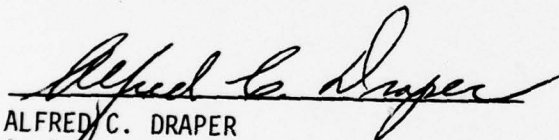


WLADIMIRO CALARESE, Ph.D.
Aerospace Engineer
Aerodynamics and Airframe Branch



RONALD E. WALTERICK
Aerospace Engineer
Aerodynamics and Airframe Branch

FOR THE COMMANDER



ALFRED C. DRAPER
Assistant for Research & Technology
Aeromechanics Division

"If your address has changed, if you wish to be removed from our mailing list, or if the addressee is no longer employed by your organization please notify AFFDL/FXM, W-PAFB, OH 45433 to help us maintain a current mailing list".

Copies of this report should not be returned unless return is required by security considerations, contractual obligations, or notice on a specific document.

UNCLASSIFIED

SECURITY CLASSIFICATION OF THIS PAGE (When Data Entered)

REPORT DOCUMENTATION PAGE		READ INSTRUCTIONS BEFORE COMPLETING FORM
1. REPORT NUMBER AFFDL-TR-78-57	2. GOVT ACCESSION NO.	3. RECIPIENT'S CATALOG NUMBER
4. TITLE (and Subtitle) MASS INJECTION AND JET FLOW SIMULATION EFFECTS ON TRANSONIC AFTERBODY DRAG		5. TYPE OF REPORT & PERIOD COVERED Final Report, Feb - Sept 1977
7. AUTHOR(s) Wladimiro Calarese Ronald E. Walterick		6. PERFORMING ORG. REPORT NUMBER
9. PERFORMING ORGANIZATION NAME AND ADDRESS Aerodynamics and Airframe Branch Air Force Flight Dynamics Laboratory Wright-Patterson Air Force Base, Ohio 45433		8. CONTRACT OR GRANT NUMBER(s)
11. CONTROLLING OFFICE NAME AND ADDRESS Air Force Flight Dynamics Laboratory Wright-Patterson Air Force Base, Ohio 45433		10. PROGRAM ELEMENT, PROJECT, TASK AREA & WORK UNIT NUMBERS 62201F, Project No. 2404 Task No. 240410 Work Unit 24041018
14. MONITORING AGENCY NAME & ADDRESS (if different from Controlling Office) <u>16</u> 2404 <u>17</u> 10		12. REPORT DATE June 1978
16. DISTRIBUTION STATEMENT (of this Report) Approved for public release; distribution unlimited. <u>12</u> 182 p.		13. NUMBER OF PAGES 182
17. DISTRIBUTION STATEMENT (of the abstract entered in Block 20, if different from Report)		15. SECURITY CLASS. (of this report) Unclassified
18. SUPPLEMENTARY NOTES		15a. DECLASSIFICATION/DOWNGRADING SCHEDULE
19. KEY WORDS (Continue on reverse side if necessary and identify by block number) Transonic Flow Drag Levels Separated Flow Boattail Mass Injection Simulated Jet Effects		
20. ABSTRACT (Continue on reverse side if necessary and identify by block number) An experimental investigation has been performed to determine the effects of boattail injection and jet flow simulation on the afterbody drag of a slender body of revolution in the transonic regime at zero angle of attack, such as engine nacelles and boattailed afterbodies with isolated engines. A correlation between sting and jet diameter has been established. The jet plume and the nozzle pressure ratio simulators have been found appropriate and useful as a testing technique. Boattail mass injection usually produces a		

DD FORM 1 JAN 73 1473 EDITION OF 1 NOV 65 IS OBSOLETE

UNCLASSIFIED

SECURITY CLASSIFICATION OF THIS PAGE (When Data Entered)

012 070

UNCLASSIFIED

SECURITY CLASSIFICATION OF THIS PAGE(When Data Entered)

drag coefficient reduction and is more effective at high nozzle pressure ratios. Boattail injection is more effective if used in regions of separated flow.

UNCLASSIFIED

SECURITY CLASSIFICATION OF THIS PAGE(When Data Entered)

FOREWORD

This report was prepared by Dr. Wladimiro Calarese and Mr. Ronald E. Walterick of the Applications Analysis Group, Aeromechanics Division, Air Force Flight Dynamics Laboratory (AFFDL/FXM), Wright-Patterson Air Force Base, Ohio. The study was performed in-house in support of Project 2404, "Aeronautics and Airframe/Propulsion Integration", Task 240410, "Aerodynamic Application Analysis", and covers work conducted between February and September 1977.

ACCESSION for	
NTIS	White Section <input checked="" type="checkbox"/>
DDC	Buff Section <input type="checkbox"/>
UNCLASSIFIED	<input type="checkbox"/>
U.S. EDITION	
DISSEMINATION ACTIVITY CODES	
SPECIAL	
A	

TABLE OF CONTENTS

SECTION	PAGE
I INTRODUCTION	1
II EQUIPMENT AND TEST DESCRIPTION	2
III RESULTS	7
1. Drag Coefficient Equations	7
2. Circular-Arc Boattail Pressure Distributions	9
3. Cut-Off B-1 Boattail Pressure Distributions	12
4. Conical Boattail Pressure Distributions	13
5. Base Pressure Levels and Afterbody Drag Coefficient	16
IV CONCLUSIONS	19
REFERENCES	170

LIST OF ILLUSTRATIONS

FIGURE		PAGE
1	Model Configuration	25
2	Boattail Coordinates, Pressure Taps, and Injection Port Location	26
3	Trisonic Gasdynamic Facility (TGF) 2' Wind Tunnel Test Section: a) Sting Mounted Circular-Arc Boattail, b) Cut-Off B-1 and Conical Boattails	27
4	a) Close-up of 2' Tunnel Test Section, b) Cone Frustum - Jet Plume Simulator at $\lambda=2''$	28
5	a) Cone Frustum - Jet Plume Simulator at $\lambda=4''$, b) Cone Frustum - Jet Plume Simulator at $\lambda=6''$	29
6	a) 1" Diameter Sting, b) 1.4" Diameter Sting	30
7	a) 1.6" Diameter Sting, b) 1.8" Diameter Sting	31
8	Base Pressure Variation Due to the Sting Versus Terminal Boattail Angle	32
9-16	Mass Injection Effect on Boattail and Base Pressure Coefficients for $NPR=2.0$, $D_S=1''$	33-40
17-20	Reynolds Number Effect on Boattail and Base Pressure Coefficients	41-44
21-22	Mach Number Effect on Boattail and Base Pressure Coefficients	45-46
23-24	Mass Injection Effect on Boattail and Base Pressure Coefficients for a Different Injection Location and Area	47-48
25	Nozzle Pressure Ratio Effect on Boattail and Base Pressure Coefficients	49
26-35	Mass Injection Effect on Boattail and Base Pressure Coefficients for $NPR>2$	50-59
36-41	Mass Injection Effect on Boattail and Base Pressure Coefficients for $NPR=2$, $D_S>1''$	60-65
42-44	Sting Size Effect on Boattail and Base Pressure Coefficients	66-68
45-52	Mass Injection Effect on Boattail and Base Pressure Coefficients for $NPR=2.0$, $D_S=1''$	69-76

LIST OF ILLUSTRATIONS (CONTINUED)

FIGURE		PAGE
53-56	Reynolds Number Effect on Boattail and Base Pressure Coefficients	77-80
57	Mach Number Effect on Boattail and Base Pressure Coefficients	81
58	Nozzle Pressure Ratio Effect on Boattail and Base Pressure Coefficients	82
59-68	Mass Injection Effect on Boattail and Base Pressure Coefficients for $NPR > 2$	83-92
69-74	Mass Injection Effect on Boattail and Base Pressure Coefficients for $NPR = 2$, $D_S > 1"$	93-98
75-77	Sting Size Effect on Boattail and Base Pressure Coefficients	99-101
78-85	Mass Injection Effect on Boattail and Base Pressure Coefficients for $NPR = 2.0$, $D_S = 1"$	102-109
86-89	Reynolds Number Effect on Boattail and Base Pressure Coefficients	110-113
90-91	Mach Number Effect on Boattail and Base Pressure Coefficients	114-115
92	Nozzle Pressure Ratio Effect on Boattail and Base Pressure Coefficients	116
93-102	Mass Injection Effect on Boattail and Base Pressure Coefficients for $NPR > 2$	117-126
103-108	Mass Injection Effect on Boattail and Base Pressure Coefficients for $NPR = 2$, $D_S > 1"$	127-132
109-111	Sting Size Effect on Boattail and Base Pressure Coefficients	133-135
112-117	Base Pressure Coefficient Variation With Sting Size	136-141
118-120	Base Drag Coefficient Variation With Sting Size	142-144
121-126	Boattail Drag Coefficient Variation With Base Pressure	145-150
127-130	Afterbody Drag Coefficient Variation With Mass Injection for Different Reynolds Numbers, and $NPR = 2$	151-154
131-132	Afterbody Drag Coefficient Variation With Mass Injection for Different Sting Sizes	155-156

LIST OF ILLUSTRATIONS (CONCLUDED)

FIGURE		PAGE
133	Afterbody Drag Coefficient Variation With Mass Injection for NPR=3.62	157
134	Afterbody Drag Coefficient Variation With Mass Injection for NPR=4.3	158
135	Afterbody Drag Coefficient Variation With Mass Injection for NPR=5.45	159
136	Afterbody Drag Coefficient Variation With Reynolds Number	160
137	Afterbody Drag Coefficient Variation With Free-Stream Mach Number for NPR=2	161
138	Afterbody Drag Coefficient Variation With Free-Stream Mach Number for NPR=3.7 and 4.34	162
139	Afterbody Drag Coefficient Variation With Nozzle Pressure Ratio Without Mass Injection	163
140	Afterbody Drag Coefficient Variation With Nozzle Pressure Ratio for Different Mass Injection Rates	164
141	Afterbody Drag Coefficient Variation With Sting Size Without Mass Injection	165
142	Afterbody Drag Coefficient Variation With Sting Size for $\dot{m}=0.033$ lbm/sec	166
143	Afterbody Drag Coefficient Variation With Sting Size for $\dot{m}=0.066$ lbm/sec	167
144	Afterbody Drag Coefficient Variation With Sting Size for $\dot{m}=0.115$ lbm/sec	168
145	Afterbody Drag Coefficient Variation With Boattail Terminal Angle	169

LIST OF TABLES AND DIAGRAMS

TABLE		PAGE
1	Pressure Taps and Injection Rows Locations	21
2	Correspondence Between Sting and Jet Size	22
3	Base Pressure Coefficient Variation With Nozzle Pressure Ratio	23
DIAGRAM		
1	Data Flow Diagram	24

LIST OF SYMBOLS

C_D	Pressure Drag Coefficient Based on Maximum Cross Sectional Area
C_p	Surface Pressure Coefficient, $\frac{p - p_\infty}{\gamma/2 p_\infty M_\infty^2}$
C_p^*	Critical Pressure Coefficient
ΔC_p	Pressure Coefficient Variation
D	Diameter
L	Axial Length
ℓ	Distance of Frustum From Model Base
M	Mach number
\dot{m}	Mass Flux
NPR	Nozzle Pressure Ratio, p_{0j}/p_∞
p	Static Pressure
p_0	Stagnation Pressure
r	Radius
r_0	Maximum Model Radius
Re_L	Reynolds Number Based on Model Length
S	Cross-Sectional Area
X	Axial Coordinate
β	Boattail Average (Chord) Angle
β_t	Boattail Terminal Angle
γ	Specific Heat Capacity Ratio
θ	Frustum Semivertex Angle
ρ_0	Radius of Curvature
ϕ	Peripheral Angle

Subscripts

β	Boattail
b	Base
f	Frustum
j	Jet
M	Maximum
s	Sting
A,j	Afterbody, Based on Jet
A,s	Afterbody, Based on Sting
b,j	Base, Based on Jet
b,s	Base, Based on Sting
∞	Infinity

Superscripts

'	First Derivative
-	Nondimensionalized With Respect to Boattail Axial Length, L_β

Flagged Symbols denote base pressure

SECTION I

INTRODUCTION

It is of utmost importance to develop new techniques capable of effectively reducing the afterbody drag of single engine fighter or engine nacelles of aircraft performing in the transonic range. It has been determined that boattail and base injection, properly used, can substantially reduce the afterbody drag levels of slender bodies of revolution in the supersonic regime (References 1, 2). Consequently an investigation was initiated in the Air Force Flight Dynamics Laboratory to determine whether the same effects would be obtained in the transonic regime. Preliminary results for boattail injection (Reference 3), using a circular-arc boattail with a boattail average angle of 10° , showed a favorable effect on the drag coefficient by injecting small amounts of air in the Mach number range of 0.8 to 0.95. Additional experimental tests have been performed on boattails of different shapes and angles to confirm and validate the previous results and also to determine the effect of different parameters such as location, area, and rate of injection, as well as boattail shape and angle, nozzle pressure ratio, jet diameter, and Reynolds number. The testing technique of jet flow simulation by means of a cone frustum-sting combination was used in the experiment.

SECTION II

EQUIPMENT AND TEST DESCRIPTION

The experiment was performed at the Trisonic Gasdynamics Facility of the Air Force Flight Dynamics Laboratory (Reference 4). The closed circuit wind tunnel in the facility can be operated in the subsonic, transonic, or supersonic regimes. The transonic configuration was used for the present experiment. The size of the tunnel test section is 15" x 15". The open area of the four slotted walls used can be varied continuously over a porosity range from 4% to 12%. The present tests used a nominal porosity of 10%. The slotted side walls can be replaced by solid side walls with optical flat inserts to allow for schlieren photography. The tests were conducted at Mach 0.8 to 0.95, at a tunnel stagnation temperature of 560°R and stagnation pressures of 2000 and 3000 psf which approximately correspond to Reynolds numbers of 8.3×10^6 and 13.4×10^6 based on the model length. The tests were performed at zero angle of attack on a sting mounted, axisymmetric ogive-cylinder model with three different boattails (Figures 1-7). The maximum model diameter was 3". The three interchangeable boattails of different shape and angle tested were: a circular-arc boattail with a nominal average angle of 10° and a terminal angle of 15°; a cut-off version of the nozzle afterbody used for the B-1 aircraft engines with a nominal average angle of 14° and a terminal angle of 20°; and a conical boattail with an angle of 25°. The boattails were equipped with four to 12 static pressure taps distributed circumferentially and longitudinally, and two to three rows of 36 injection ports per row (Table 1). Additional pressure taps were located in the base region. The boattail coordinates are given in Figure 2.

The injection air was supplied through the rear sting to a settling chamber inside the boattail.

In Reference 5, a correlation between the effects of the support sting-cone frustum combination on base pressure variation and the effects of a real jet plume was obtained. Based on this correlation, a cone frustum of 20° angle and 2.75" axial length, L_f , acted as plume simulator and could be positioned over the sting at different distances from the

boattail end (Figures 4 and 5). The sting diameter could also be varied using sleeves of different diameters (Figures 1, 6, and 7). The jet flow for a nozzle pressure ratio (NPR) of approximately 2, which represents a fully expanded sonic flow at the exit of a convergent nozzle, was simulated by the support sting without the frustum. The base pressure variation due to the sting for constant model diameter is

$$\Delta C_{p_b}|_s = \frac{\partial C_{p_b}}{\partial (D_s/D_b)^2} (D_s/D_b)^2 \quad (1)$$

Similarly, the variation due to the jet is

$$\Delta C_{p_b}|_j = \Delta C_{p_b}(D_j^2=0) + \frac{\partial \Delta C_{p_b}}{\partial (D_j^2/D_b D_M)} D_j^2/D_b D_M \quad (2)$$

The right hand side terms of Equation 2 have been obtained as functions of NPR by correlation with flight tests. Equating the pressure variation of the sting to that caused by the jet yields a correspondence between sting and jet diameter, which is shown in Table 2. Note that the base pressure variation due to jet effects consists of two terms. One is due to the jet flow, the other $\Delta C_{p_b}(D_j^2=0)$, is the hypothetical contribution when the jet diameter is reduced to zero.

Even though the wind tunnel simulation produces the same base pressure as a real jet, the drag coefficient obtained with the sting is different from the one obtained with the jet due to the difference in the effective base area,

$$\frac{\pi(D_b^2 - D_s^2)}{4} \neq \frac{\pi(D_b^2 - D_j^2)}{4} \quad (3)$$

Then, in general

$$C_{D_{A,s}} \neq C_{D_{A,j}} \quad (4)$$

Both drag coefficients are listed in this report but the present parametric study is mainly based on experimentally obtained values of $C_{D_{A,s}}$.

For $NPR > 2$ the simulation was accomplished by positioning the frustum on the sting at different distances from the model while holding the sting-diameter fixed at 1". The effect of the frustum on the base pressure, given in Reference 5, is obtained by adding the following term to the right hand side of Equation 1:

$$\Delta C_{p_b} \Big|_f = \tan \theta \left[\frac{1}{\{(\ell/r_s)^2 Z^2\}^{1/2}} - \frac{(L/r_s) \tan \theta + 1}{\{[(L/r_s) + (\ell/r_s)]^2 + Z^2\}^{1/2}} \right] \\ + \tan^2 \theta \left[\sinh^{-1} \left\{ \frac{(L/r_s) + (\ell/r_s)}{Z} \right\} - \sinh^{-1} \left(\frac{\ell/r_s}{Z} \right) \right]$$

where Z is a function of Mach number.

The term $\frac{\partial C_{p_b}}{\partial (D_s/D_b)^2}$ of Equation 1 is plotted in Figure 8 versus boattail

terminal angle and its value seems to have little dependence on Mach number in the range of the present experiment and is consistent with the value of Reference 5, except for $\beta_t = 25^\circ$, (conical boattail). As will be seen later, the flow over the 25° conical boattail separates and therefore the base pressure is not significantly affected by changes in the sting diameter. This is one of the limitations of the correlation of Reference 5 which is valid for attached flows only and for zero base bleed. Also, conical boattails do not correlate well with simulation results obtained on different boattail shapes. Table 3 shows the correspondence between NPR , ΔC_{p_b} , ℓ , D_s , D_j for each boattail used. For the conical boattail, $\beta_t = 25^\circ$, the value of Reference 5 for $\frac{\partial C_{p_b}}{\partial (D_s/D_b)^2}$ was used and the results for NPR should be taken with some reservation.

The model blockage was approximately 3%. The base was equipped with two pressure taps and 36 more pressure taps were mounted in the wall and in the diffuser to check for possible wall interference. Tunnel wall static pressures were connected to the Hg manometer board to monitor the wind tunnel pressure levels. The model pressure

transducers were connected to a Hewlett Packard 2100 on-line computer for calculation of the afterbody pressure and drag coefficients (Diagram 1).

The mass flow system provided the secondary flow for air injection. The orifice used in the system was 0.36247" in diameter. Two equations were used to calculate the mass flow rates, namely

$$\dot{m} = k p_{o_1} \left(\gamma / R T_{o_1} \right)^{1/2} g A^* \quad (\text{lbm/sec}) \quad (5)$$

for choked flow and

$$\dot{m} = A p_{o_1} \left\{ \frac{2\gamma}{R T_{o_1} (\gamma - 1)} \left[\left(\frac{p_{o_1}}{p_2} \right)^{\frac{\gamma-1}{\gamma}} - 1 \right] \right\}^{1/2} g / \left(\frac{p_{o_1}}{p_2} \right)^{\frac{\gamma+1}{2\gamma}} \quad (6)$$

for unchoked flow

where

$$k = 0.579$$

$$p_{o_1} = \text{stagnation pressure ahead of orifice, psia}$$

$$p_2 = \text{pressure behind orifice, psia}$$

$$T_{o_1} = \text{stagnation temperature ahead of orifice, } ^\circ\text{R}$$

$$R = \text{gas constant, } 1716 \text{ ft}^2/\text{sec}^2\text{ } ^\circ\text{R}$$

$$\gamma = \text{specific heat capacity ratio, 1.4 for cold air}$$

$$g = \text{acceleration of gravity, ft/sec}^2$$

$$A^* = \text{choked orifice area, in}^2$$

$$A = \text{orifice area, in}^2$$

The pressure and temperature data from the mass flow system were directly fed to the Hewlett Packard computer for the calculation of the injected mass flow. The sequence of signal inputs, their conditioning and the resultant outputs are shown in Diagram 1.

A test matrix was assembled to test different configurations: air injection for the three boattails was varied from 0.033 to 0.114 lbm/sec. When the correct wind tunnel and injection conditions were attained, the data acquisition system was triggered (Diagram 1).

It will be seen later that the injection rate that gave the best drag reduction was between 0.03 and 0.06 lbm/sec, which corresponds to about 2% to 3% of the mass flow captured by a stream tube of area equal to the model's maximum cross-sectional area.

SECTION III

RESULTS

1. DRAG COEFFICIENT EQUATIONS

Experimental data were obtained, reduced, and analyzed. The pressure coefficients for different configurations were plotted in order to investigate the effects of mass injection, Mach number, plume simulator, and sting diameter on the flow field and on the drag coefficient. The purpose of using different configurations, injection locations, and mass fluxes was to find those for which the overall integrated boattail and base pressure would give a drag reduction.

The afterbody pressure drag coefficient was calculated using the following equations

$$C_{D_{A,s}} = C_{D_{\beta}} + C_{D_{b,s}} \quad (7)$$

where

$$C_{D_{\beta}} = \frac{1}{\bar{S}_M} \int_0^1 C_{P_{\beta}} \bar{S}'_{\beta} d\bar{x} \quad (8)$$

$$C_{D_{b,s}} = -C_{P_b} (\bar{S}_b - \bar{S}_s) / \bar{S}_M \quad (9)$$

or, if the jet flow is considered,

$$C_{D_{A,j}} = C_{D_{\beta}} + C_{D_{b,j}} \quad (10)$$

where

$$C_{D_{b,j}} = -C_{P_b} (\bar{S}_b - \bar{S}_j) / \bar{S}_M \quad (11)$$

For the circular-arc boattail

$$\bar{S}'_{\beta} = 2 \pi \bar{r} \frac{d\bar{r}}{d\bar{x}} \quad (12)$$

$$C_{P_{\beta}} = \frac{P_{\beta} - P_{\infty}}{\gamma/2 P_{\infty} M_{\infty}^2} \quad (13)$$

$$\bar{r} = -(\bar{\rho}_o - \bar{r}_o) + (\bar{\rho}_o^2 - \bar{x}^2)^{1/2} \quad (14)$$

$$\bar{r}_b = -(\bar{\rho}_o - \bar{r}_o) + (\bar{\rho}_o^2 - 1)^{1/2} \quad (15)$$

The barred quantities are nondimensionalized with respect to the boattail axial length, in this case $L_\beta = 3.024$ ". The boattail radius of curvature is $\rho_o = 10.971$ ", and $r_o = 1.5$ ".

Therefore

$$C_{D_{A,s}} = C_1 \int_0^1 C_{p_\beta} \frac{\bar{x} d\bar{x}}{\sqrt{\bar{\rho}_o^2 - \bar{x}^2}} - C_2 \int_0^1 C_{p_\beta} \bar{x} d\bar{x} - C_{p_b} \left\{ \frac{[-(2\bar{\rho}_o - \bar{D}_M) + 2(\bar{\rho}_o^2 - 1)^{1/2}]^2 - \bar{D}_s^2}{\bar{D}_M^2} \right\} \quad (16)$$

where $C_1 = 25.457568$ and $C_2 = 8.128513$

For the cut-off B-1 boattail, a curve fit was obtained for $\bar{r} = f(\bar{x})$, viz.

$$\bar{r} = C_1 + C_2 \bar{x} + C_3 \bar{x}^2 \quad (17)$$

where $L_\beta = 1.905$ ", $C_1 = 0.78547$, $C_2 = -0.084826$, $C_3 = -0.13249$

Therefore

$$C_{D_{A,s}} = \frac{8}{\bar{D}^2} \int_0^1 C_{p_\beta} (C_1 + C_2 \bar{x} + C_3 \bar{x}^2)(C_2 + 2C_3 \bar{x}) d\bar{x} - C_{p_b} \frac{[(C_1 + C_2 + C_3)^2 - \bar{D}_s^2/4]}{C_1^2} \quad (18)$$

For the conical boattail ($\beta = 25^\circ$)

$$\bar{r} = \frac{1}{2} (\bar{D}_M - 2\bar{x} \tan \beta) \quad (19)$$

where $L_\beta = 0.922$

Therefore

$$C_{D_{A,s}} = \frac{4}{\bar{D}_M^2} \left[-\bar{D}_M \tan \beta \int_0^1 C_{p\beta} d\bar{x} + 2 \tan^2 \beta \int_0^1 C_{p\beta} \bar{x} d\bar{x} \right] - C_{p_b} \frac{[(\bar{D}_M - 2 \tan \beta)^2 - \bar{D}_s^2]}{\bar{D}_M^2} \quad (20)$$

2. CIRCULAR-ARC BOATTAIL PRESSURE DISTRIBUTIONS

a. Mass Injection

Figures 9 through 16 show the influence of mass injection on the pressure distribution and on the drag coefficient at free-stream Mach numbers from 0.8 to 0.95, a NPR of 2, and a sting diameter of 1". In general the injection attenuates the expansion of the flow over the boattail shoulder ahead of the injection ports but it degrades the recompression process on the terminal section of the boattail. The rate of injection is of critical importance in producing drag reduction or increase. In Figures 9 and 10, an injection rate of 0.033 lbm/sec produces a drag reduction while increasing the injection rate increases the drag. An examination of the pressure distribution shows that, for the lower injection rates, the injected flow produces a mild compression in front without causing a large separated region behind. The extent of the supersonic pocket is therefore reduced. At higher rates, the expansion over the boattail shoulder is at first favorably reduced but the expansion peak reaches an even lower value. This lower peak occurs immediately after the injection ports, revealing the occurrence of vortical flow with an extended separated region produced by the lateral jet issuing into the embedded supersonic field. Then, a stronger reattachment shock takes place.

b. Reynolds Number

The effect of Reynolds number is shown in Figures 17 through 20. The difference in the pressure distribution at $Re_L \approx 8.5 \times 10^6$ and 13×10^6 is small for any NPR and is mainly seen in the value of the

base pressure and at $x=2.25''$. It is possible that the pressure tap at this location did not work properly since the value of the drag coefficient at $M_\infty=0.8$ is higher than the drag coefficient at $M_\infty=0.85$ for $Re_L=8.3 \times 10^6$ (Figures 17 and 18) and this is incompatible with the well known results of increasing drag coefficient with increasing Mach number for attached flows in this Mach number range. Except for $M_\infty=0.8$, there is an increase in drag coefficient with increasing Re_L . In Reference 6 it is stated that this increase in the afterbody region is cancelled by a drag decrease in the forebody so that it is necessary to consider the overall pressure drag to show that it is independent of Reynolds number. This result, however, has recently been questioned. Other results have shown that the boattail drag is not affected by the Reynolds number (Reference 7). However, the Re_L range considered is much wider than the present range, up to 43×10^6 , and the base drag is not considered.

It is important to state that, in the present experiment, the boundary layer flow is naturally turbulent over the afterbody for both Re_L . It is then correct to assume that in the present small Re_L range, the boundary layer does not alter appreciably the external pressure distribution.

c. Mach Number

The effect of Mach number on the pressure distribution is shown in Figures 21 and 22. An increase of the free-stream Mach number usually results in a stronger expansion over the boattail shoulder creating a higher drag coefficient. From $M_\infty=0.85$ to 0.95 the supersonic pocket increases in size and higher shock losses occur. These losses are partially compensated by a greater subsonic recompression on the boattail terminal section.

d. Injection Location and Area

Previous tests (Reference 3) have shown that for those small injection rates that produce drag reduction, a further reduction can be obtained when the injection ports are concentrated near the boattail shoulder instead of being uniformly distributed over the boattail

(Figures 23 and 24). In addition, reducing the injection area at low injection rates increases the momentum of the injected flow, which reduces the expansion over the boattail shoulder with consequent drag decrease.

e. Nozzle Pressure Ratio

The nozzle pressure ratio (NPR) influences considerably the boattail pressure distribution and the base pressure. The expansion over the boattail shoulder becomes weaker and the recompression over the boattail terminal section and in the base region becomes stronger with increasing NPR (Figure 25). This effect is verified at Mach numbers and Reynolds numbers between $M_\infty=0.9$ and 0.95 and $Re_L=8.3 \times 10^6$ and 13.4×10^6 .

Figures 26 through 33 show the effect of mass injection for NPR from 3.62 to 4.26. The same results as reported for NPR=2 in Section III-2,a are obtained, namely a drag reduction is experienced at low injection rates followed by a drag increase at higher rates. However, for NPR>2, the drag reduction obtained with injection is higher than the one obtained for NPR=2, up to 12% instead of about 5%.

Figures 34 and 35 show the effect of mass injection at NPR=5.45. At this high NPR, a thrust is experienced in the afterbody region. In this case, the injection is not beneficial producing a decrease in thrust.

f. Sting

Figures 36 through 41 show the pressure distributions when the sting diameter is increased. Qualitatively, the distributions are similar to those obtained with the 1" diameter sting. The injection at first decreases the expansion over the boattail shoulder but weakens the recompression on the boattail terminal part. Increasing injection rate increases the shoulder expansion. Consequently the drag coefficient decreases for low injection rates while it increases for higher rates.

Quantitatively, the overall drag levels are reduced with bigger sting sizes. The sting simulates the jet diameter and, therefore, the volumetric jet flow. An increase in sting size decreases the boattail

shoulder expansion and increases the recompression on the terminal part of the boattail and the base pressure (Figures 42 through 44). The beneficial effect is experienced at any injection rate.

3. CUT-OFF B-1 BOATTAIL PRESSURE DISTRIBUTIONS

a. Mass Injection

A pattern somewhat different than the circular-arc boattails is seen in the pressure distributions of the cut-off B-1 at NPR=2 (Figures 45 through 52). In the case of supersonic flow occurring on the boattail, when the mass injection is used, the extent of the supersonic pocket is larger than the one that develops on the circular arc boattail. This is due to the different location and area of injection, three rows of injection extending downstream up to about 1" from the boattail end (Figure 45) while for the circular-arc only two rows extending downstream up to about 2" from the boattail end (Figure 9). The separation and reattachment shocks generated by the injection are farther apart and the separated flow region is larger. These phenomena consequently produce stronger shock and separation losses and a drag increase with injection even though the base pressure at times rises with it. Clearly the pressure distribution of Figure 46 shows a strong compression with subsequent expansion, at $x \approx 1$ " caused mainly by the air injected from the third row of injection ports. The effect of injection seems to be detrimental when used with this particular boattail shape, except in sporadic cases (Figure 51).

b. Reynolds Number

As in the case of the circular-arc boattail, the Reynolds number, in the range of the present experiment, has little effect on the pressure distribution for any NPR (Figures 53 through 56), except at the shoulder expansion and on the value of the base pressure. Again, except at $M_\infty = 0.8$ where an increase in Reynolds number produces lower drag, a higher Reynolds number produces higher drag in the Mach number range of $M_\infty = 0.85$ to 0.95.

c. Mach Number

The Mach number effect on the pressure distribution (Figure 57) is the same as for the circular-arc boattail. The increase of Mach number produces a stronger boattail shoulder expansion, a bigger supersonic pocket and a drag increase.

d. Injection Location and Area

As mentioned in Section III-3,a, the location and area of injection for the cut-off B-1 boattail is not very favorable inasmuch as it generally produces a drag increase at all Mach numbers.

e. Nozzle Pressure Ratio

Figure 58 shows the effect of NPR on the pressure distribution. As for the circular-arc boattail, a higher NPR produces a better boattail recompression and a higher base pressure. Consequently the drag coefficient is reduced.

Figures 59-68 show that at any $NPR > 2$ and up to 5.18, mass injection produces a drag increase as was the case for $NPR = 2$.

f. Sting

The sting size does not change qualitatively the pressure distribution with or without injection (Figures 69 through 74). The plots are similar to those for $D_s = 1"$ (Figures 45 through 52, Section III-3,a).

The increase in sting size produces a compression over the boattail and an increase in base pressure (Figures 75 through 77). The values of the drag coefficient are consequently reduced.

4. CONICAL BOATTAIL PRESSURE DISTRIBUTIONS

a. Mass Injection

The pressure distributions for the conical boattail are shown in Figures 78 through 85. Because of the high boattail angle, $\beta = 25^\circ$, an incipient separation is detected for $M_\infty = 0.8$ and $\dot{m} = 0$ downstream of the boattail shoulder (Figure 80). This is confirmed by the inflection of

the pressure distribution over the boattail terminal section, signifying a brief lack of recompression. For $M_\infty > 0.8$, the flow is fully separated and no recompression occurs.

When mass injection is used, a drag reduction is obtained inasmuch as the injection energizes the flow in the separated region and delays separation; even though the expansion over the shoulder is bigger, a stronger recompression occurs downstream. As reported in Reference 8, gas injection in a separated region is always beneficial and reduces the drag levels.

b. Reynolds Number

Figures 86 through 89 show the effect of Reynolds number on the pressure distributions for $NPR=2$. The pressure distribution for $M_\infty=0.8$ and $p_0=2000$ (Figure 86) seems to be in error as was the case for the other boattails. The drag obtained is too high to be acceptable. As will be seen later its value is much higher than the one obtained for $M_\infty=0.95$.

The other distributions show little Reynolds number effect but it should be noted, that contrary to the results for the other boattails, the drag values are lower for the higher Reynolds numbers.

Reynolds number effects for $NPR > 2$ will be discussed later on in Section III-4,e.

c. Mach Number

Figures 90 and 91 show that the Mach number influence on the pressure distribution is much smaller than it was for the other two boattails for $NPR=2$. This is due to the fact that the flow is separated and, therefore, the amount of shoulder expansion does not increase with Mach number any more. Excluding the erroneous value for $M_\infty=0.8$ and $p_0=2000$ mentioned before, the drag coefficient rise with Mach number is small.

For $NPR > 2$, the drag coefficient actually decreases with M_∞ , as it will be seen later. This is attributed to the earlier boattail separation occurring at higher NPR. When the local boattail flow is subsonic, there is little change in the drag coefficient, but when the local flow is supersonic, as in the case of $M_\infty = 0.95$, an earlier separation produces a drag decrease.

d. Injection Location and Area

The location and area of injection do not influence the pressure distribution and the drag values as long as the gas is injected in the separated flow region.

e. Nozzle Pressure Ratio

Figure 92 shows the effect of NPR on the pressure distribution. As for the other two boattails, a higher NPR gives rise to a better boattail recompression and higher base pressure. For the conical boattail, an NPR of 5.42 eliminates almost completely the expansion over the shoulder and the base pressure becomes higher than free-stream.

Figures 93 through 102 show that, for $NPR > 2$, small mass injection produces a drag reduction. For high mass fluxes, $\dot{m} > 0.066$, a reversal takes place and the drag increases again (Figures 97, 101, and 102).

It is important to notice that, at high NPR, mass injection produces a reattachment of the flow field for the lower Reynolds number cases (Figures 97 and 101) while leaving the flow separated at higher Reynolds number (Figure 102). The Reynolds number effect is thus evident.

f. Sting

As for the other boattails, the sting size does not alter qualitatively the pressure distributions (Figures 103 through 108). The increase in sting size produces a better boattail recompression with consequent drag reduction (Figures 109 through 111).

5. BASE PRESSURE LEVELS AND AFTERBODY DRAG COEFFICIENTS

The base pressure levels and the afterbody drag coefficients, which are the sum of the base and boattail drag coefficients, are analyzed.

Figures 112 through 117 show how the base pressure is affected by the sting size. The base pressure coefficient increases with an increase in the value of D_s/D_b for both the circular-arc and the cut-off B-1 boattails at any injection rate. It remains almost unchanged for the conical boattail. This happens because of the separated boattail flow caused by the high boattail angle. Consequently, its value is much lower than the value obtained for the other two boattails.

The base pressure values for zero sting diameter have been obtained by extrapolation and are indicated with dash lines. They are hypothetical and only indicative of the conditions that might exist in the base region in absence of the sting.

Figures 118 through 120 show the corresponding base drag coefficients. At $\dot{m}=0$, the circular-arc boattail exhibits a higher base thrust than the cut-off B-1, while at $\dot{m}=0.066$ the values are reversed and practically identical at $\dot{m}=0.115$. The conical boattail produces instead the highest base drag. The base drag curves tend to zero when $D_s/D_b \rightarrow 1$.

Figures 121 through 126 show correlations between boattail drag coefficient and base pressure coefficient with and without mass injection for different free-stream Mach numbers. The correlation for the circular-arc of Figure 121 exhibits a higher negative slope than the McDonald-Hughes correlation (Reference 5) and is also slightly different when compared with the results of Reference 3 (see Figure 12 of Reference 3). Nevertheless, the influence of the mass injection is well defined. Figures 121 and 122 show, first, a boattail drag decrease with small injection rates, and then, an increase with higher injection rates for the circular-arc boattail. Figures 123 and 124 show a continuous boattail drag increase with injection rates for the cut-off B-1 boattail as do Figures 125 and 126 for the conical boattail.

Comparing the correlations for the three different boattail terminal angles, β_t , it is observed that the rate of boattail drag reduction with increasing base pressure diminishes with increasing boattail terminal angle.

The plots of the afterbody drag coefficient versus mass injection are reported in Figures 127 through 135. The effect of boattail angle is evident in these figures. As expected at these high β 's, a higher boattail angle produces a higher drag coefficient because of the higher boattail shoulder expansion and lower subsequent recompression.

The conical boattail has the highest afterbody drag coefficient because of the high β and the occurrence of separated flow, but is the most sensitive to mass injection. This injection produces considerable drag reduction. In Figures 127 and 128, the circular-arc boattail shows a very small drag reduction with injection at $M_\infty=0.8$ and 0.85, while the drag of the cut-off B-1 increases rapidly with injection. For $M_\infty=0.95$ (Figure 130), the drag reduction with injection is sizeable not only for the conical boattail but for the circular-arc as well. The drag reversal with injection (decrease-increase) is evident in all the figures. The best configuration for lowest drag is the circular-arc, followed by the cut-off B-1, and then the conical boattail. The Reynolds number affects the drag values. Its effect changes irregularly with the injection rates. No definite pattern is observed.

Figures 131 and 132 are plots of afterbody drag coefficient versus mass injection for various sting sizes. Again, the drag reversal with \dot{m} is observed. For each boattail configuration, the lowest drag coefficient is obtained with the maximum sting size. The minimum overall drag is obtained for the circular-arc boattail, which also requires the lowest amount of mass injection to reach this minimum.

Figures 133 through 135 present the drag coefficient values with mass injection at $NPR>2$. The favorable effect of mass injection for the circular-arc and conical boattails decreases with increasing NPR and for $NPR\approx 5.45$ the effect of injection becomes unfavorable for the circular-arc. This high NPR produces an adverse pressure gradient which, when added to the one generated by the injected flow, causes at times a separation

of the boundary layer over the boattail and an adverse interference. Note in Figure 133 that the conical boattail produces less drag at $M_\infty=0.95$ than at $M_\infty=0.9$ for $NPR=3.62$ as it was anticipated in Section III-4,c.

The Reynolds number effect on the drag coefficient for $NPR=2$ and zero injection is shown in Figure 136. Taking with reservation the high drag values for $M_\infty=0.8$, it is evident that there is little Reynolds number effect on the drag coefficient. For the circular-arc and cut-off B-1 boattails there is a slight increase in drag with Re_L while for the conical boattail a slight decrease.

Figure 137 is a plot of $C_{D_{A,s}}$ versus M_∞ for $NPR=2$ and zero mass injection. The rate of drag increase with M_∞ is less for the conical than for the other boattails because of separation effects. The drag values for $M_\infty=0.8$ and $P_0=2,000$ psfa are too high. As mentioned before, this is attributed to a defective pressure tap. At higher NPR a decrease in drag with M_∞ is actually obtained for the conical boattail (Figure 138).

Figures 139 and 140 show that the increase of NPR considerably reduces the drag coefficient for any condition as expected. The maximum decreasing rate occurs between $NPR=4$ and 5. The increase of the sting diameter also reduces the drag coefficient as illustrated in Figures 141 through 144 for any amount of mass injection. The reduction is considerable.

Figure 145 finally shows the predicted increasing drag coefficient trend with boattail terminal angle for $NPR=2$ and $M_\infty=0.8$ to 0.9. For $M_\infty=0.95$ the drag coefficient increases up to $\beta_t=20^\circ$ but then decreases because of the separation effects of the conical boattail which were discussed earlier. At higher NPR , the beneficial effects due to the injection in the separated region over the conical boattail are felt at $M_\infty=0.9$ as well as $M_\infty=0.95$. Consequently the drag values drop considerably for $\beta_t=25^\circ$.

SECTION IV

CONCLUSIONS

An experimental investigation of the effects of boattail mass injection and jet flow on the transonic afterbody drag of a slender body of revolution at zero angle of attack has been performed.

The conclusions are:

1. A correlation between sting, used as jet simulator, and corresponding jet diameter has been established.
2. The jet plume and the nozzle pressure ratio simulations by the sting-frustum combination have been found appropriate and useful and are considered a good testing technique.
3. Small rates of boattail mass injection in general produce a drag coefficient reduction and are more effective at high nozzle pressure ratios for the circular-arc and conical boattails. For the cut-off B-1 boattail, mass injection increases the drag levels in the present set-up. This boattail shape should not be used in conjunction with injection, in this fashion. It is suggested that the injection port location should be reexamined in light of the present results and eventually replaced.
4. Mass injection is more effective in zones of separated flow.
5. For the boattail angle range used in the present report the afterbody drag increases with boattail angle provided the boattail flow remains attached.
6. The conical boattail has the highest afterbody drag coefficient for $M_\infty=0.8$ to 0.9 , $NPR=2$ and no injection, but is the most sensitive to mass injection which produces considerable drag reduction. For $M_\infty=0.95$ the cut-off B-1 boattail exhibits the highest drag coefficient; the same is true when mass injection is considered at $NPR>2$. In general, the circular-arc boattail gives the lowest drag values.

7. The Reynolds number has a negligible effect on the drag coefficient at NPR=2 and zero injection. At higher NPR and injection rates the Reynolds number affects the boattail pressure distribution of the conical boattail. The boattail flow seems to be attached at low Reynolds number.

8. An increase in Mach number produces a drag coefficient increase for all boattails at NPR=2. At higher NPR values, the drag coefficient increases with increasing M_∞ for the circular-arc and cut-off B-1 boattails but decreases for the conical boattail.

9. Concentrating the injection ports near the boattail shoulder attenuates the expansion at that location and produces a drag reduction for the circular-arc and conical boattails.

10. The nozzle pressure ratio is very effective in changing the afterbody drag. An increase in NPR produces a substantial decrease in drag for all boattails.

11. Increasing the diameter of the sting, which simulates an increase in jet diameter, reduces the afterbody drag for all boattails.

TABLE 1
PRESSURE TAPS AND INJECTION ROWS LOCATION
CIRCULAR ARC BOATTAIL PRESSURE TAPS

NUMBER	X (INCHES)
1	FIXED CYLINDER
2	0.10
3	0.25
4	0.50
5	0.75
6	1.00
7	1.25
8	1.50
9	1.75
10	1.80
11	2.00
12	2.25
13	2.50
14	2.75
15	BASE
16	BASE

INJECTION ROWS

INJECTION ROWS AT

x = 0.756"

x = 1.135"

CUT-OFF B-1 BOATTAIL

NUMBER	X (INCHES)
1	FIXED CYLINDER
2	0.10
3	0.25
4	0.50
5	0.75
6	1.00
7	1.25
8	1.50
9	1.75
10	1.85
11	BASE
12	BASE

INJECTION ROWS AT

x = 0.322"

x = 0.643"

x = 0.965"

CONICAL BOATTAIL

NUMBER	X (INCHES)
1	FIXED CYLINDER
2	0.236
3	0.436
4	0.636
5	0.836
6	BASE
7	BASE

INJECTION ROWS AT

x = 0.25"

x = 0.45"

x = 0.65"

TABLE 2
CORRESPONDENCE BETWEEN STING AND JET SIZE
CIRCULAR ARC BOATTAIL

NPR	D_s (in)	D_j (in)
2	1.0	1.25
2	1.4	1.52
2	1.6	1.66
2	1.8	1.80

CUT-OFF B-1 BOATTAIL

NPR	D_s (in)	D_j (in)
2	1.0	1.24
2	1.4	1.48
2	1.6	1.60
2	1.8	1.73

CONICAL BOATTAIL

NPR	D_s (in)	D_j (in)
2	1.0	1.15
2	1.4	1.29
2	1.6	1.36
2	1.8	1.45

TABLE 3

BASE PRESSURE COEFFICIENT VARIATION WITH NOZZLE PRESSURE RATIO

z (in.)	D_s (in.)	D_j (in.)	ΔC_{p_b}	NPR	
6.0	1.0	1.25	0.02873	3.61	CIRCULAR ARC BOATTAIL
↓			0.02932	3.62	
↓			0.03015	3.64	
↓			0.03051	3.65	
4.0			0.04048	4.26	
↓			0.04131	4.28	
↓			0.04203	4.30	
↓			0.04309	4.41	
2.0			0.08257	5.42	
↓			0.08458	5.45	
↓			0.08650	5.48	CUT-OFF B-1 BOATTAIL
↓			0.08788	5.51	
6.0		1.24	0.02653	3.60	
↓			0.02712	3.61	
↓			0.02795	3.63	
↓			0.02831	3.63	
4.0			0.03828	4.13	
↓			0.03911	4.14	
↓			0.03983	4.15	
↓			0.04089	4.17	
2.0			0.08037	5.15	CONICAL BOATTAIL
↓			0.08238	5.18	
↓			0.08430	5.22	
↓			0.08568	5.24	
6.0		1.15	0.01788	3.69	
↓			0.01847	3.70	
↓			0.01930	3.82	
↓			0.01966	3.83	
4.0			0.02963	4.30	
↓			0.03046	4.32	
↓			0.03118	4.34	
↓			0.03224	4.37	
2.0			0.07172	5.38	
↓			0.07373	5.42	
↓			0.07565	5.45	
↓			0.07703	5.48	

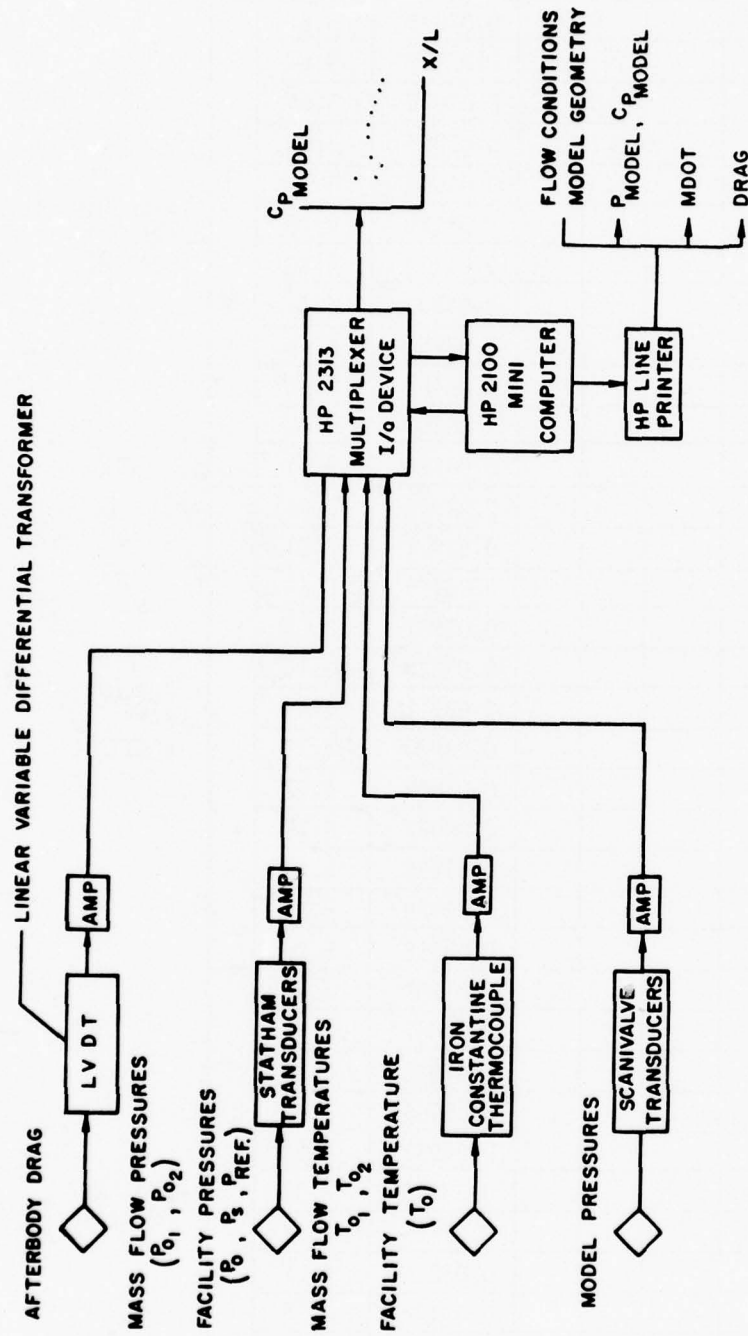


Diagram 1. Flow Data Diagram

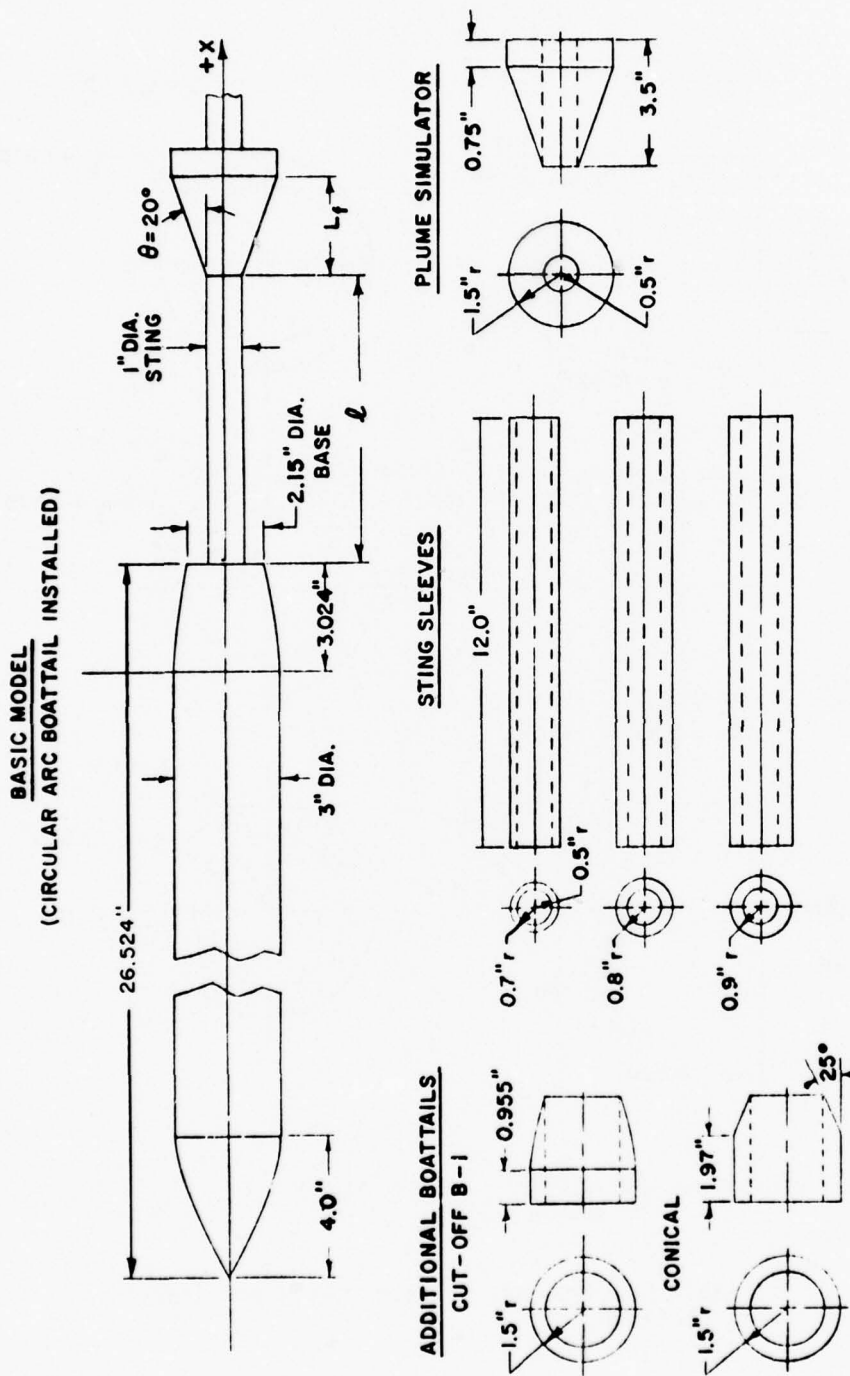
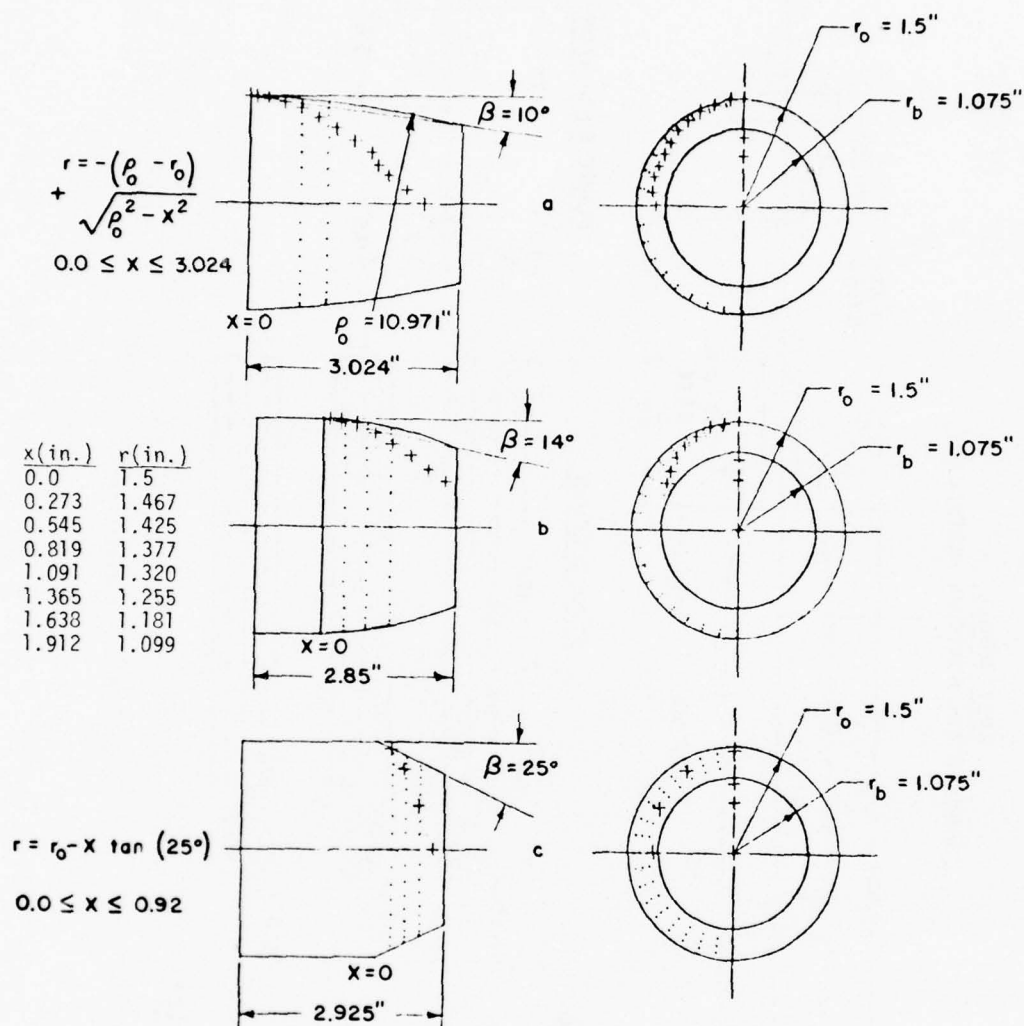


Figure 1. Model Configuration

• = INJECTION PORTS
+ = STATIC PRESSURE TAP



a. = CIRCULAR ARC BOATTAIL b. = CUT-OFF B-1 BOATTAIL
c. = 25° CONICAL BOATTAIL

Figure 2. Boattail Coordinates, Pressure Taps, and Injection Port Location

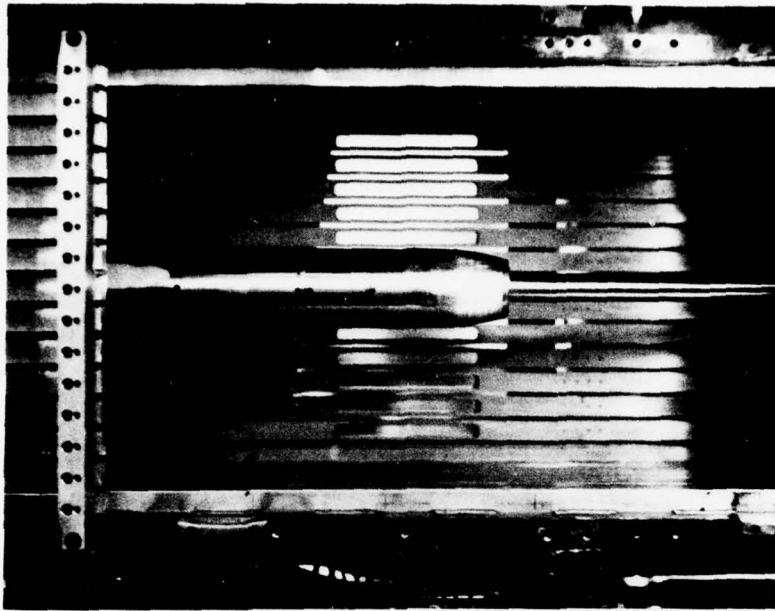


Figure 3a. Trisonic Gasdynamic Facility (TGF) 2' Wind Tunnel Test Section
Sting Mounted Circular-Arc Boattail

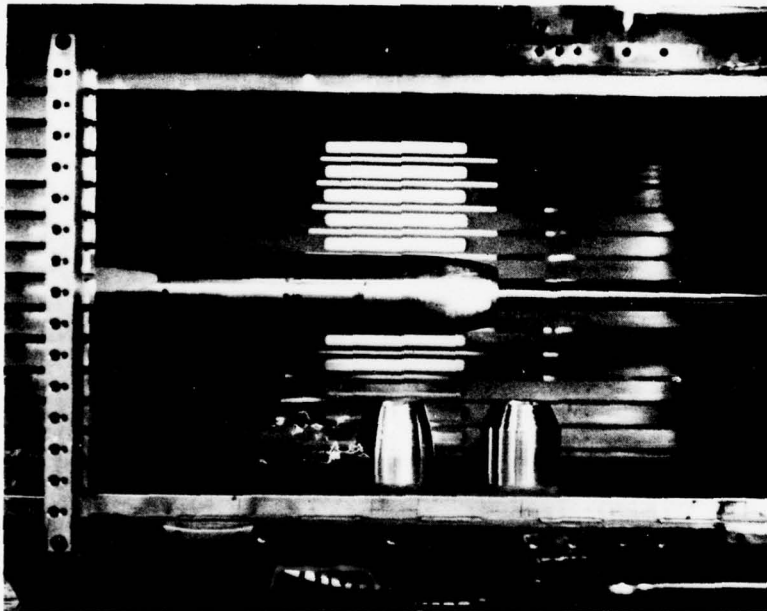


Figure 3b. Trisonic Gasdynamic Facility (TGF) 2' Wind Tunnel Test Section
Cut-Off B-1 and Conical Boattails

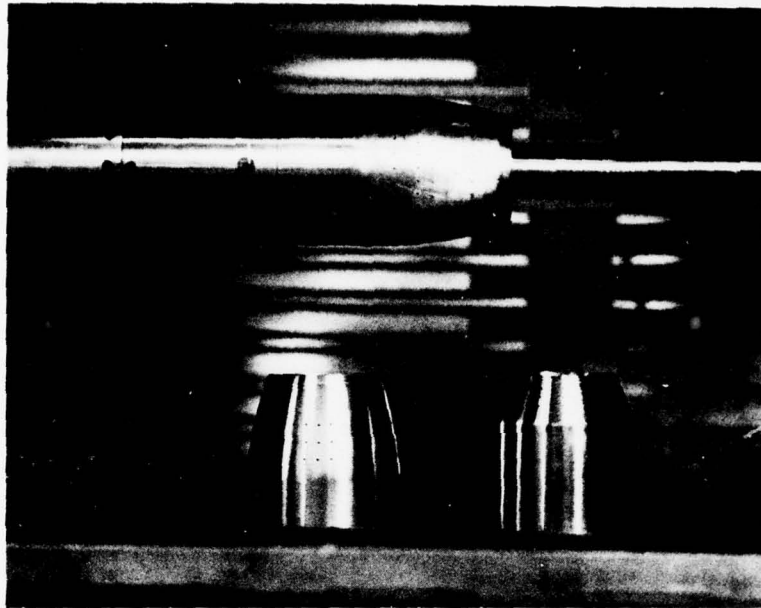


Figure 4a. Close-up of 2' Tunnel Test Section

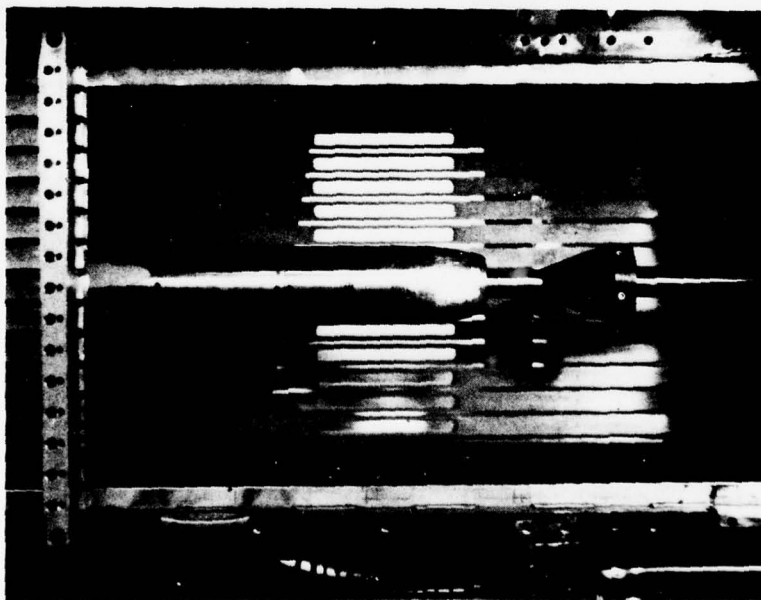


Figure 4b. Cone Frustum - Jet Plume Simulator at $l=2$

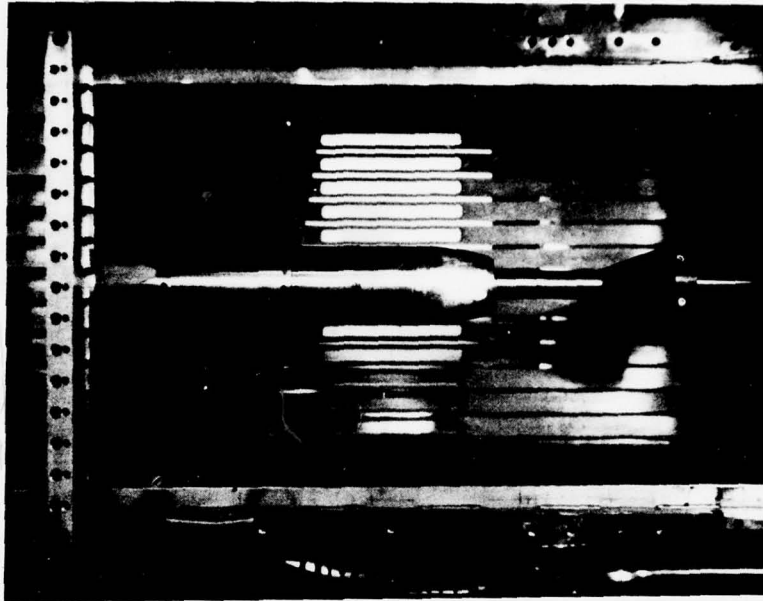


Figure 5a. Cone Frustum - Jet Plume Simulator at $\ell=4''$

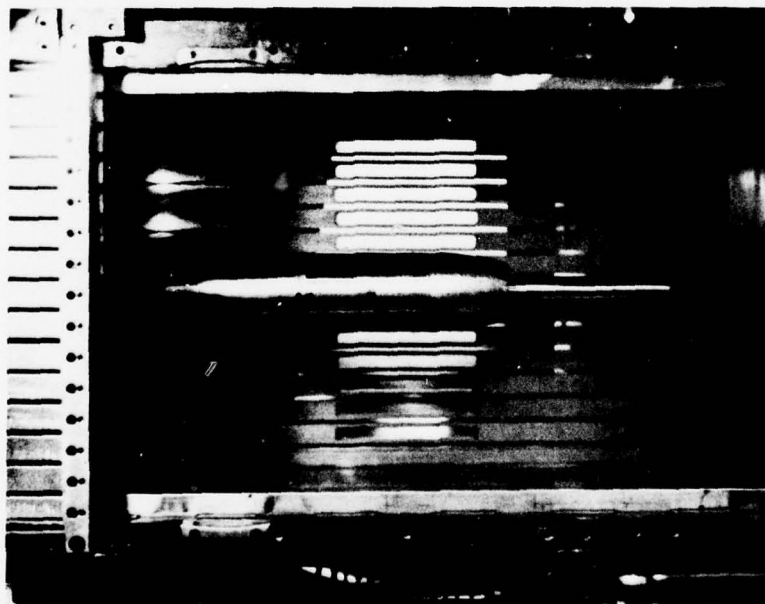


Figure 5b. Cone Frustum - Jet Plume Simulator at $\ell=6''$

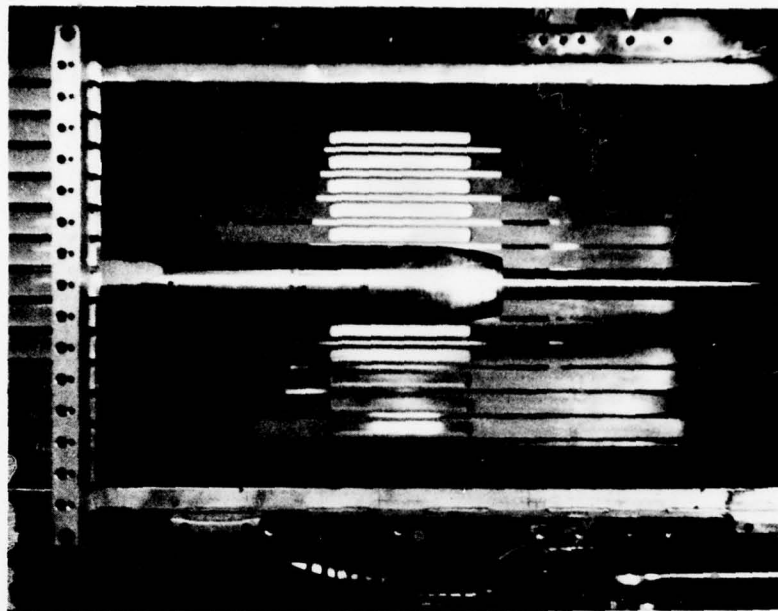


Figure 6a. 1" Diameter Sting

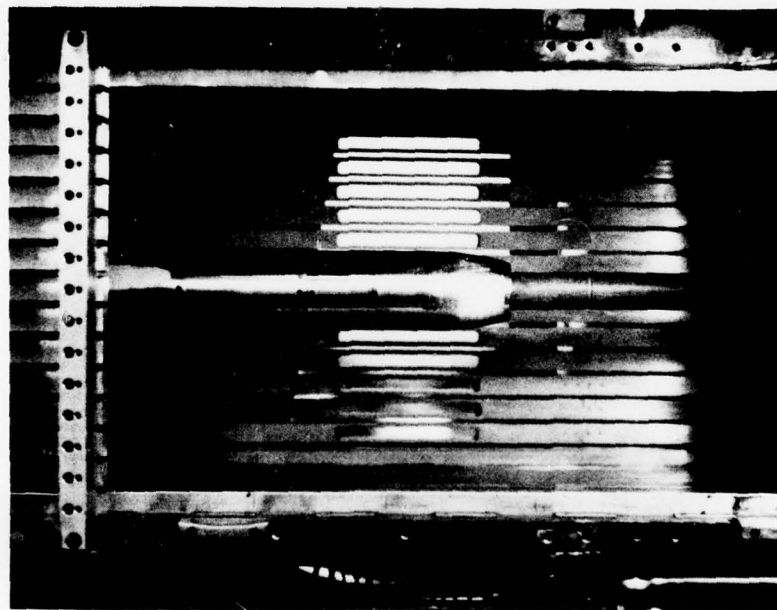


Figure 6b. 1.4" Diameter Sting

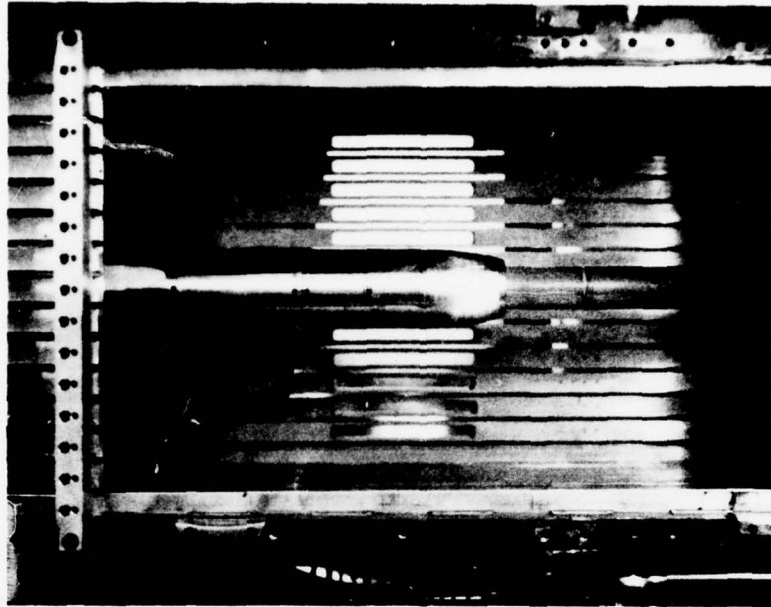


Figure 7a. 1.6" Diameter Sting

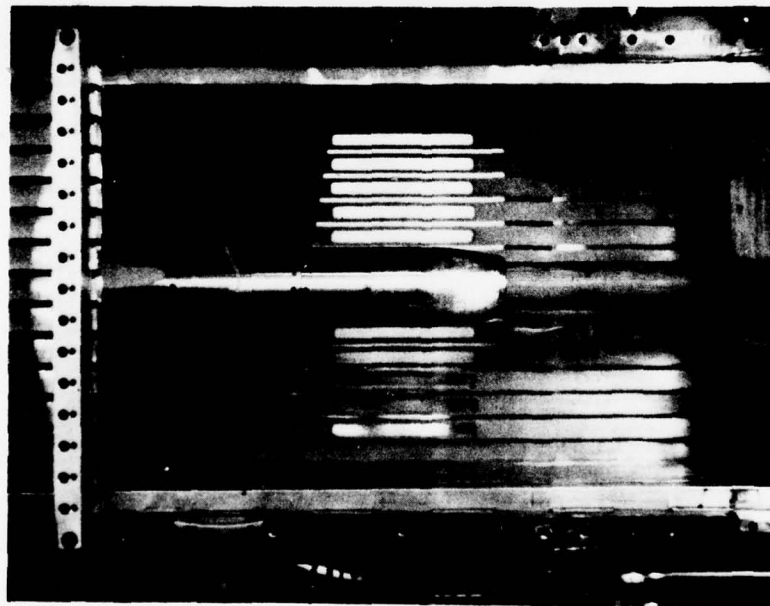


Figure 7b. 1.8" Diameter Sting

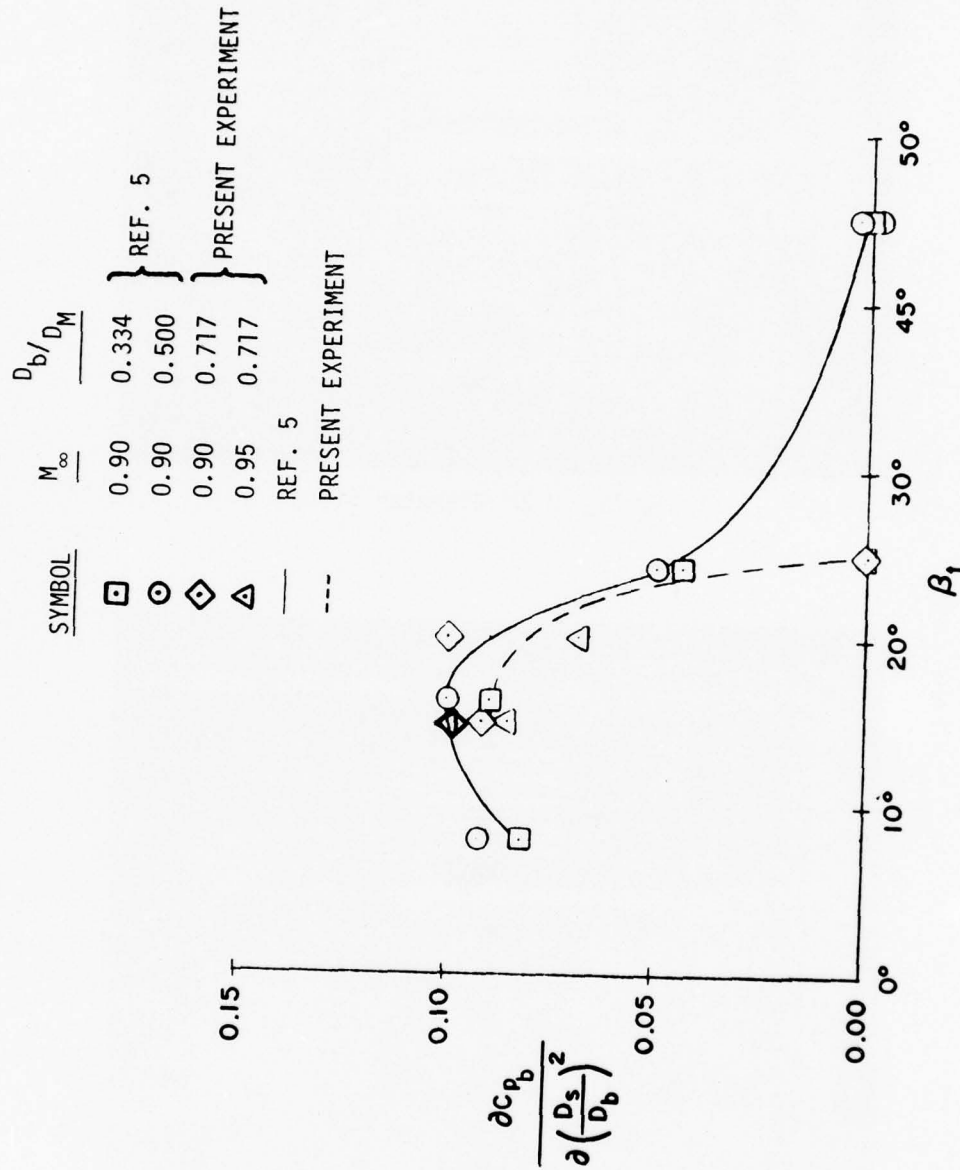


Figure 8. Base Pressure Variation Due to the Sting Versus Terminal Boattail Angle

SYMBOL	NPR	M_∞	p_o (psfa)	Re_L	\dot{m} (lbm/sec)	$C_{D_{A,s}}$	$C_{D_{A,j}}$	$\frac{D_j^2}{D_b D_M}$
○	2.0	.90	2000	8.7×10^6	0.000	.07016	.07408	0.242
□	2.0	.90	2000	8.7×10^6	0.033	.06985	.07361	0.242
◇	2.0	.90	2000	8.7×10^6	0.065	.07390	.07771	0.242
△	2.0	.90	2000	8.7×10^6	0.116	.07854	.08293	0.242

CIRCULAR ARC BOATTAIL

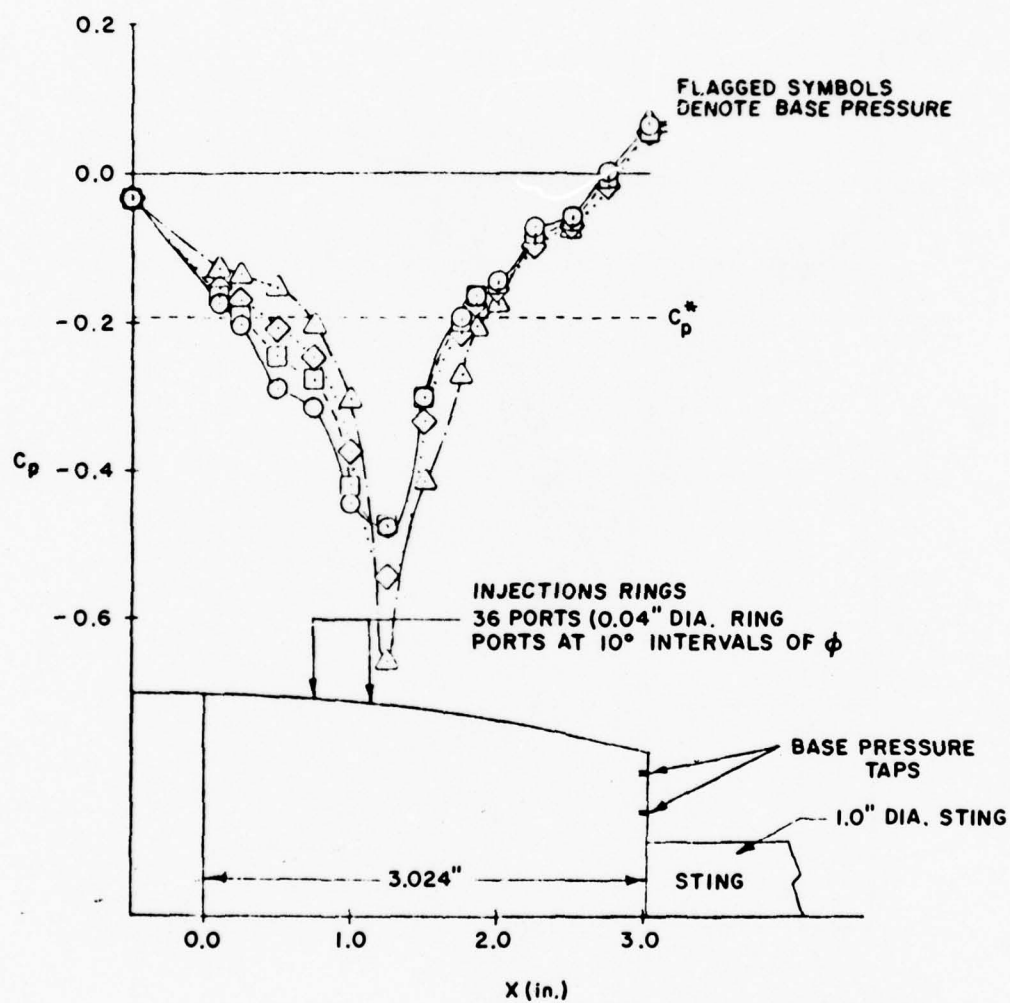


Figure 9. Mass Injection Effect on Boattail and Base Pressure Coefficients for NPR=2.0, $D_S=1"$

SYMBOL	NPR	M_∞	p_o (psfa)	Re_L	\dot{m} (lbm/sec)	$C_{DA,s}$	$C_{DA,j}$	$\frac{D_j^2}{D_b D_M}$
—○—	2.0	.95	2000	8.9×10^6	0.000	.10119	.10391	0.242
—□—	2.0	.95	2000	8.9×10^6	0.033	.09482	.09790	0.242
...◇...	2.0	.95	2000	8.9×10^6	0.066	.09911	.10300	0.242
---△---	2.0	.95	2000	8.9×10^6	0.116	.10487	.10965	0.242

CIRCULAR ARC BOATTAIL

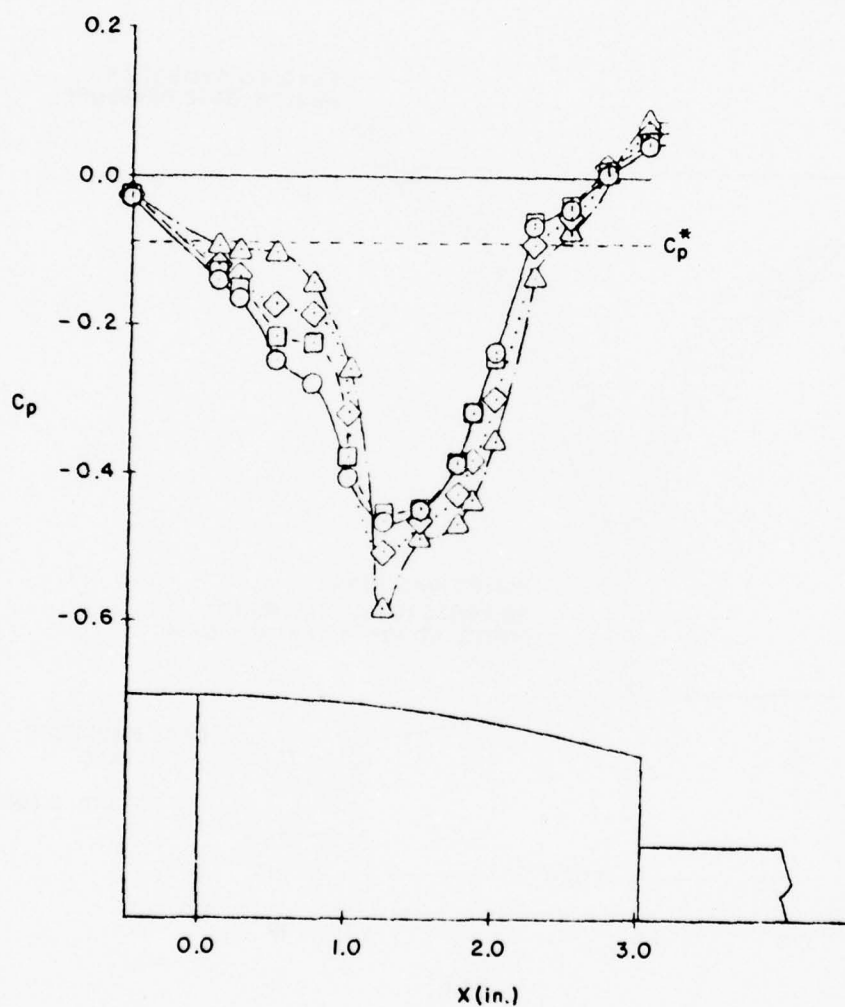


Figure 10. Mass Injection Effect on Boattail and Base Pressure Coefficients for NPR=2.0, $D_b=1"$

SYMBOL	NPR	M_∞	p_o (psfa)	Re_L	\dot{m} (lbm/sec)	$C_{D_A,s}$	$C_{D_A,j}$	$\frac{D_j^2}{D_b D_m}$
—○—	2.0	.80	2000	8.3×10^6	0.000	.06333	.06741	0.242
—□—	2.0	.80	2000	8.3×10^6	0.034	.06635	.07005	0.242
...◇...	2.0	.80	2000	8.3×10^6	0.066	.07151	.07505	0.242
—△—	2.0	.80	2000	8.3×10^6	0.113	.07464	.07845	0.242

CIRCULAR ARC BOATTAIL

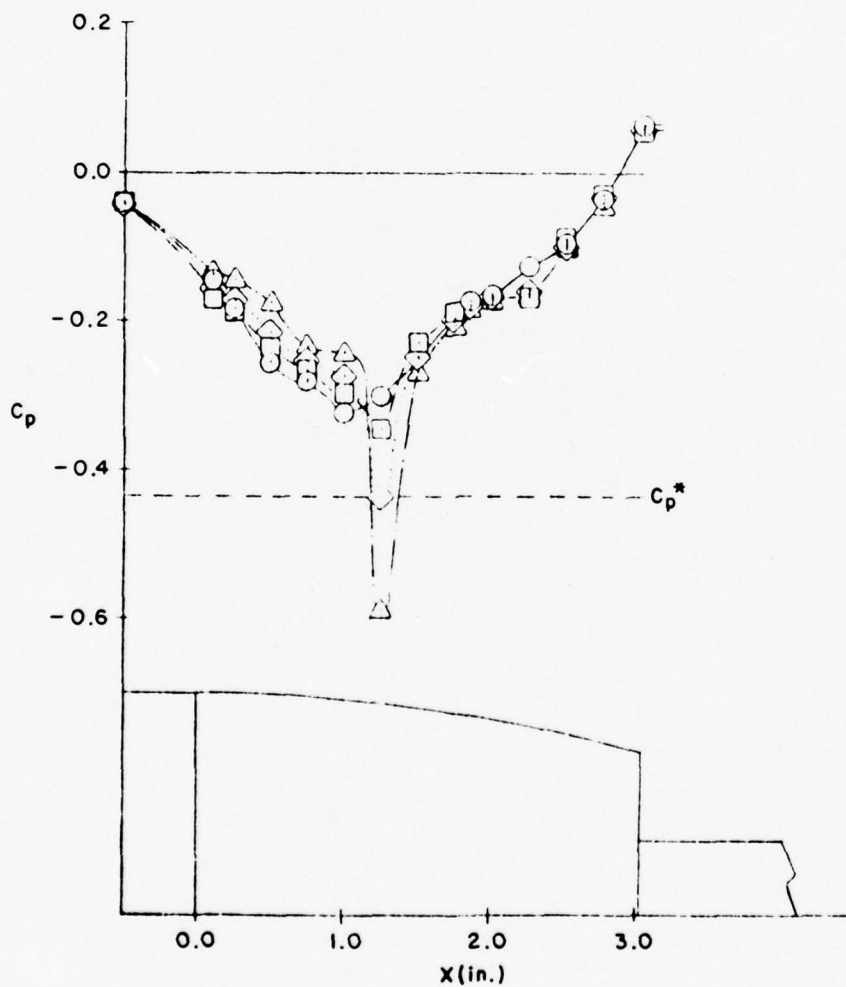


Figure 11. Mass Injection Effect on Boattail and Base Pressure Coefficients for NPR=2.0, $D_S=1"$

SYMBOL	NPR	M_∞	p_o (psfa)	Re_L	\dot{m} (lbm/sec)	$C_{D_A,s}$	$C_{D_A,j}$	$\frac{D_j^2}{D_b D_M}$
—○—	2.0	0.85	2000	8.4×10^6	0.000	.05965	.06410	0.242
—□—	2.0	0.85	2000	8.4×10^6	0.034	.06417	.06813	0.242
...◇...	2.0	0.85	2000	8.4×10^6	0.068	.06430	.06849	0.242
—△—	2.0	0.85	2000	8.4×10^6	0.115	.06986	.07419	0.242

CIRCULAR ARC BOATTAIL

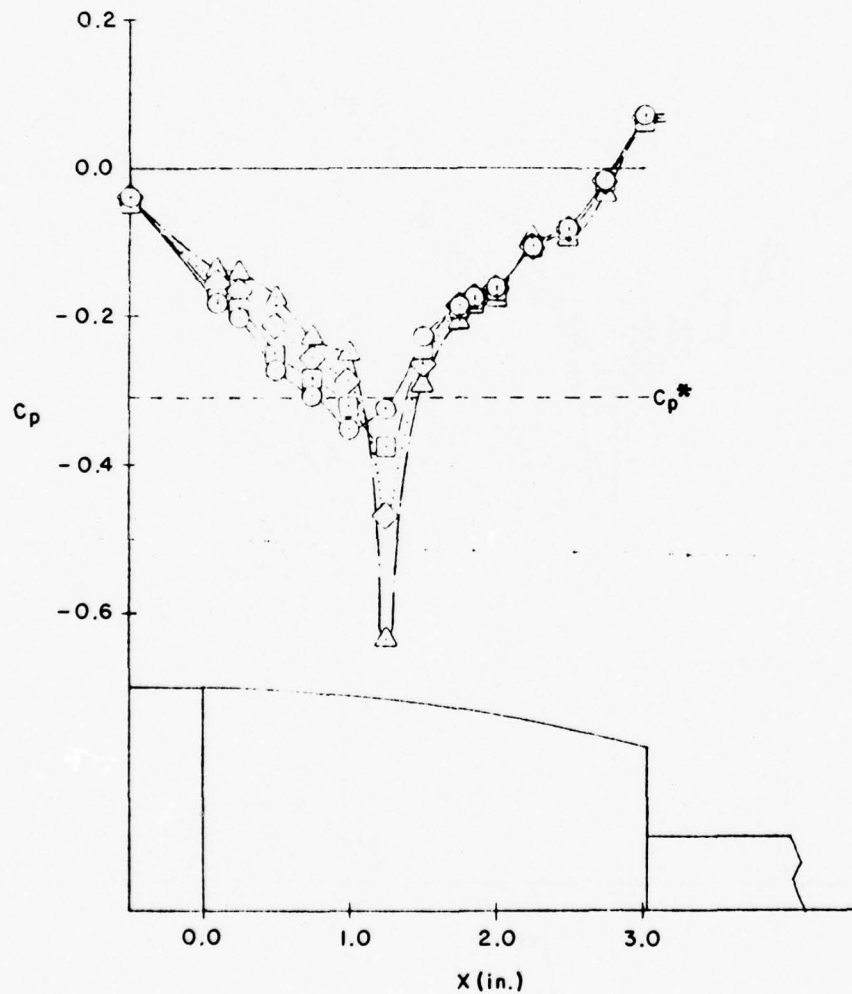


Figure 12. Mass Injection Effect on Boattail and Base Pressure Coefficients for NPR=2.0, $D_S=1"$

SYMBOL	NPR	M_∞	p_o (psfa)	Re_L	\dot{m} (lbm/sec)	$C_{DA,s}$	$C_{DA,j}$	$\frac{D_j^2}{D_b D_M}$
—○—	2.0	.80	3000	12.4×10^6	0.000	.05904	.06355	0.242
-□-	2.0	.80	3000	12.4×10^6	0.033	.06094	.06522	0.242
...◇...	2.0	.80	3000	12.4×10^6	0.066	.05941	.06378	0.242
-△-	2.0	.80	3000	12.4×10^6	0.115	.06414	.06850	0.242

CIRCULAR ARC BOATTAIL

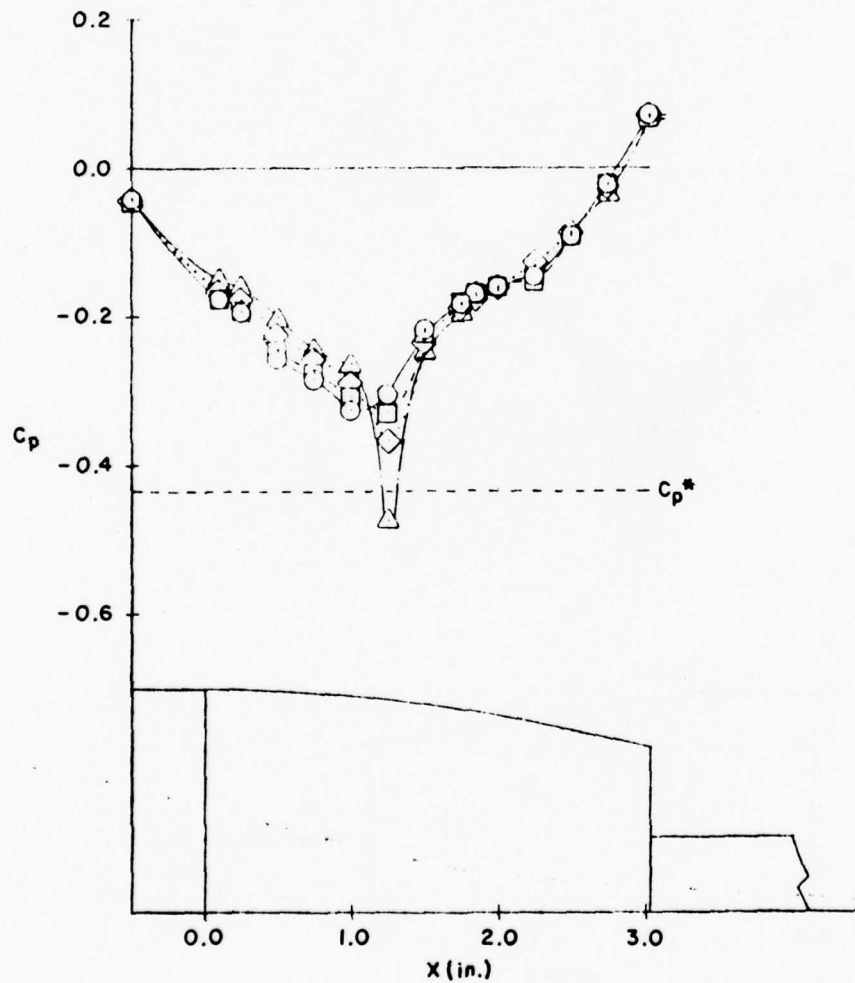


Figure 13. Mass Injection Effect on Boattail and Base Pressure Coefficients for NPR=2.0, $D_S=1"$

SYMBOL	NPR	M_∞	p_o (psfa)	Re_L	\dot{m} (lbm/sec)	$C_{D_A,s}$	$C_{D_A,j}$	$\frac{D_j^2}{D_b D_M}$
○	2.0	.85	3000	12.7×10^6	0.000	.06424	.06849	0.242
□	2.0	.85	3000	12.7×10^6	0.034	.06325	.06745	0.242
◇	2.0	.85	3000	12.7×10^6	0.068	.06506	.06927	0.242
△	2.0	.85	3000	12.7×10^6	0.115	.07037	.07452	0.242

CIRCULAR ARC BOATTAIL

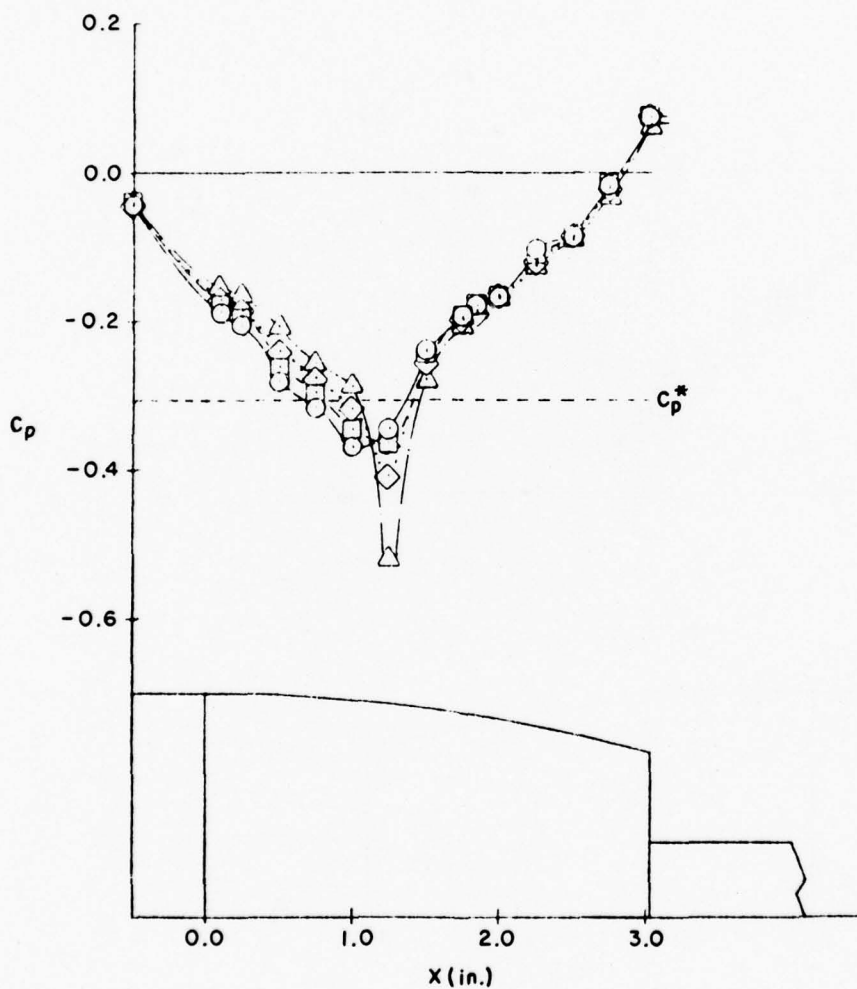


Figure 14. Mass Injection Effect on Boattail and Base Pressure Coefficients for NPR=2.0, $D_S=1"$

SYMBOL	NPR	M_∞	p_0 (psfa)	Re_L	\dot{m} (lbm/sec)	$C_{D_A,s}$	$C_{D_A,j}$	$\frac{D_j^2}{D_b D_M}$
—○—	2.0	.90	3000	13.1×10^6	0.000	.07320	.07744	0.242
—□—	2.0	.90	3000	13.1×10^6	0.033	.07428	.07820	0.242
...◇...	2.0	.90	3000	13.1×10^6	0.067	.07323	.07740	0.242
---△---	2.0	.90	3000	13.1×10^6	0.114	.07504	.07965	0.242

CIRCULAR ARC BOATTAIL

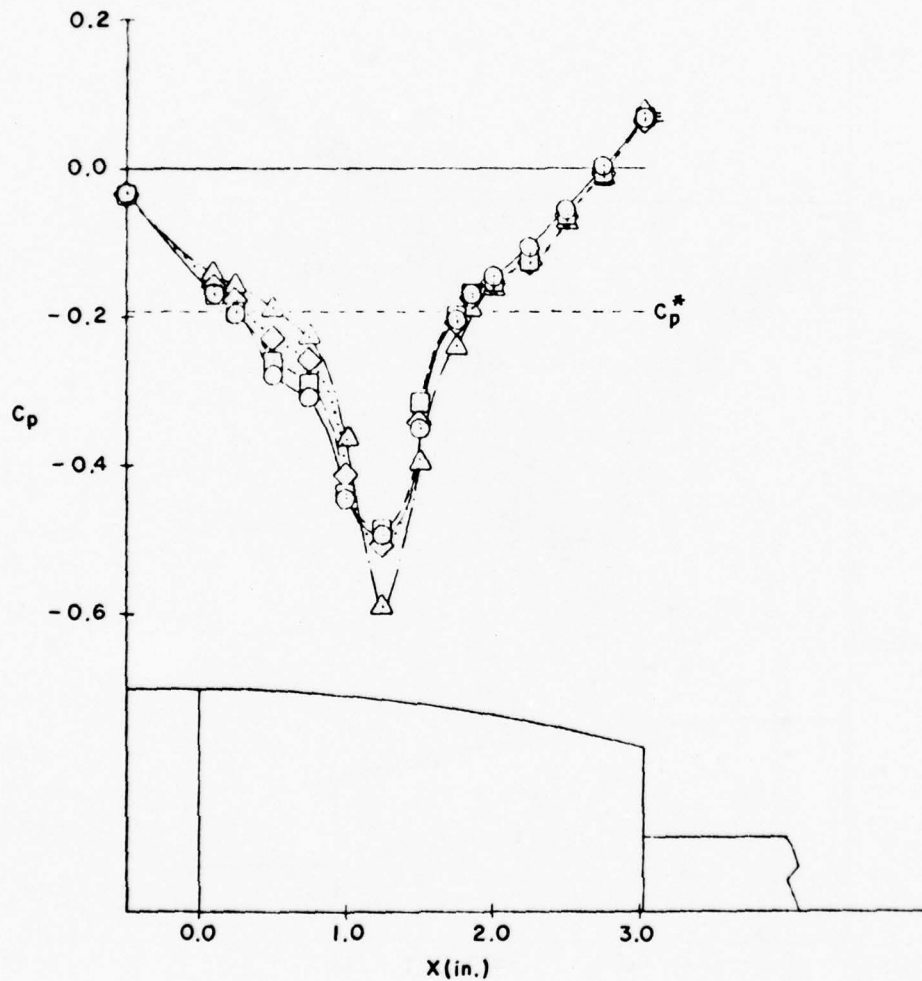


Figure 15. Mass Injection Effect on Boattail and Base Pressure Coefficients for NPR=2.0, $D_S=1"$

SYMBOL	NPR	M_∞	p_0 (psfa)	Re_L	\dot{m} (lbm/sec)	$C_{DA,s}$	$C_{DA,j}$	$\frac{D_j^2}{D_b D_M}$
—○—	2.0	.95	3000	13.4×10^6	0.000	.10239	.10539	0.242
—□—	2.0	.95	3000	13.4×10^6	0.034	.10178	.10478	0.242
...◇...	2.0	.95	3000	13.4×10^6	0.067	.09729	.10120	0.242
---△---	2.0	.95	3000	13.4×10^6	0.116	.10515	.10952	0.242

CIRCULAR ARC BOATTAIL

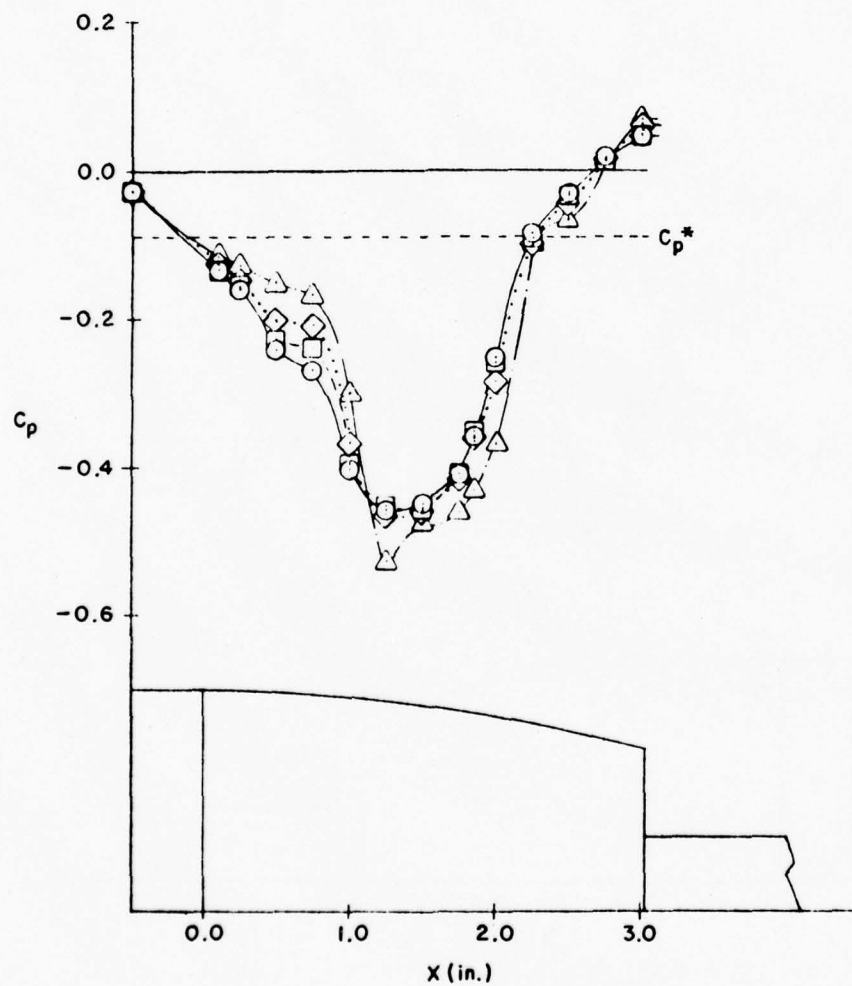


Figure 16. Mass Injection Effect on Boattail and Base Pressure Coefficients for NPR=2.0, $D_S=1"$

SYMBOL	NPR	M_∞	p_o (psfa)	Re_L	\dot{m} (lbm/sec)	$C_{DA,s}$	$C_{DA,j}$	$\frac{D_j^2}{D_b D_M}$
\square	2.0	.80	2000	8.3×10^6	0.000	.06333	.06766	0.242
\circ	2.0	.80	3000	12.4×10^6	0.000	.05904	.06355	0.242

CIRCULAR ARC BOATTAIL

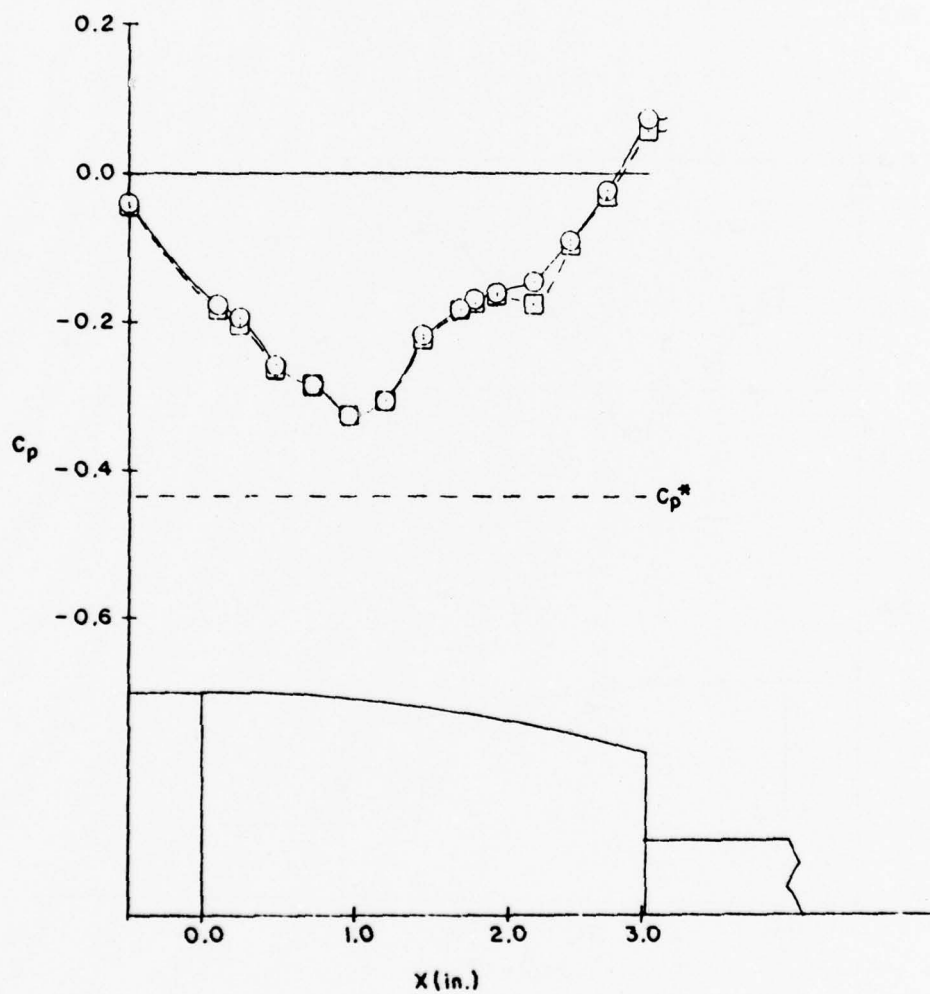


Figure 17. Reynolds Number Effect on Boattail and Base Pressure Coefficients

SYMBOL	NPR	M_∞	p_o (psfa)	Re_L	\dot{m} (lbm/sec)	$C_{D,A,s}$	$C_{D,A,j}$	$\frac{D_j^2}{D_b D_M}$
—○—	2.0	.85	2000	8.3×10^6	0.000	.05965	.06410	0.242
--□--	2.0	.85	3000	12.4×10^6	0.000	.06424	.06849	0.242

CIRCULAR ARC BOATTAIL

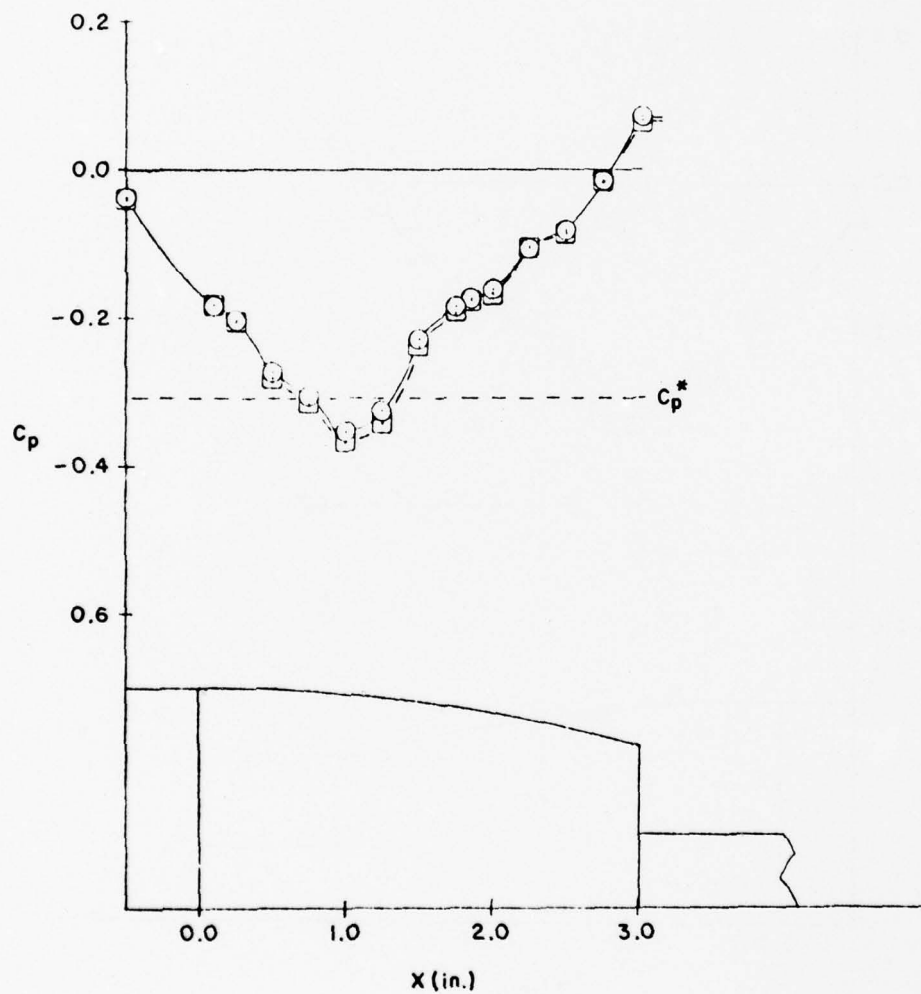


Figure 18. Reynolds Number Effect on Boattail and Base Pressure Coefficients

SYMBOL	NPR	M_∞	p_o (psfa)	Re_L	\dot{m} (lbm/sec)	$C_{DA,s}$	$C_{DA,j}$	$\frac{D_j^2}{D_b^2 M}$
—○—	2.0	.90	2000	8.7×10^6	0.000	.07016	.07408	0.242
—□—	2.0	.90	3000	13.1×10^6	0.000	.07320	.07744	0.242

CIRCULAR ARC BOATTAIL

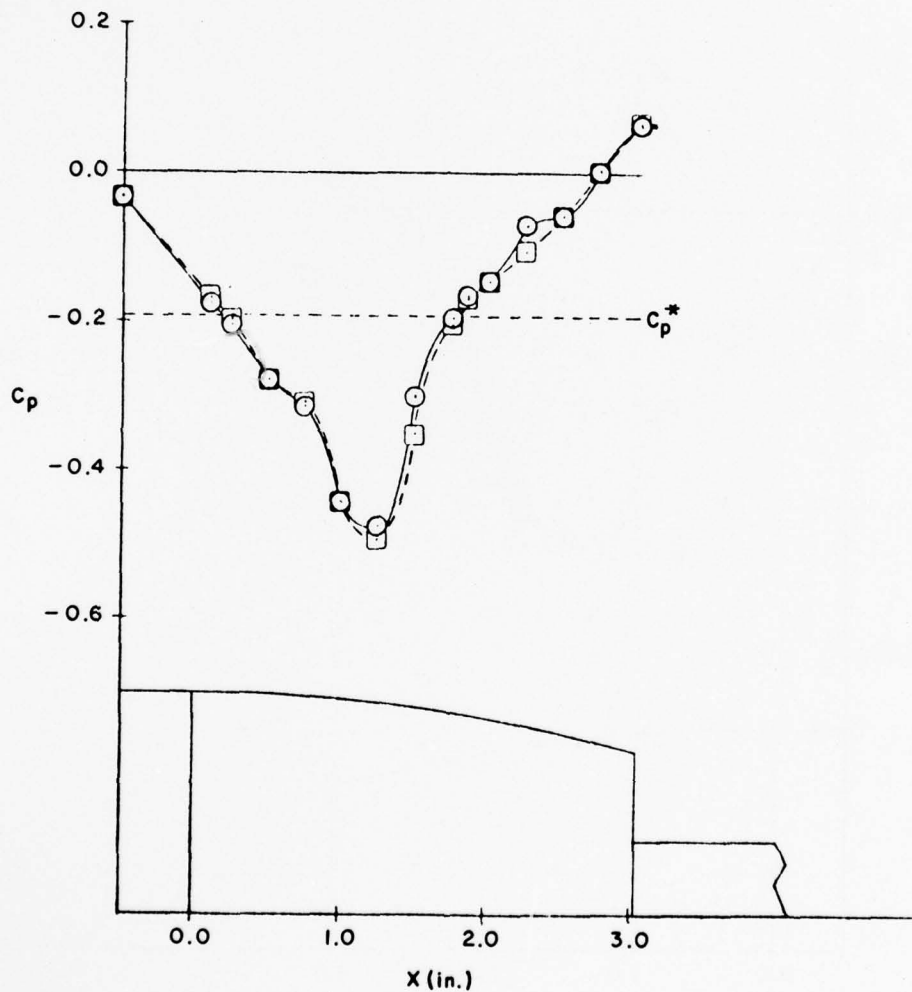


Figure 19. Reynolds Number Effect on Boattail and Base Pressure Coefficients

SYMBOL	NPR	M_∞	p_o (psfa)	Re_L	\dot{m} (lbm/sec)	$C_{DA,s}$	$C_{DA,j}$	$\frac{D_j^2}{D_b D_M}$
—○—	2.0	.95	2000	8.8×10^6	0.000	.10119	.10391	0.242
--□--	2.0	.95	3000	13.2×10^6	0.000	.10239	.10539	0.242

CIRCULAR ARC BOATTAIL

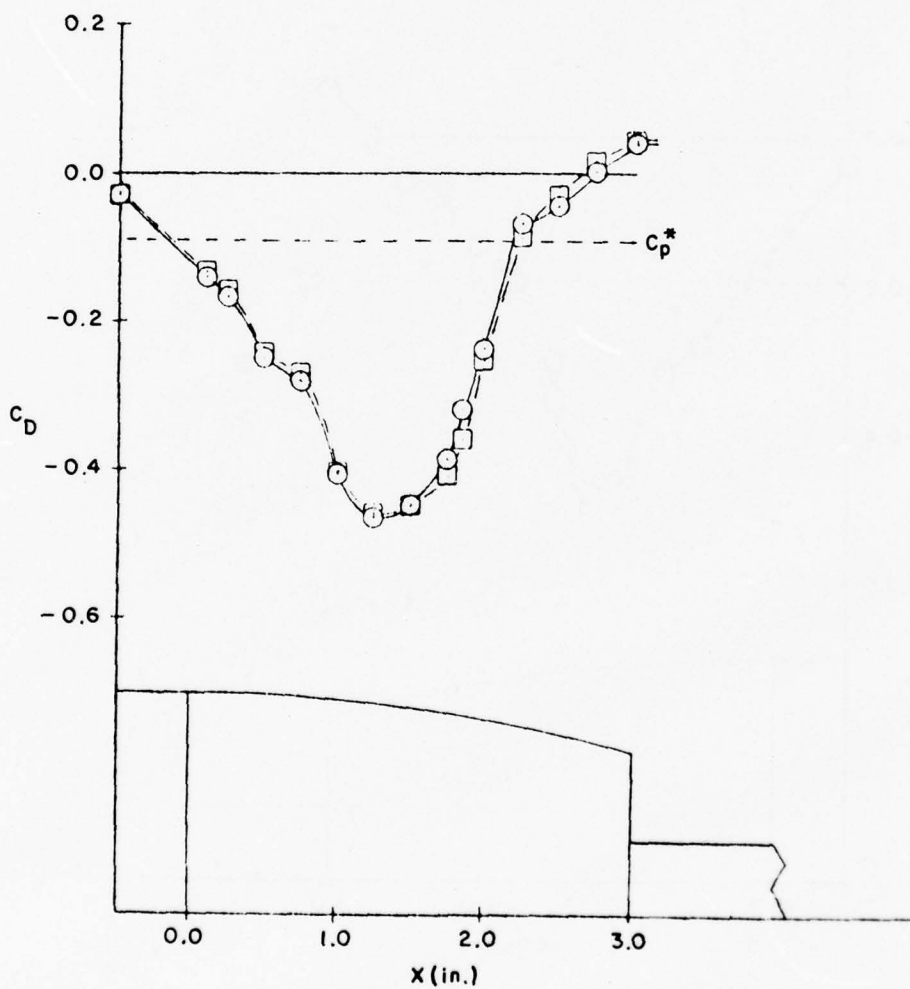


Figure 20. Reynolds Number Effect on Boattail and Base Pressure Coefficients

SYMBOL	NPR	M_∞	p_o (psfa)	Re_L	\dot{m} (lbm/sec)	$C_{DA,s}$	$C_{DA,j}$	$\frac{D_j^2}{D_b D_M}$
—○—	2.0	.80	2000	8.3×10^6	0.000	.06333	.06741	0.242
—□—	2.0	.85	2000	8.4×10^6	0.000	.05965	.06410	0.242
...◇...	2.0	.90	2000	8.7×10^6	0.000	.07016	.07408	0.242
---△---	2.0	.95	2000	8.9×10^6	0.000	.10119	.10391	0.242

CIRCULAR ARC BOATTAIL

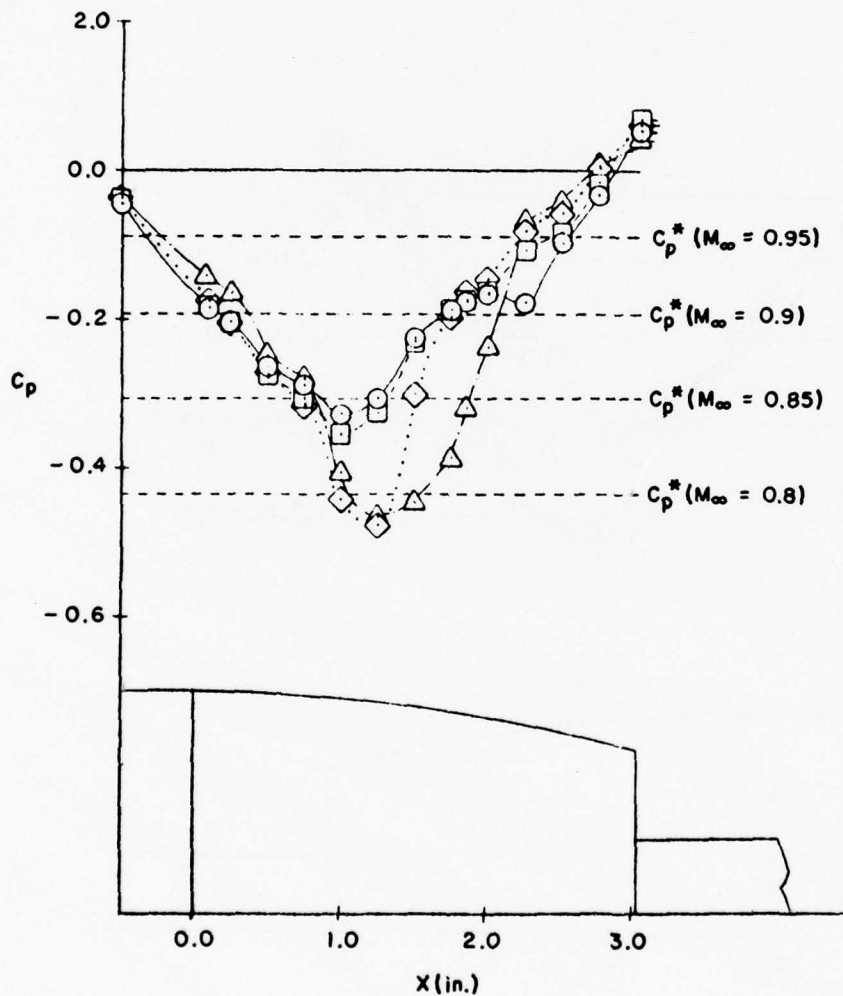


Figure 21. Mach Number Effect on Boattail and Base Pressure Coefficients

SYMBOL	NPR	M_∞	p_0 (psfa)	Re_L	\dot{m} (lbm/sec)	$C_{DA,s}$	$C_{DA,j}$	$\frac{D_j^2}{D_b D_M}$
—○—	2.0	.80	3000	12.4×10^6	0.000	.05904	.06355	0.242
—□—	2.0	.85	3000	12.7×10^6	0.000	.06424	.06849	0.242
...◇...	2.0	.90	3000	13.1×10^6	0.000	.07320	.07744	0.242
---△---	2.0	.95	3000	13.4×10^6	0.000	.10239	.10539	0.242

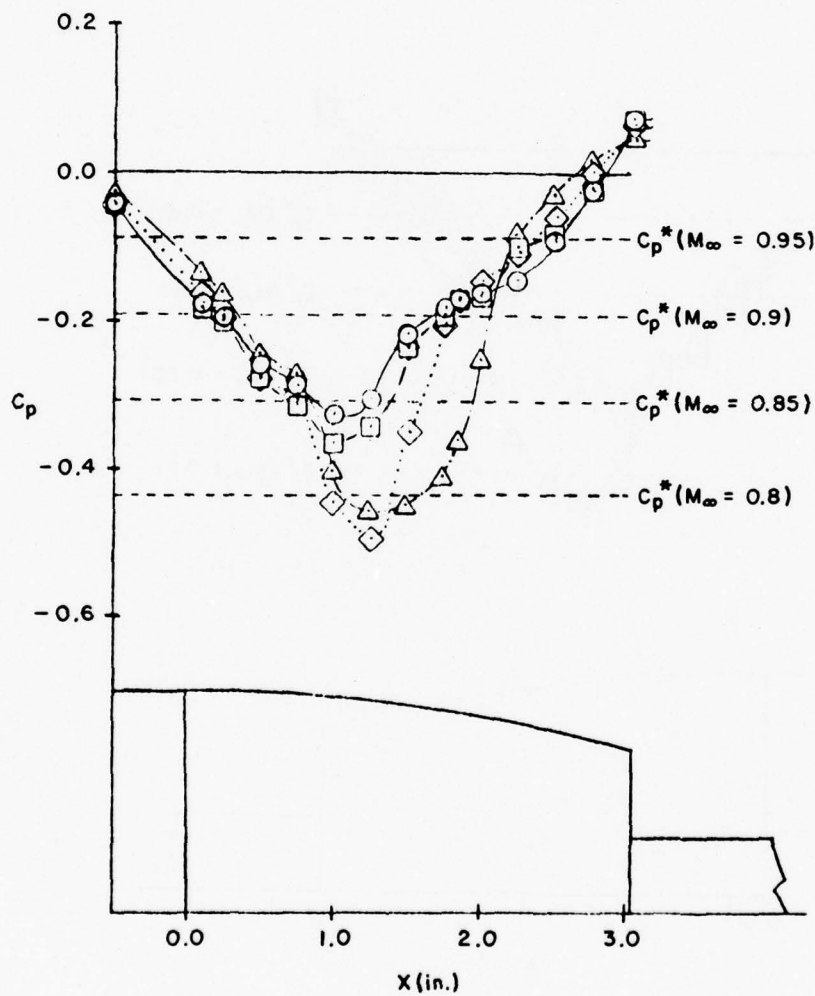


Figure 22. Mach Number Effect on Boattail and Base Pressure Coefficients

SYMBOL	NPR	M_∞	p_0 (psfa)	Re_L	\dot{m} (lbm/sec)	l	$C_{D_{A,j}}$	$\frac{D_j^2}{D_b D_M}$
—○—	3.61	0.95	3000	13.4×10^6	0.000	6.0	.0816	0.242
—◇—	3.61	0.95	3000	13.4×10^6	0.066	6.0	.0731	0.242
—△—	3.61	0.95	3000	13.4×10^6	0.114	6.0	.0803	0.242

CIRCULAR ARC BOATTAIL

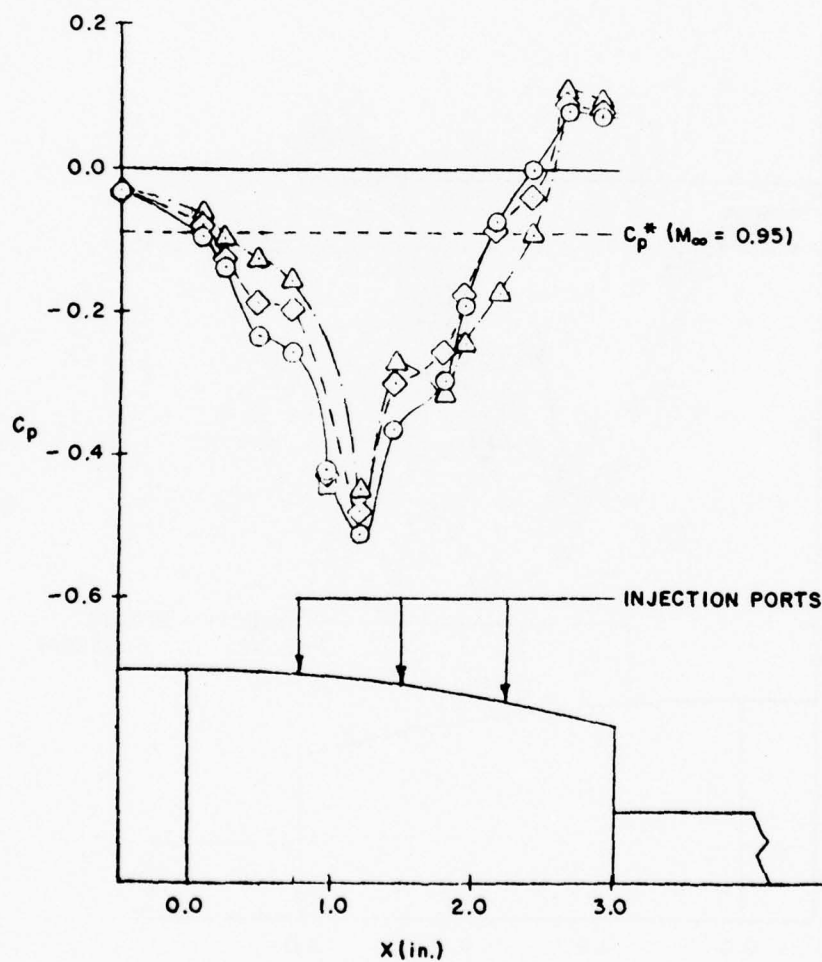


Figure 23. Mass Injection Effect on Boattail and Base Pressure Coefficients for a Different Injection Location and Area

SYMBOL	NPR	M_∞	p_o (psfa)	Re_L	\dot{m} (lbm/sec)	ℓ	$C_{DA,j}$	$\frac{D_j^2}{D_b D_M}$
—○—	3.61	0.95	3000	13.4×10^6	0.000	6.0	.0816	0.242
—◇—	3.61	0.95	3000	13.4×10^6	0.066	6.0	.0648	0.242
—△—	3.61	0.95	3000	13.4×10^6	0.114	6.0	.0837	0.242

CIRCULAR ARC BOATTAIL

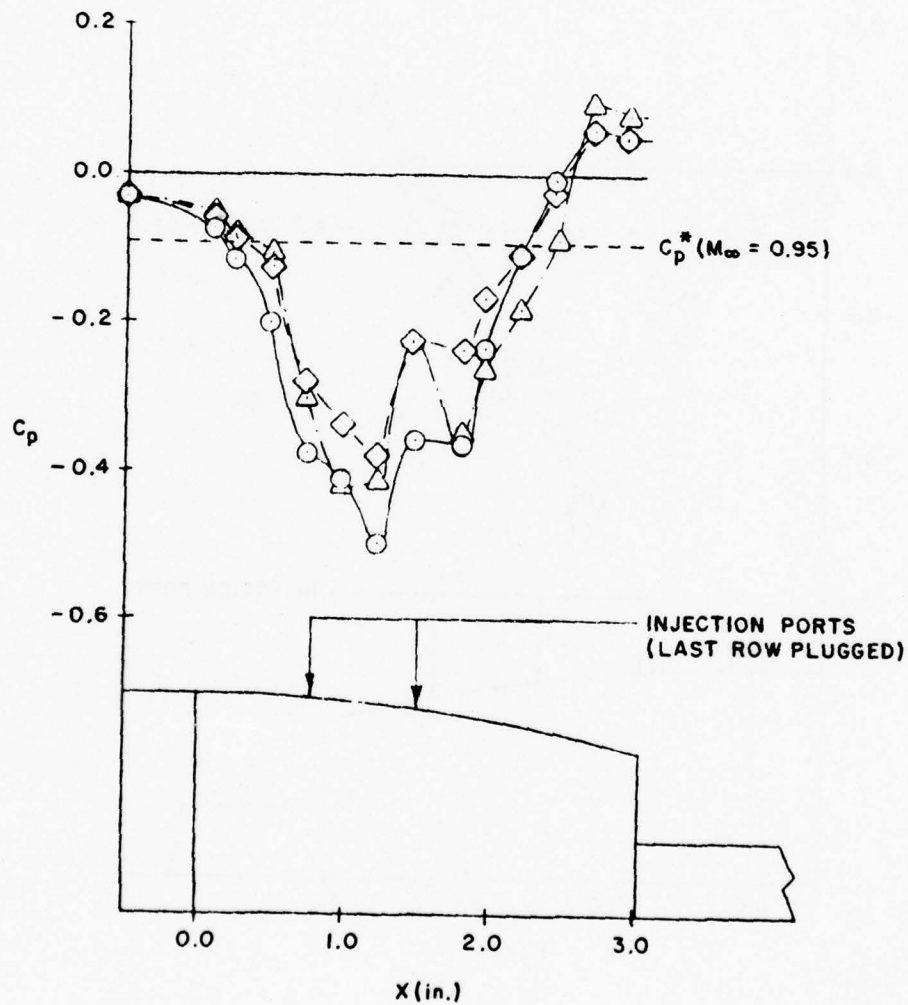


Figure 24. Mass Injection Effect on Boattail and Base Pressure Coefficients for a Different Injection Location and Area

SYMBOL	NPR	M_∞	p_o (psfa)	Re_L	\dot{m} (lbm/sec)	l (in.)	$C_{D_A,s}$	$C_{D_A,j}$	$\frac{D_j^2}{D_b D_M}$
—○—	2.0	.90	2000	8.7×10^6	0.000	REMOVED	.07016	.07408	0.242
—□—	3.62	.90	2000	8.7×10^6	0.000	6	.05083	.05611	0.242
---◇---	4.28	.90	2000	8.7×10^6	0.000	4	.00934	.01738	0.242
---△---	5.45	.90	2000	8.7×10^6	0.000	2	-.04469	-.03382	0.242

CIRCULAR ARC BOATTAIL

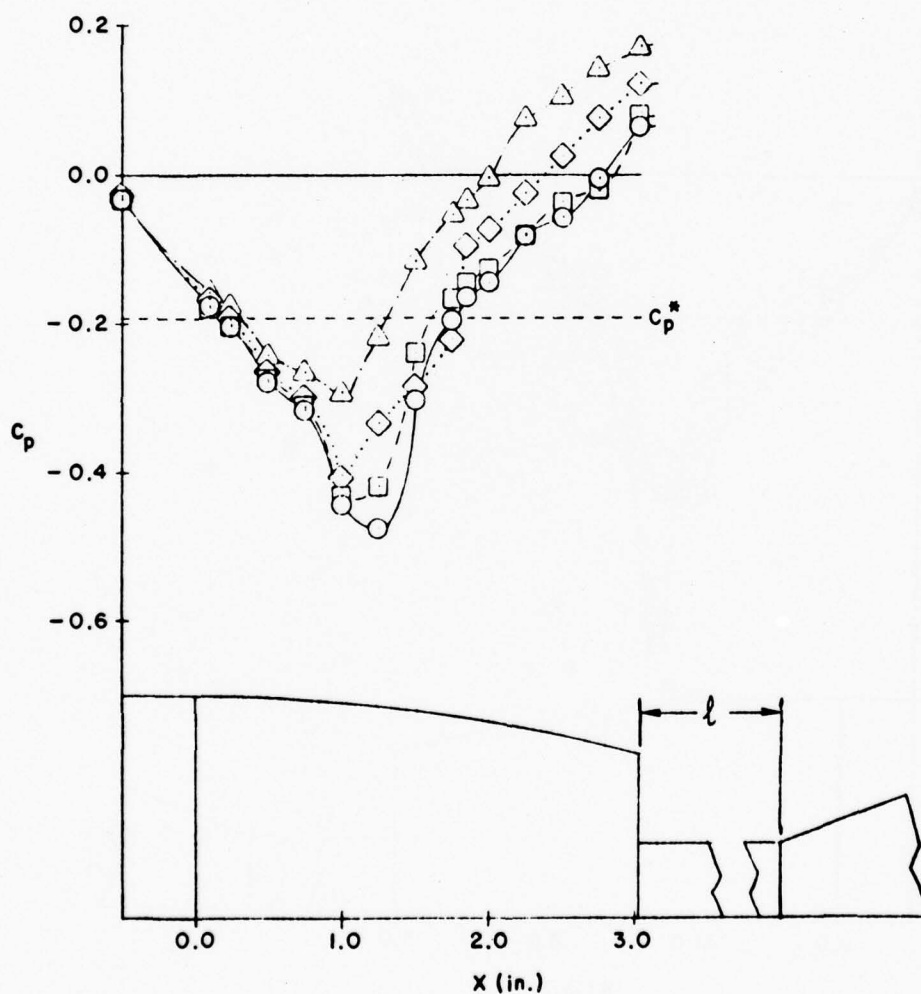


Figure 25. Nozzle Pressure Ratio Effect on Boattail and Base Pressure Coefficients

SYMBOL	NPR	M_∞	p_o (psfa)	Re_L	\dot{m} (lbm/sec)	ℓ (in.)	$C_{D_A,s}$	$C_{D_A,j}$	$\frac{D_j^2}{D_b D_M}$
—○—	3.62	.90	2000	8.7×10^6	0.000	6	.05083	.05611	0.242
—□—	3.62	.90	2000	8.7×10^6	0.033	6	.04560	.05096	0.242
...◇...	3.62	.90	2000	8.7×10^6	0.066	6	.05106	.05650	0.242
---△---	3.62	.90	2000	8.7×10^6	0.113	6	.05780	.06360	0.242

CIRCULAR ARC BOATTAIL

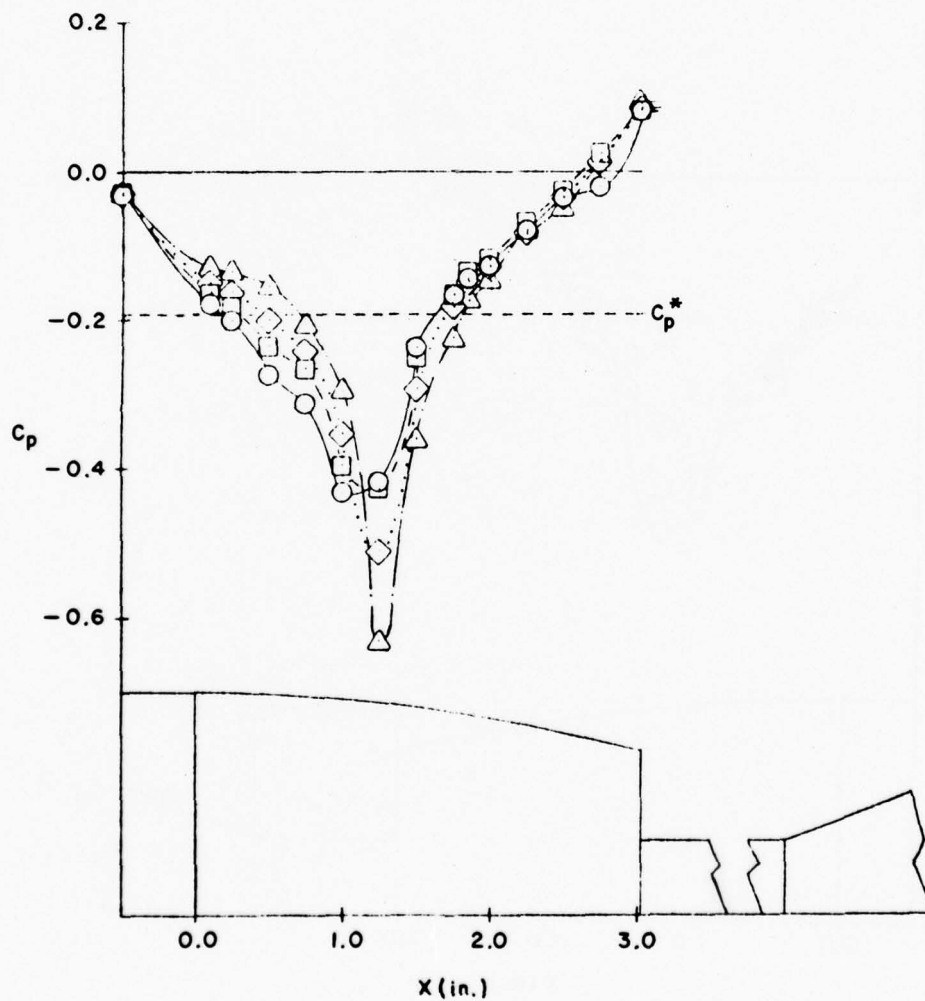


Figure 26. Mass Injection Effect on Boattail and Base Pressure Coefficients for NPR>2

SYMBOL	NPR	M_∞	p_o (psfa)	Re_L	\dot{m} (lbm/sec)	l (in.)	$C_{D_{A,s}}$	$C_{D_{A,j}}$	$\frac{D_j^2}{D_b D_M}$
—○—	3.62	.90	3000	13.1×10^6	0.000	6	.05378	.05939	0.242
—□—	3.62	.90	3000	13.1×10^6	0.033	6	.05264	.05811	0.242
...◇...	3.62	.90	3000	13.1×10^6	0.067	6	.05211	.05765	0.242
—△—	3.62	.90	3000	13.1×10^6	0.116	6	.05472	.06064	0.242

CIRCULAR ARC BOATTAIL

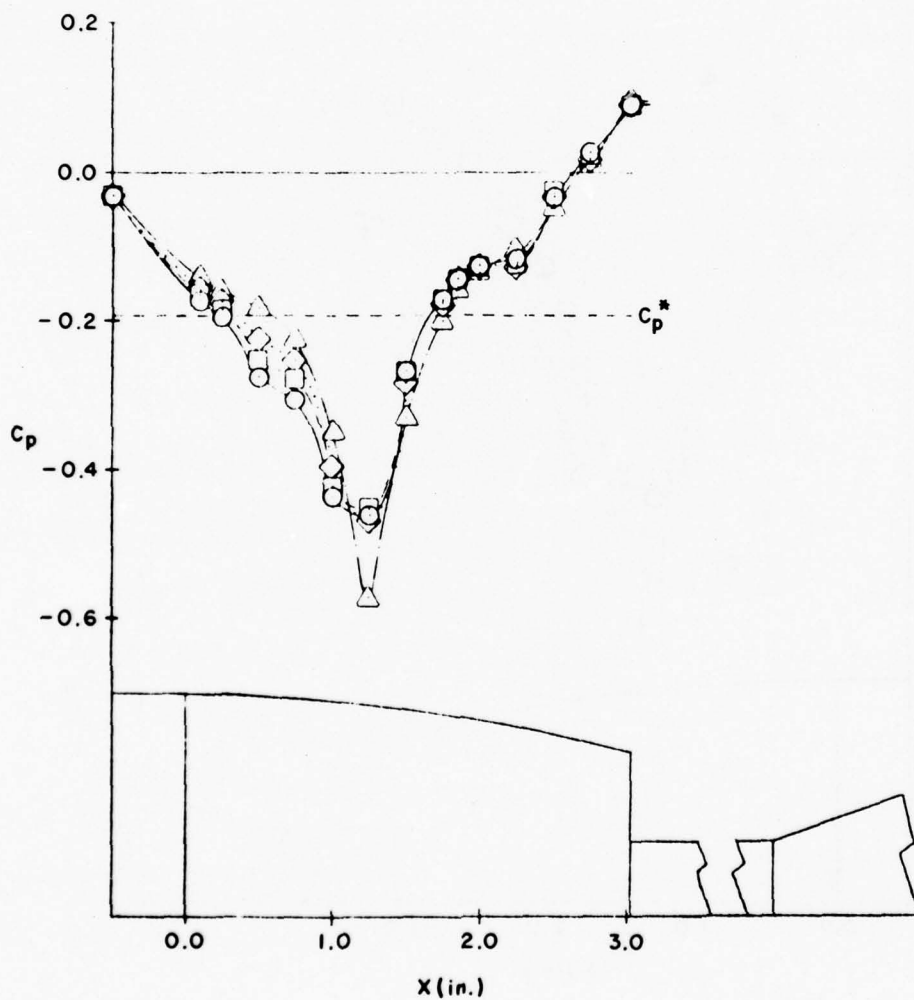


Figure 27. Mass Injection Effect on Boattail and Base Pressure Coefficients for $NPR > 2$

SYMBOL	NPR	M_∞	p_0 (psfa)	Re_L	\dot{m} (lbm/sec)	ℓ (in.)	$C_{DA,s}$	$C_{DA,j}$	$\frac{D_j^2}{D_b D_M}$
○—	3.61	.95	2000	8.7×10^6	0.000	6	.06823	.07294	0.242
□—	3.61	.95	2000	8.7×10^6	0.034	6	.06291	.06770	0.242
◇—	3.61	.95	2000	8.7×10^6	0.067	6	.06966	.07546	0.242
△—	3.61	.95	2000	8.7×10^6	0.116	6	.07619	.08267	0.242

CIRCULAR ARC BOATTAIL

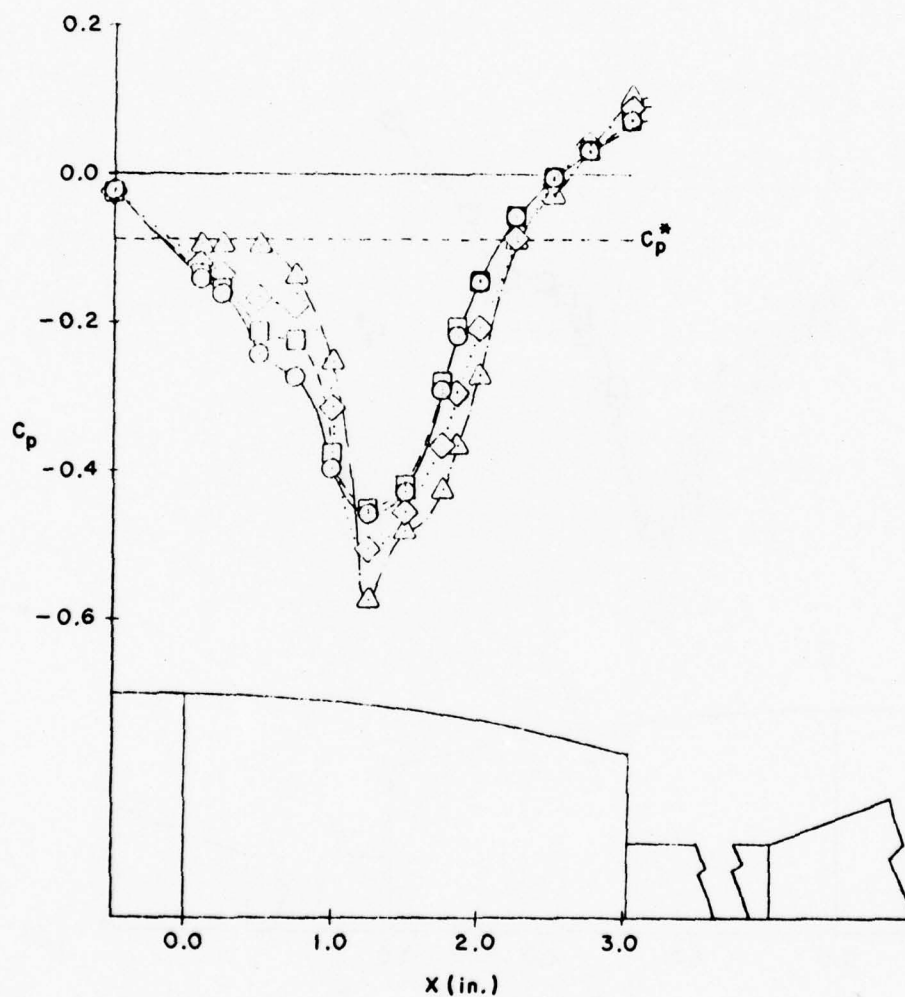


Figure 28. Mass Injection Effect on Boattail and Base Pressure Coefficients for $NPR > 2$

SYMBOL	NPR	M_∞	p_o (psfa)	Re_L	\dot{m} (lbm/sec)	l (in.)	$C_{DA,s}$	$C_{DA,j}$	$\frac{D_j^2}{D_b D_M}$
—○—	3.61	.95	3000	13.4×10^6	0.000	6	.07632	.08060	0.242
—□—	3.61	.95	3000	13.4×10^6	0.033	6	.07153	.07626	0.242
...◇...	3.61	.95	3000	13.4×10^6	0.067	6	.06789	.07344	0.242
—△—	3.61	.95	3000	13.4×10^6	0.114	6	.07886	.08505	0.242

CIRCULAR ARC BOATTAIL

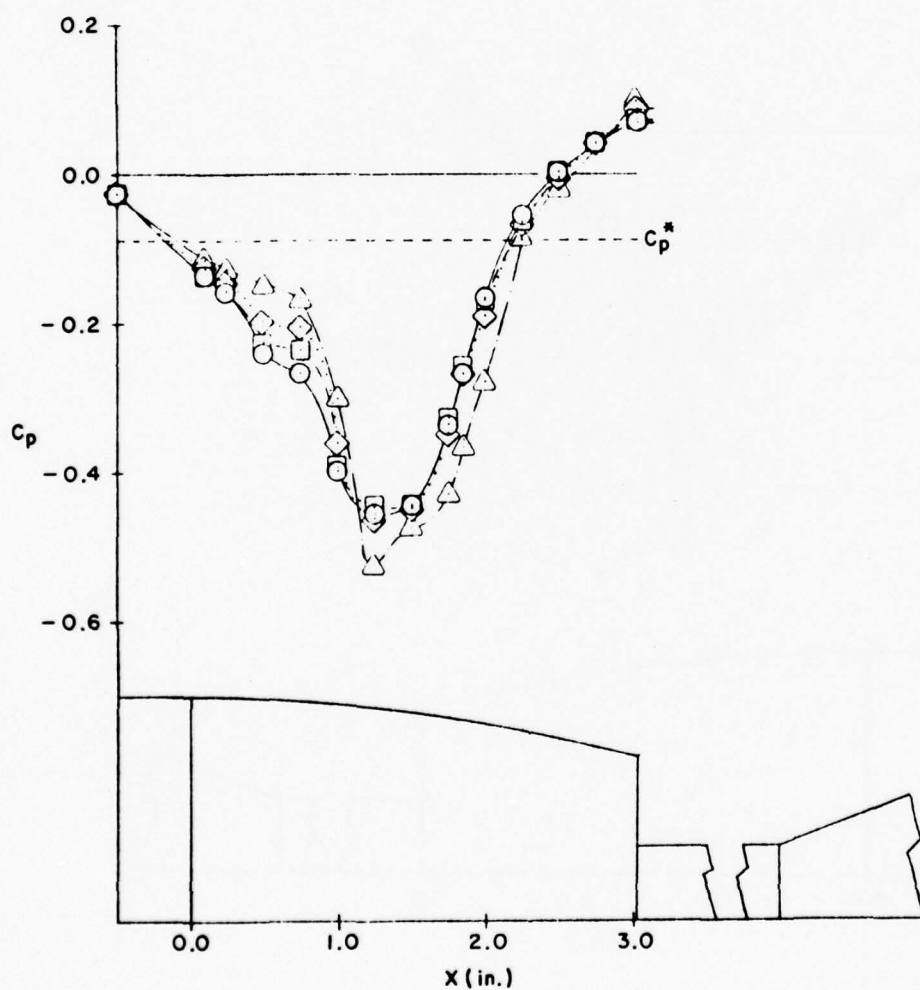


Figure 29. Mass Injection Effect on Boattail and Base Pressure Coefficients for $NPR > 2$

SYMBOL	NPR	M_∞	p_o (psfa)	Re_L	\dot{m} (lbm/sec)	x (in.)	$C_{D_A,s}$	$C_{D_A,j}$	$\frac{D_j^2}{D_b D_M}$
—○—	4.30	.85	2000	8.4×10^6	0.000	4	.00957	.01739	0.242
—□—	4.30	.85	2000	8.4×10^6	0.032	4	.00848	.01610	0.242
...◇...	4.30	.85	2000	8.4×10^6	0.066	4	.01396	.02149	0.242
—△—	4.30	.85	2000	8.4×10^6	0.114	4	.02204	.02972	0.242

CIRCULAR ARC BOATTAIL

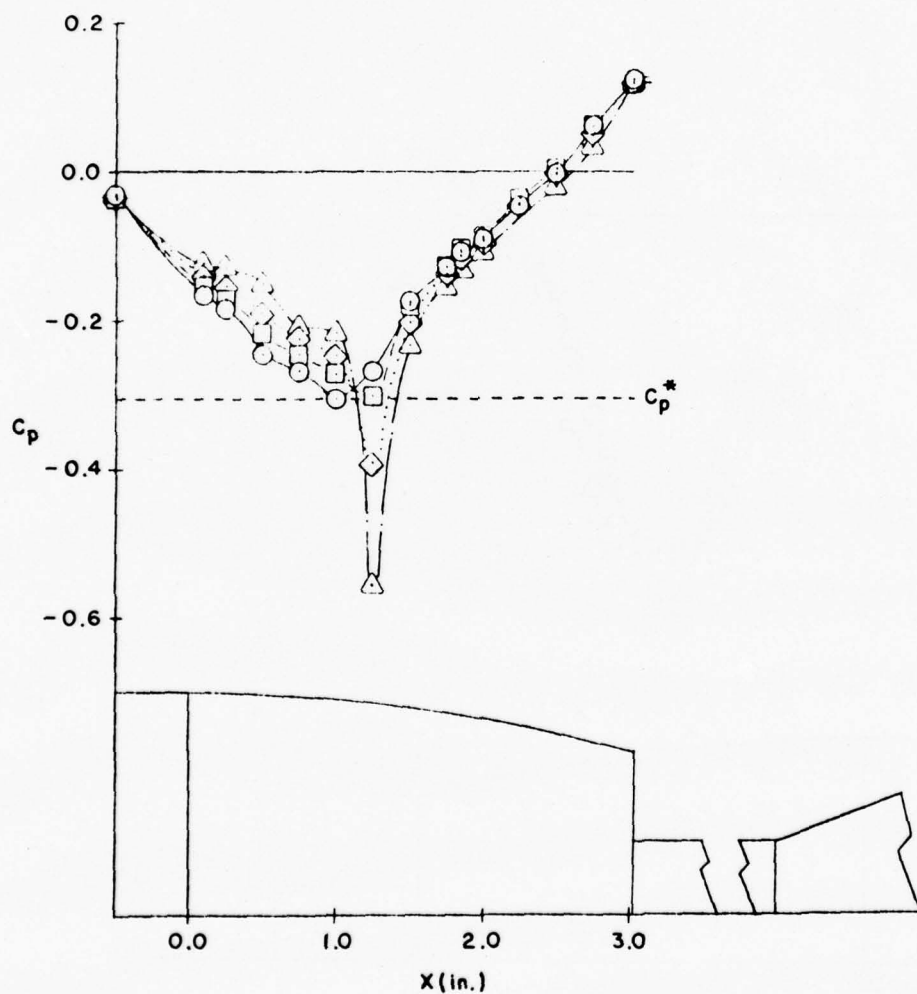


Figure 30. Mass Injection Effect on Boattail and Base Pressure Coefficients for NPR>2

SYMBOL	NPR	M_∞	p_o (psfa)	Re_L	\dot{m} (lbm/sec)	ℓ (in.)	$C_{D_A,s}$	$C_{D_A,j}$	$\frac{D_j^2}{D_b D_M}$
○—	4.28	.90	2000	8.7×10^6	0.002	4	.00934	.01738	0.242
□—	4.28	.90	2000	8.7×10^6	0.034	4	.00808	.01589	0.242
◇—	4.28	.90	2000	8.7×10^6	0.067	4	.01301	.02092	0.242
△—	4.28	.90	2000	8.7×10^6	0.114	4	.02471	.03275	0.242

CIRCULAR ARC BOATTAIL

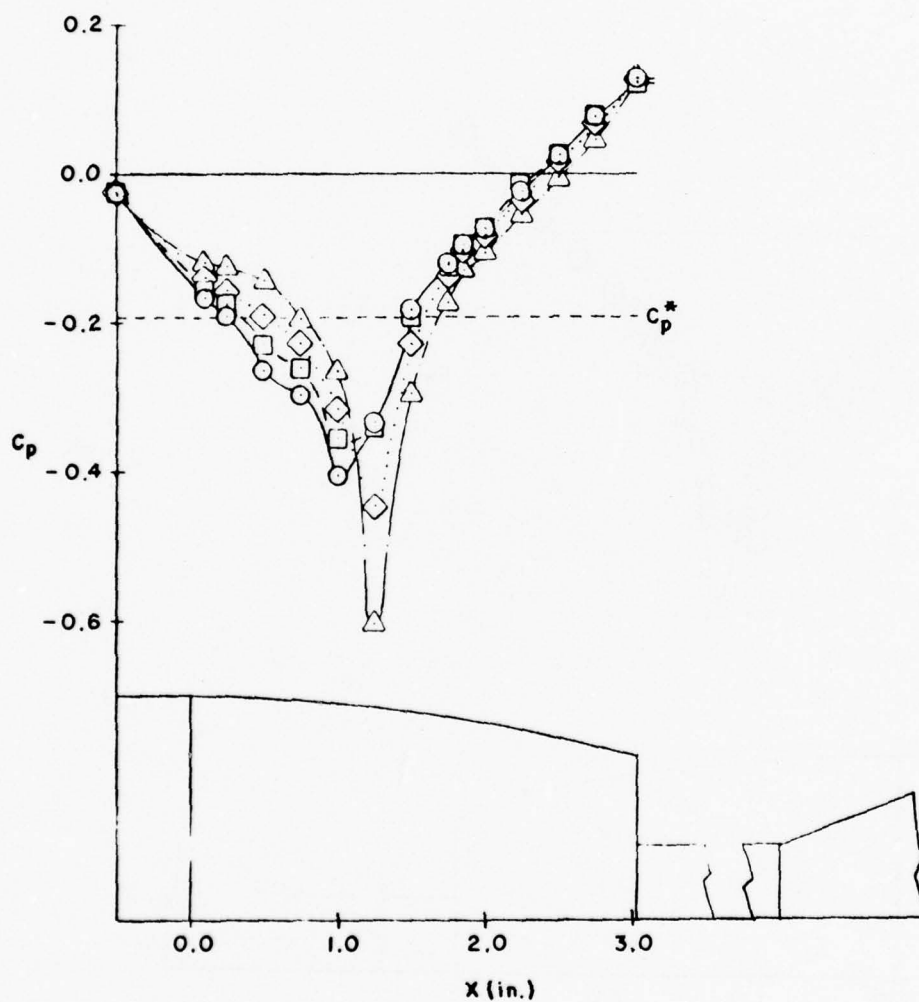
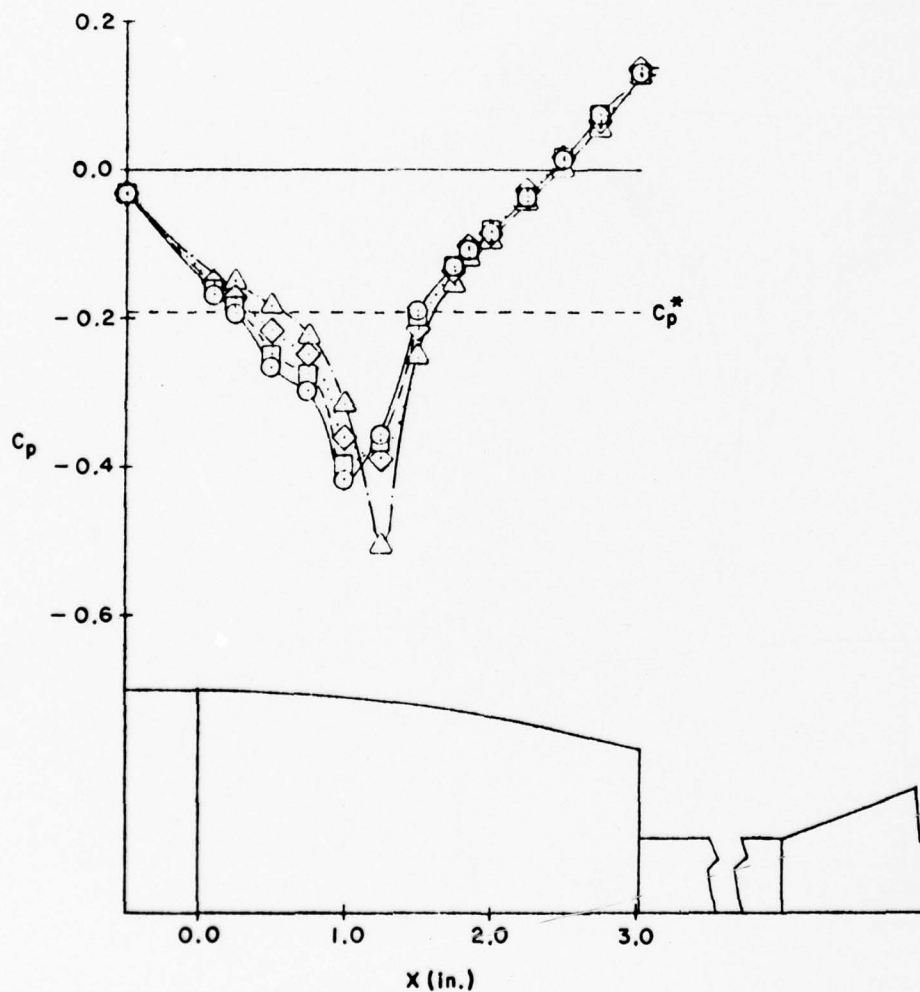


Figure 31. Mass Injection Effect on Boattail and Base Pressure Coefficients for $NPR > 2$

SYMBOL	NPR	M_∞	p_o (psfa)	Re_L	\dot{m} (lbm/sec)	ℓ (in.)	$C_{D_A,s}$	$C_{D_A,j}$	$\frac{D_j^2}{D_b D_M}$
—○—	4.28	.90	3000	13.1×10^6	0.000	4	.01358	.02175	0.242
—□—	4.28	.90	3000	13.1×10^6	0.034	4	.01290	.02093	0.242
...◇...	4.28	.90	3000	13.1×10^6	0.066	4	.01186	.01993	0.242
---△---	4.28	.90	3000	13.1×10^6	0.115	4	.01856	.02668	0.242

CIRCULAR ARC BOATTAIL

Figure 32. Mass Injection Effect on Boattail and Base Pressure Coefficients for $NPR > 2$

SYMBOL	NPR	M_∞	p_o (psfa)	Re_L	\dot{m} (lbm/sec)	l (in.)	$C_{DA,s}$	$C_{DA,j}$	$\frac{D_j^2}{D_b D_M}$
—○—	4.26	.95	3000	13.4×10^6	0.000	4	.02197	.02917	0.242
—□—	4.26	.95	3000	13.4×10^6	0.035	4	.01796	.02534	0.242
...◇...	4.26	.95	3000	13.4×10^6	0.067	4	.01806	.02600	0.242
---△---	4.26	.95	3000	13.4×10^6	0.114	4	.02986	.03869	0.242

CIRCULAR ARC BOATTAIL

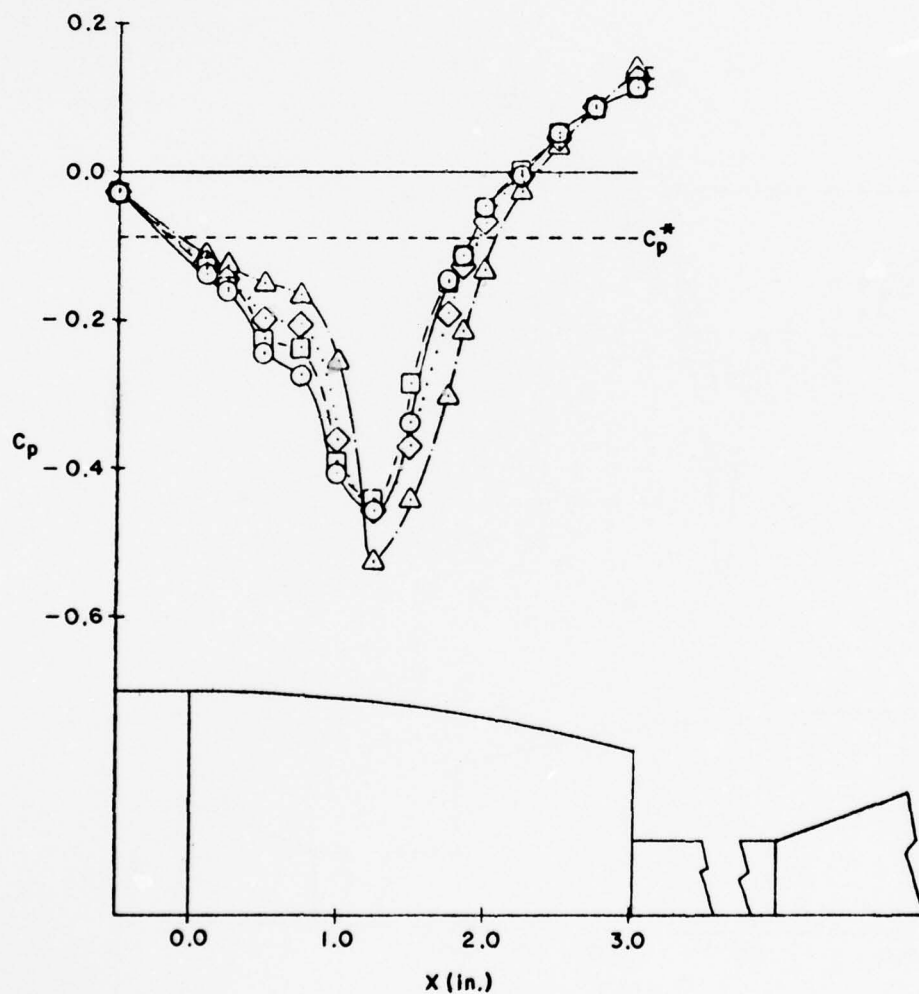


Figure 33. Mass Injection Effect on Boattail and Base Pressure Coefficients for $NPR > 2$

SYMBOL	NPR	M_∞	p_o (psfa)	Re_L	\dot{m} (lbm/sec)	ℓ (in.)	$C_{D_A,s}$	$C_{D_A,j}$	$\frac{D_j^2}{D_b D_M}$
—○—	5.45	.90	2000	8.7×10^6	0.000	2	-.04469	-.03382	0.242
—□—	5.45	.90	2000	8.7×10^6	0.034	2	-.03796	-.07290	0.242
...◇...	5.45	.90	2000	8.7×10^6	0.067	2	-.03505	-.02448	0.242
---△---	5.45	.90	2000	8.7×10^6	0.116	2	-.02211	-.01136	0.242

CIRCULAR ARC BOATTAIL

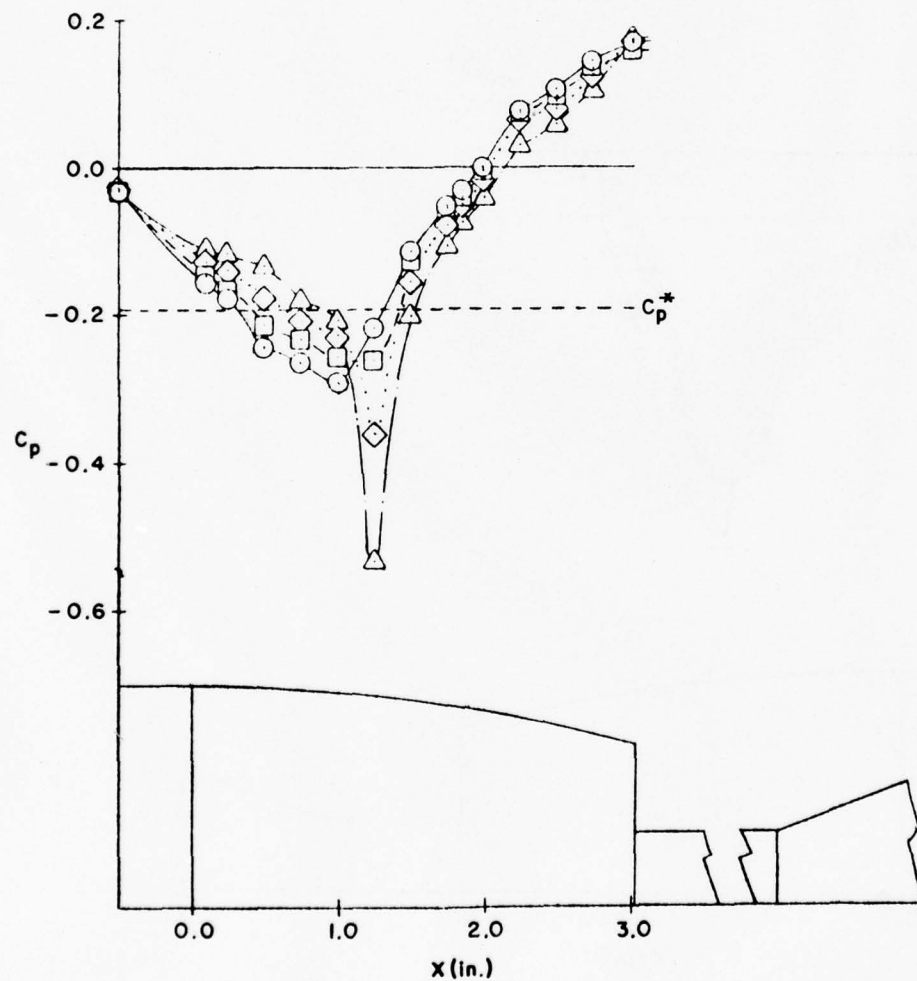


Figure 34. Mass Injection Effect on Boattail and Base Pressure Coefficients for $NPR > 2$

SYMBOL	NPR	M_α	p_o (psfa)	Re_L	\dot{m} (lbm/sec)	x (in.)	$C_{D_{A,s}}$	$C_{D_{A,j}}$	$\frac{D_j^2}{D_b D_M}$
—○—	5.45	.90	3000	13.1×10^6	0.000	2	-.04357	-.03227	0.242
—□—	5.45	.90	3000	13.1×10^6	0.034	2	-.04268	-.03177	0.242
...◇...	5.45	.90	3000	13.1×10^6	0.066	2	-.03597	-.02539	0.242
—△—	5.45	.90	3000	13.1×10^6	0.114	2	-.03261	-.02151	0.242

CIRCULAR ARC BOATTAIL

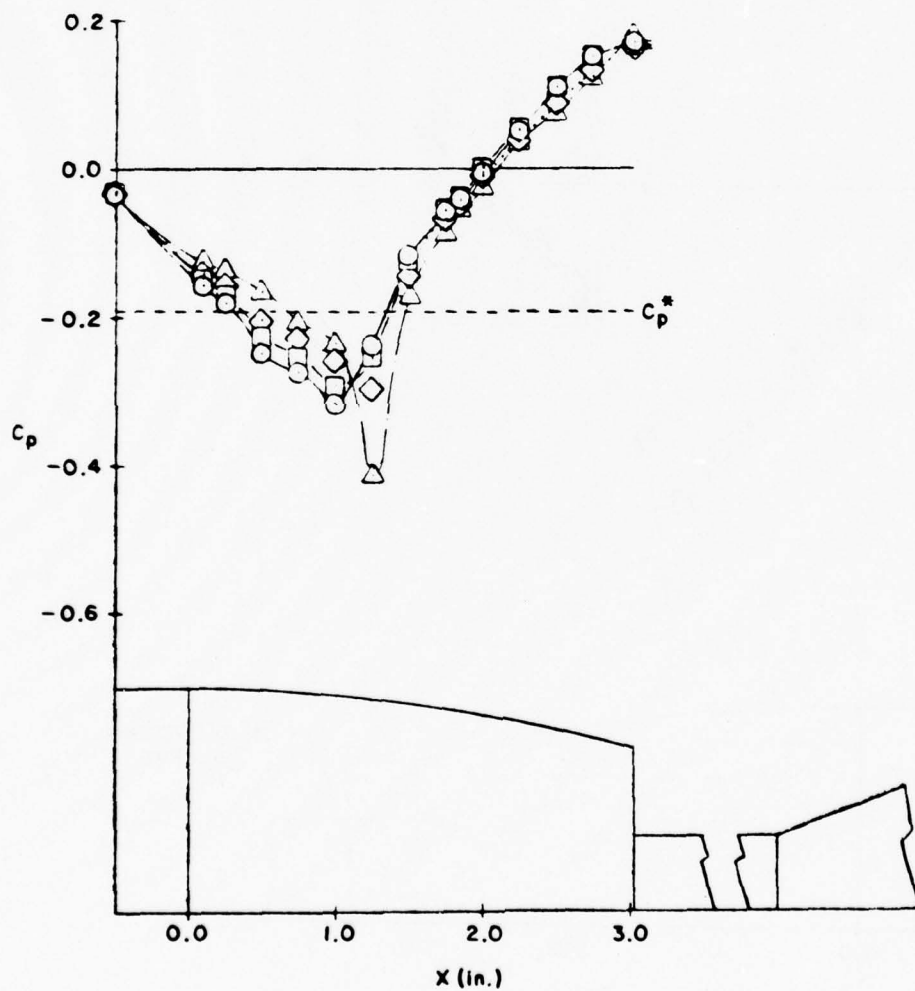


Figure 35. Mass Injection Effect on Boattail and Base Pressure Coefficients for NPR>2

SYMBOL	NPR	M_∞	p_o (psfa)	Re_L	\dot{m} (lbm/sec)	$C_{DA,s}$	$C_{DA,j}$	$\frac{D_j^2}{D_b D_M}$
—○—	2.0	.90	2000	8.7×10^6	0.000	.06515	.06822	0.358
—□—	2.0	.90	2000	8.7×10^6	0.034	.06322	.06614	0.358
...◇...	2.0	.90	2000	8.7×10^6	0.067	.06879	.07171	0.358
---△---	2.0	.90	2000	8.7×10^6	0.115	.07236	.07569	0.358

C CIRCULAR ARC BOATTAIL

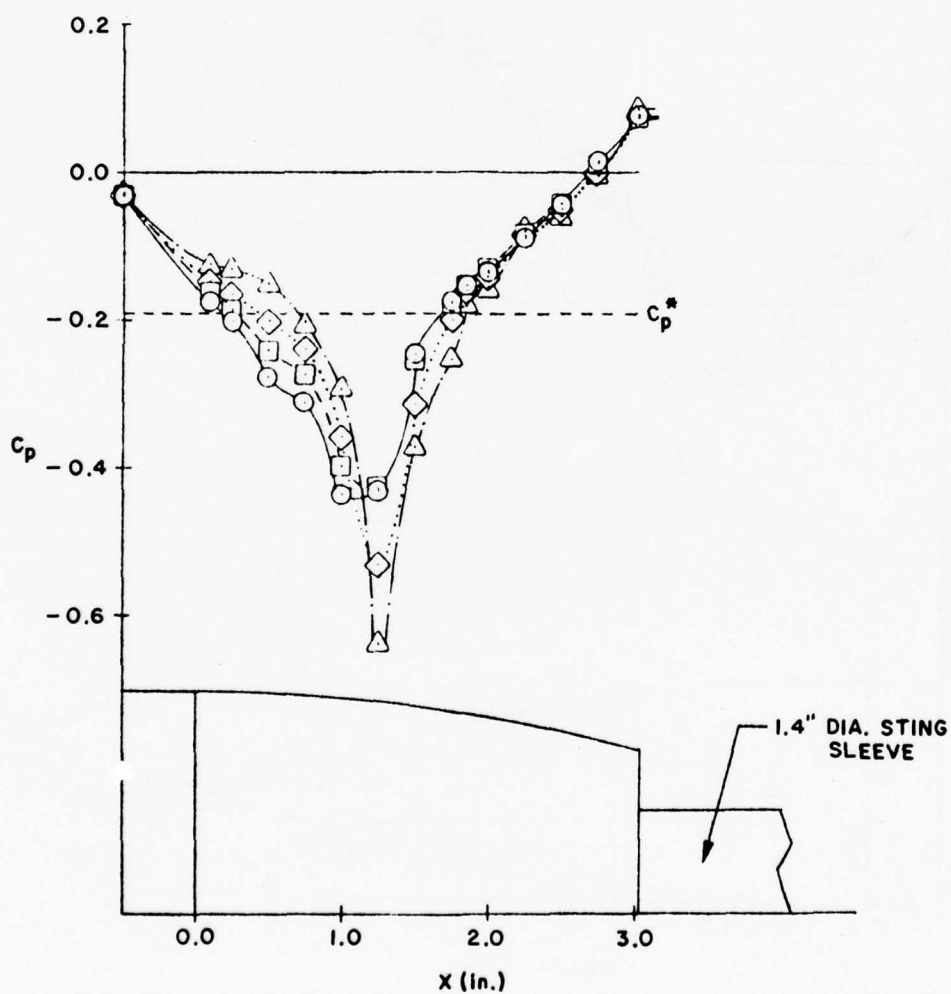


Figure 36. Mass Injection Effect on Boattail and Base Pressure Coefficients for NPR=2, $D_S > 1"$

SYMBOL	NPR	M_∞	p_o (psfa)	Re_L	\dot{m} (lbm/sec)	$C_{D_A,s}$	$C_{D_A,j}$	$\frac{D_j^2}{D_b D_M}$
○—	2.0	.95	2000	8.9×10^6	0.000	.09134	.09358	0.358
□—	2.0	.95	2000	8.9×10^6	0.033	.08818	.09047	0.358
◇····	2.0	.95	2000	8.9×10^6	0.068	.09588	.09881	0.358
△---	2.0	.95	2000	8.9×10^6	0.114	.10100	.10448	0.358

CIRCULAR ARC BOATTAIL

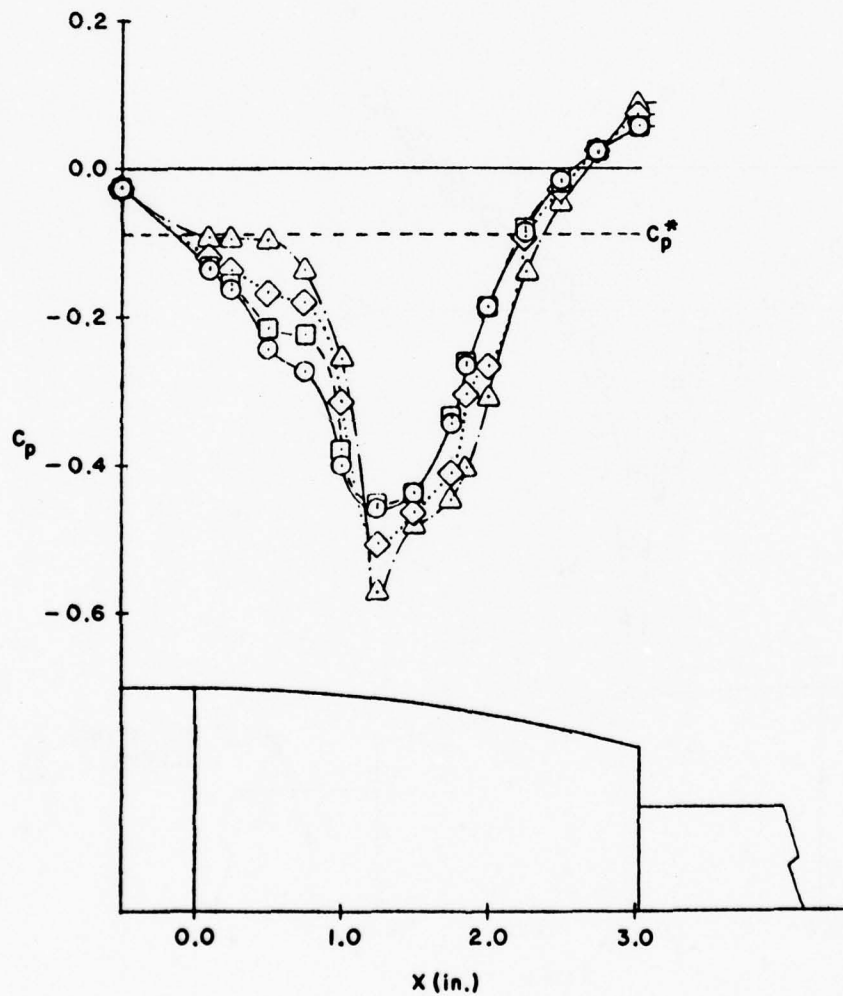


Figure 37. Mass Injection Effect on Boattail and Base Pressure Coefficients for NPR=2, $D_S > 1"$

SYMBOL	NPR	M_∞	p_o (psfa)	Re_L	\dot{m} (lbm/sec)	$C_{DA,s}$	$C_{DA,j}$	$\frac{D_j^2}{D_b D_M}$
—○—	2.0	.90	2000	8.7×10^6	0.000	.05894	.06100	0.427
—□—	2.0	.90	2000	8.7×10^6	0.034	.05827	.06019	0.427
...◇...	2.0	.90	2000	8.7×10^6	0.066	.06426	.06617	0.427
—△—	2.0	.90	2000	8.7×10^6	0.114	.06965	.07177	0.427

CIRCULAR ARC BOATTAIL

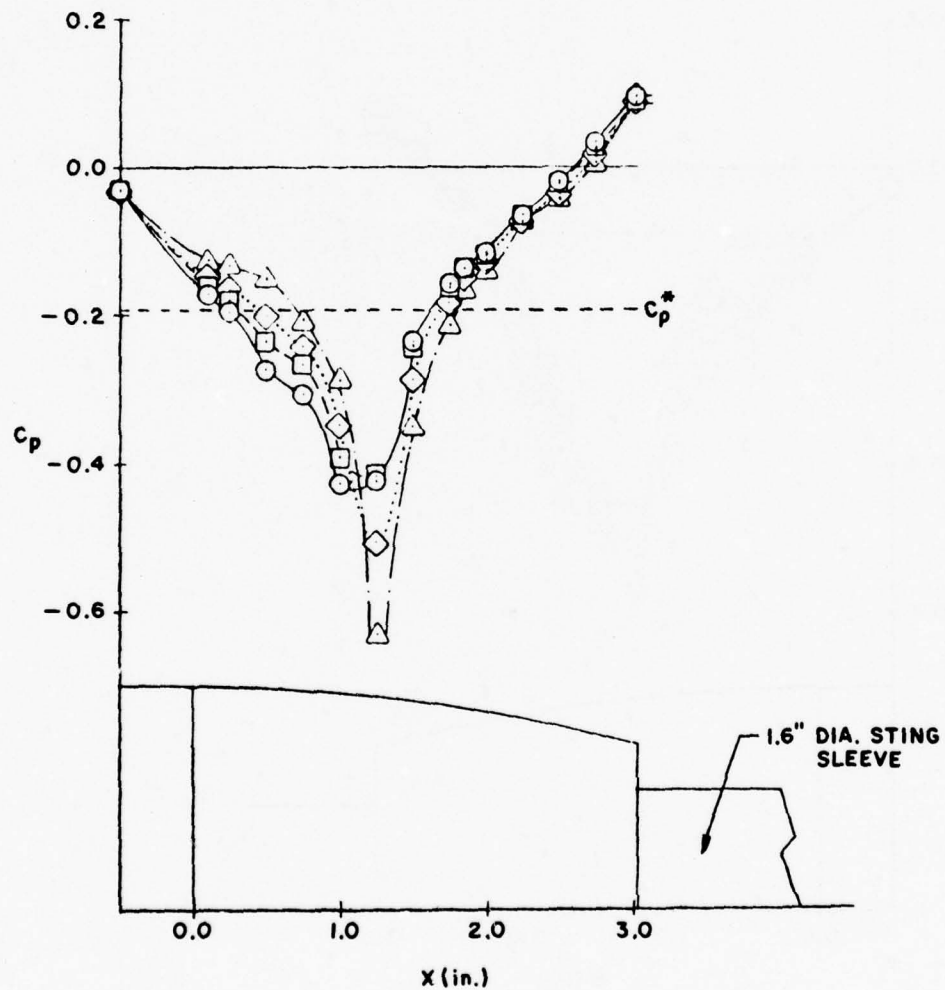


Figure 38. Mass Injection Effect on Boattail and Base Pressure Coefficients for $NPR=2$, $D_S > 1"$

SYMBOL	NPR	M_∞	p_o (psfa)	Re_L	\dot{m} (lbm/sec)	$C_{DA,s}$	$C_{DA,j}$	$\frac{D_j^2}{D_b D_M}$
—○—	2.0	.95	2000	8.9×10^6	0.000	.08203	.08352	0.427
—□—	2.0	.95	2000	8.9×10^6	0.033	.08005	.08152	0.427
...◇...	2.0	.95	2000	8.9×10^6	0.067	.08502	.08698	0.427
---△---	2.0	.95	2000	8.9×10^6	0.114	.09309	.09535	0.427

CIRCULAR ARC BOATTAIL



Figure 39. Mass Injection Effect on Boattail and Base Pressure Coefficients for $NPR=2$, $D_S > 1"$

SYMBOL	NPR	M_∞	p_o (psfa)	Re_L	\dot{m} (lbm/sec)	$C_{DA,s}$	$C_{DA,j}$	$\frac{D_j^2}{D_b D_M}$
—○—	2.0	.90	2000	8.7×10^6	0.000	.05779	.05779	0.502
—□—	2.0	.90	2000	8.7×10^6	0.033	.05617	.05617	0.502
---◇---	2.0	.90	2000	8.7×10^6	0.067	.05964	.05964	0.502
---△---	2.0	.90	2000	8.7×10^6	0.114	.06335	.06335	0.502

CIRCULAR ARC BOATTAIL

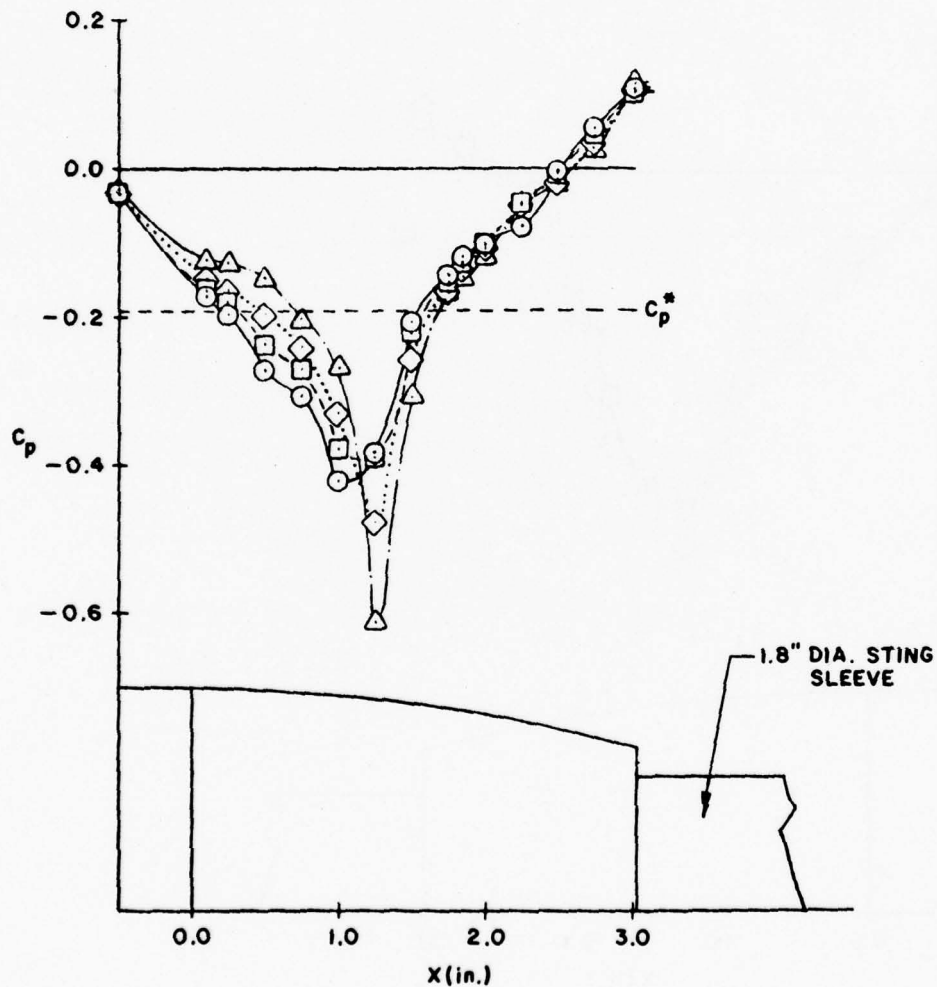


Figure 40. Mass Injection Effect on Boattail and Base Pressure Coefficients for NPR=2, $D_S > 1"$

SYMBOL	NPR	M_∞	p_o (psfa)	Re_L	\dot{m} (lbm/sec)	$C_{DA,s}$	$C_{DA,j}$	$\frac{D_j^2}{D_b D_M}$
—○—	2.0	.95	2000	8.9×10^6	0.000	.07276	.07276	0.502
—□—	2.0	.95	2000	8.9×10^6	0.034	.06898	.06898	0.502
...◇...	2.0	.95	2000	8.9×10^6	0.066	.08137	.08137	0.502
---△---	2.0	.95	2000	8.9×10^6	0.113	.05931	.06667	0.502

CIRCULAR ARC BOATTAIL

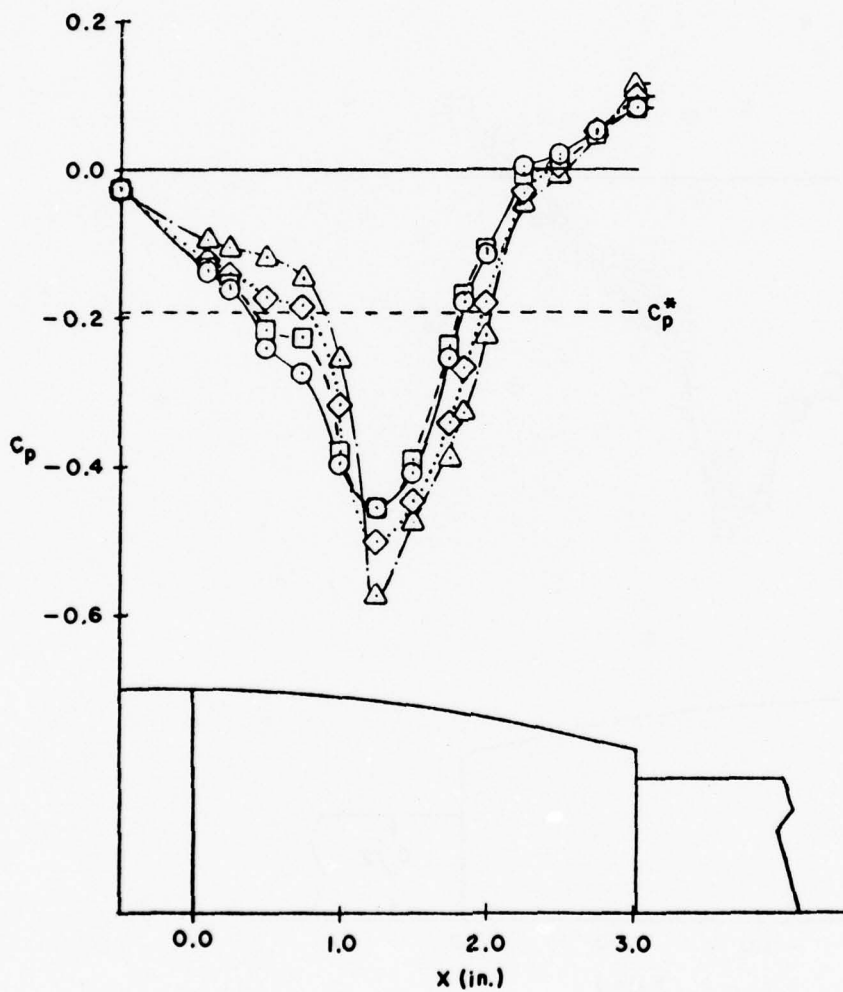


Figure 41. Mass Injection Effect on Boattail and Base Pressure Coefficients for NPR=2, $D_S > 1"$

SYMBOL	NPR	M_∞	p_o (psfa)	Re_L	\dot{m} (lmb/sec)	$C_{DA,s}$	$C_{DA,j}$	$\frac{D_j^2}{D_b D_M}$	$\frac{D_s}{D_b}$
---△---	2.0	.90	2000	8.7×10^6	0.000	.07016	.07408	0.242	.465
—○—	2.0	.90	2000	8.7×10^6	0.000	.06515	.06822	0.358	.651
—□—	2.0	.90	2000	8.7×10^6	0.000	.05894	.06100	0.427	.744
...◇...	2.0	.90	2000	8.7×10^6	0.000	.05779	.05779	0.502	.837

CIRCULAR ARC BOATTAIL

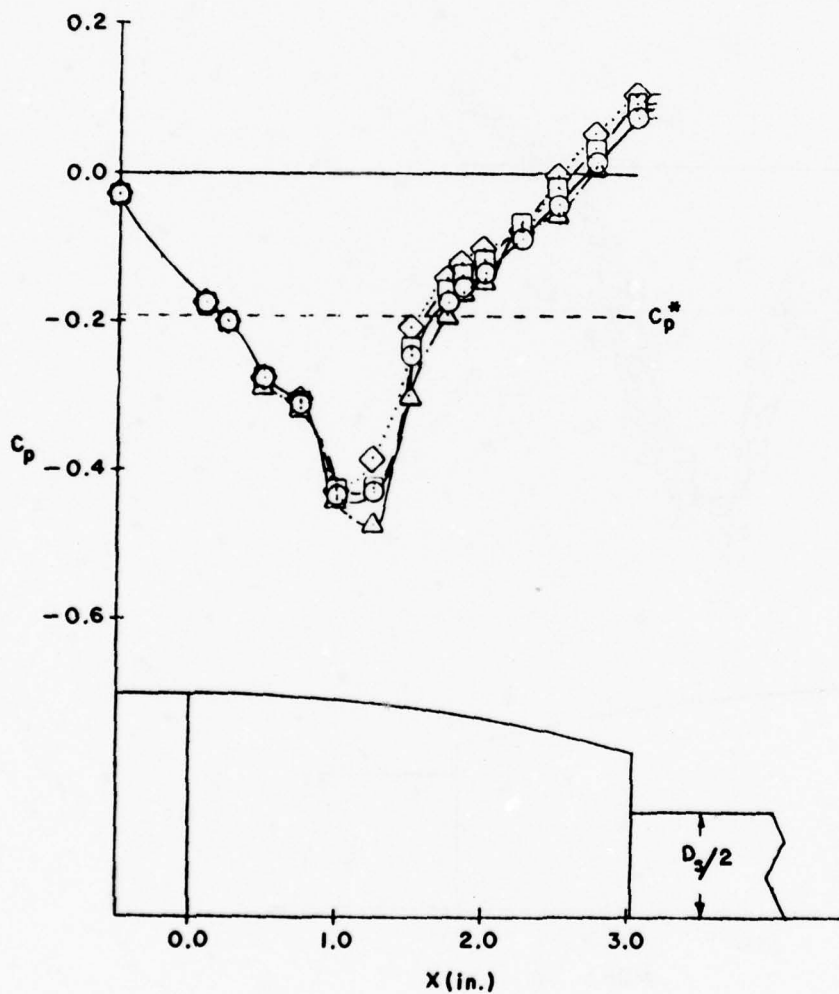


Figure 42. Sting Size Effect on Boattail and Base Pressure Coefficients

SYMBOL	NPR	M_∞	p_o (psfa)	Re_L	\dot{m} (lbm/sec)	$C_{DA,s}$	$C_{DA,j}$	$\frac{D_j^2}{D_b D_M}$	$\frac{D_s}{D_b}$
—△—	2.0	.90	2000	8.7×10^6	0.033	.06985	.07361	0.242	.465
—○—	2.0	.90	2000	8.7×10^6	0.034	.06322	.06614	0.358	.651
—□—	2.0	.90	2000	8.7×10^6	0.034	.05827	.06019	0.427	.744
...◇...	2.0	.90	2000	8.7×10^6	0.033	.05617	.05617	0.502	.837

CIRCULAR ARC BOATTAIL

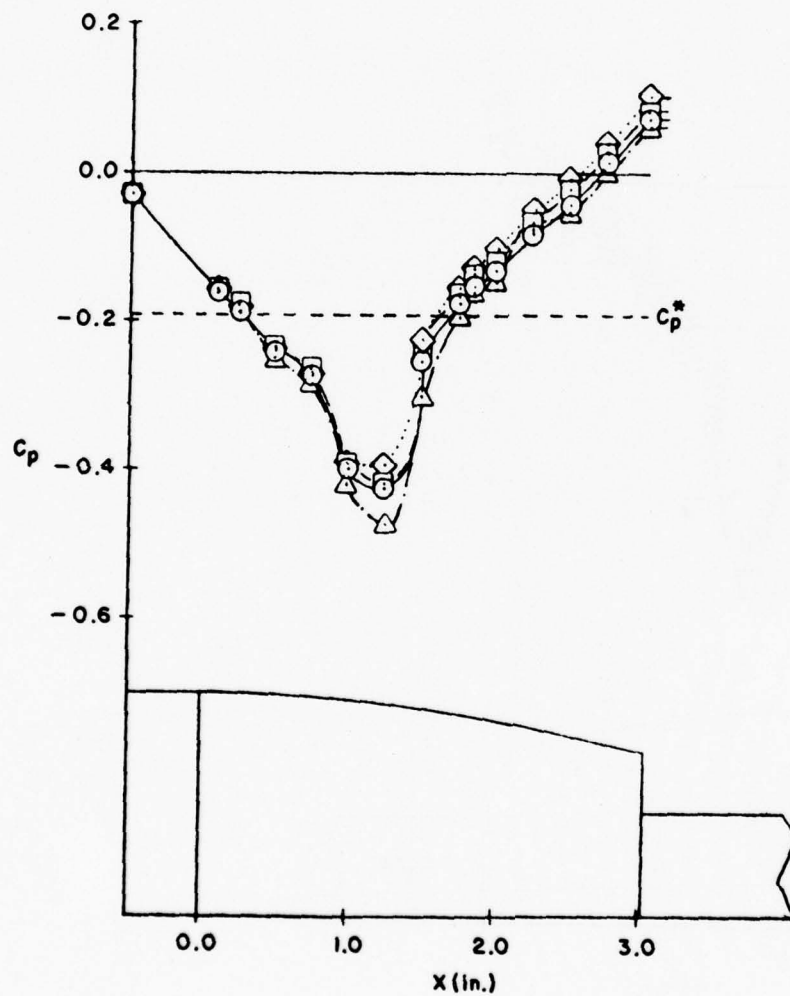


Figure 43. Sting Size Effect on Boattail and Base Pressure Coefficients

SYMBOL	NPR	M_∞	p_o (psfa)	Re_L	\dot{m} (lbm/sec)	$C_{D_A,s}$	$C_{D_A,j}$	$\frac{D_j^2}{D_b D_M}$	$\frac{D_s}{D_b}$
---△---	2.0	.90	2000	8.7×10^6	0.065	.07390	.07771	0.242	.465
—○—	2.0	.90	2000	8.7×10^6	0.067	.06879	.07171	0.358	.651
—□—	2.0	.90	2000	8.7×10^6	0.066	.06426	.06617	0.427	.744
...◇...	2.0	.90	2000	8.7×10^6	0.067	.05964	.05964	0.502	.837

CIRCULAR ARC BOATTAIL

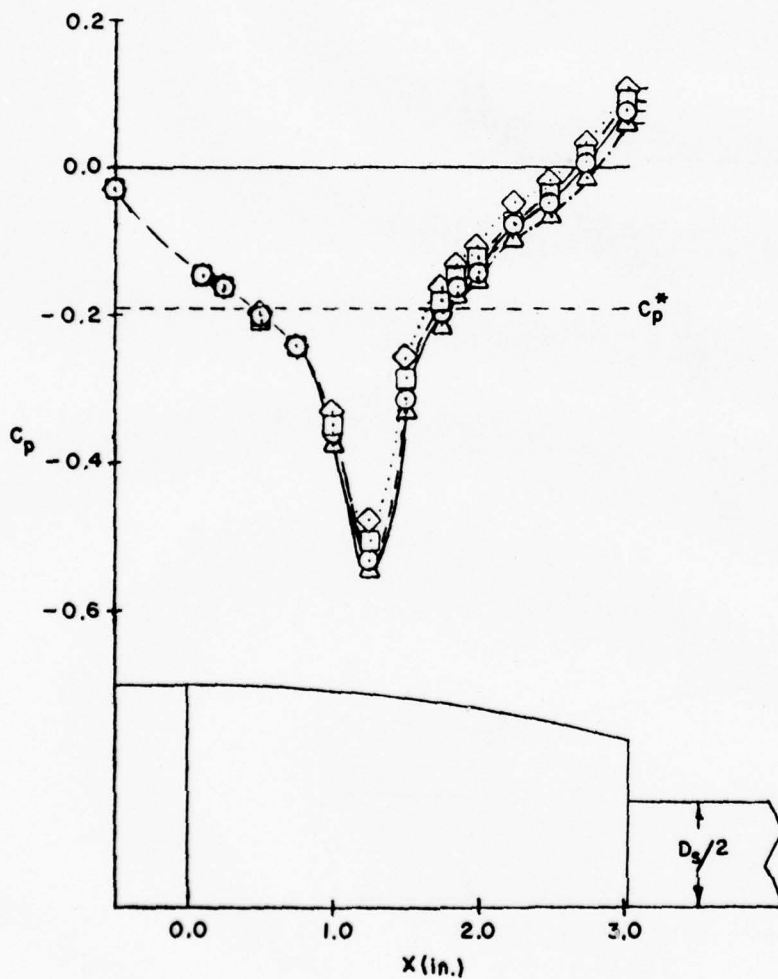


Figure 44. Sting Size Effect on Boattail and Base Pressure Coefficients

SYMBOL	NPR	M_∞	p_o (psfa)	Re_L	\dot{m} (lbm/sec)	$C_{DA,s}$	$C_{DA,j}$	$\frac{D_j^2}{D_b D_M}$
—○—	2.0	.90	2000	8.7×10^6	0.000	.09607	.09843	.240
—□—	2.0	.90	2000	8.7×10^6	0.063	.09717	.10089	.240
...◇...	2.0	.90	2000	8.7×10^6	0.116	.09730	.10206	.240

CUT-OFF
B-I BOATTAIL

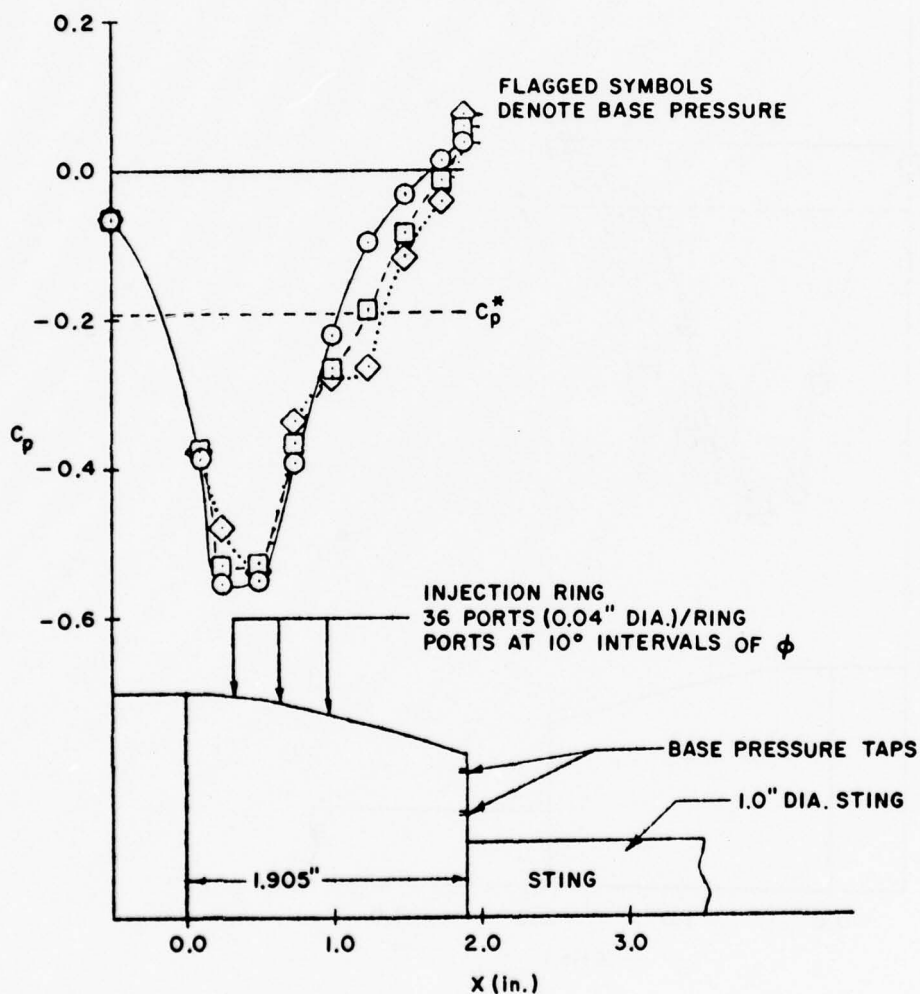


Figure 45. Mass Injection Effect on Boattail and Base Pressure Coefficients for NPR=2.0, $D_s=1"$

SYMBOL	NPR	M_∞	p_o (psfa)	Re_L	\dot{m} (lbm/sec)	$C_{D_A,s}$	$C_{D_A,j}$	$\frac{D_j^2}{D_b D_M}$
—○—	2.0	.95	2000	8.9×10^6	0.000	.11593	.11525	.240
—□—	2.0	.95	2000	8.9×10^6	0.062	.12002	.12228	.240
...◇...	2.0	.95	2000	8.9×10^6	0.119	.12025	.12456	.240

CUT-OFF
B-I BOATTAIL

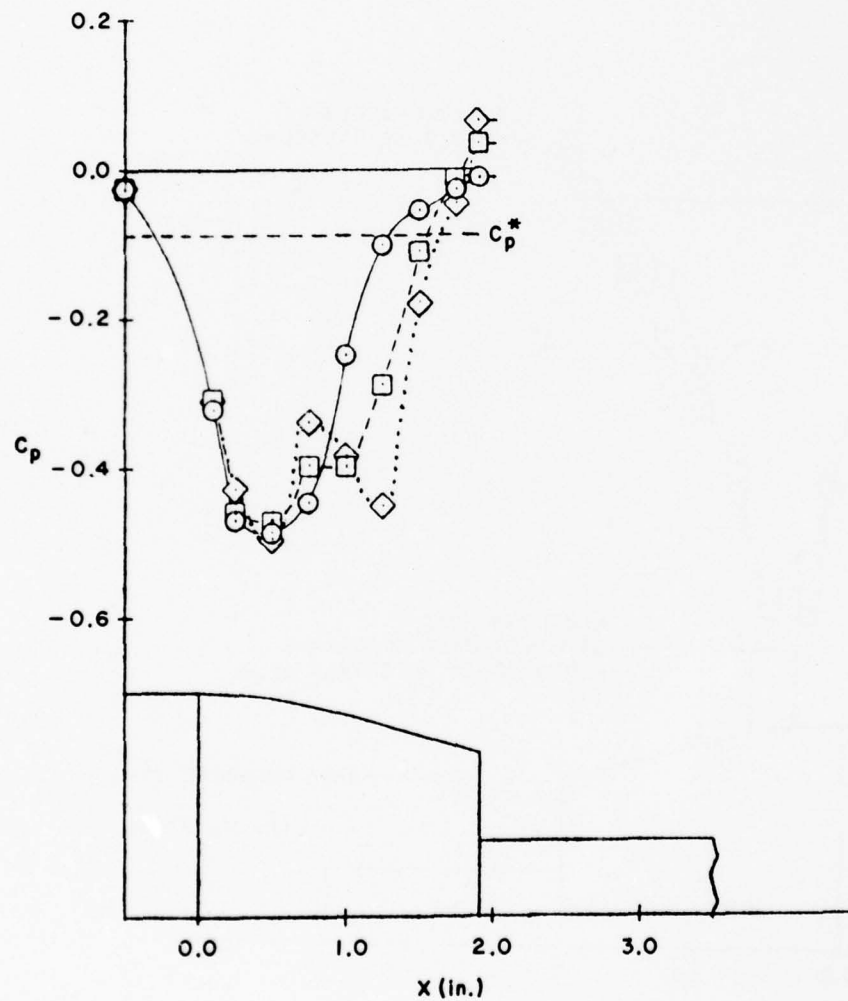


Figure 46. Mass Injection Effect on Boattail and Base Pressure Coefficients for NPR=2.0, $D_S=1"$

SYMBOL	NPR	M_∞	p_o (psfa)	Re_L	\dot{m} (lbm/sec)	$C_{DA,s}$	$C_{DA,j}$	$\frac{D_j^2}{D_b D_M}$
—○—	2.0	.80	2000	8.3×10^6	0.000	.07169	.07559	.240
—□—	2.0	.80	2000	8.3×10^6	0.059	.07524	.07875	.240
...◇...	2.0	.80	2000	8.3×10^6	0.112	.08322	.08739	.240

CUT-OFF
B-I BOATTAIL

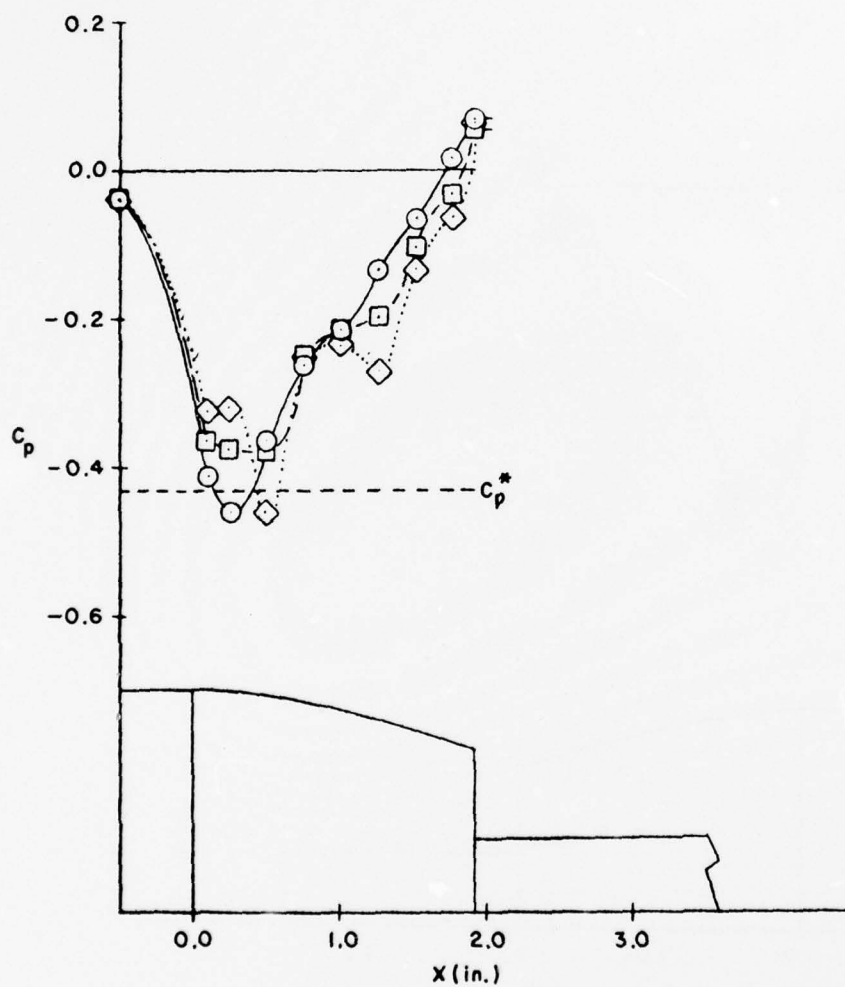


Figure 47. Mass Injection Effect on Boattail and Base Pressure Coefficients for NPR=2.0, $D_S=1"$

SYMBOL	NPR	M_∞	p_o (psfa)	Re_L	\dot{m} (lbm/sec)	$C_{DA,s}$	$C_{DA,j}$	$\frac{D_j^2}{D_b D_M}$
—○—	2.0	.85	2000	8.4×10^6	0.000	.07262	.07699	.240
—□—	2.0	.85	2000	8.4×10^6	0.060	.07462	.07872	.240
...◇...	2.0	.85	2000	8.4×10^6	0.112	.07949	.08441	.240

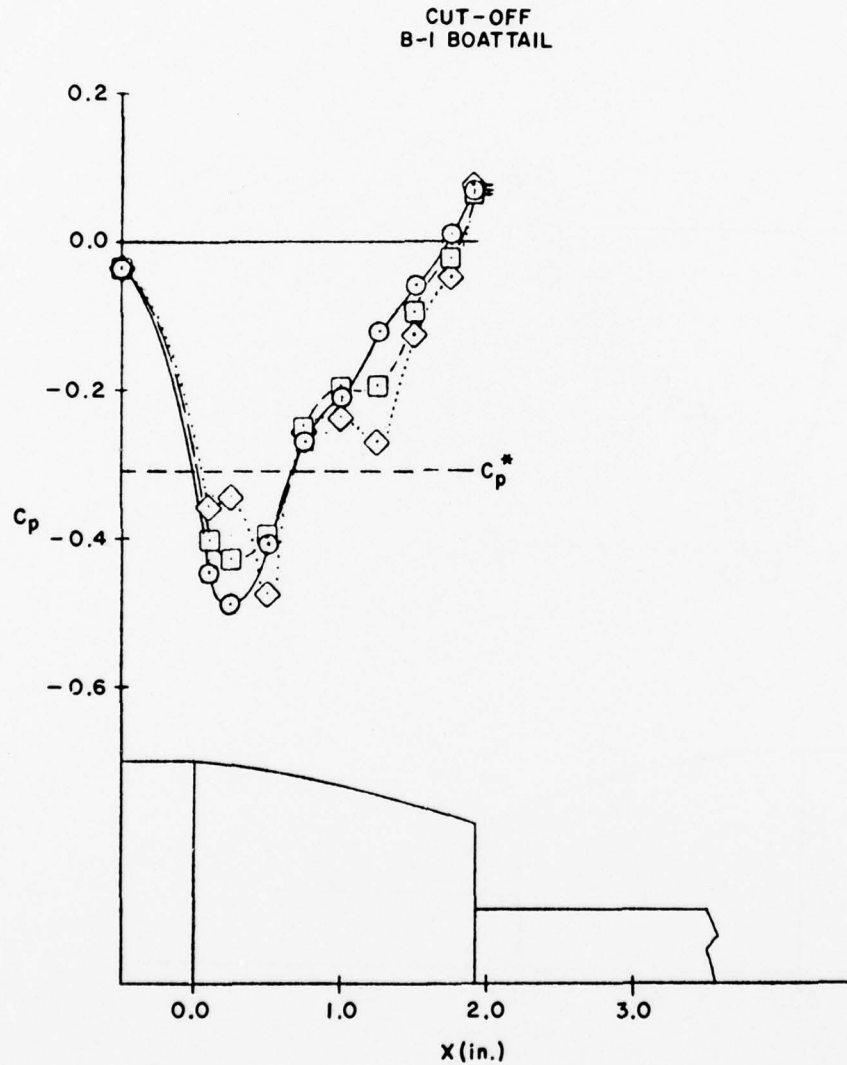


Figure 48. Mass Injection Effect on Boattail and Base Pressure Coefficients for NPR=2.0, $D_S=1"$

SYMBOL	NPR	M_∞	p_o (psfa)	Re_L	\dot{m} (lbm/sec)	$C_{DA,s}$	$C_{DA,j}$	$\frac{D_j^2}{D_b D_M}$
—○—	2.0	.80	3000	12.4×10^6	0.000	.06487	.06946	.240
—□—	2.0	.80	3000	12.4×10^6	0.063	.06727	.07110	.240
...◇...	2.0	.80	3000	12.4×10^6	0.114	.07066	.07502	.240

**CUT-OFF
B-I BOATTAIL**

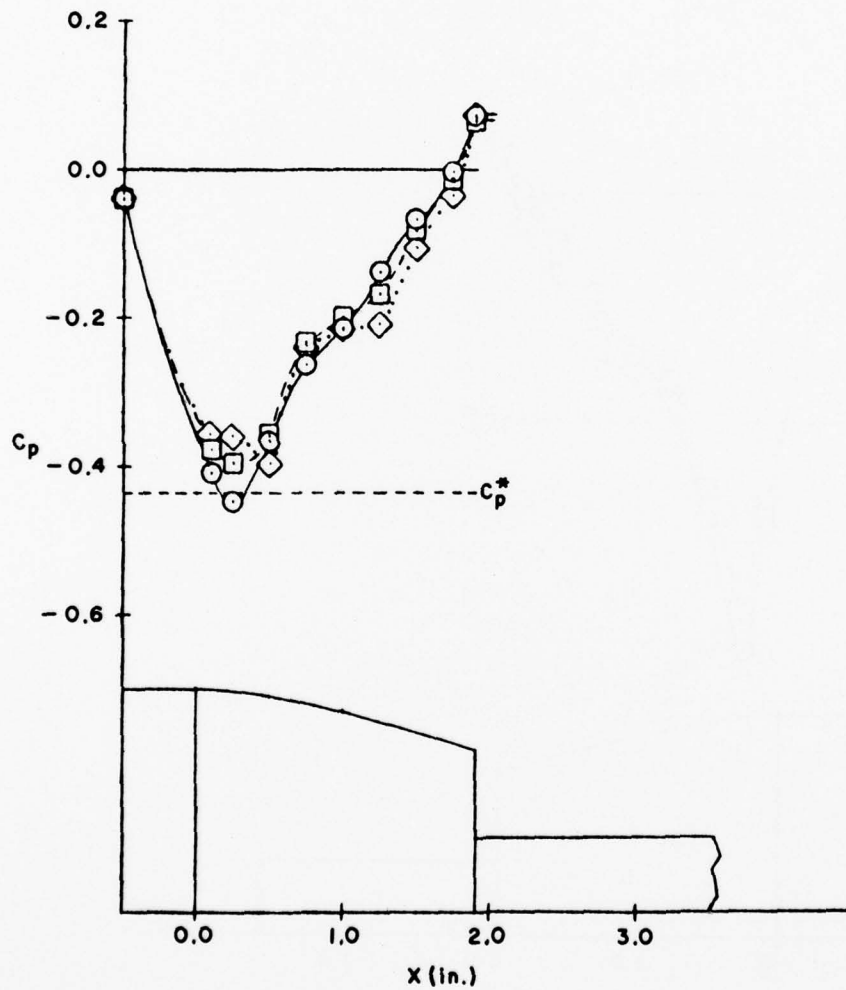


Figure 49. Mass Injection Effect on Boattail and Base Pressure Coefficients for NPR=2.0, $D_S=1"$

SYMBOL	NPR	M_∞	p_o (psfa)	Re_L	\dot{m} (lbm/sec)	$C_{DA,s}$	$C_{DA,j}$	$\frac{D_j^2}{D_b D_M}$
—○—	2.0	.85	3000	12.7×10^6	0.000	.07704	.08160	.240
—□—	2.0	.85	3000	12.7×10^6	0.063	.07957	.08316	.240
...◇...	2.0	.85	3000	12.7×10^6	0.118	.08126	.08553	.240

CUT-OFF
B-I BOATTAIL

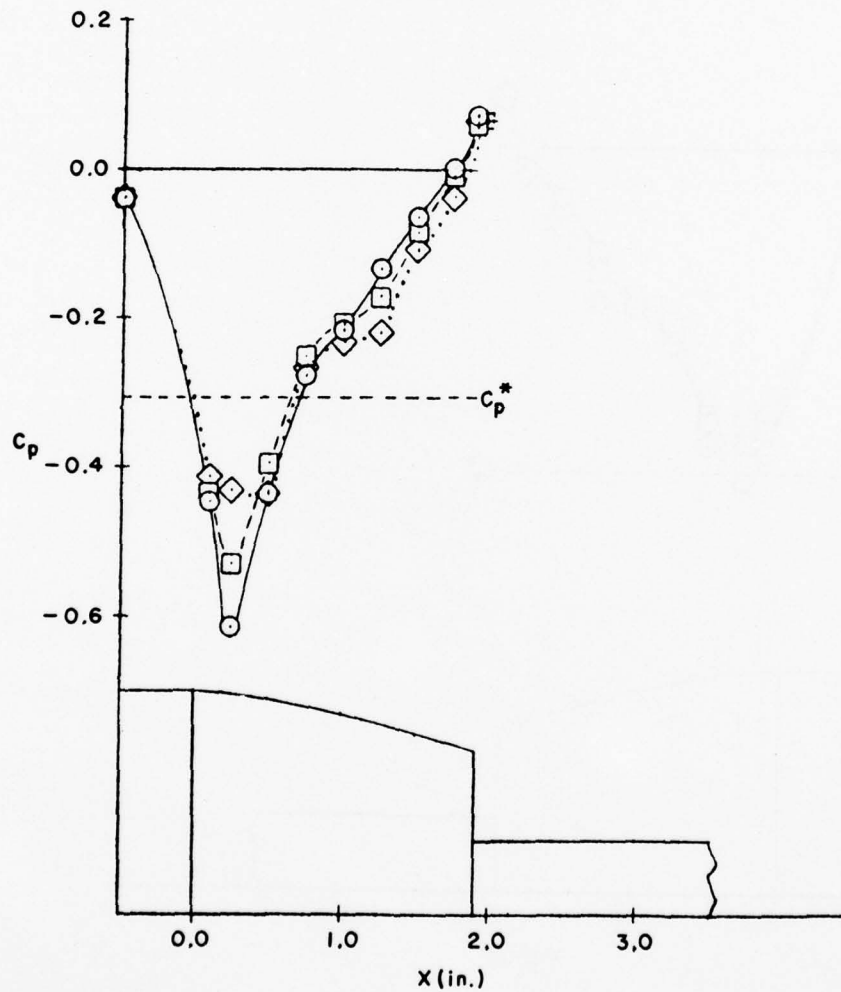


Figure 50. Mass Injection Effect on Boattail and Base Pressure Coefficients for NPR=2.0, $D_S=1"$

SYMBOL	NPR	M_∞	p_o (psfa)	Re_L	\dot{m} (lbm/sec)	$C_{D_A,s}$	$C_{D_A,j}$	$\frac{D_j^2}{D_b D_M}$
—○—	2.0	.90	3000	13.1×10^6	0.000	.09781	.10055	0.240
—□—	2.0	.90	3000	13.1×10^6	0.064	.09574	.09888	0.240
...◇...	2.0	.90	3000	13.1×10^6	0.117	.09689	.10124	0.240

CUT - OFF
B-I BOATTAIL

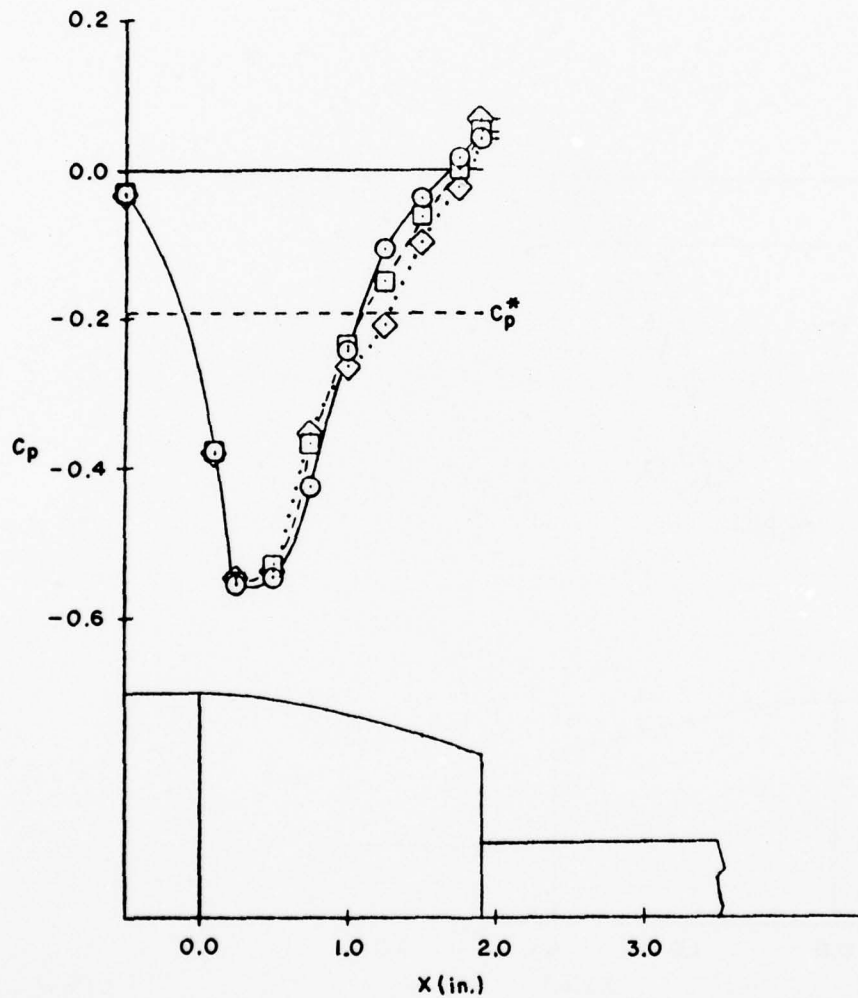


Figure 51. Mass Injection Effect on Boattail and Base Pressure Coefficients for NPR=2.0, $D_S=1"$

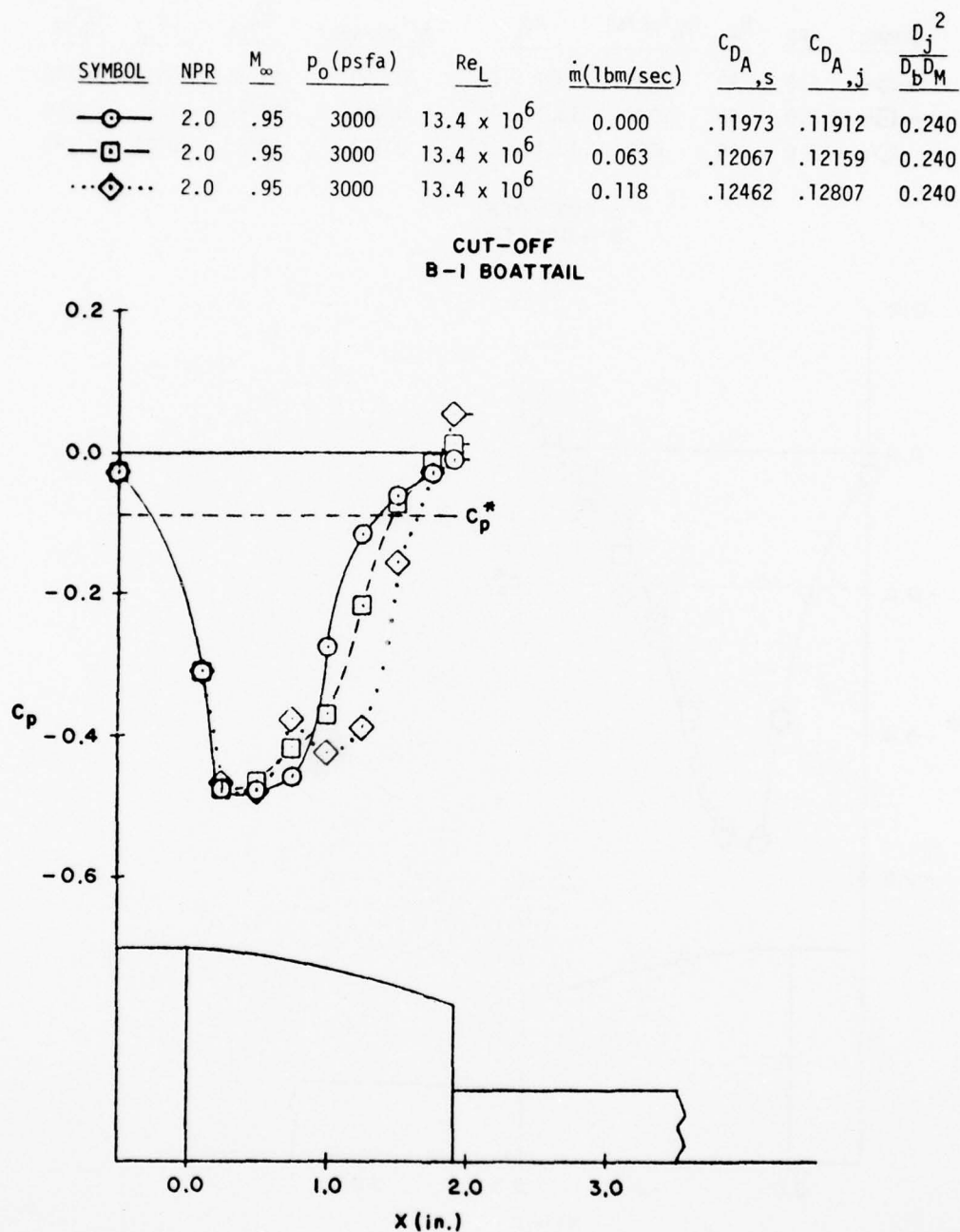


Figure 52. Mass Injection Effect on Boattail and Base Pressure Coefficients for NPR=2.0, $D_S=1"$

SYMBOL	NPR	M_∞	p_o (psfa)	Re_L	\dot{m} (lbm/sec)	$C_{DA,s}$	$C_{DA,j}$	$\frac{D_j^2}{D_b D_M}$
—○—	2.0	.80	2000	8.3×10^6	0.000	.07169	.07559	.240
—□—	2.0	.80	3000	12.4×10^6	0.000	.06487	.06946	.240

CUT-OFF
B-1 BOATTAIL

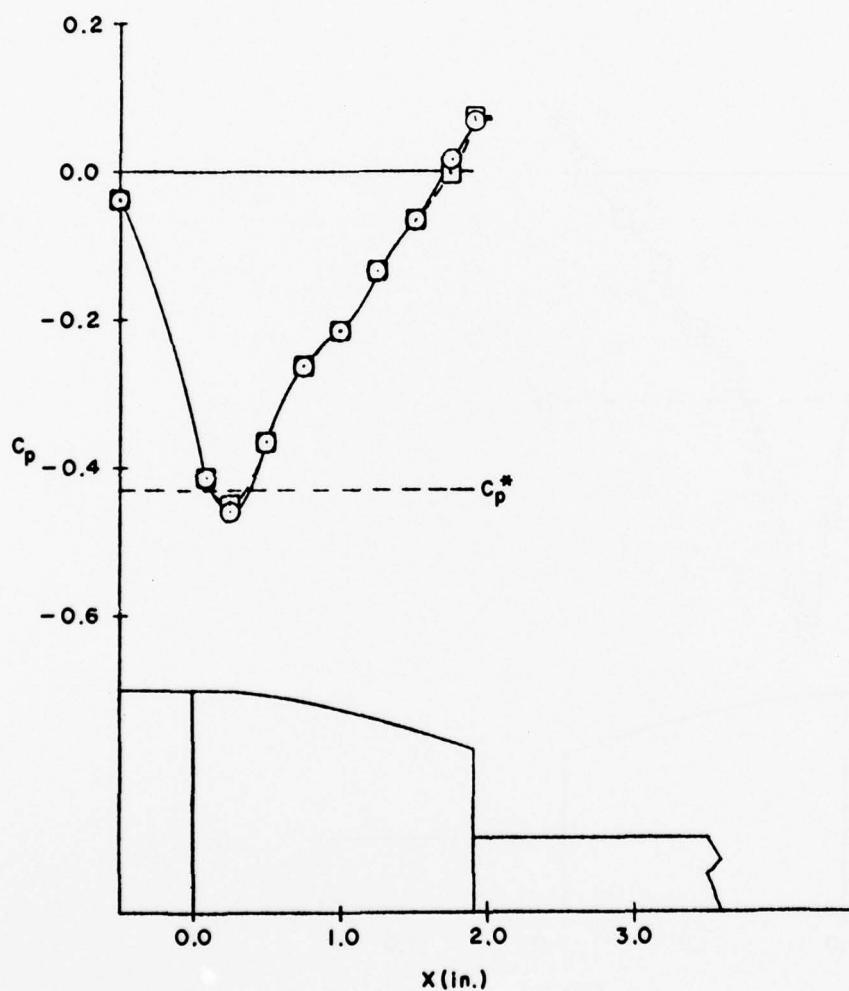


Figure 53. Reynolds Number Effect on Boattail and Base Pressure Coefficients

SYMBOL	NPR	M_∞	p_o (psfa)	Re_L	\dot{m} (lbm/sec)	$C_{DA,s}$	$C_{DA,j}$	$\frac{D_j^2}{D_b D_M}$
—○—	2.0	.85	2000	8.4×10^6	0.000	.07262	.07699	.240
—□—	2.0	.85	3000	12.7×10^6	0.000	.07704	.08160	.240

CUT - OFF
B-1 BOATTAIL

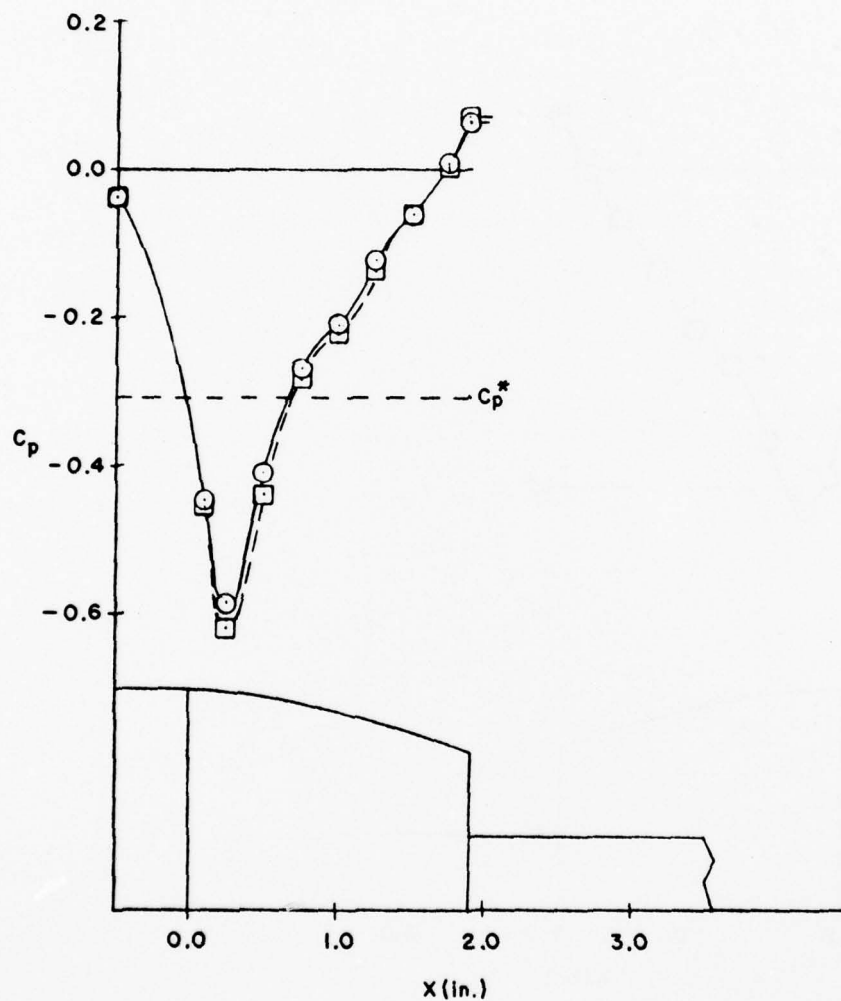


Figure 54. Reynolds Number Effect on Boattail and Base Pressure Coefficients

SYMBOL	NPR	M_∞	p_o (psfa)	Re_L	\dot{m} (lbm/sec)	$C_{DA,s}$	$C_{DA,j}$	$\frac{D_j^2}{D_b D_M}$
—○—	2.0	.90	2000	8.7×10^6	0.000	.09607	.09843	0.240
—□—	2.0	.90	3000	13.1×10^6	0.000	.09781	.10055	0.240

CUT-OFF
B-I BOATTAIL

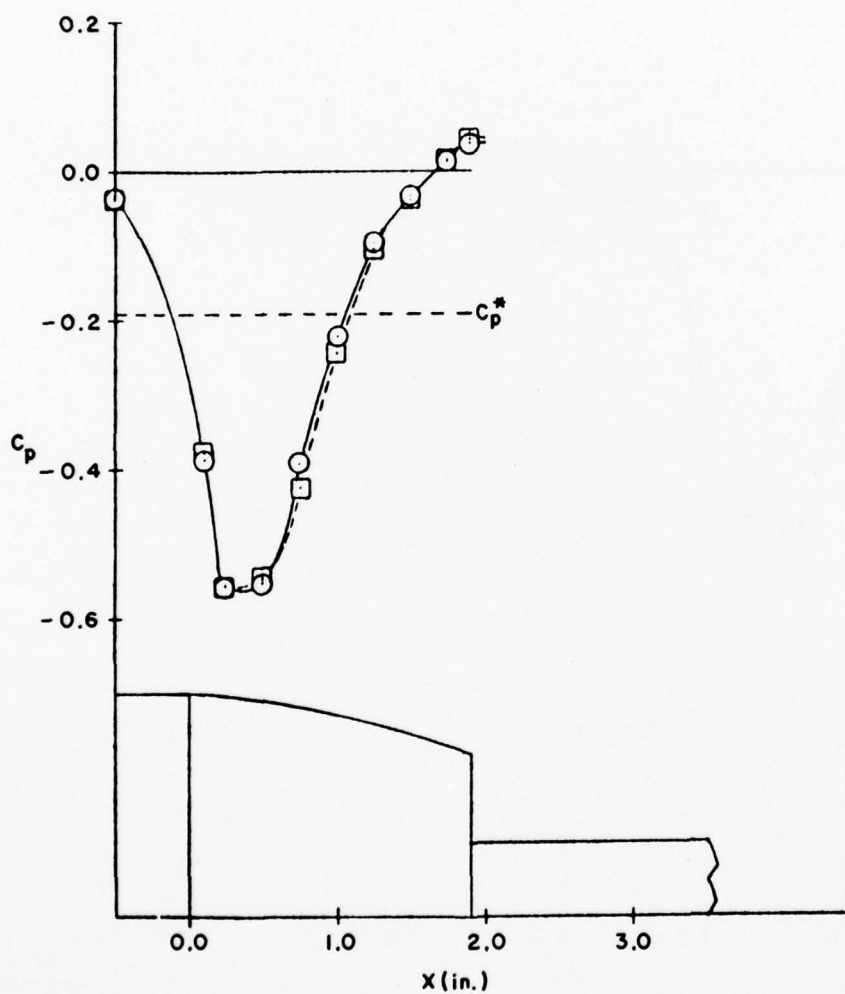


Figure 55. Reynolds Number Effect on Boattail and Base Pressure Coefficients

SYMBOL	NPR	M_∞	p_o (psfa)	Re_L	\dot{m} (lbm/sec)	$C_{D,A,s}$	$C_{D,A,j}$	$\frac{D_j^2}{D_b D_M}$
—○—	2.0	.95	2000	8.9×10^6	0.000	.11593	.11525	.240
—□—	2.0	.95	3000	13.4×10^6	0.000	.11973	.11912	.240

CUT - OFF
B-1 BOATTAIL

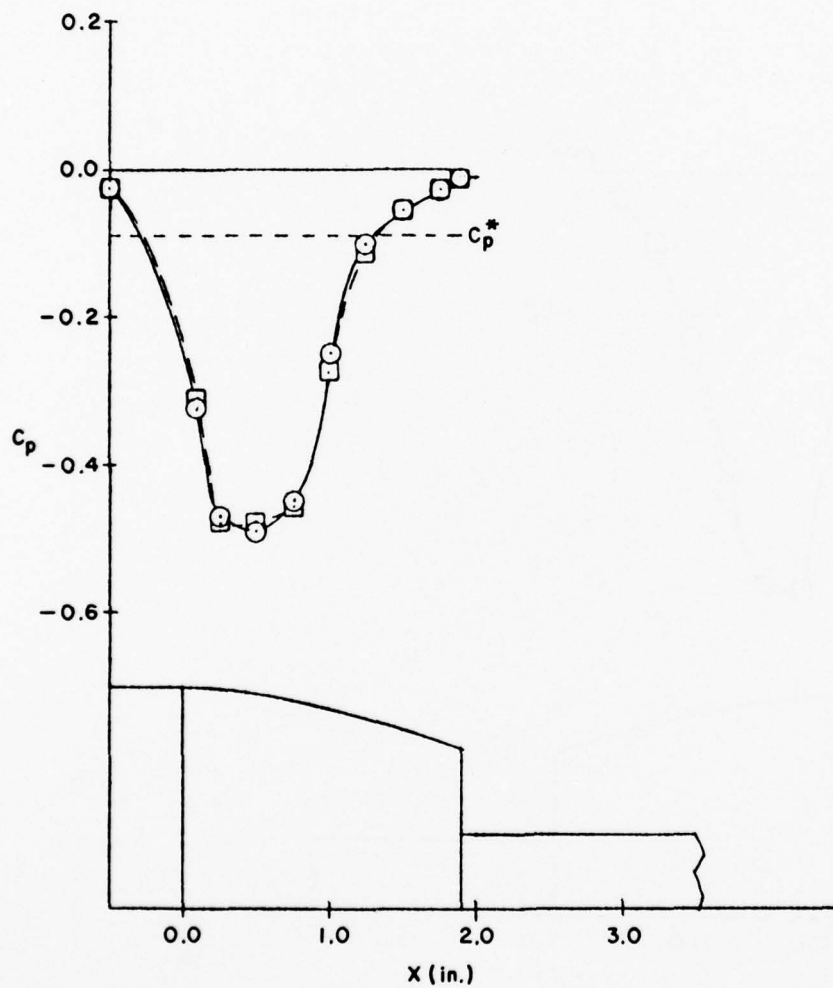


Figure 56. Reynolds Number Effect on Boattail and Base Pressure Coefficients

SYMBOL	NPR	M_∞	p_o (psfa)	Re_L	\dot{m} (lbm/sec)	$C_{D_A,s}$	$C_{D_A,j}$
—○—	2.0	.80	2000	8.3×10^6	0.000	.07169	.07559
—□—	2.0	.85	2000	8.4×10^6	0.000	.07261	.07699
...◇...	2.0	.90	2000	8.7×10^6	0.000	.09607	.09843
---△---	2.0	.95	2000	8.9×10^6	0.000	.11593	.11525

CUT-OFF
B-I BOATTAIL

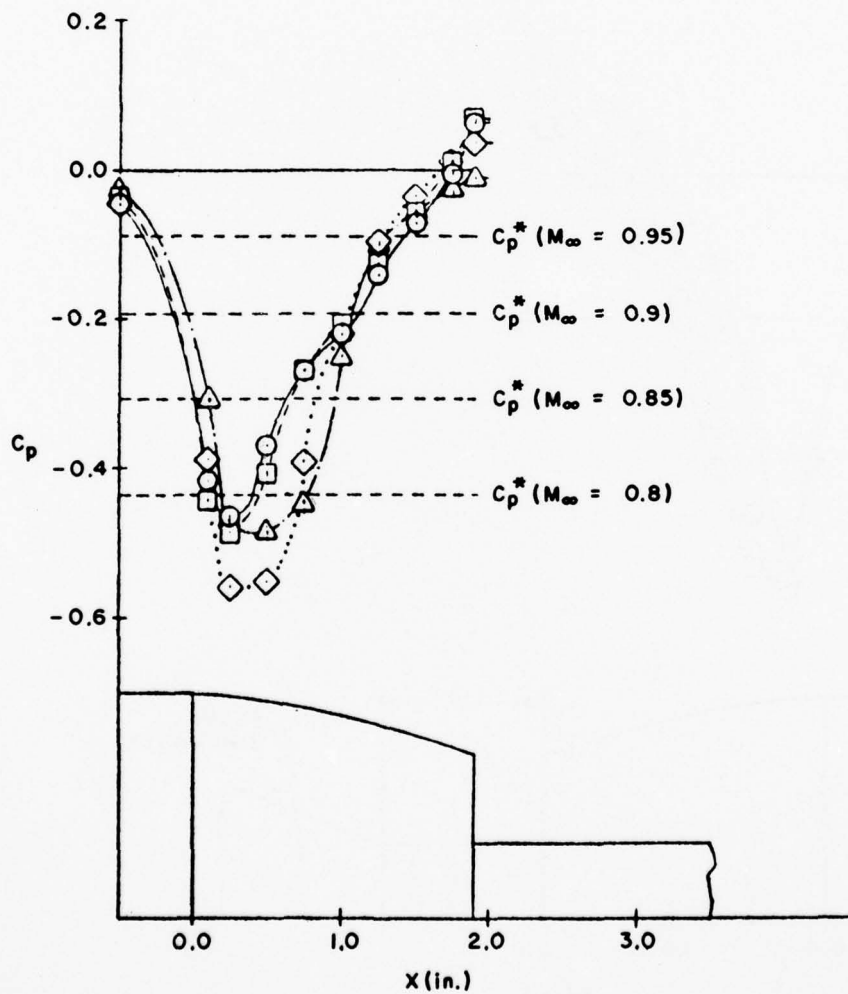


Figure 57. Mach Number Effect on Boattail and Base Pressure Coefficients

SYMBOL	NPR	M_∞	p_o (psfa)	Re_L	\dot{m} (lbm/sec)	ℓ (in.)	$C_{DA,s}$	$C_{DA,j}$	$\frac{D_j^2}{D_b D_M}$
—○—	2.0	.90	2000	8.7×10^6	0.000	REMOVED	.09607	.09843	0.240
—□—	3.61	.90	2000	8.7×10^6	0.000	6	.06937	.07330	0.240
...◇...	4.14	.90	2000	8.7×10^6	0.000	4	.03070	.03740	0.240
---△---	5.18	.90	2000	8.7×10^6	0.000	2	-.02585	-.01602	0.240

CUT-OFF
B-I BOATTAIL

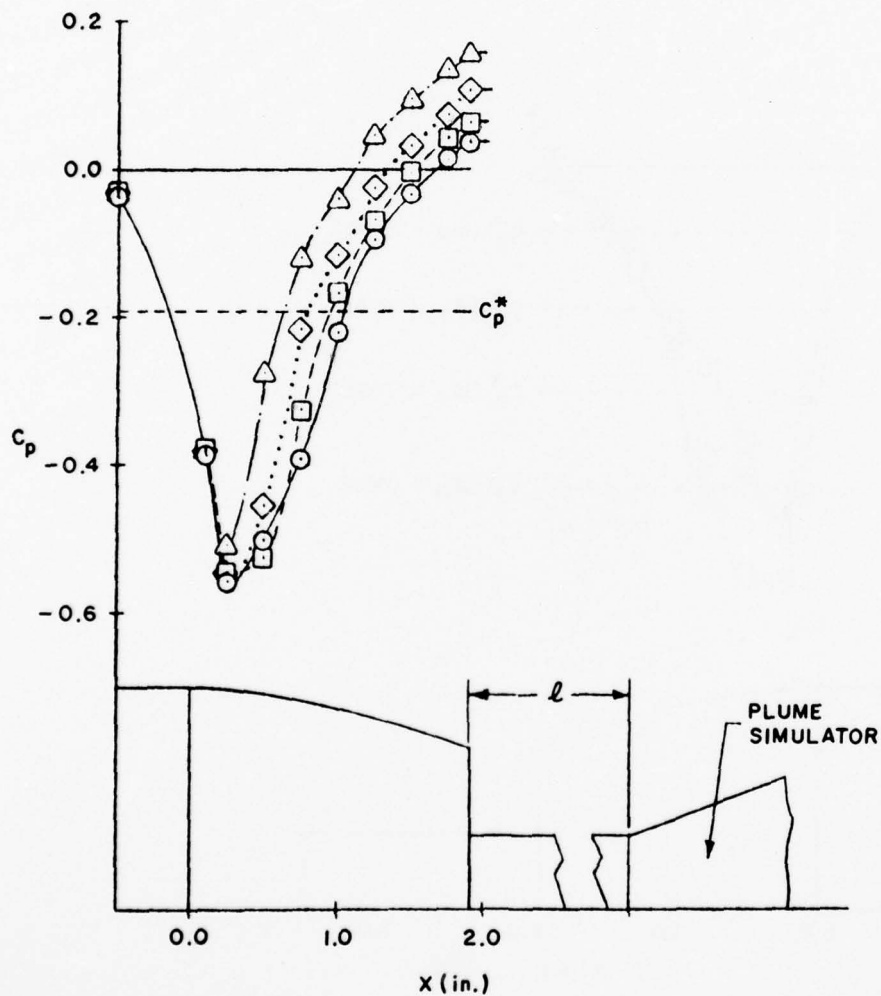


Figure 58. Nozzle Pressure Ratio Effect on Boattail and Base Pressure Coefficients

SYMBOL	NPR	M_∞	p_o (psfa)	Re_L	\dot{m} (lbm/sec)	x (in.)	$C_{DA,s}$	$C_{DA,j}$	$\frac{D_j^2}{D_b D_M}$
—○—	3.61	.90	2000	8.7×10^6	0.000	6	.06937	.07330	0.240
--□--	3.61	.90	2000	8.7×10^6	0.063	6	.07118	.07638	0.240
...◇...	3.61	.90	2000	8.7×10^6	0.114	6	.07432	.08050	0.240

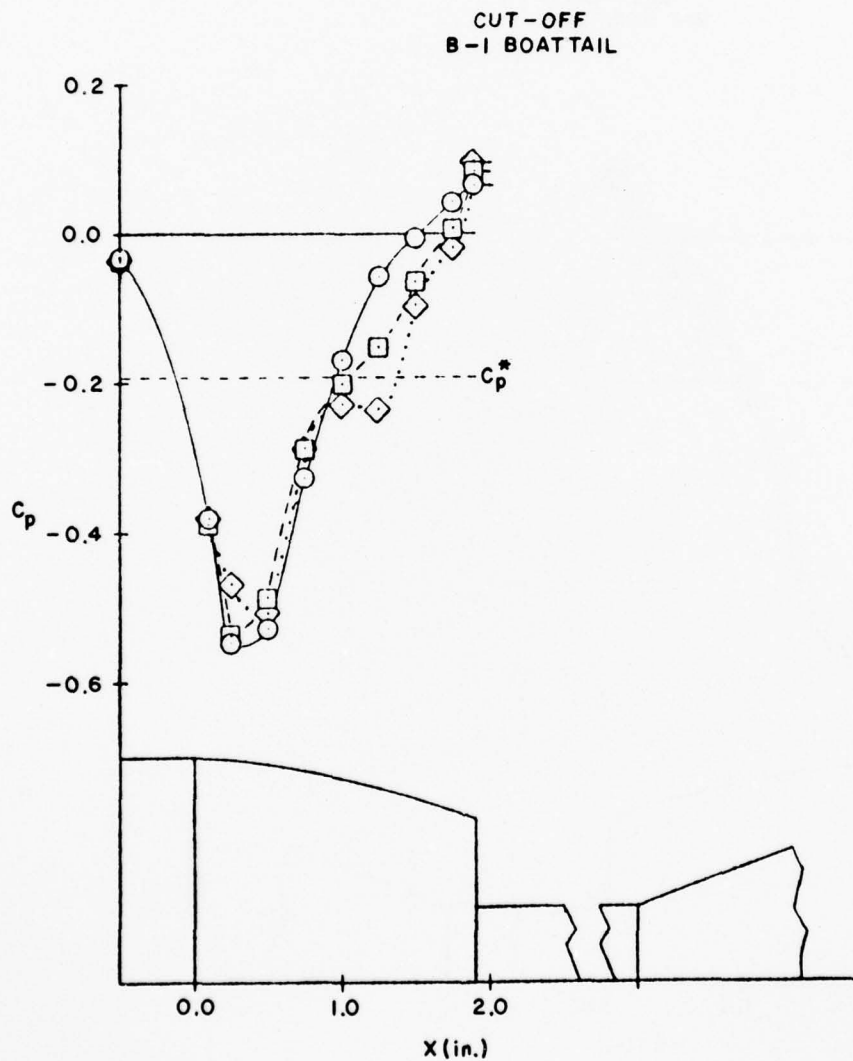


Figure 59. Mass Injection Effect on Boattail and Base Pressure Coefficients for $NPR > 2$

SYMBOL	NPR	M_∞	p_0 (psfa)	Re_L	\dot{m} (lbm/sec)	x (in.)	$C_{DA,s}$	$C_{DA,j}$	$\frac{D_j^2}{D_b D_M}$
—○—	3.61	.90	3000	13.1×10^6	0.000	6	.06981	.07464	0.240
—□—	3.61	.90	3000	13.1×10^6	0.065	6	.07321	.07775	0.240
...◇...	3.61	.90	3000	13.1×10^6	0.115	6	.07353	.07940	0.240

CUT-OFF
B-I BOATTAIL

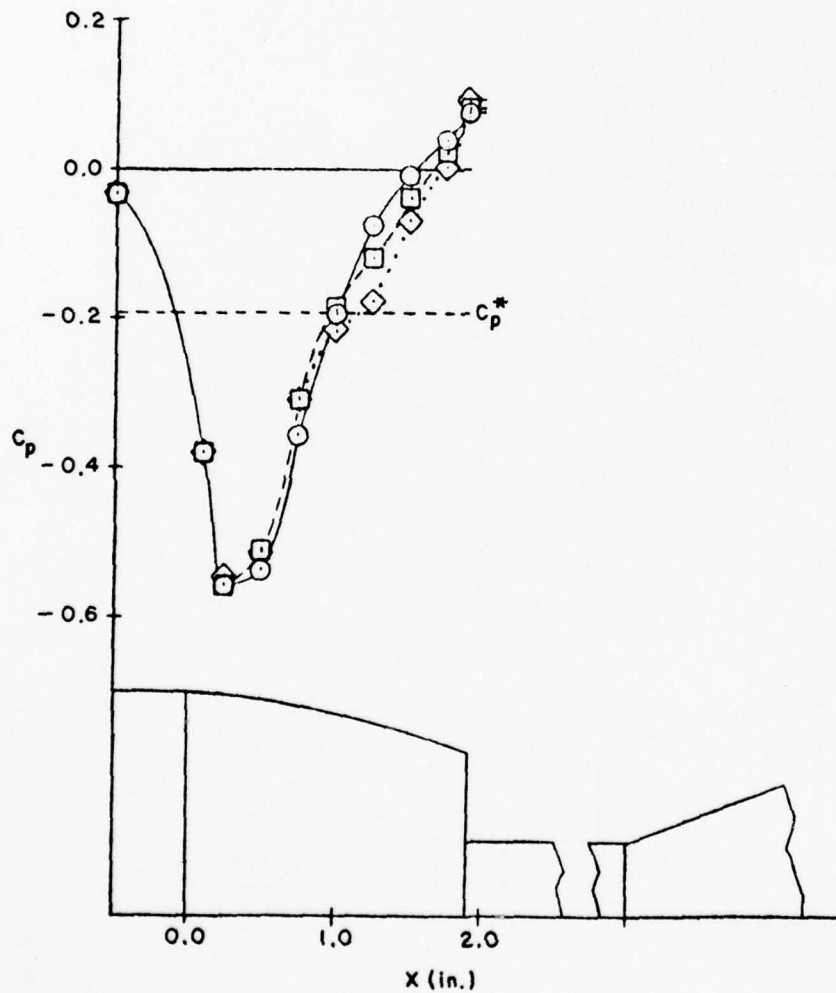


Figure 60. Mass Injection Effect on Boattail and Base Pressure Coefficients for NPR>2

AD-A061 378

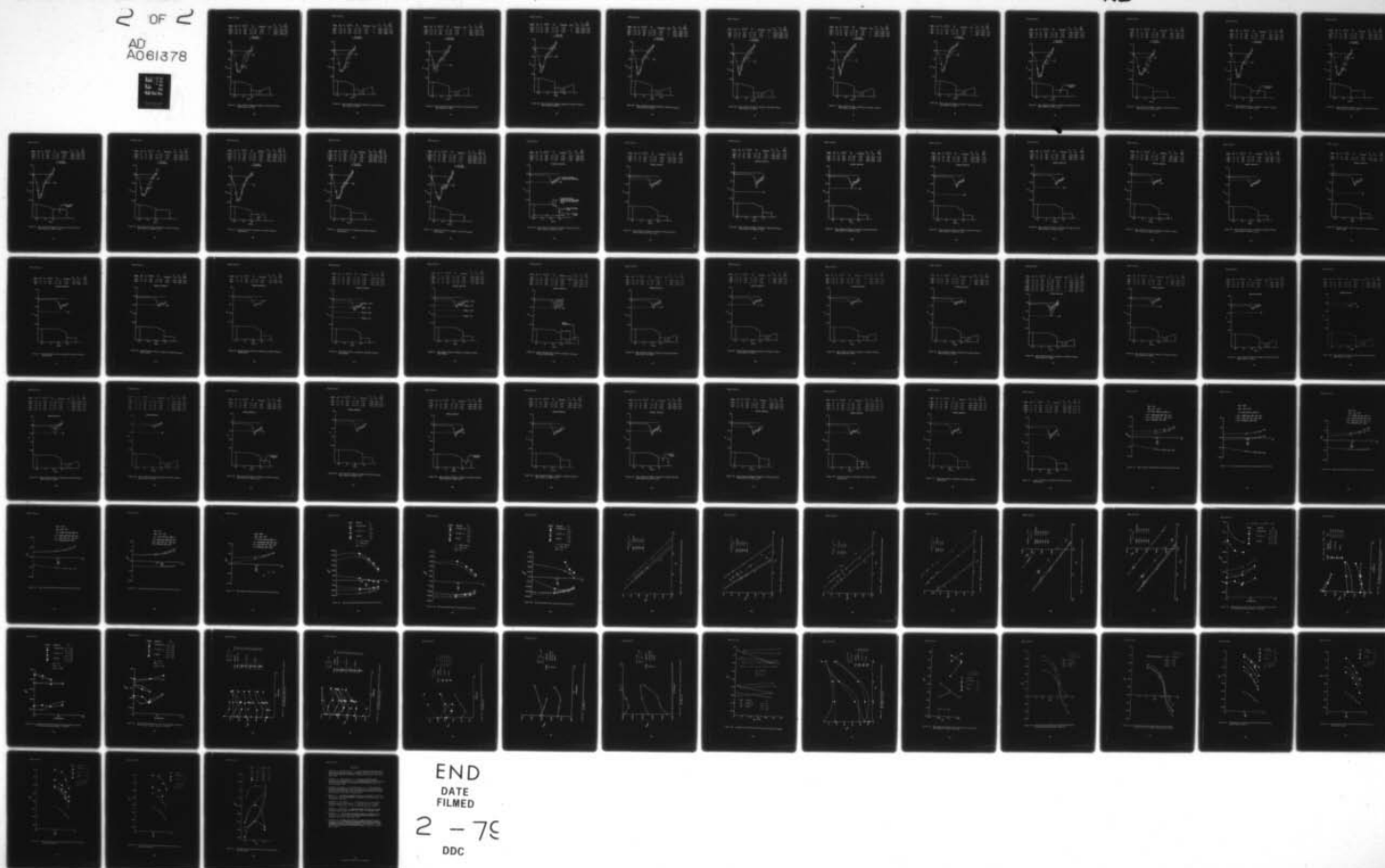
AIR FORCE FLIGHT DYNAMICS LAB WRIGHT-PATTERSON AFB OHIO F/G 20/4
MASS INJECTION AND JET FLOW SIMULATION EFFECTS ON TRANSONIC AFT--ETC(U)
JUN 78 W CALARESE, R E WALTERICK
AFFDL-TR-78-57

UNCLASSIFIED

NL

2 OF 2

AD
A061378



SYMBOL	NPR	M_∞	p_o (psfa)	Re_L	\dot{m} (lbm/sec)	l (in.)	$C_{D_A,s}$	$C_{D_A,j}$	$\frac{D_j^2}{D_b D_M}$
—○—	3.60	.95	2000	8.9×10^6	0.000	6	.07961	.08114	0.240
—□—	3.60	.95	2000	8.9×10^6	0.065	6	.09158	0.9581	0.240
...◇...	3.60	.95	2000	8.9×10^6	0.115	6	.09687	.10289	0.240

CUT-OFF
B-I BOATTAIL

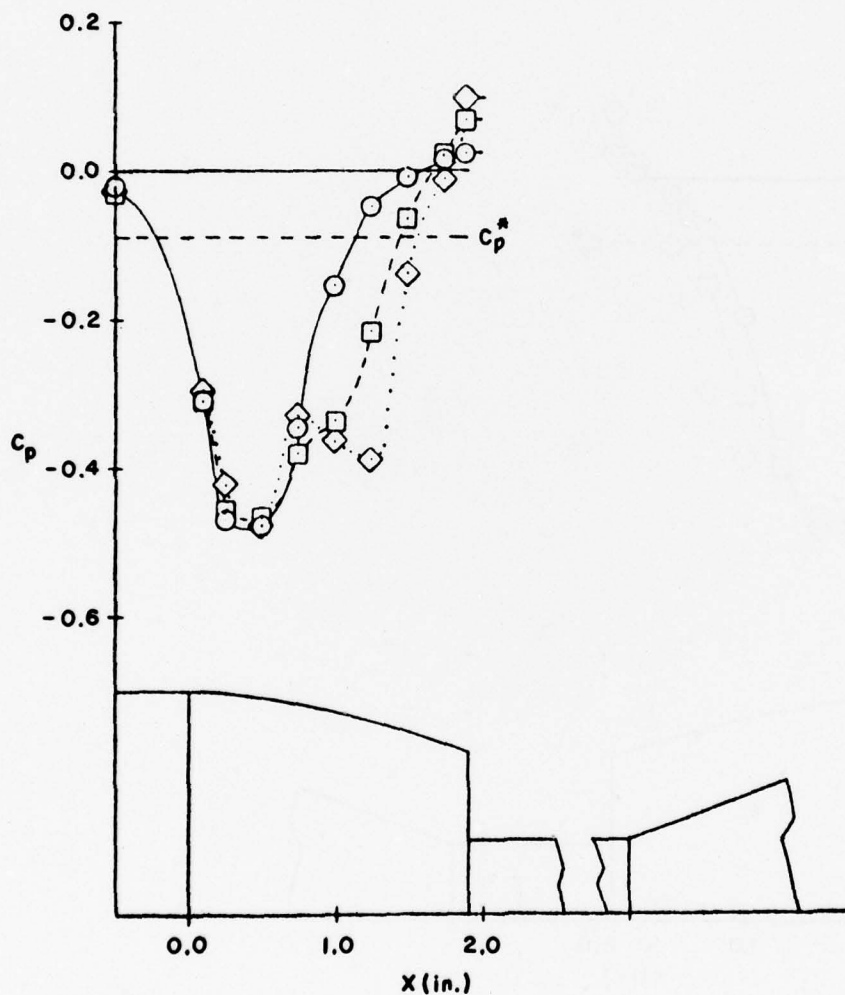


Figure 61. Mass Injection Effect on Boattail and Base Pressure Coefficients for NPR>2

SYMBOL	NPR	M_∞	p_o (psfa)	Re_L	\dot{m} (lbm/sec)	l (in.)	$C_{D_A,s}$	$C_{D_A,j}$	$\frac{D_j^2}{D_b D_M}$
—○—	3.60	.95	3000	13.4×10^6	0.000	6	.08427	.08618	0.240
—□—	3.60	.95	3000	13.4×10^6	0.063	6	.09022	.09315	0.240
...◇...	3.60	.95	3000	13.4×10^6	0.118	6	.09342	.09888	0.240

CUT-OFF
8-1 BOATTAIL

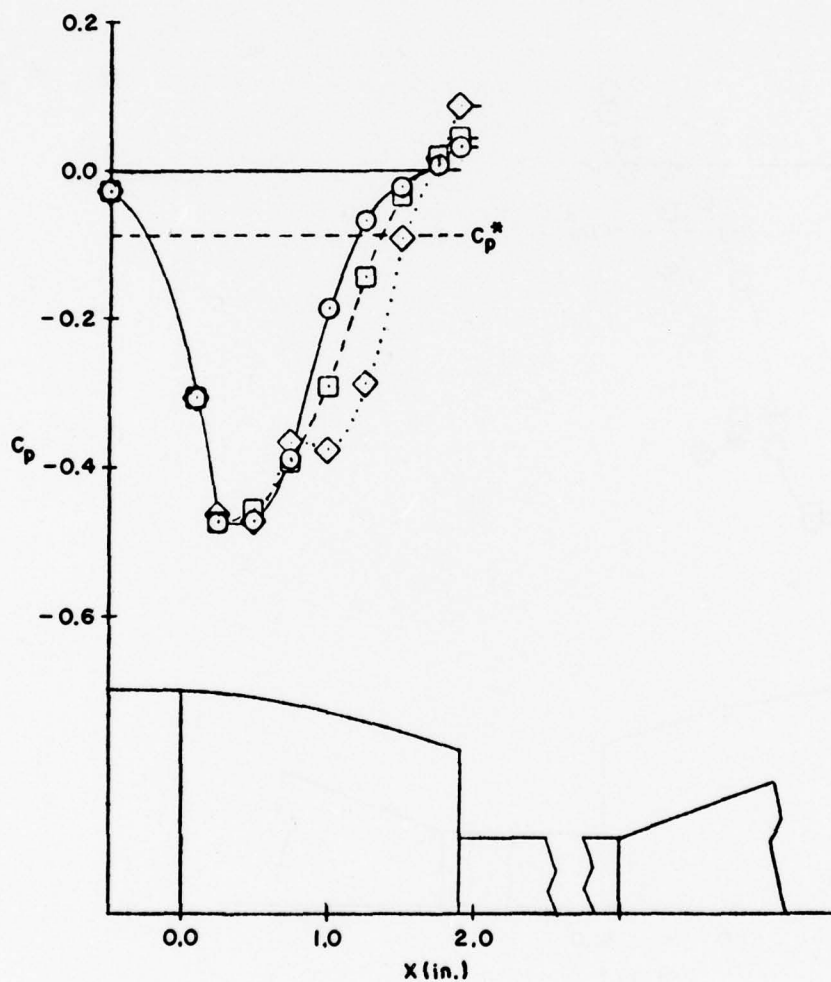


Figure 62. Mass Injection Effect on Boattail and Base Pressure Coefficients for $NPR > 2$

SYMBOL	NPR	M_∞	p_o (psfa)	Re_L	\dot{m} (lbm/sec)	l (in.)	$C_{DA,s}$	$C_{DA,j}$	$\frac{D_j^2}{D_b D_M}$
—○—	4.15	.85	2000	8.4×10^6	0.000	4	.02480	.03166	0.240
—□—	4.15	.85	2000	8.4×10^6	0.063	4	.02551	.03278	0.240
...◇...	4.15	.85	2000	8.4×10^6	0.117	4	.03465	.04276	0.240

CUT-OFF
B-I BOATTAIL

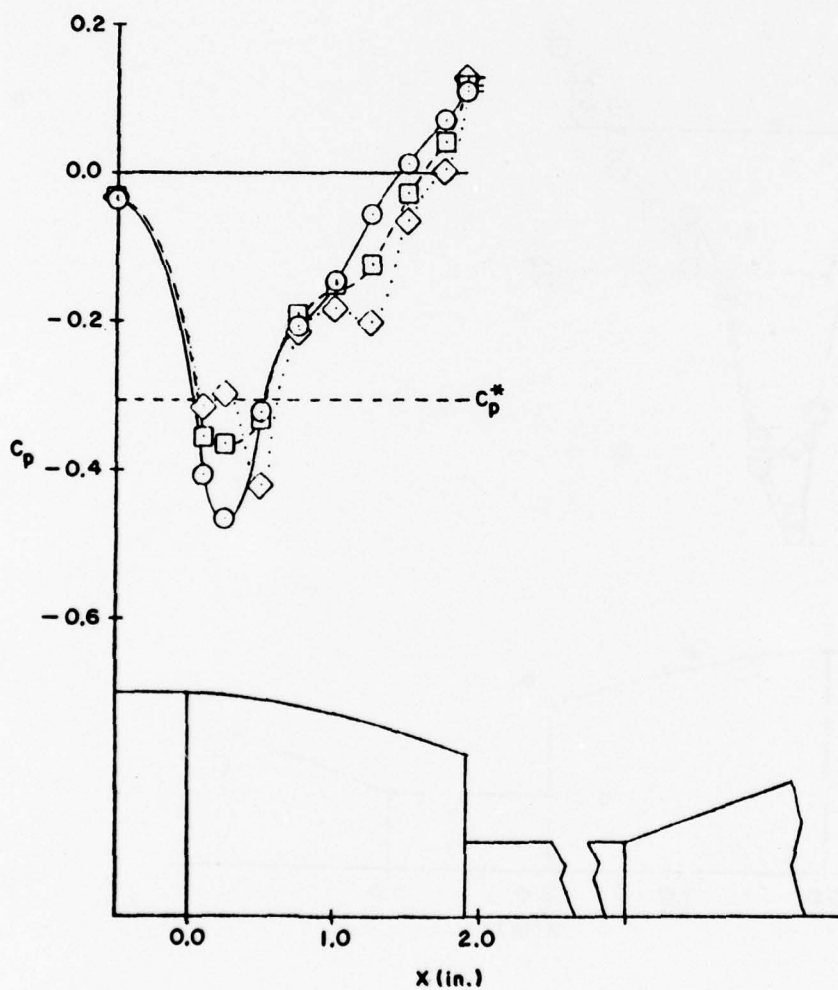


Figure 63. Mass Injection Effect on Boattail and Base Pressure Coefficients for NPR>2

SYMBOL	NPR	M_∞	p_o (psfa)	Re_L	\dot{m} (lbm/sec)	x (in.)	$C_{DA,s}$	$C_{DA,j}$	$\frac{D_j^2}{D_b D_M}$
—○—	4.14	.90	2000	8.7×10^6	0.000	4	.03070	.03740	0.240
—□—	4.14	.90	2000	8.7×10^6	0.062	4	.03550	.04295	0.240
...◇...	4.14	.90	2000	8.7×10^6	0.115	4	.04009	.04850	0.240

CUT - OFF
B - I BOATTAIL

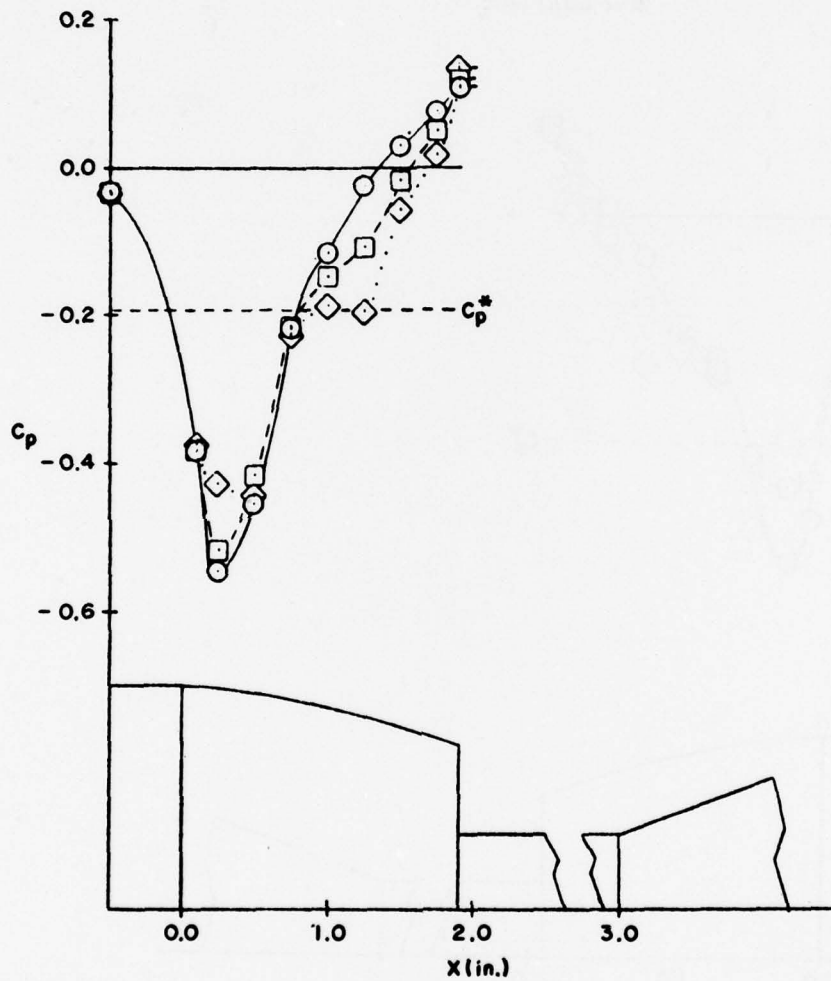


Figure 64. Mass Injection Effect on Boattail and Base Pressure Coefficients for $NPR > 2$

SYMBOL	NPR	M_∞	p_0 (psfa)	Re_L	\dot{m} (lbm/sec)	x (in.)	$C_{D_{A,s}}$	$C_{D_{A,j}}$	$\frac{D_j^2}{D_b^2 M}$
—○—	4.14	.90	3000	13.1×10^6	0.000	4	.02937	.03676	0.240
—□—	4.14	.90	3000	13.1×10^6	0.061	4	.03311	.03992	0.240
...◇...	4.14	.90	3000	13.1×10^6	0.119	4	.03858	.04669	0.240

CUT-OFF
B-I BOATTAIL

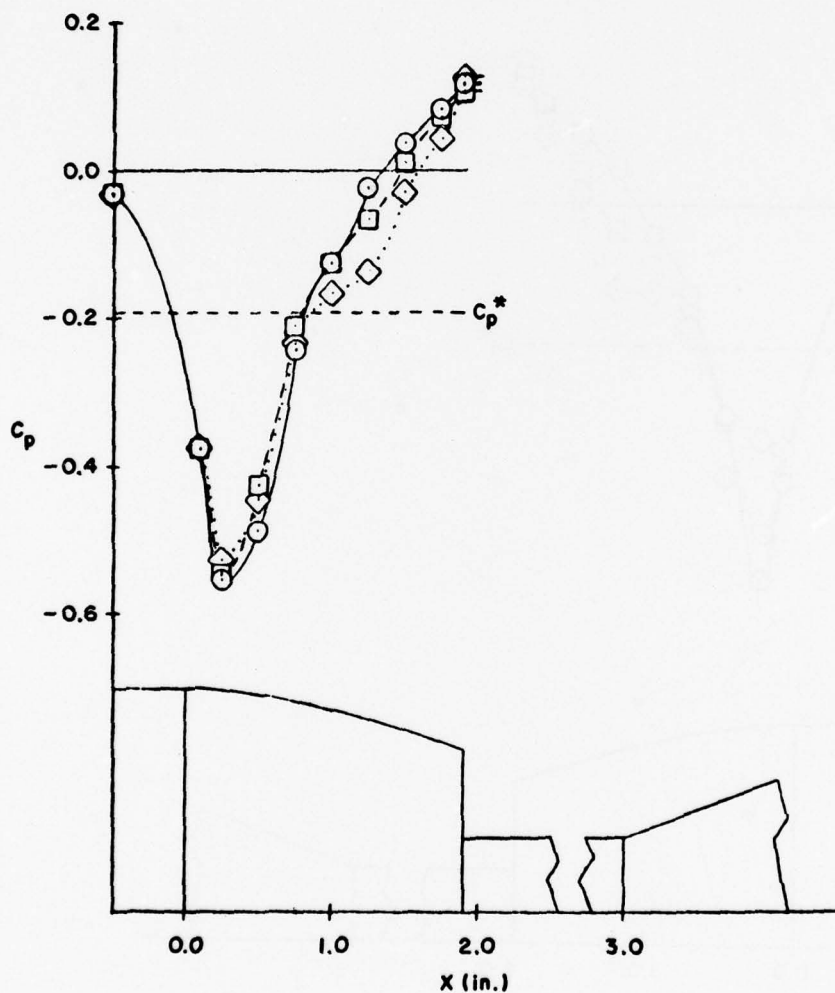


Figure 65. Mass Injection Effect on Boattail and Base Pressure Coefficients for $NPR > 2$

SYMBOL	NPR	M_∞	p_0 (psfa)	Re_L	\dot{m} (lbm/sec)	ℓ (in.)	$C_{DA,s}$	$C_{DA,j}$	$\frac{D_j^2}{D_b D_M}$
—○—	5.18	.90	2000	8.7×10^6	0.000	2	-.02585	-.01602	0.240
—□—	5.18	.90	2000	8.7×10^6	0.062	2	-.01969	-.00883	0.240
...◇...	5.18	.90	2000	8.7×10^6	0.115	2	-.01833	-.00600	0.240

CUT-OFF
B-I BOATTAIL

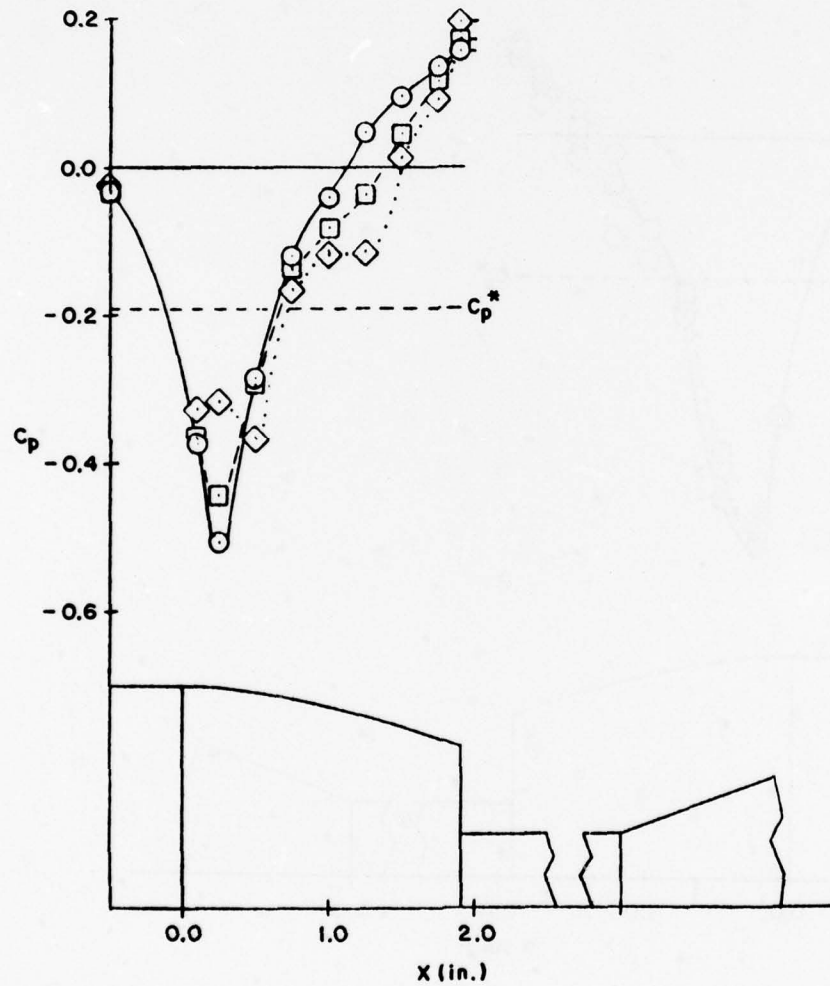


Figure 66. Mass Injection Effect on Boattail and Base Pressure Coefficients for NPR>2

SYMBOL	NPR	M_∞	p_0 (psfa)	Re_L	\dot{m} (lbm/sec)	x (in.)	$C_{D_A,s}$	$C_{D_A,j}$	$\frac{D_j^2}{D_b D_M}$
—○—	5.18	.90	3000	13.1×10^6	0.000	2	-.02615	-.01549	0.240
—□—	5.18	.90	3000	13.1×10^6	0.062	2	-.02244	-.01243	0.240
...◇...	5.18	.90	3000	13.1×10^6	0.117	2	-.01957	-.00786	0.240

CUT-OFF
8-1 BOATTAIL

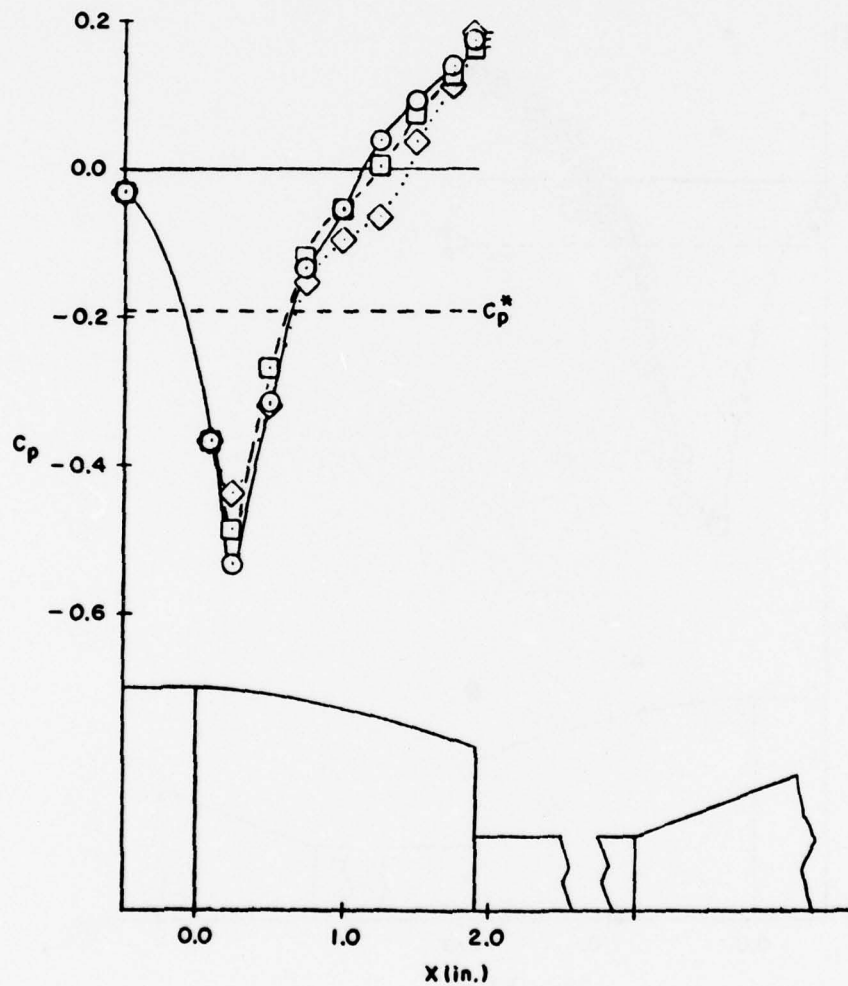


Figure 67. Mass Injection Effect on Boattail and Base Pressure Coefficients for $NPR > 2$

SYMBOL	NPR	M_∞	p_0 (psfa)	Re_L	\dot{m} (lbm/sec)	x (in.)	$C_{DA,s}$	$C_{DA,j}$	$\frac{D_j^2}{D_b D_M}$
—○—	5.15	.95	3000	13.4×10^6	0.000	2	-.02312	-.01398	0.240
—□—	5.15	.95	3000	13.4×10^6	0.064	2	-.01696	-.00714	0.240
...◇...	5.15	.95	3000	13.4×10^6	0.115	2	-.00934	-.00240	0.240

CUT-OFF
B-I BOATTAIL

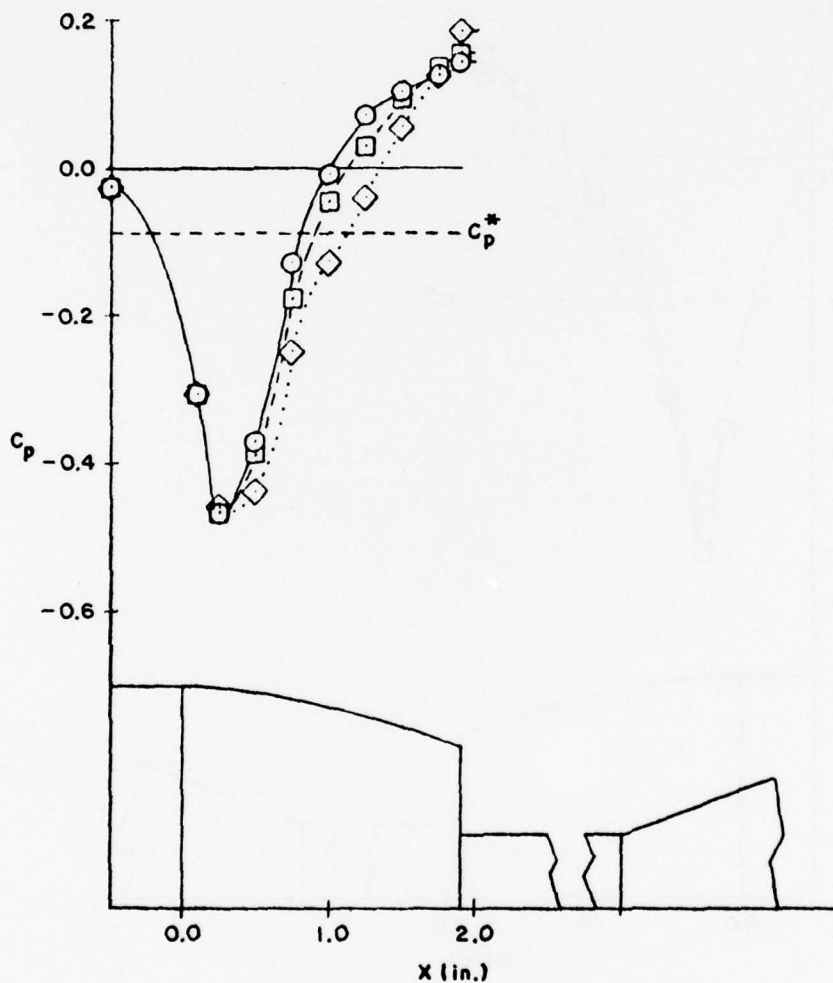


Figure 68. Mass Injection Effect on Boattail and Base Pressure Coefficients for $NPR > 2$

SYMBOL	NPR	M_∞	p_o (psfa)	Re_L	\dot{m} (lbm/sec)	$C_{DA,s}$	$C_{DA,j}$	$\frac{D_j^2}{D_b D_M}$
—○—	2.0	.90	2000	8.7×10^6	0.000	.08832	.08984	0.340
—□—	2.0	.90	2000	8.7×10^6	0.062	.09130	.09317	0.340
...◇...	2.0	.90	2000	8.7×10^6	0.118	.09227	.09463	0.340

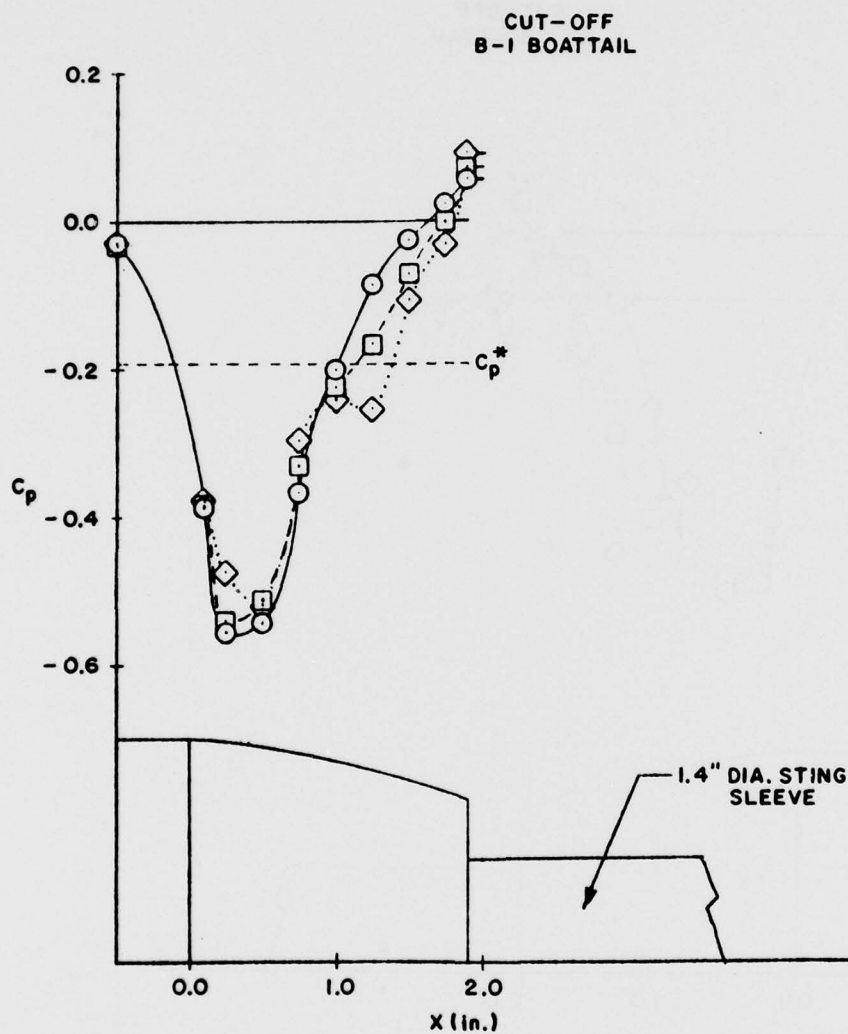


Figure 69. Mass Injection Effect on Boattail and Base Pressure Coefficients for NPR=2, $D_S > 1"$

SYMBOL	NPR	M_∞	p_o (psfa)	Re_L	\dot{m} (lbm/sec)	$C_{DA,s}$	$C_{DA,j}$	$\frac{D_j^2}{D_b D_M}$
—○—	2.0	.95	2000	8.9×10^6	0.000	.10859	.10860	0.340
—□—	2.0	.95	2000	8.9×10^6	0.062	.11774	.11883	0.340
...◇...	2.0	.95	2000	8.9×10^6	0.115	.12002	.12209	0.340

CUT-OFF
B-1 BOATTAIL

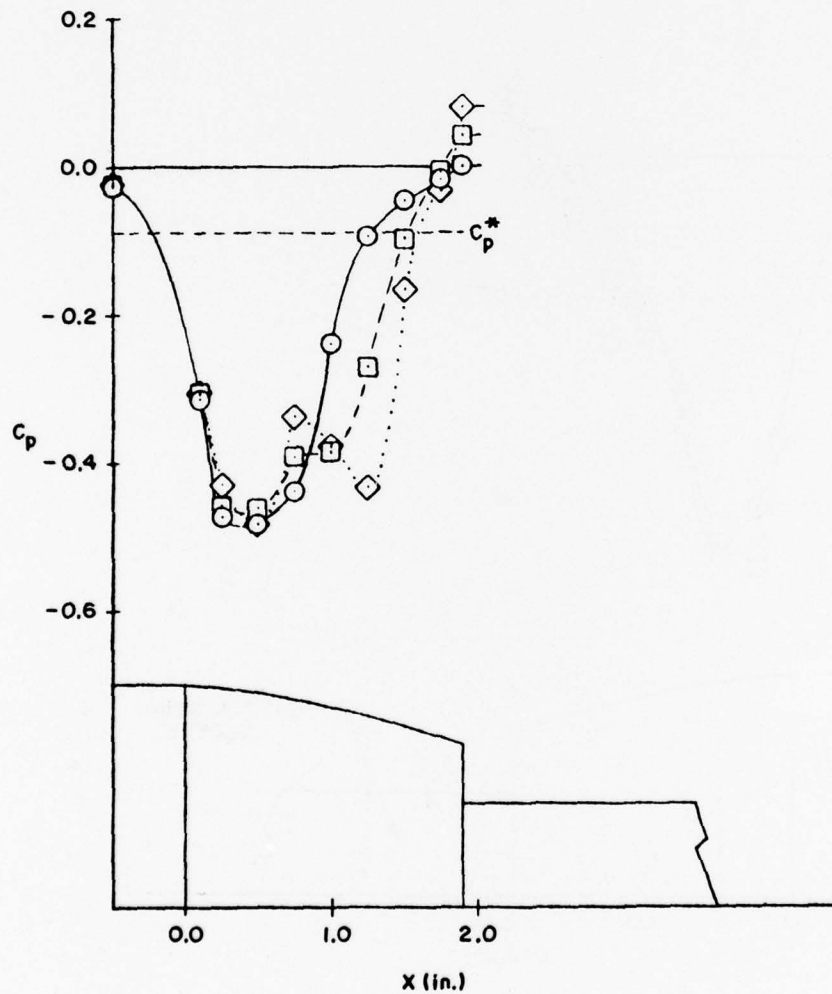


Figure 70. Mass Injection Effect on Boattail and Base Pressure Coefficients for NPR=2, $D_S > 1"$

SYMBOL	NPR	M_∞	p_o (psfa)	Re_L	\dot{m} (lbm/sec)	$C_{DA,s}$	$C_{DA,j}$	$\frac{D_j^2}{D_b D_M}$
—○—	2.0	.90	2000	8.7×10^6	0.000	.08171	.08171	0.397
—□—	2.0	.90	2000	8.7×10^6	0.061	.08331	.08331	0.397
...◇...	2.0	.90	2000	8.7×10^6	0.114	.08440	.08440	0.397

CUT-OFF
B-I BOATTAIL

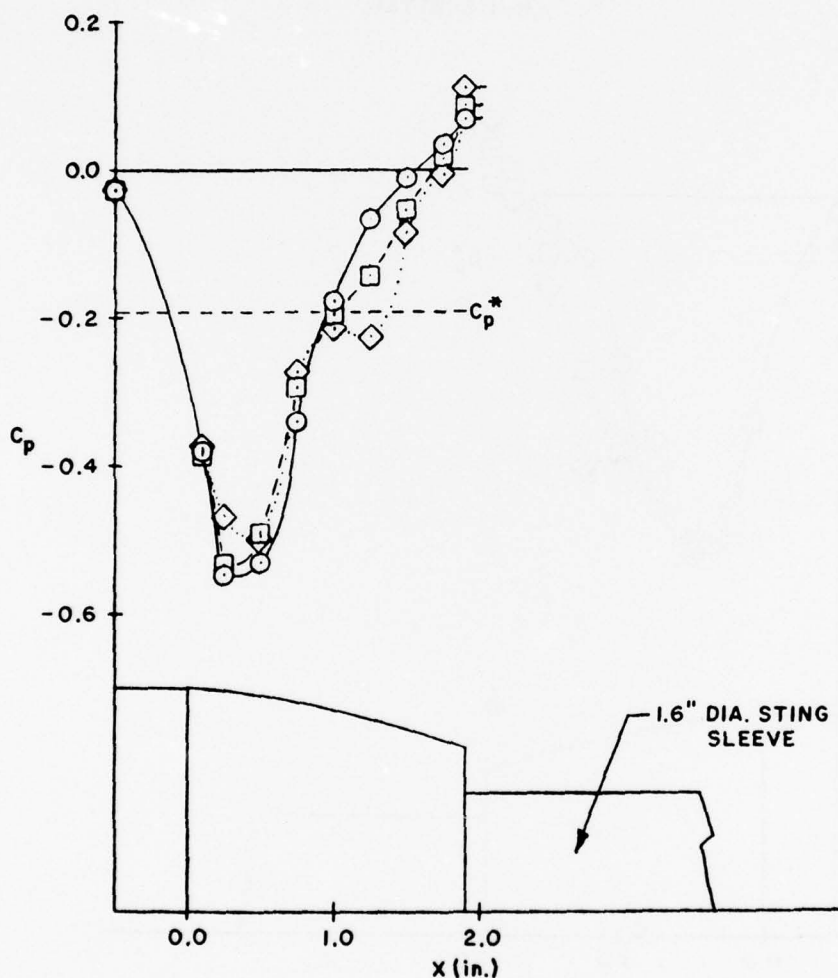


Figure 71. Mass Injection Effect on Boattail and Base Pressure Coefficients for NPR=2, $D_S > 1"$

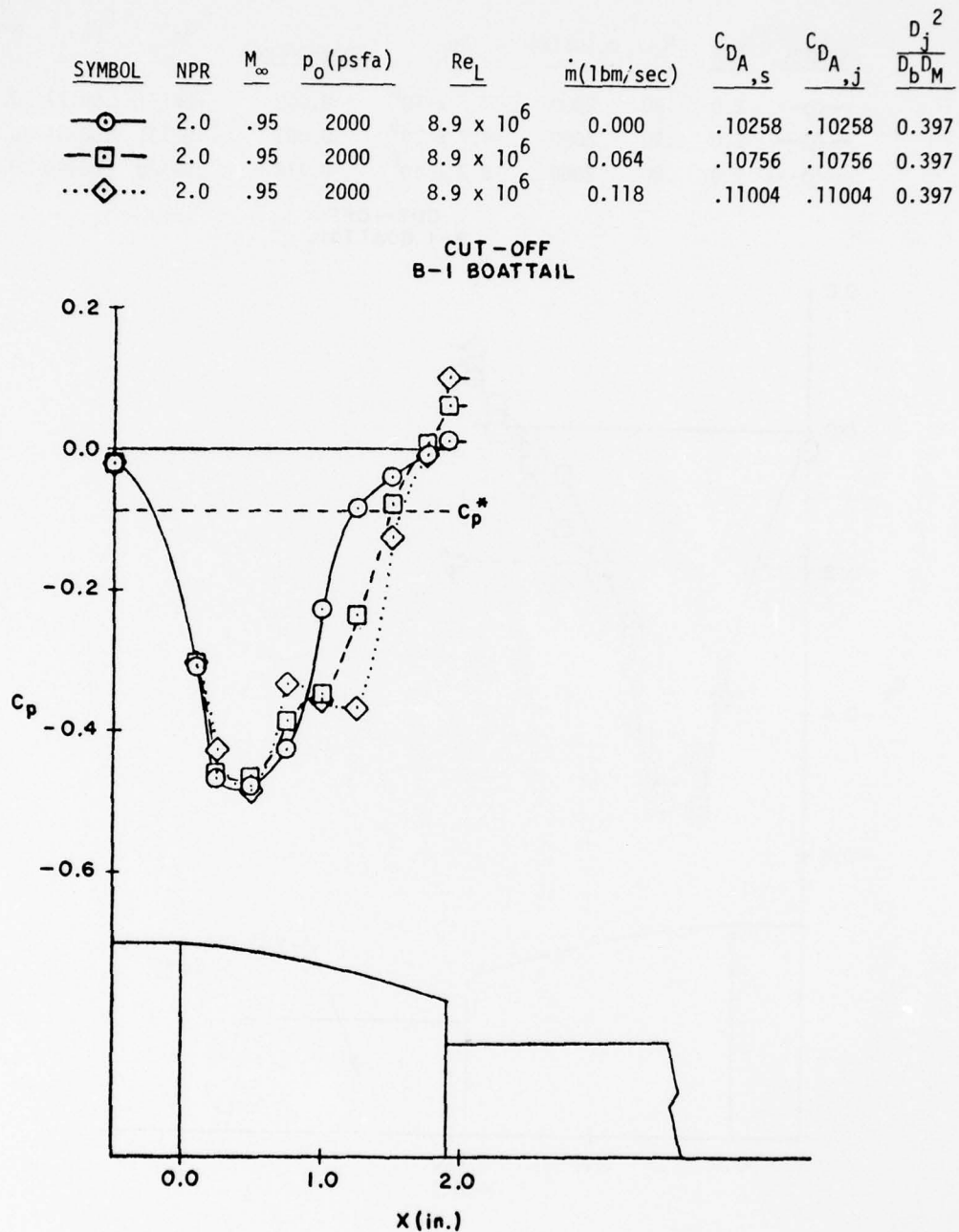


Figure 72. Mass Injection Effect on Boattail and Base Pressure Coefficients for NPR=2, $D_S > 1"$

SYMBOL	NPR	M_∞	p_o (psfa)	Re_L	\dot{m} (lbm/sec)	$C_{DA,s}$	$C_{DA,j}$	$\frac{D_j^2}{D_b D_M}$
—○—	2.0	.90	2000	8.7×10^6	0.000	.07629	.07366	0.464
—□—	2.0	.90	2000	8.7×10^6	0.062	.07686	.07378	0.464
...◇...	2.0	.90	2000	8.7×10^6	0.114	.07895	.07526	0.464

CUT-OFF
B-I BOATTAIL

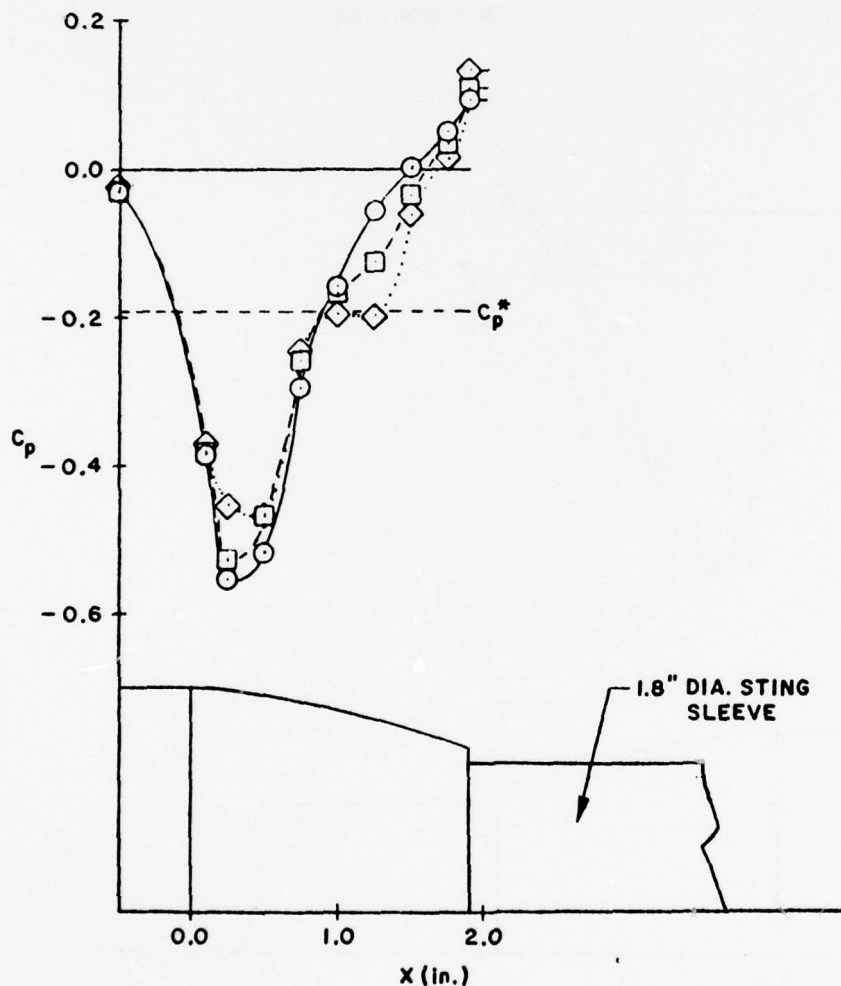


Figure 73. Mass Injection Effect on Boattail and Base Pressure Coefficients for NPR=2, $D_S > 1"$

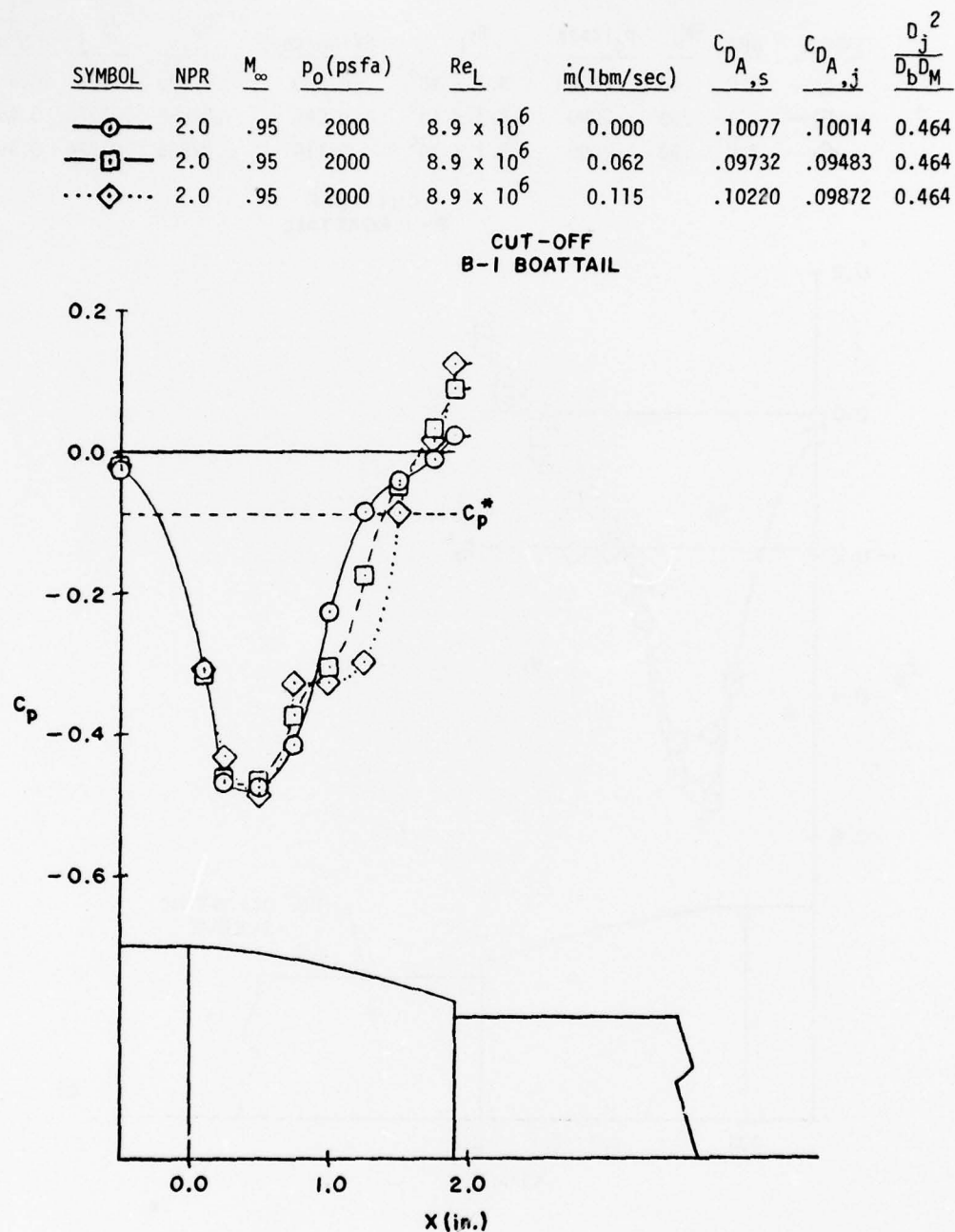


Figure 74. Mass Injection Effect on Boattail and Base Pressure Coefficients for NPR=2, $D_S > 1"$

SYMBOL	NPR	M_∞	p_o (psfa)	Re_L	\dot{m} (lbm/sec)	$C_{DA,s}$	$C_{DA,j}$	$\frac{D_j^2}{D_b D_M}$	$\frac{D_s}{D_b}$
---△---	2.0	.90	2000	8.7×10^6	0.000	.09607	.09843	0.240	.465
—○—	2.0	.90	2000	8.7×10^6	0.000	.08832	.08984	0.340	.651
—□—	2.0	.90	2000	8.7×10^6	0.000	.08171	.08171	0.397	.744
...◇...	2.0	.90	2000	8.7×10^6	0.000	.07629	.07366	0.464	.837

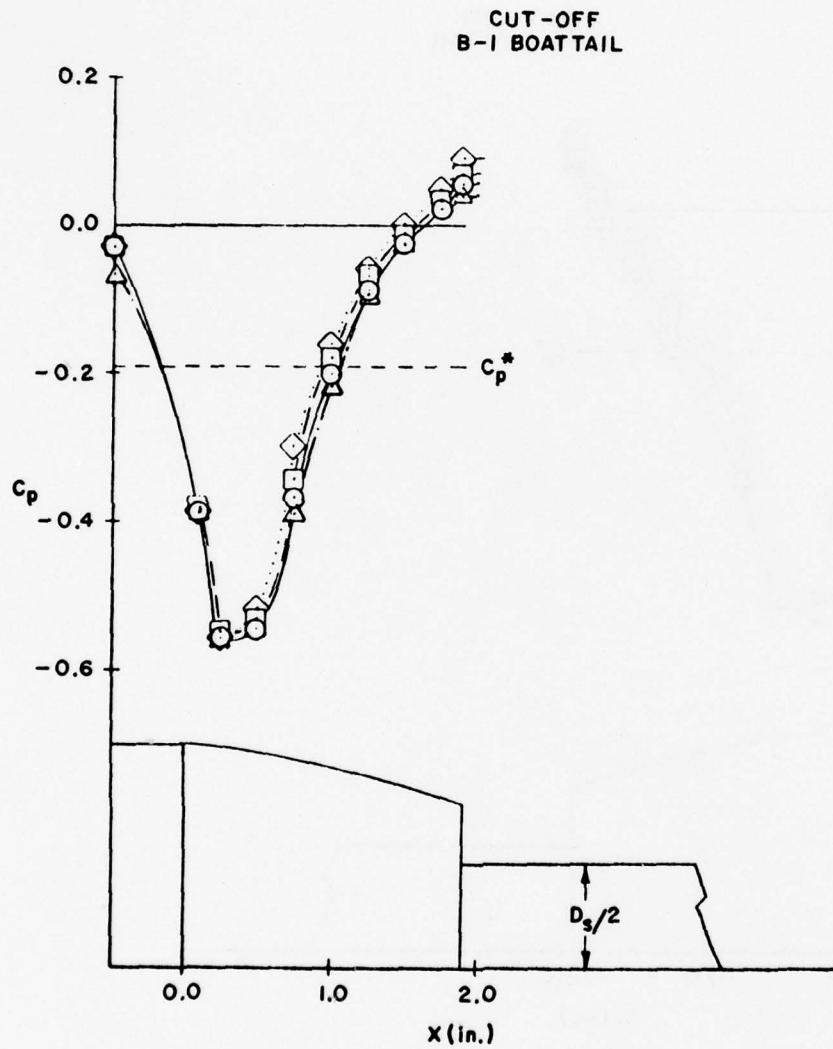


Figure 75. Sting Size Effect on Boattail and Base Pressure Coefficients

SYMBOL	NPR	M_∞	p_o (psfa)	Re_L	\dot{m} (lbm/sec)	$C_{DA,s}$	$C_{DA,j}$	$\frac{D_j^2}{D_b D_M}$	$\frac{D_s}{D_b}$
---△---	2.0	.90	2000	8.7×10^6	0.063	.09717	.10089	0.240	.465
---○---	2.0	.90	2000	8.7×10^6	0.062	.09130	.09317	0.340	.651
---□---	2.0	.90	2000	8.7×10^6	0.061	.08331	.08331	0.397	.744
---◇---	2.0	.90	2000	8.7×10^6	0.062	.07686	.07378	0.464	.837

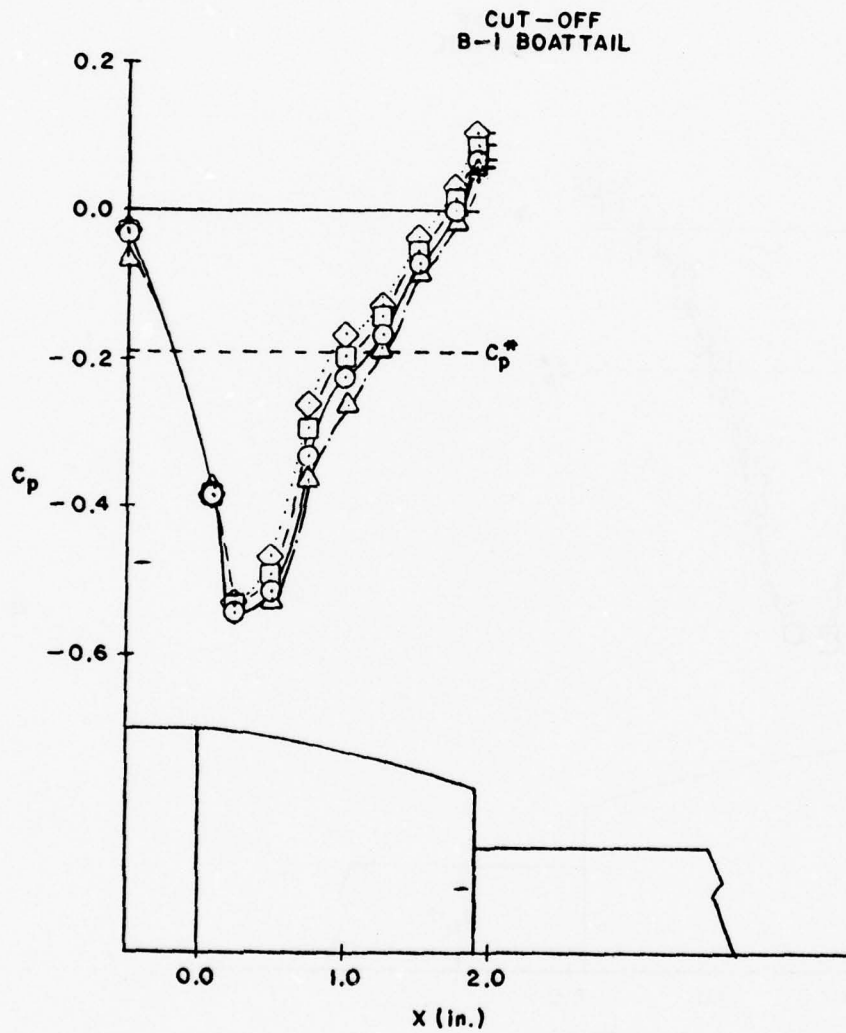


Figure 76. Sting Size Effect on Boattail and Base Pressure Coefficients

SYMBOL	NPR	M_∞	p_o (psfa)	Re_L	\dot{m} (lbm/sec)	$C_{DA,s}$	$C_{DA,j}$	$\frac{D_j^2}{D_b D_M}$	$\frac{D_s}{D_b}$
---△---	2.0	.90	2000	8.7×10^6	0.116	.09730	.10206	0.240	.465
---○---	2.0	.90	2000	8.7×10^6	0.118	.09227	.09463	0.340	.651
---□---	2.0	.90	2000	8.7×10^6	0.114	.08440	.08440	0.397	.744
---◇---	2.0	.90	2000	8.7×10^6	0.114	.07695	.07526	0.464	.837

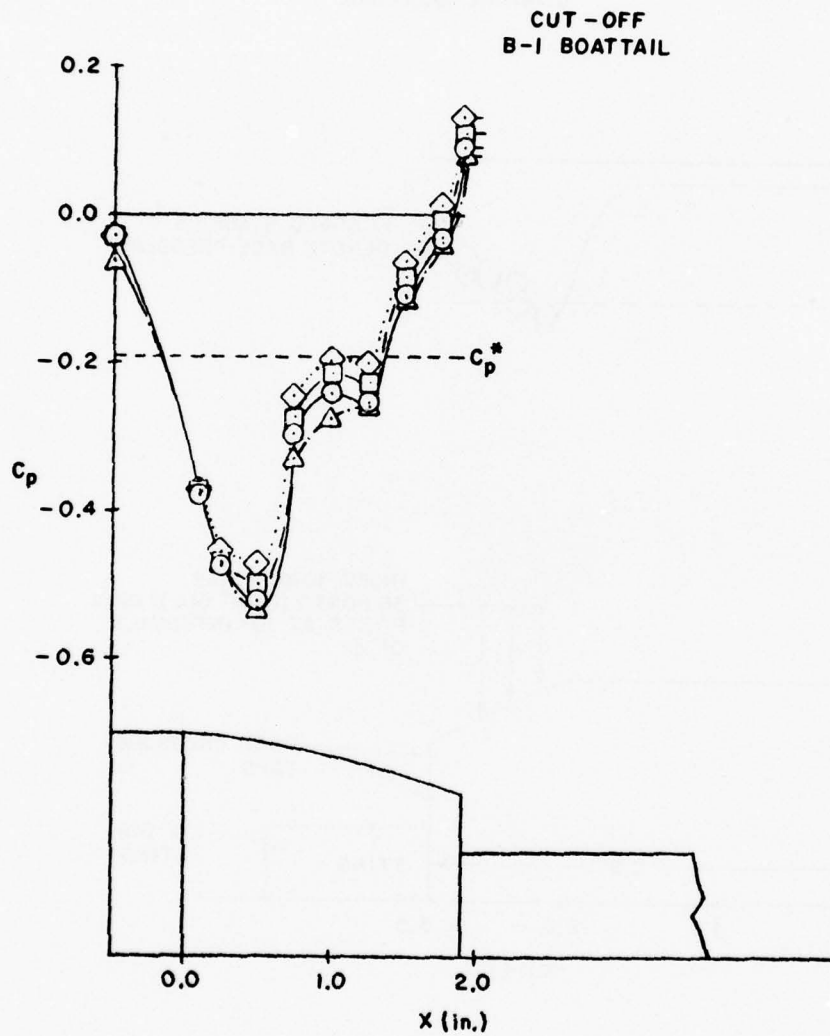


Figure 77. Sting Size Effect on Boattail and Base Pressure Coefficients

SYMBOL	NPR	M_∞	p_o (psfa)	Re_L	\dot{m} (lbm/sec)	$C_{DA,s}$	$C_{DA,j}$	$\frac{D_j^2}{D_b D_M}$
—○—	2.0	.90	2000	8.7×10^6	0.000	.10732	.10300	0.205
—□—	2.0	.90	2000	8.7×10^6	0.033	.10163	.09766	0.205
...◇...	2.0	.90	2000	8.7×10^6	0.066	.10102	.09787	0.205

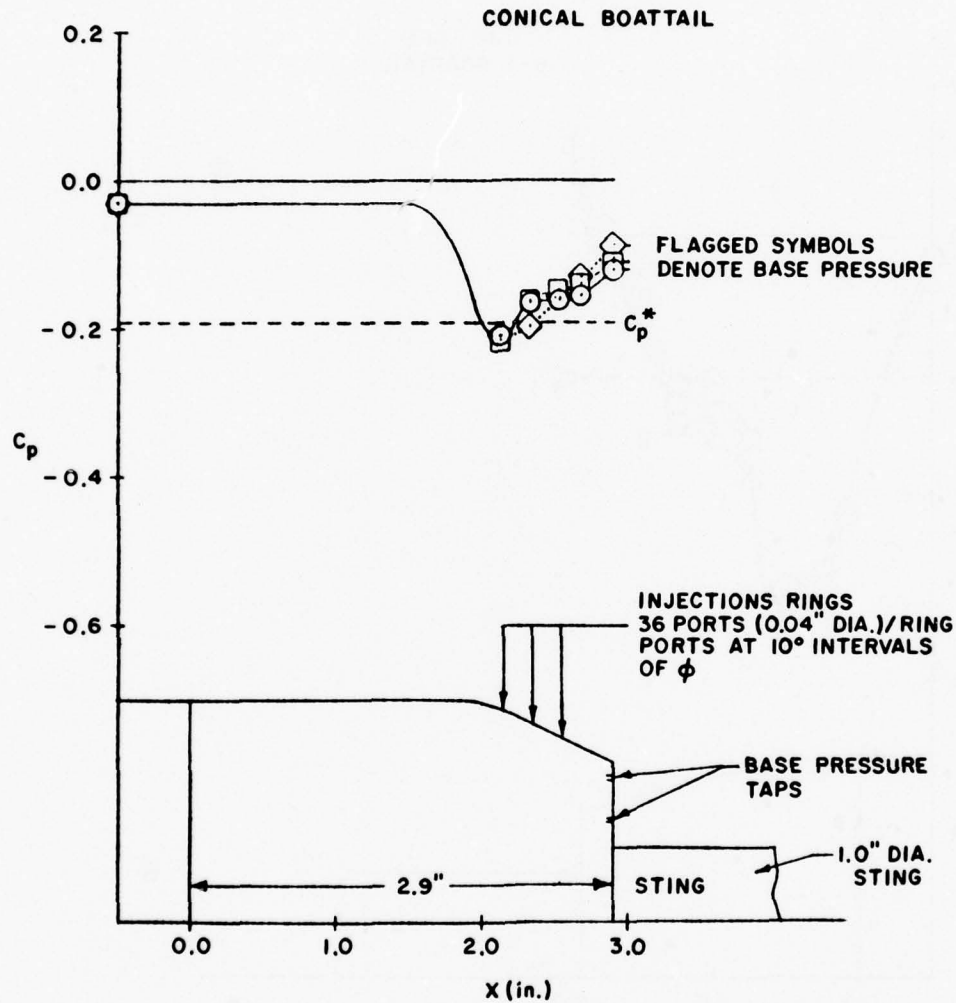


Figure 78. Mass Injection Effect on Boattail and Base Pressure Coefficients for NPR=2.0, $D_S=1"$

SYMBOL	NPR	M_∞	p_o (psfa)	Re_L	\dot{m} (lbm/sec)	$C_{D_A,s}$	$C_{D_A,j}$	$\frac{D_j^2}{D_b^2 M}$
—○—	2.0	.95	2000	8.9×10^6	0.000	.11335	.10861	0.205
—□—	2.0	.95	2000	8.9×10^6	0.035	.11235	.10771	0.205
...◇...	2.0	.95	2000	8.9×10^6	0.066	.10768	.10389	0.205

CONICAL BOATTAIL

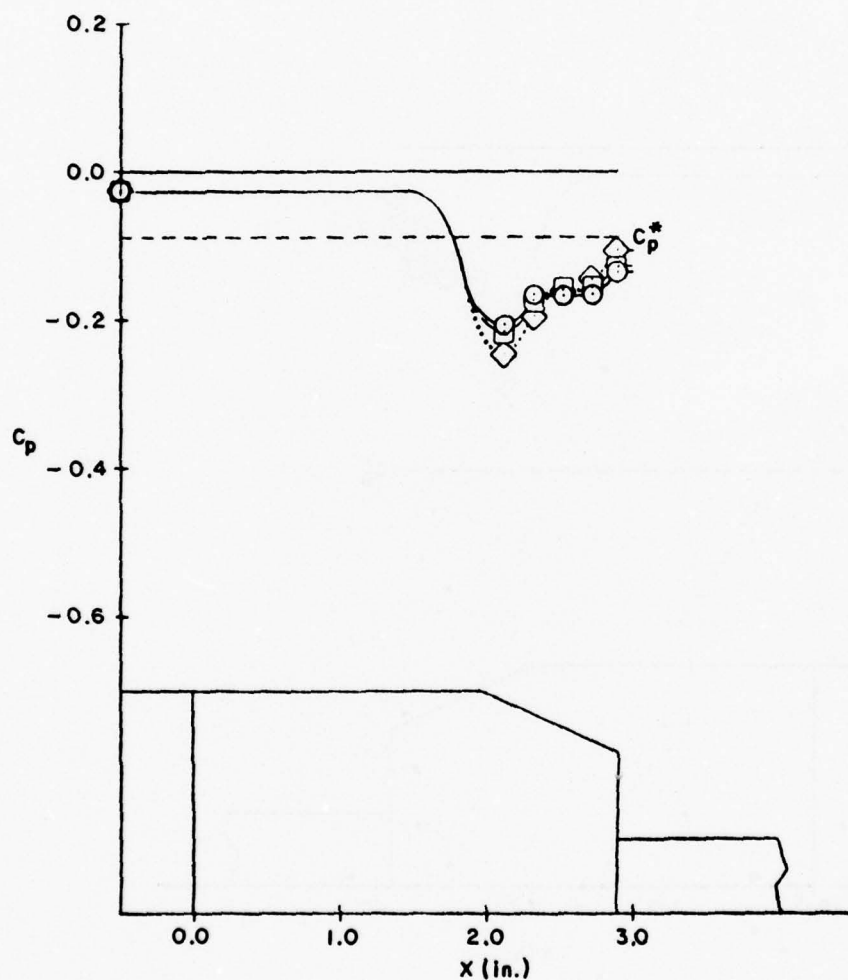


Figure 79. Mass Injection Effect on Boattail and Base Pressure Coefficients for NPR=2.0, $D_S=1"$

SYMBOL	NPR	M_∞	p_o (psfa)	Re_L	\dot{m} (lbm/sec)	$C_{DA,s}$	$C_{DA,j}$	$\frac{D_j^2}{D_b D_M}$
—○—	2.0	.80	2000	8.3×10^6	0.000	.11616	.11183	0.205
—□—	2.0	.80	2000	8.3×10^6	0.033	.10389	.09751	0.205
...◇...	2.0	.80	2000	8.3×10^6	0.066	.09942	.09512	0.205

CONICAL BOATTAIL

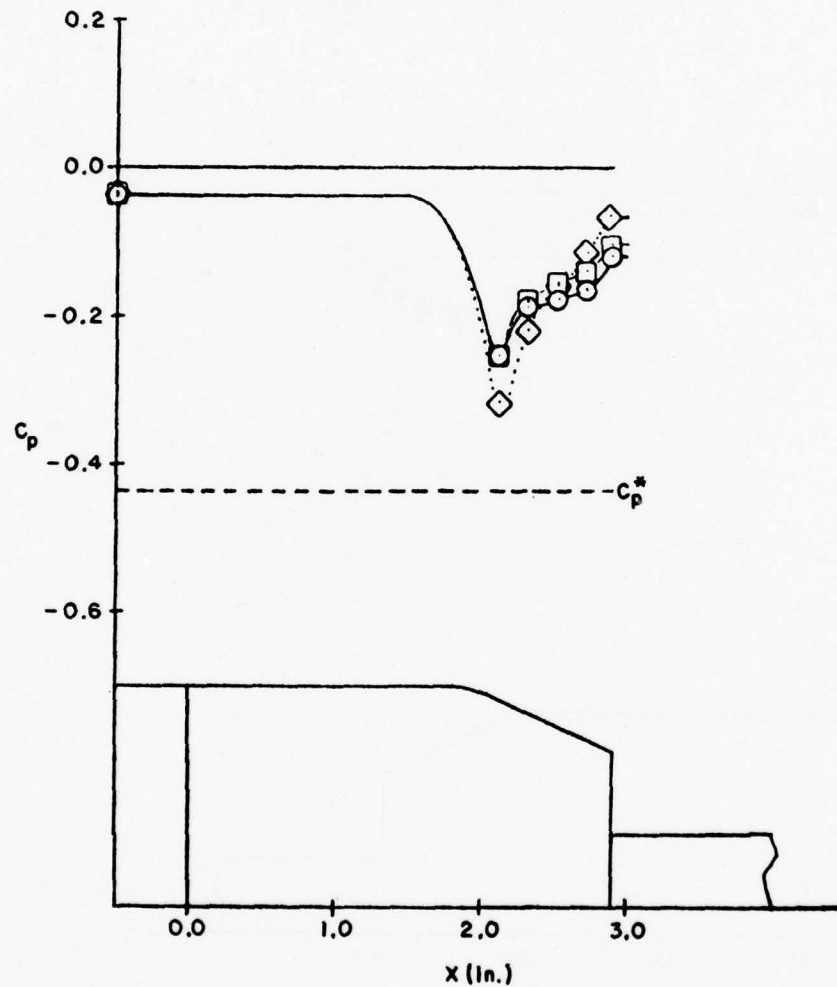


Figure 80. Mass Injection Effect on Boattail and Base Pressure Coefficients for NPR=2.0, $D_S=1"$

SYMBOL	NPR	M_∞	p_o (psfa)	Re_L	\dot{m} (lbm/sec)	$C_{DA,s}$	$C_{DA,j}$	$\frac{D_j^2}{D_b D_M}$
—○—	2.0	.85	2000	8.4×10^6	0.000	.10512	.10111	0.205
—□—	2.0	.85	2000	8.4×10^6	0.035	.09919	.09284	0.205
...◇...	2.0	.85	2000	8.4×10^6	0.065	.09529	.09082	0.205

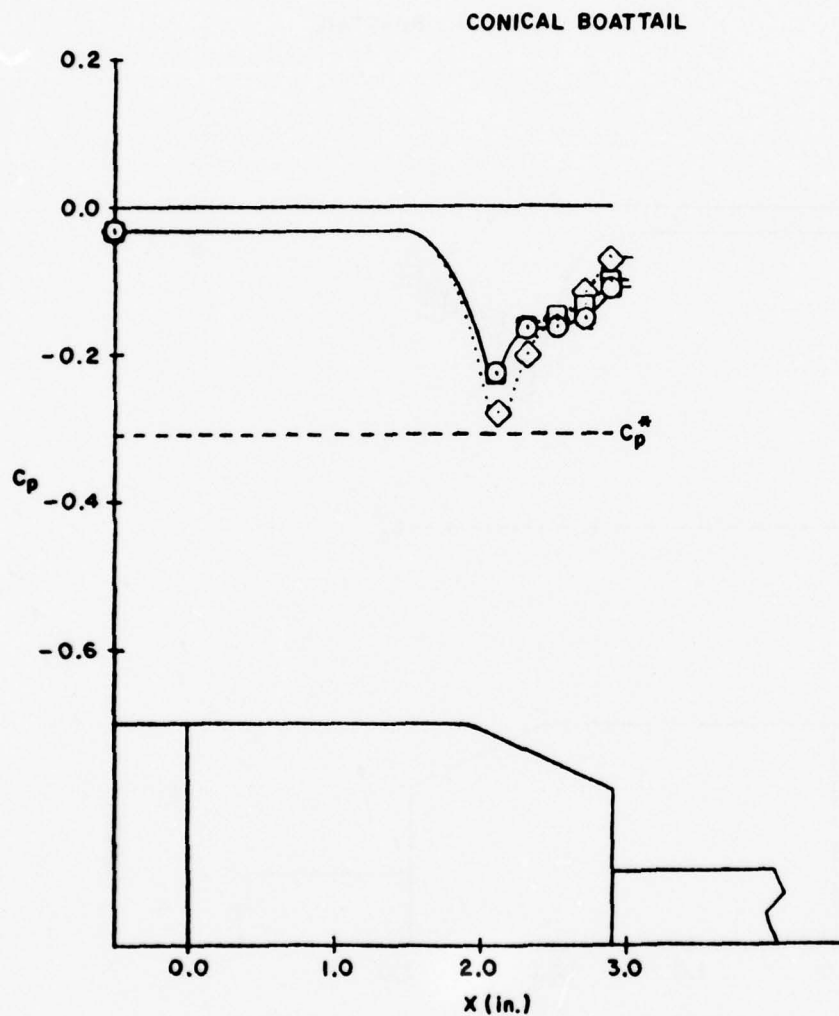


Figure 81. Mass Injection Effect on Boattail and Base Pressure Coefficients for NPR=2.0, $D_S=1"$

SYMBOL	NPR	M_∞	p_o (psfa)	Re_L	\dot{m} (lbm/sec)	$C_{DA,s}$	$C_{DA,j}$	$\frac{D_j^2}{D_b D_M}$
—○—	2.0	.80	3000	12.4×10^6	0.000	.10184	.09805	0.205
—□—	2.0	.80	3000	12.4×10^6	0.032	.09170	.08842	0.205
...◇...	2.0	.80	3000	12.4×10^6	0.066	.09016	.08725	0.205

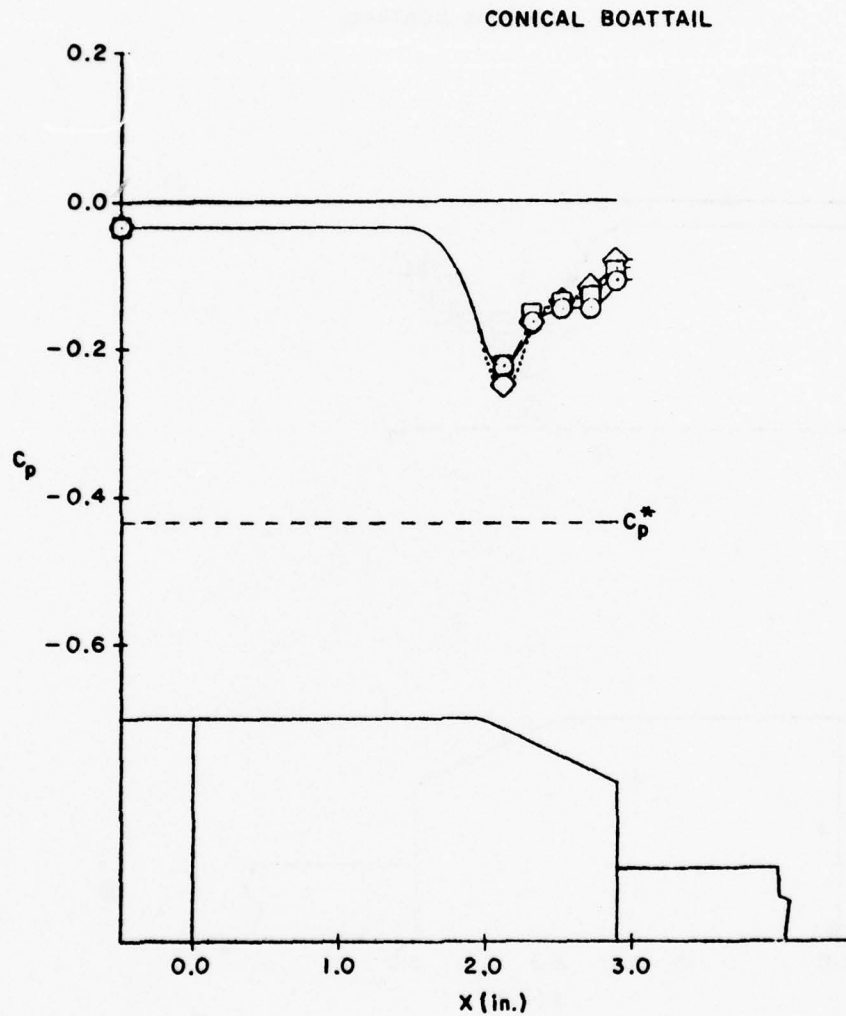


Figure 82. Mass Injection Effect on Boattail and Base Pressure Coefficients for NPR=2.0, $D_S=1"$

SYMBOL	NPR	M_∞	p_0 (psfa)	Re_L	\dot{m} (lbm/sec)	$C_{DA,s}$	$C_{DA,j}$	$\frac{D_j^2}{D_b D_M}$
—○—	2.0	.85	3000	12.7×10^6	0.000	.10241	.09845	.0205
—□—	2.0	.85	3000	12.7×10^6	0.033	.09806	.09428	.0205
—◇—	2.0	.85	3000	12.7×10^6	0.067	.09527	.09195	.0205

CONICAL BOATTAIL

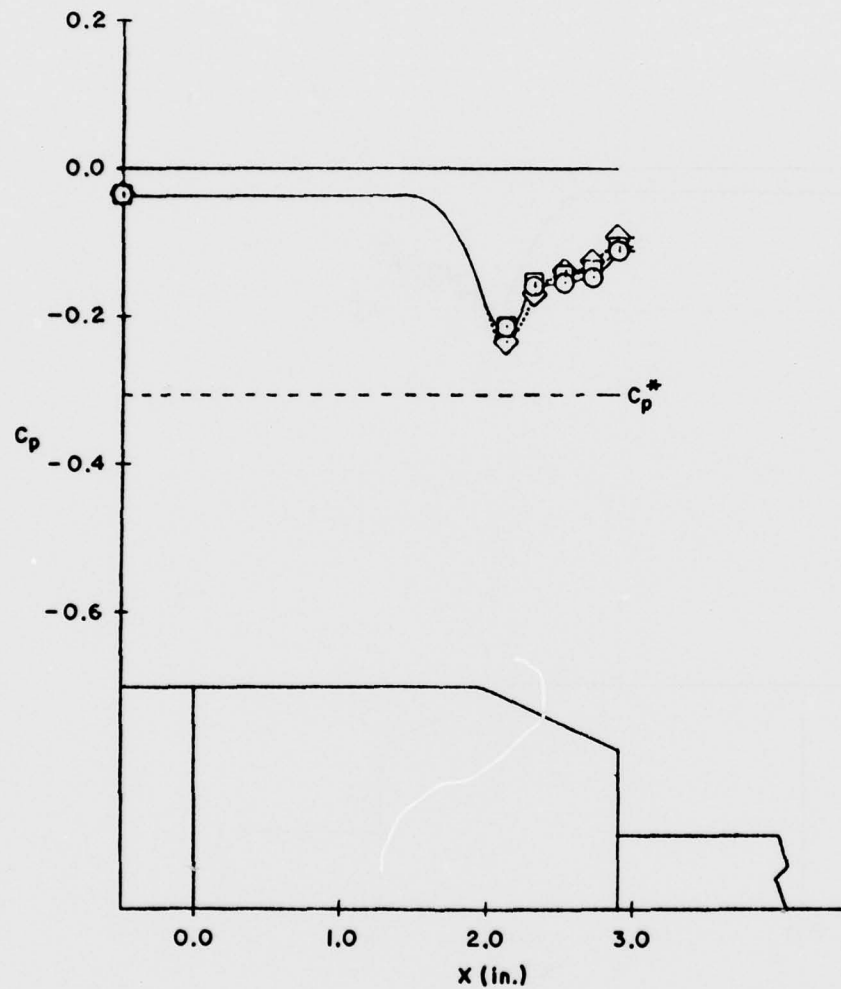


Figure 83. Mass Injection Effect on Boattail and Base Pressure Coefficients for NPR=2.0, $D_S=1"$

SYMBOL	NPR	M_∞	p_o (psfa)	Re_L	\dot{m} (lbm/sec)	$C_{DA,s}$	$C_{DA,j}$	$\frac{D_j^2}{D_b D_M}$
—○—	2.0	.90	3000	13.1×10^6	0.000	.10477	.10047	0.205
—□—	2.0	.90	3000	13.1×10^6	0.033	.10390	.09961	0.205
—◇—	2.0	.90	3000	13.1×10^6	0.066	.09915	.09546	0.205

CONICAL BOATTAIL

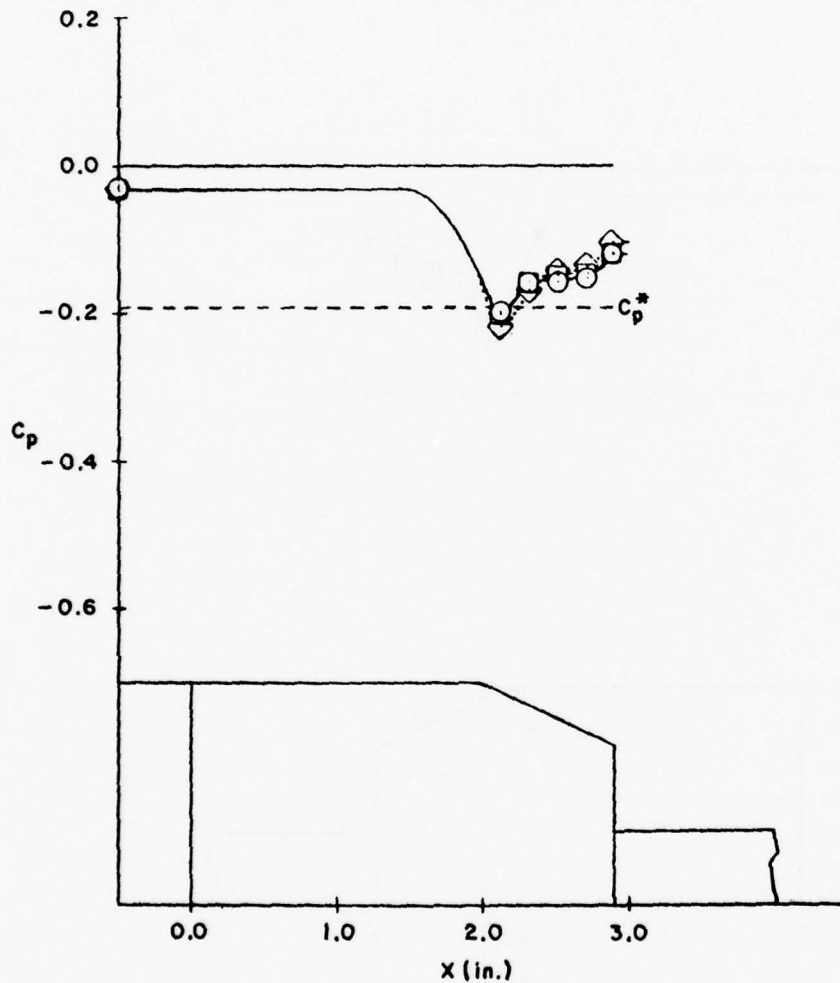


Figure 84. Mass Injection Effect on Boattail and Base Pressure Coefficients for NPR=2.0, $D_S=1"$

SYMBOL	NPR	M_∞	p_o (psfa)	Re_L	\dot{m} (lbm/sec)	$C_{DA,s}$	$C_{DA,j}$	$\frac{D_j^2}{D_b D_M}$
—○—	2.0	.95	3000	13.4×10^6	0.000	.11374	.10892	0.205
—□—	2.0	.95	3000	13.4×10^6	0.033	.10950	.10497	0.205
...◇...	2.0	.95	3000	13.4×10^6	0.066	.10723	.10301	0.205

CONICAL BOATTAIL

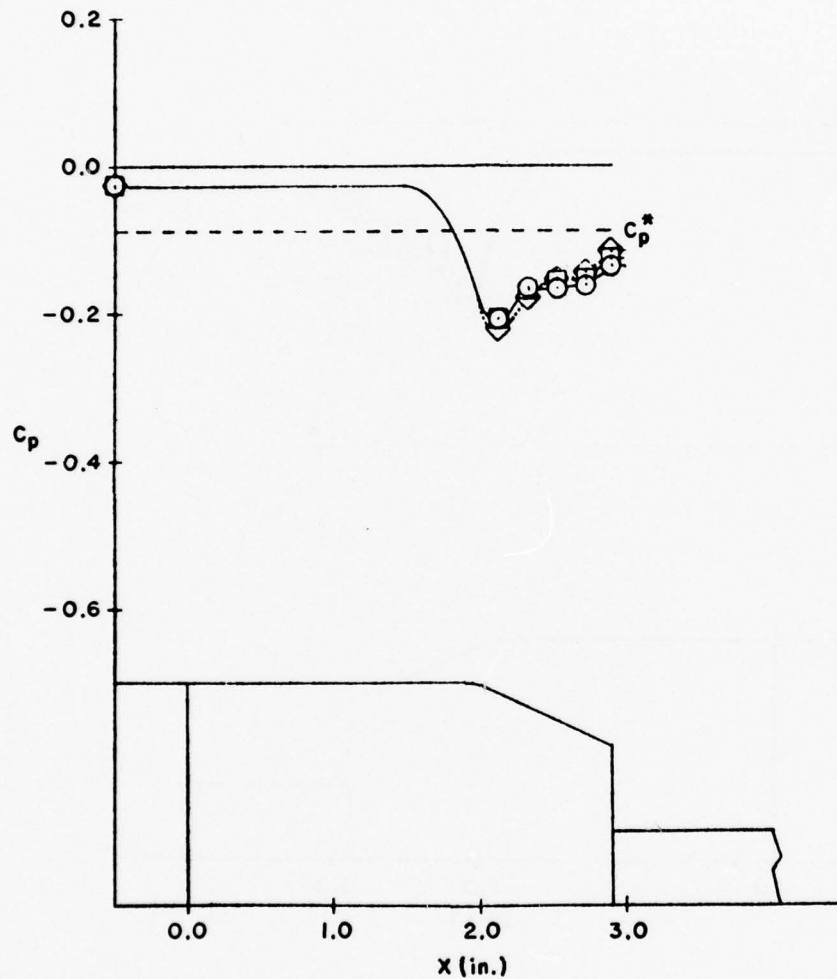


Figure 85. Mass Injection Effect on Boattail and Base Pressure Coefficients for NPR=2.0, $D_S=1"$

SYMBOL	NPR	M_∞	p_o (psfa)	Re_L	\dot{m} (lbm/sec)	$C_{DA,s}$	$C_{DA,j}$	$\frac{D_j^2}{D_b D_M}$
—○—	2.0	.80	2000	8.3×10^6	0.000	.11616	.11183	0.205
—□—	2.0	.80	3000	12.4×10^6	0.000	.10184	.09805	0.205

CONICAL BOATTAIL

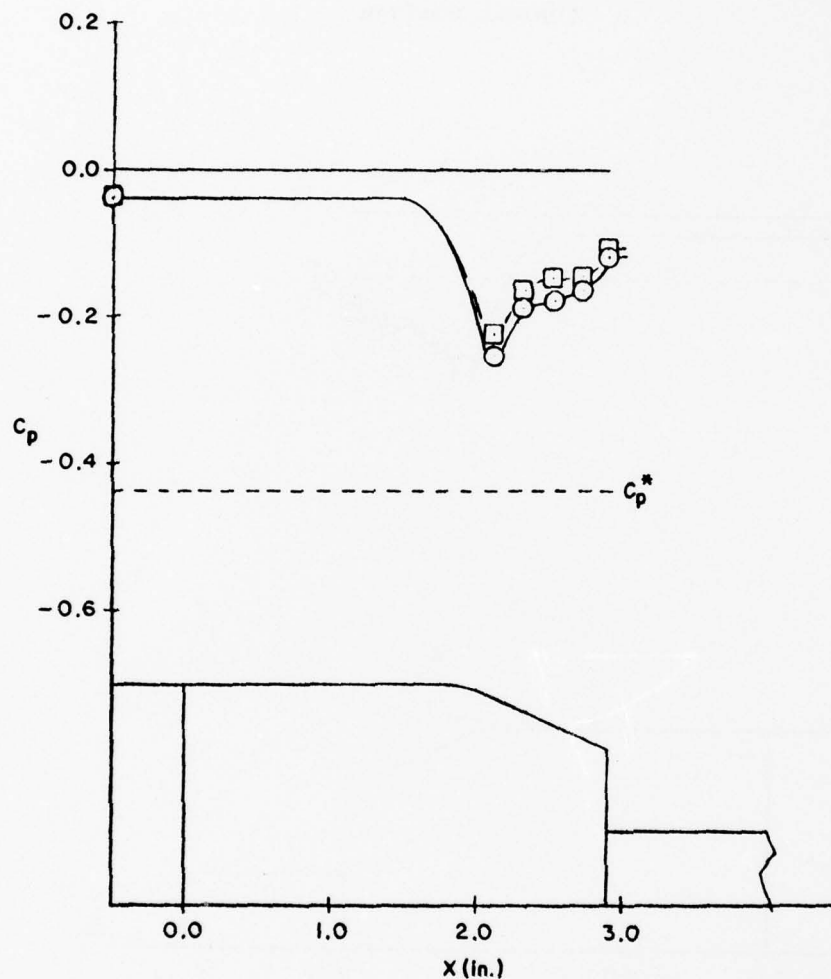


Figure 86. Reynolds Number Effect on Boattail and Base Pressure Coefficients

SYMBOL	NPR	M_∞	p_o (psfa)	Re_L	\dot{m} (lbm/sec)	$C_{DA,s}$	$C_{DA,j}$	$\frac{D_j^2}{D_b D_M}$
—○—	2.0	.85	2000	8.4×10^6	0.000	.10512	.10111	0.205
—□—	2.0	.85	3000	12.7×10^6	0.000	.10241	.09845	0.205

CONICAL BOATTAIL

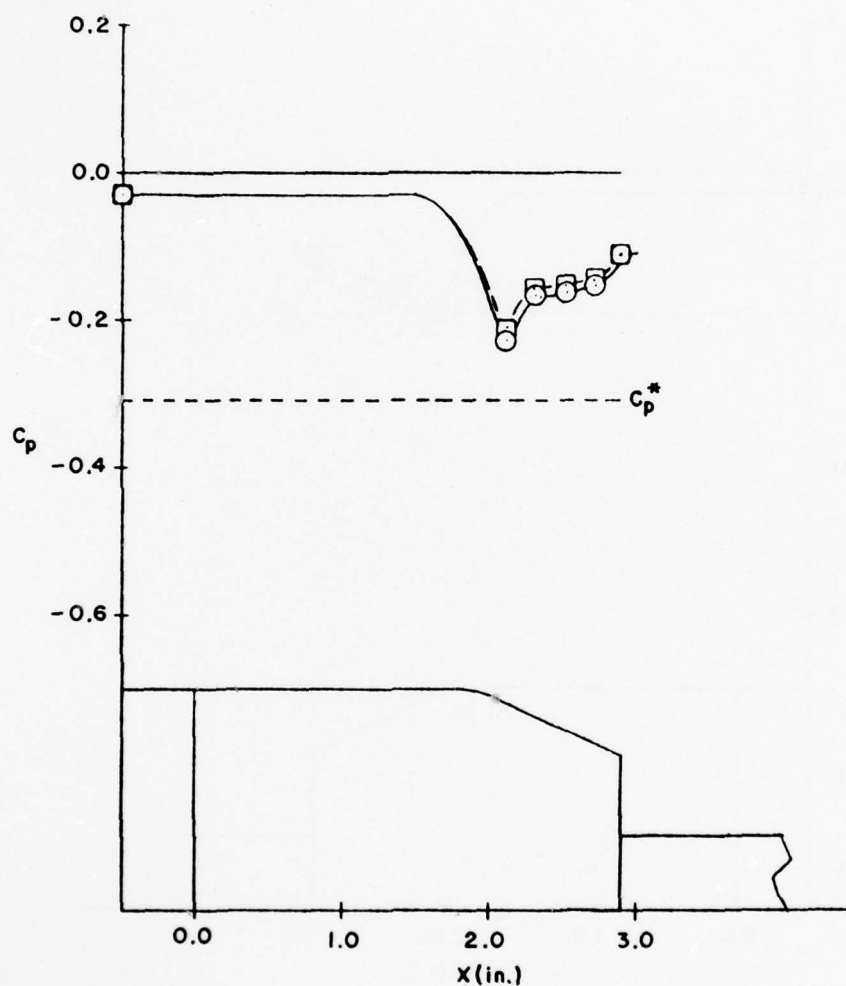


Figure 87. Reynolds Number Effect on Boattail and Base Pressure Coefficients

SYMBOL	NPR	M_∞	p_o (psfa)	Re_L	\dot{m} (lbm/sec)	$C_{D_A,s}$	$C_{D_A,j}$	$\frac{D_j^2}{D_b D_M}$
—○—	2.0	.90	2000	8.7×10^6	0.000	.10732	.10300	0.205
—□—	2.0	.90	3000	13.1×10^6	0.035	.10477	.10047	0.205

CONICAL BOATTAIL

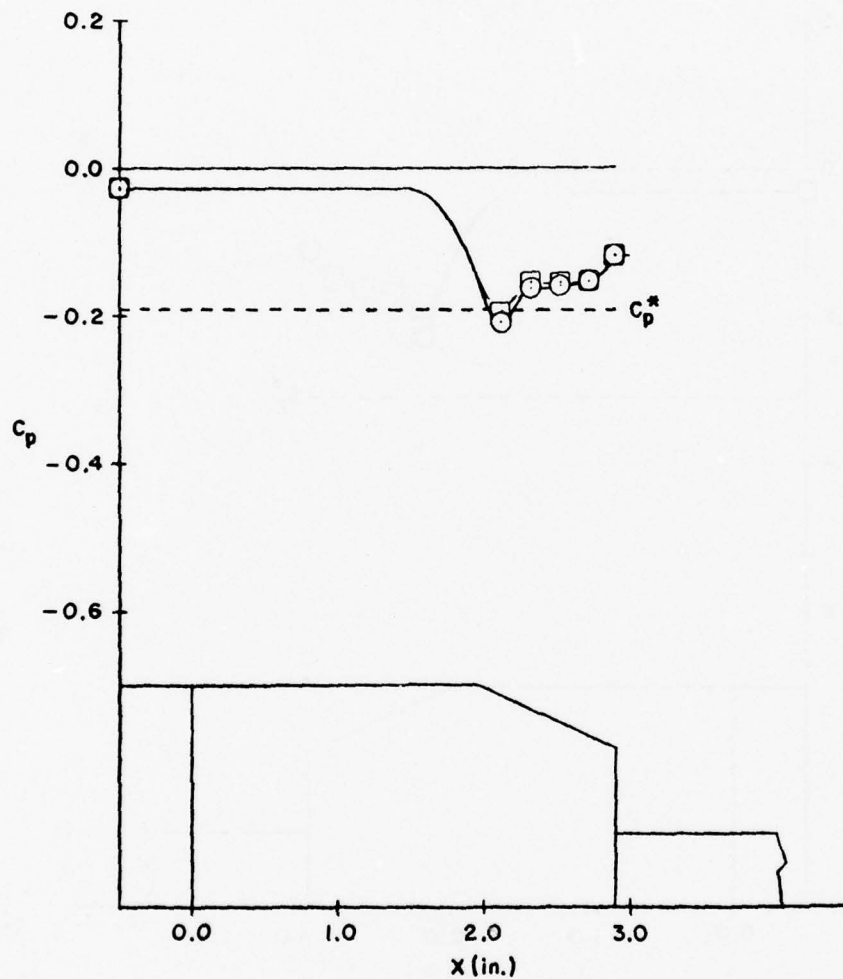


Figure 88. Reynolds Number Effect on Boattail and Base Pressure Coefficients

SYMBOL	NPR	M_∞	p_o (psfa)	Re_L	\dot{m} (lbm/sec)	$C_{D_{A,s}}$	$C_{D_{A,j}}$	$\frac{D_j^2}{D_b D_M}$
—○—	2.0	.95	2000	8.9×10^6	0.000	.11335	.10861	0.205
—□—	2.0	.95	3000	13.4×10^6	0.000	.11374	.10892	0.205

CONICAL BOATTAIL

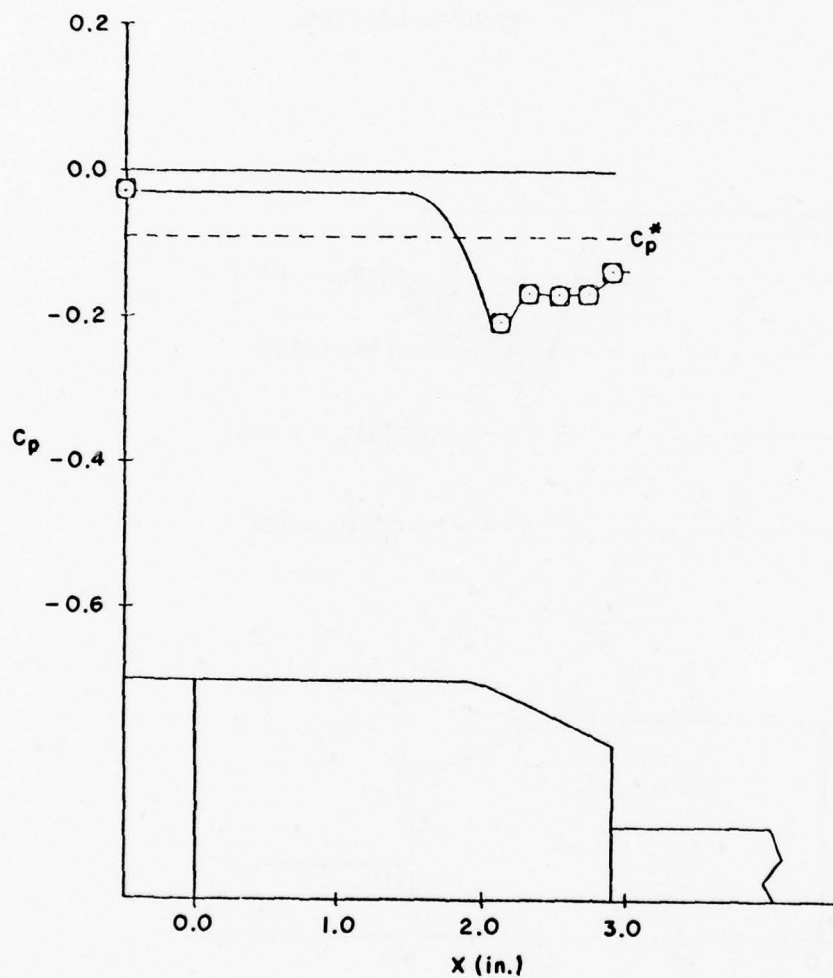


Figure 89. Reynolds Number Effect on Boattail and Base Pressure Coefficients

SYMBOL	NPR	M_∞	p_o (psfa)	Re_L	\dot{m} (lbm/sec)	$C_{DA,s}$	$C_{DA,j}$	$\frac{D_j^2}{D_b D M}$
—○—	2.0	.80	2000	8.3×10^6	0.000	.11616	.11183	0.205
—□—	2.0	.85	2000	8.4×10^6	0.000	.10512	.10111	0.205
—◇—	2.0	.90	2000	8.7×10^6	0.000	.10732	.10300	0.205
—△—	2.0	.95	2000	8.9×10^6	0.000	.11335	.10861	0.205

CONICAL BOATTAIL

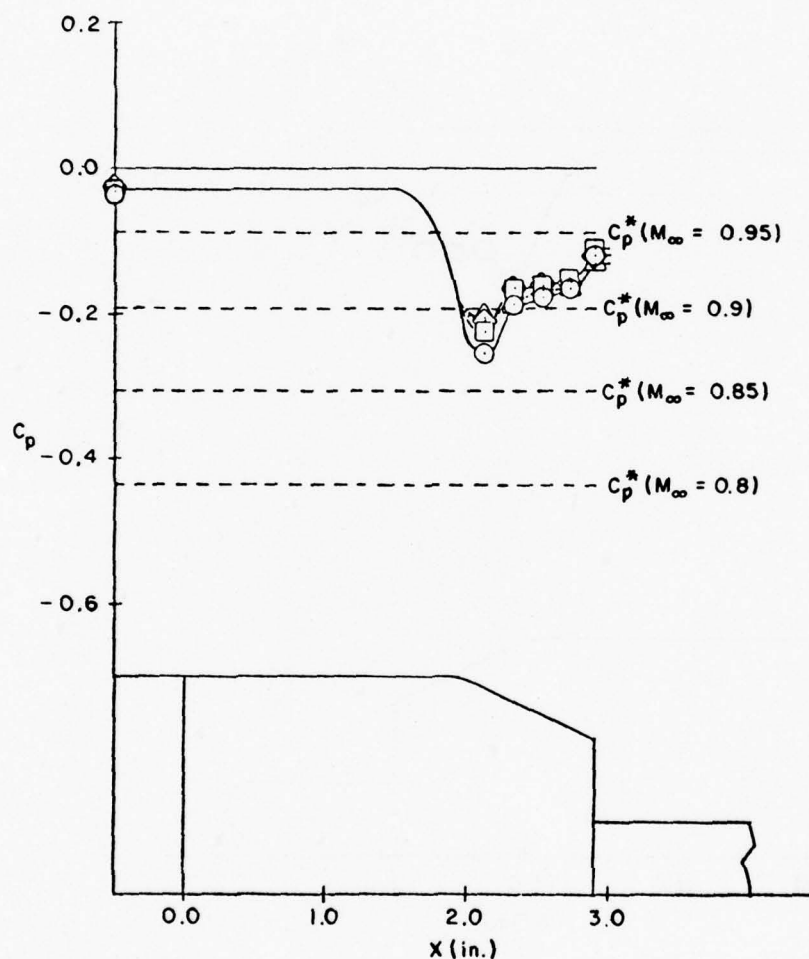


Figure 90. Mach Number Effect on Boattail and Base Pressure Coefficients

SYMBOL	NPR	M_∞	p_0 (psfa)	Re_L	\dot{m} (lbm/sec)	$C_{DA,s}$	$C_{DA,j}$	$\frac{D_j^2}{D_b^2 M}$
—○—	2.0	.80	3000	12.4×10^6	0.000	.10184	.09805	0.205
—□—	2.0	.85	3000	12.7×10^6	0.000	.10241	.09428	0.205
---◇---	2.0	.90	3000	13.1×10^6	0.000	.10477	.10047	0.205
---△---	2.0	.95	3000	13.4×10^6	0.000	.11374	.10892	0.205

CONICAL BOATTAIL

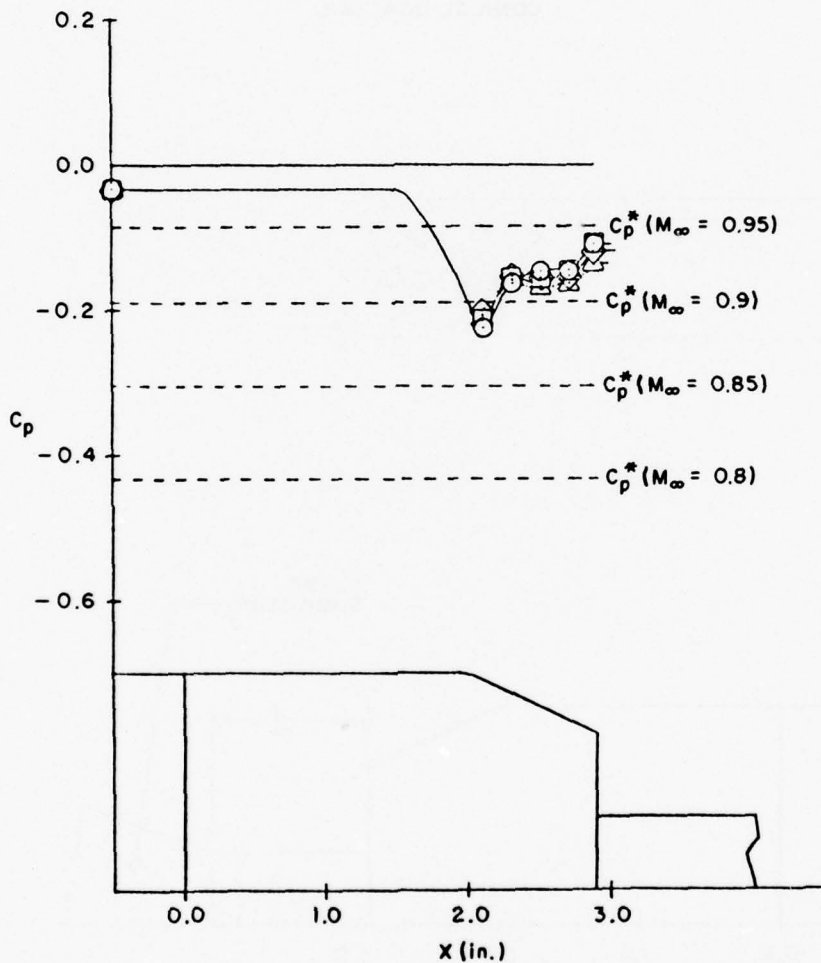


Figure 91. Mach Number Effect on Boattail and Base Pressure Coefficients

SYMBOL	NPR	M_∞	p_o (psfa)	Re_L	\dot{m} (lbm/sec)	l (in.)	$C_{DA,s}$	$C_{DA,j}$	$\frac{D_j^2}{D_b D_M}$
—○—	2.0	.90	2000	8.7×10^6	0.000	REMOVED	.10732	.10300	0.205
—□—	3.70	.90	2000	8.7×10^6	0.000	6	.07649	.07347	0.205
...◇...	4.32	.90	2000	8.7×10^6	0.000	4	.03287	.03188	0.205
---△---	5.42	.90	2000	8.7×10^6	0.000	2	-.00089	-.00024	0.205

CONICAL BOATTAIL

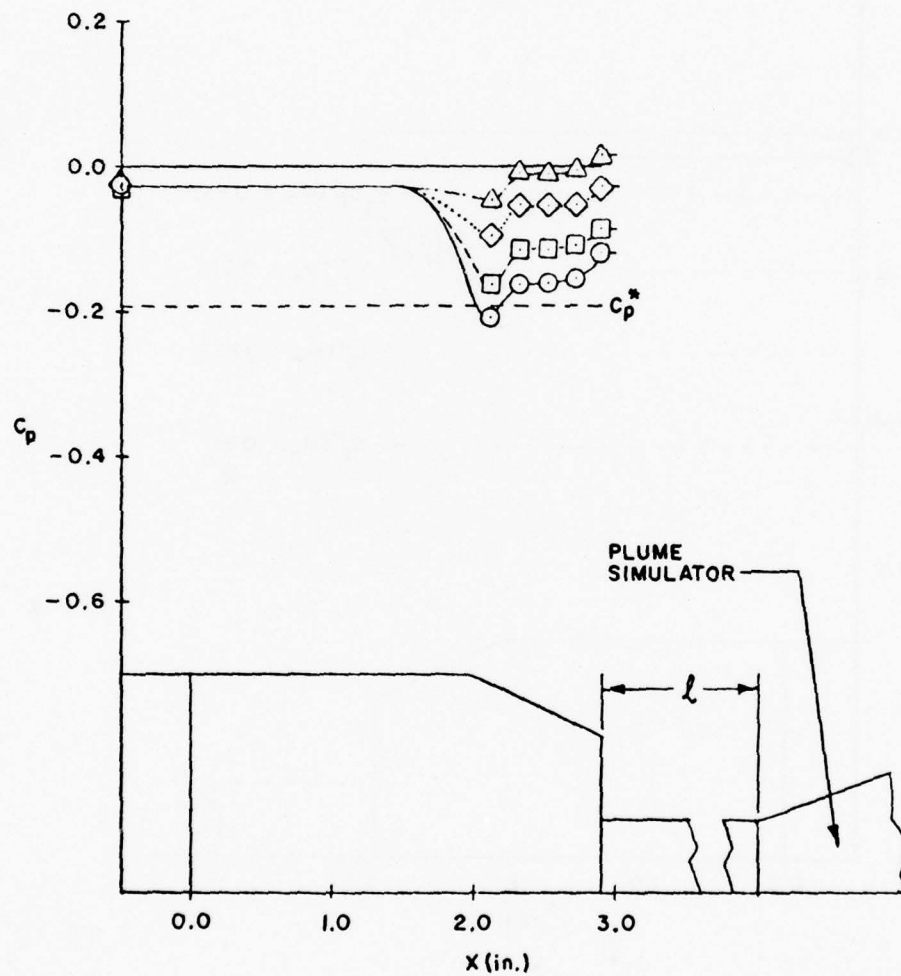


Figure 92. Nozzle Pressure Ratio Effect on Boattail and Base Pressure Coefficients

SYMBOL	NPR	M_∞	p_o (psfa)	Re_L	\dot{m} (lbm/sec)	l (in.)	$C_{DA,s}$	$C_{DA,j}$	$\frac{D_j^2}{D_b D_M}$
—○—	3.70	.90	2000	8.7×10^6	0.000	6	.07649	.07347	0.205
—□—	3.70	.90	2000	8.7×10^6	0.034	6	.07112	.06852	0.205
...◇...	3.70	.90	2000	8.7×10^6	0.066	6	.06460	.06305	0.205

CONICAL BOATTAIL

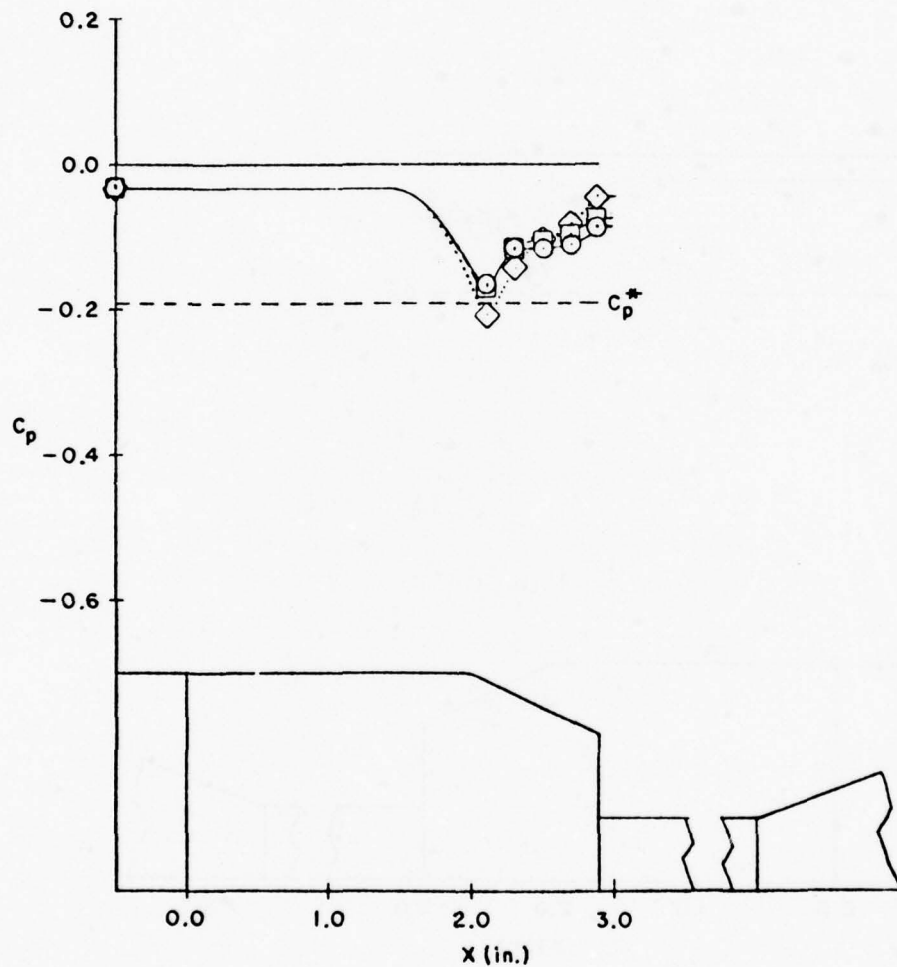


Figure 93. Mass Injection Effect on Boattail and Base Pressure Coefficients for $NPR > 2$

SYMBOL	NPR	M_∞	p_o (psfa)	Re_L	\dot{m} (lbm/sec)	l (in.)	$C_{DA,s}$	$C_{DA,j}$	$\frac{D_j^2}{D_b^2 M}$
—○—	3.70	.90	3000	13.1×10^6	0.000	6	.07082	.06804	0.205
—□—	3.70	.90	3000	13.1×10^6	0.035	6	.06699	.06433	0.205
...◇...	3.70	.90	3000	13.1×10^6	0.066	6	.06423	.06207	0.205

CONICAL BOATTAIL

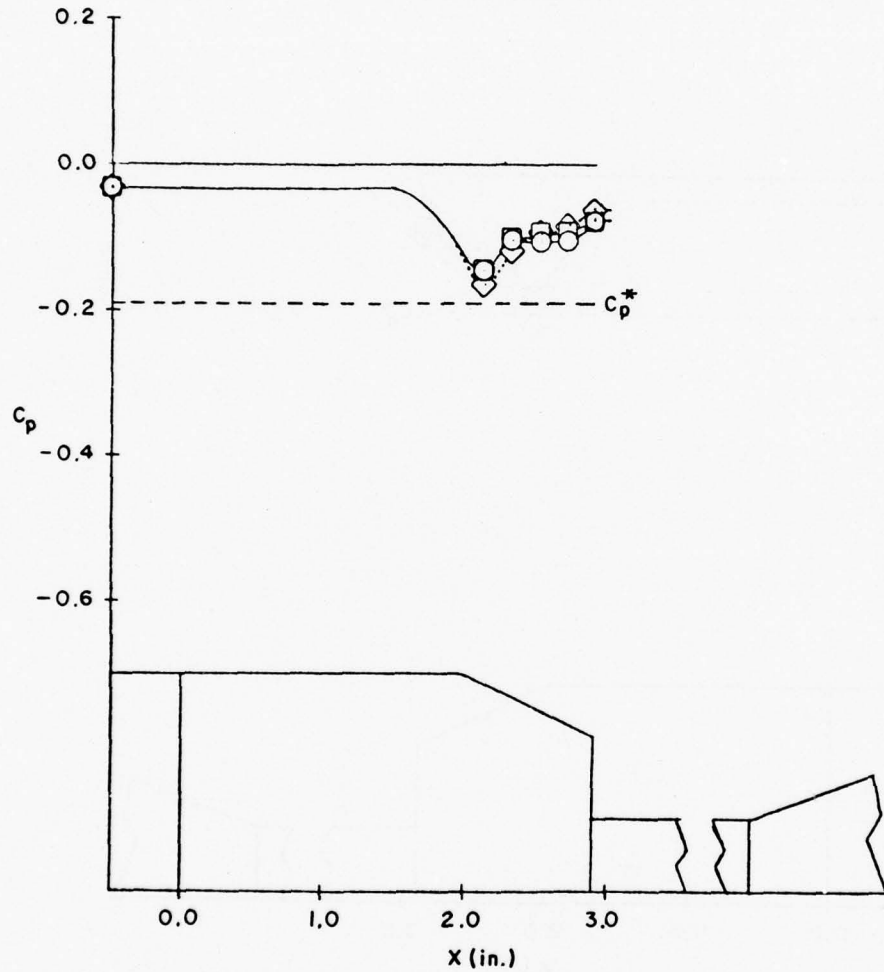


Figure 94. Mass Injection Effect on Boattail and Base Pressure Coefficients for $NPR > 2$

SYMBOL	NPR	M_∞	p_o (psfa)	Re_L	\dot{m} (lbm/sec)	l (in.)	$C_{DA,s}$	$C_{DA,j}$	$\frac{D_j^2}{D_b D_M}$
—○—	3.69	.95	2000	8.9×10^6	0.000	6	.07040	.06751	0.205
—□—	3.69	.95	2000	8.9×10^6	0.033	6	.06177	.13943	0.205
...◇...	3.69	.95	2000	8.9×10^6	0.066	6	.06126	.05958	0.205

CONICAL BOATTAIL

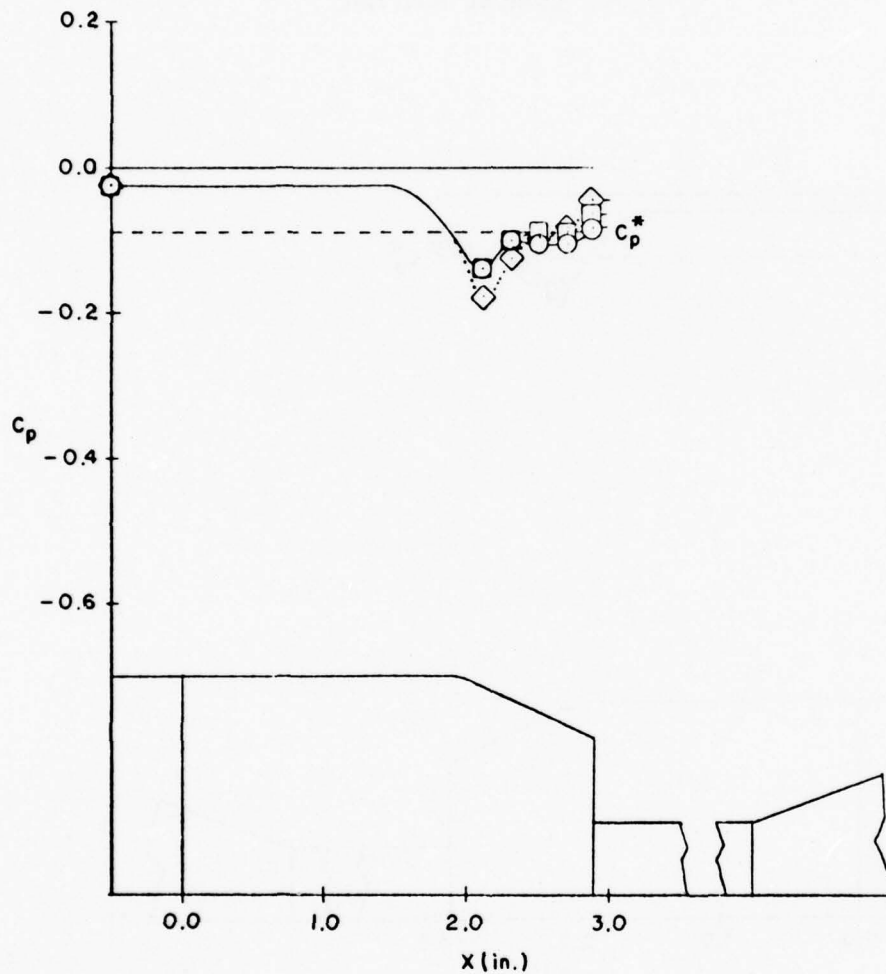


Figure 95. Mass Injection Effect on Boattail and Base Pressure Coefficients for $NPR > 2$

SYMBOL	NPR	M_∞	p_o (psfa)	Re_L	\dot{m} (lbm/sec)	ℓ (in.)	$C_{DA,s}$	$C_{DA,j}$	$\frac{D_j^2}{D_b D_M}$
—○—	3.69	.95	3000	13.4×10^6	0.000	6	.06767	.06486	0.205
—□—	3.69	.95	3000	13.4×10^6	0.033	6	.06232	.05986	0.205
...◇...	3.69	.95	3000	13.4×10^6	0.067	6	.05884	.05680	0.205

CONICAL BOATTAIL

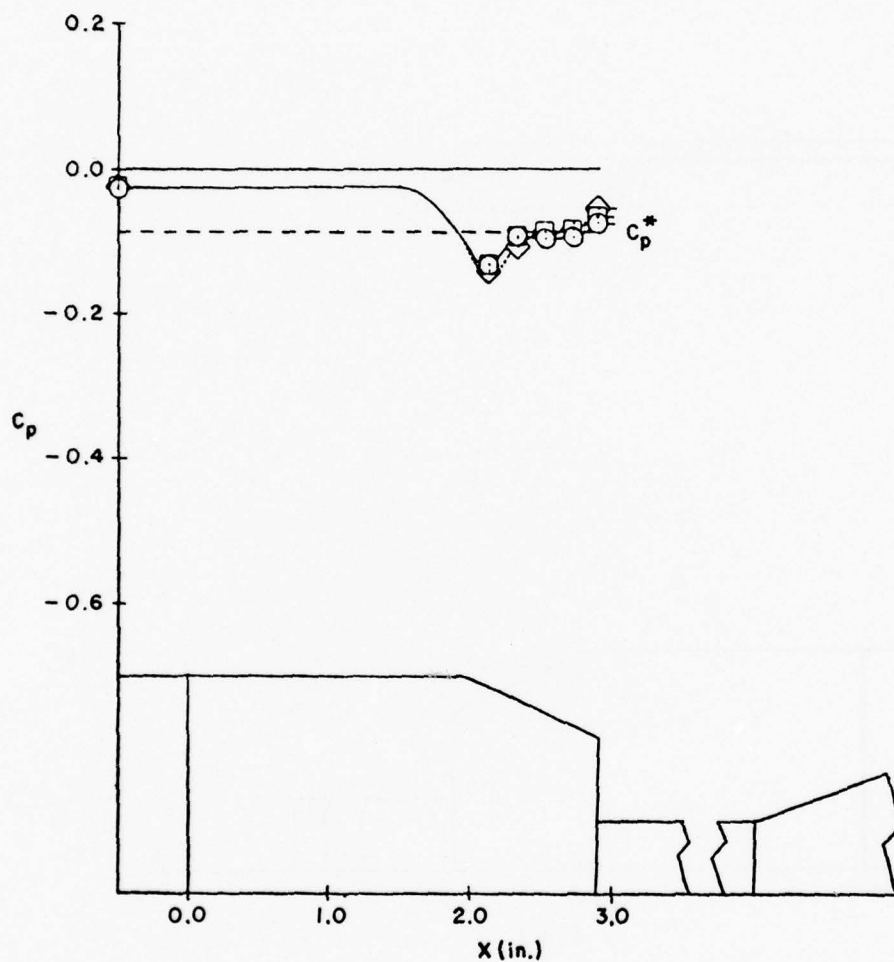


Figure 96. Mass Injection Effect on Boattail and Base Pressure Coefficients for NPR>2

SYMBOL	NPR	M_∞	p_o (psfa)	Re_L	\dot{m} (lbm/sec)	l (in.)	$C_{DA,s}$	$C_{DA,j}$	$\frac{D_j^2}{D_b D_M}$
—○—	4.34	.85	2000	8.4×10^6	0.000	4	.04104	.03977	0.205
—□—	4.34	.85	2000	8.4×10^6	0.034	4	.03139	.03063	0.205
...◇...	4.34	.85	2000	8.4×10^6	0.039	4	.03096	.03026	0.205
---△---	4.34	.85	2000	8.4×10^6	0.066	4	.03041	.03061	0.205
-♦-△-♦-	4.34	.85	2000	8.4×10^6	0.070	4	.03196	.03223	0.205
-x-△-x-	4.34	.85	2000	8.4×10^6	0.114	4	.04357	.04523	0.205

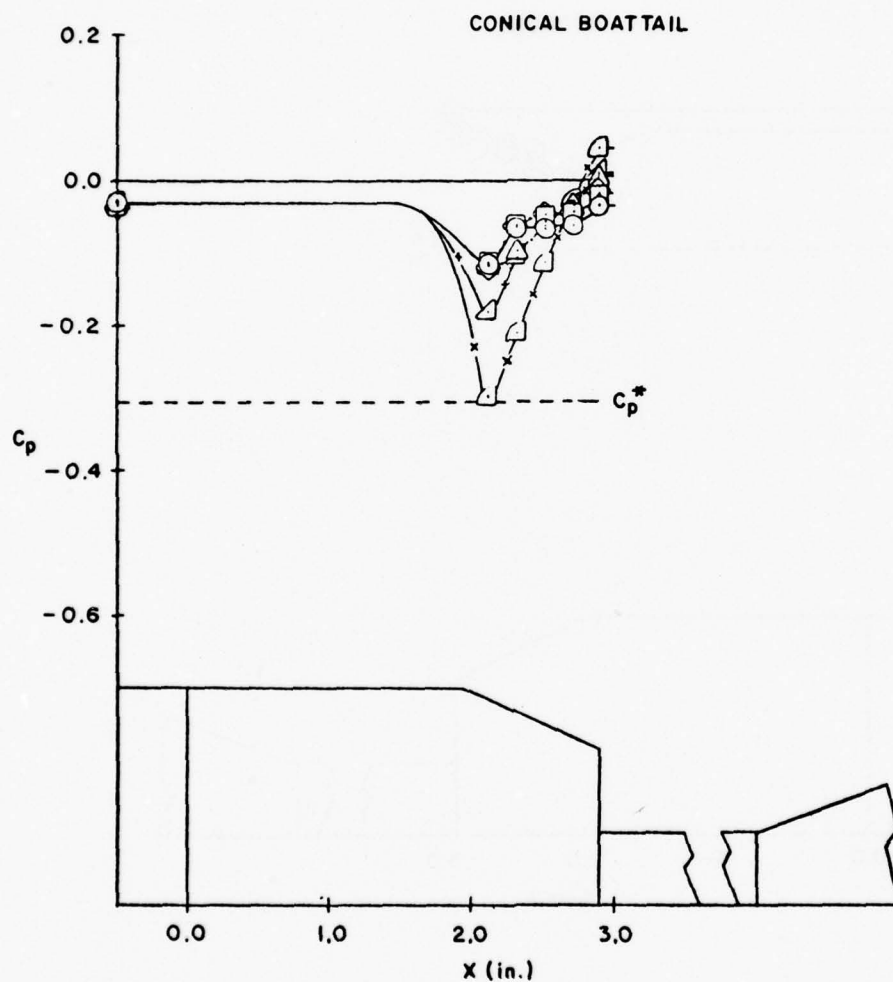


Figure 97. Mass Injection Effect on Boattail and Base Pressure Coefficients for NPR>2

SYMBOL	NPR	M_∞	p_o (psfa)	Re_L	\dot{m} (lbm/sec)	l (in.)	$C_{D_A,s}$	$C_{D_A,j}$	$\frac{D_j^2}{D_b D_M}$
—○—	4.32	.90	2000	8.7×10^6	0.000	4	.03287	.03188	0.205
—□—	4.32	.90	2000	8.7×10^6	0.032	4	.02912	.02841	0.205
...◇...	4.32	.90	2000	8.7×10^6	0.068	4	.02951	.02958	0.205

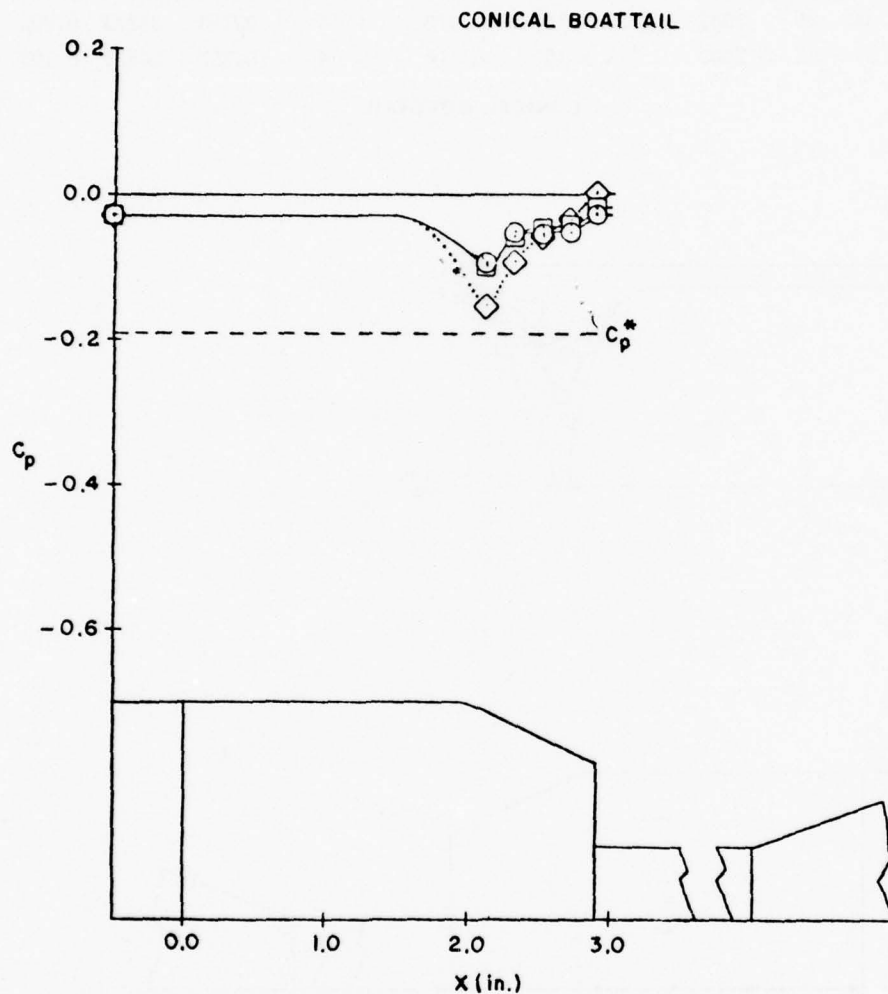


Figure 98. Mass Injection Effect on Boattail and Base Pressure Coefficients for $NPR > 2$

SYMBOL	NPR	M_∞	p_o (psfa)	Re_L	m (lbm/sec)	l (in.)	$C_{D_A,s}$	$C_{D_A,j}$	$\frac{D_j^2}{D_b D_M}$
—○—	4.32	.90	3000	13.1×10^6	0.000	4	.03155	.03060	0.205
—□—	4.32	.90	3000	13.1×10^6	0.033	4	.02806	.02721	0.205
....◇....	4.32	.90	3000	13.1×10^6	0.067	4	.02581	.02540	0.205

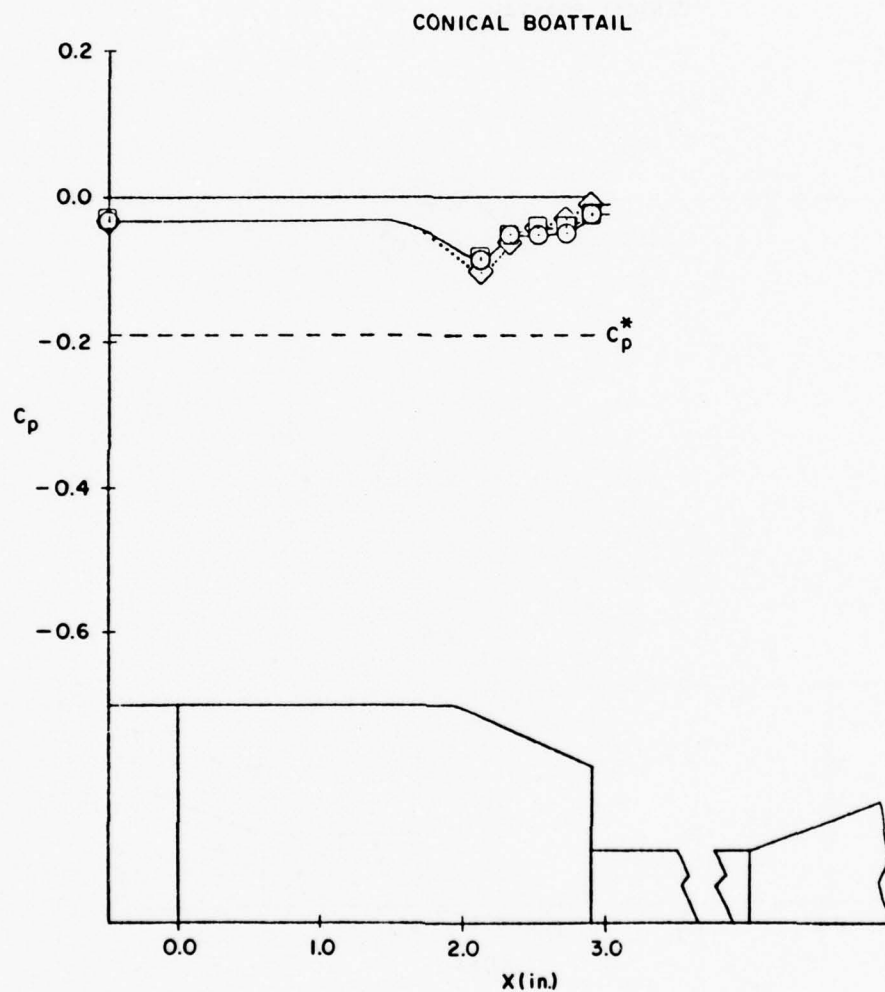


Figure 99. Mass Injection Effect on Boattail and Base Pressure Coefficients for $NPR > 2$

SYMBOL	NPR	M_∞	p_o (psfa)	Re_L	\dot{m} (lbm/sec)	x (in.)	$C_{DA,s}$	$C_{DA,j}$	$\frac{D_j^2}{D_b D_M}$
—○—	4.30	.95	3000	13.4×10^6	0.000	4	.02475	.02393	0.205
—□—	4.30	.95	3000	13.4×10^6	0.033	4	.01952	.01903	0.205
...◇...	4.30	.95	3000	13.4×10^6	0.066	4	.01826	.01810	0.205

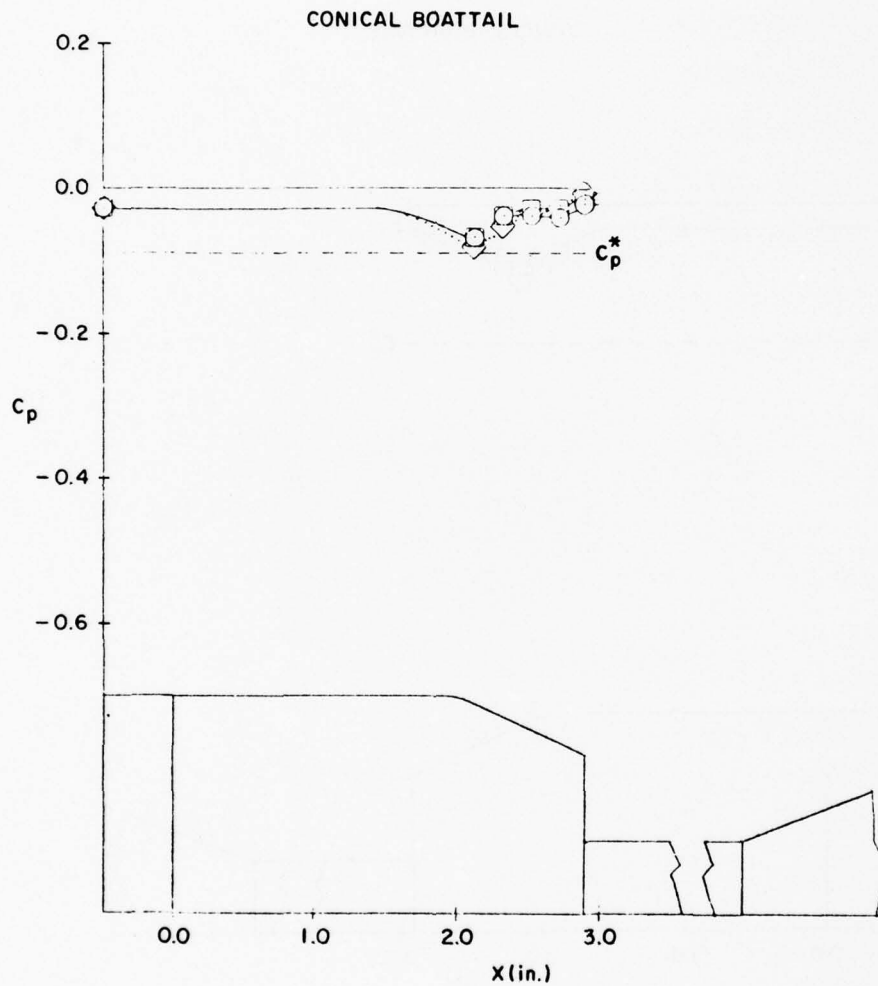


Figure 100. Mass Injection Effect on Boattail and Base Pressure Coefficients for $NPR > 2$

SYMBOL	NPR	M_∞	p_o (psfa)	Re_L	\dot{m} (lbm/sec)	x (in.)	$C_{DA,s}$	$C_{DA,j}$	$\frac{D_j^2}{D_b D_M}$
—○—	5.42	.90	2000	8.7×10^6	0.000	2	-.00089	-.00024	0.205
—□—	5.42	.90	2000	8.7×10^6	0.033	2	-.00576	-.00487	0.205
...◇...	5.42	.90	2000	8.7×10^6	0.063	2	-.00358	-.00228	0.205
---△---	5.42	.90	2000	8.7×10^6	0.066	2	-.00207	-.00067	0.205
---+△---	5.42	.90	2000	8.7×10^6	0.115	2	-.00262	-.00554	0.205

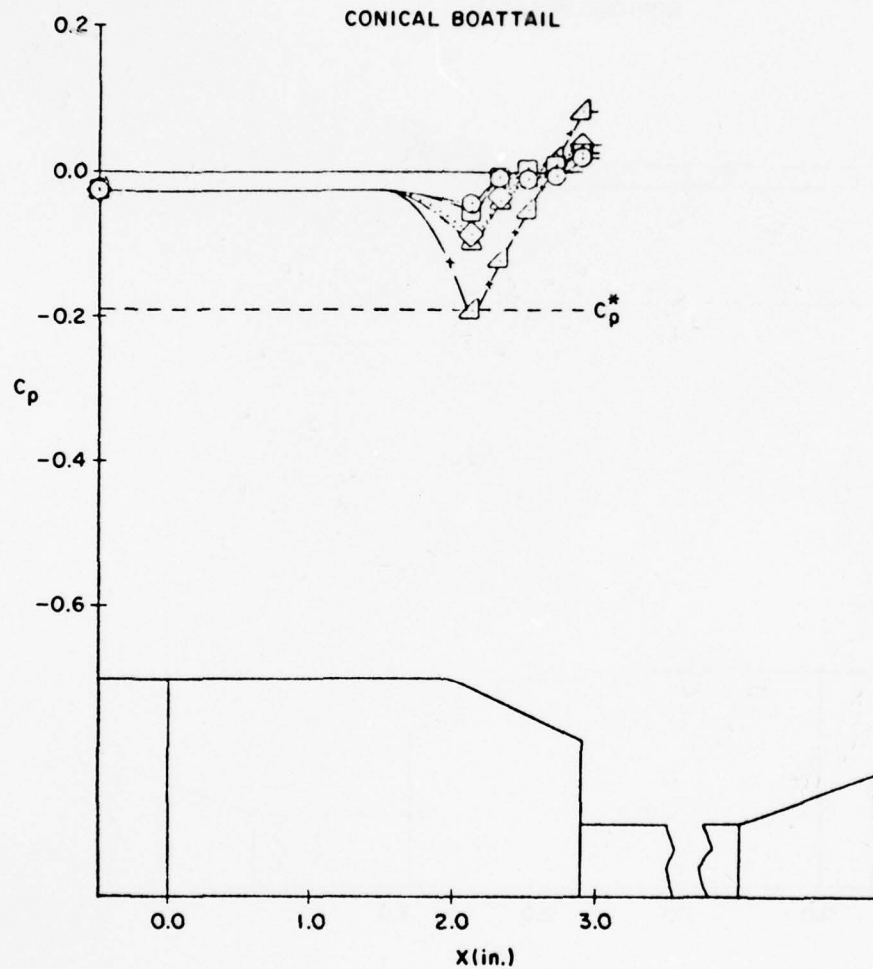


Figure 101. Mass Injection Effect on Boattail and Base Pressure Coefficients for NPR>2

SYMBOL	NPR	M_∞	p_o (psfa)	Re_L	\dot{m} (lbm/sec)	x (in.)	$C_{DA,s}$	$C_{DA,j}$	$\frac{D_j^2}{D_b D_M}$
—○—	5.42	.90	3000	13.1×10^6	0.000	2	.00277	.00312	0.205
—□—	5.42	.90	3000	13.1×10^6	0.034	2	-.00462	-.00388	0.205
...◇...	5.42	.90	3000	13.1×10^6	0.064	2	-.00513	-.00427	0.205
—△—	5.42	.90	3000	13.1×10^6	0.067	2	-.00561	-.00467	0.205
—+△+—	5.42	.90	3000	13.1×10^6	0.116	2	-.00328	-.00143	0.205

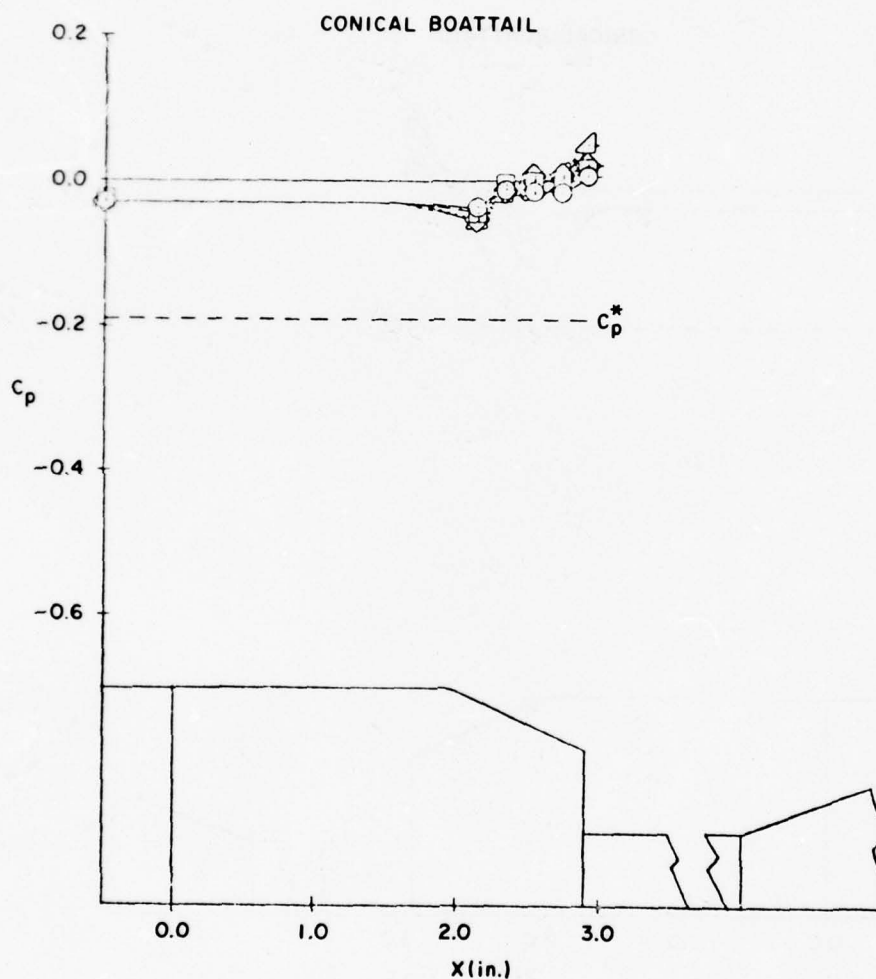


Figure 102. Mass Injection Effect on Boattail and Base Pressure Coefficients for $NPR > 2$

SYMBOL	NPR	M_∞	p_o (psfa)	Re_L	\dot{m} (lbm/sec)	$C_{DA,s}$	$C_{DA,j}$	$\frac{D_j^2}{D_b D_M}$
—○—	2.0	.90	2000	8.7×10^6	0.000	.09917	.10331	0.258
—□—	2.0	.90	2000	8.7×10^6	0.034	.09369	.09744	0.258
...◇...	2.0	.90	2000	8.7×10^6	0.066	.09242	.09753	0.258

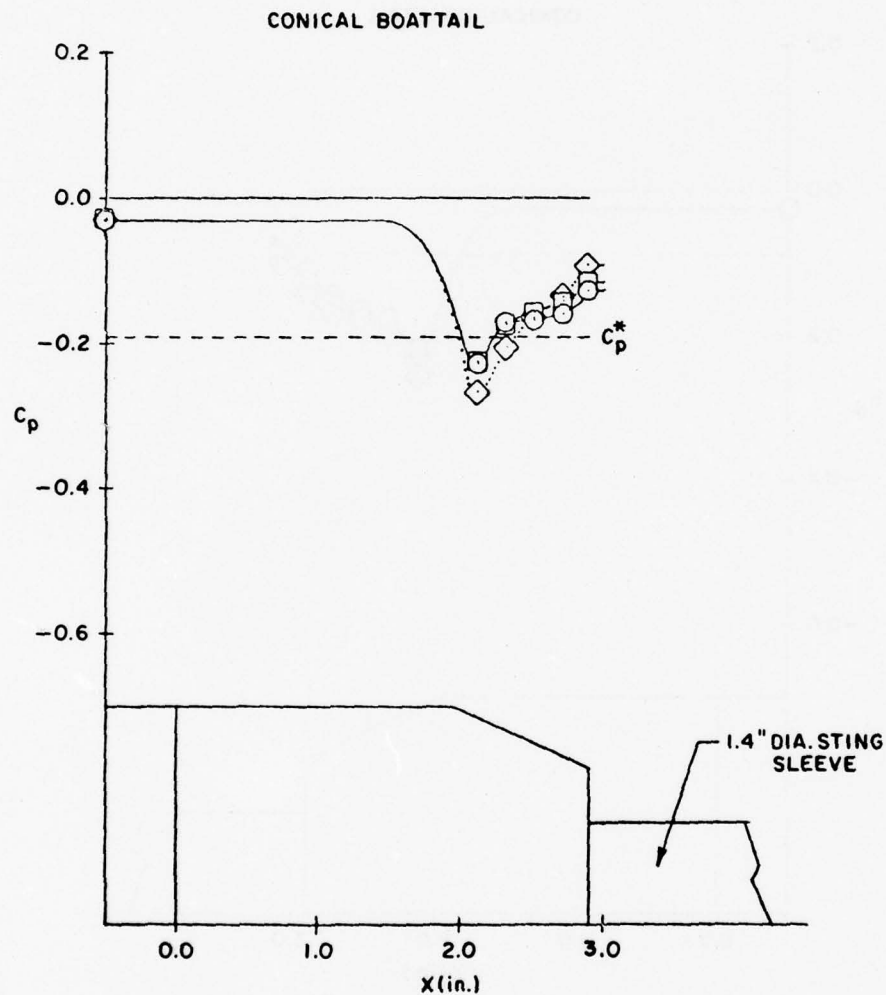


Figure 103. Mass Injection Effect on Boattail and Base Pressure Coefficients for NPR=2, $D_S > 1"$

SYMBOL	NPR	M_∞	p_0 (psfa)	Re_L	\dot{m} (lbm/sec)	$C_{DA,s}$	$C_{DA,j}$	$\frac{D_j^2}{D_b D_M}$
—○—	2.0	.95	2000	8.9×10^6	0.000	.10660	.11137	0.258
—□—	2.0	.95	2000	8.9×10^6	0.034	.10240	.10682	0.258
...◇...	2.0	.95	2000	8.9×10^6	0.066	.10095	.10339	0.258

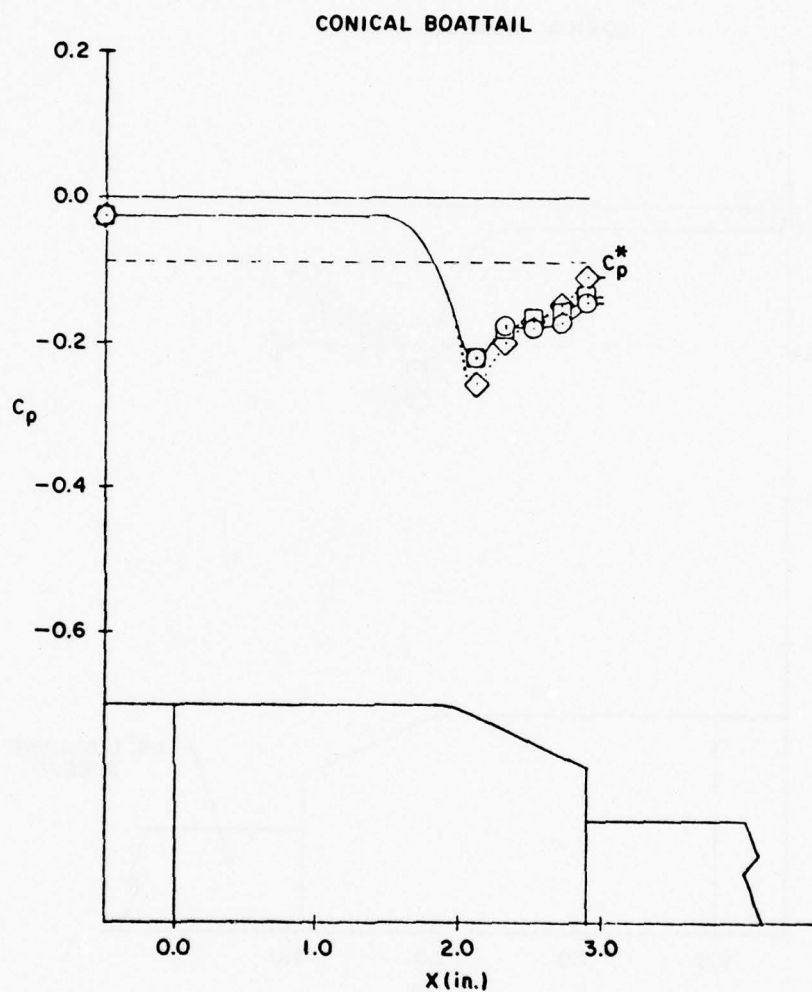


Figure 104. Mass Injection Effect on Boattail and Base Pressure Coefficients for NPR=2, $D_S > 1"$

SYMBOL	NPR	M_∞	p_o (psfa)	Re_L	\dot{m} (lbm/sec)	$C_{D_A,s}$	$C_{D_A,j}$	$\frac{D_j^2}{D_b D_M}$
—○—	2.0	.90	2000	8.7×10^6	0.000	.09236	.10262	0.287
—□—	2.0	.90	2000	8.7×10^6	0.034	.08683	.09601	0.287
...◇...	2.0	.90	2000	8.7×10^6	0.066	.08810	.09517	0.287

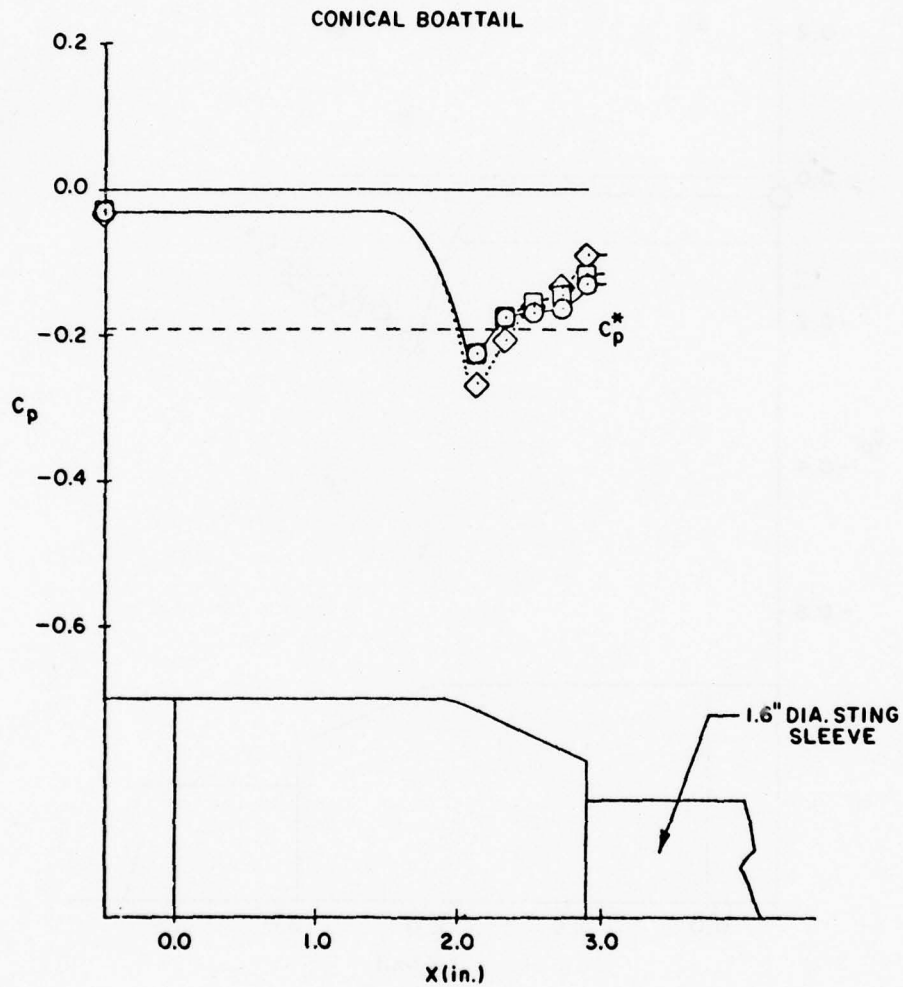


Figure 105. Mass Injection Effect on Boattail and Base Pressure Coefficients for NPR=2, $D_S > 1"$

SYMBOL	NPR	M_∞	p_0 (psfa)	Re_L	\dot{m} (lbm/sec)	$C_{D,A,s}$	$C_{D,A,j}$	$\frac{D_j^2}{D_b D_M}$
—○—	2.0	.95	2000	8.9×10^6	0.000	.10020	.11199	0.287
—□—	2.0	.95	2000	8.9×10^6	0.033	.09432	.10515	0.287
...◇...	2.0	.95	2000	8.9×10^6	0.066	.09246	.10339	0.287

CONICAL BOATTAIL

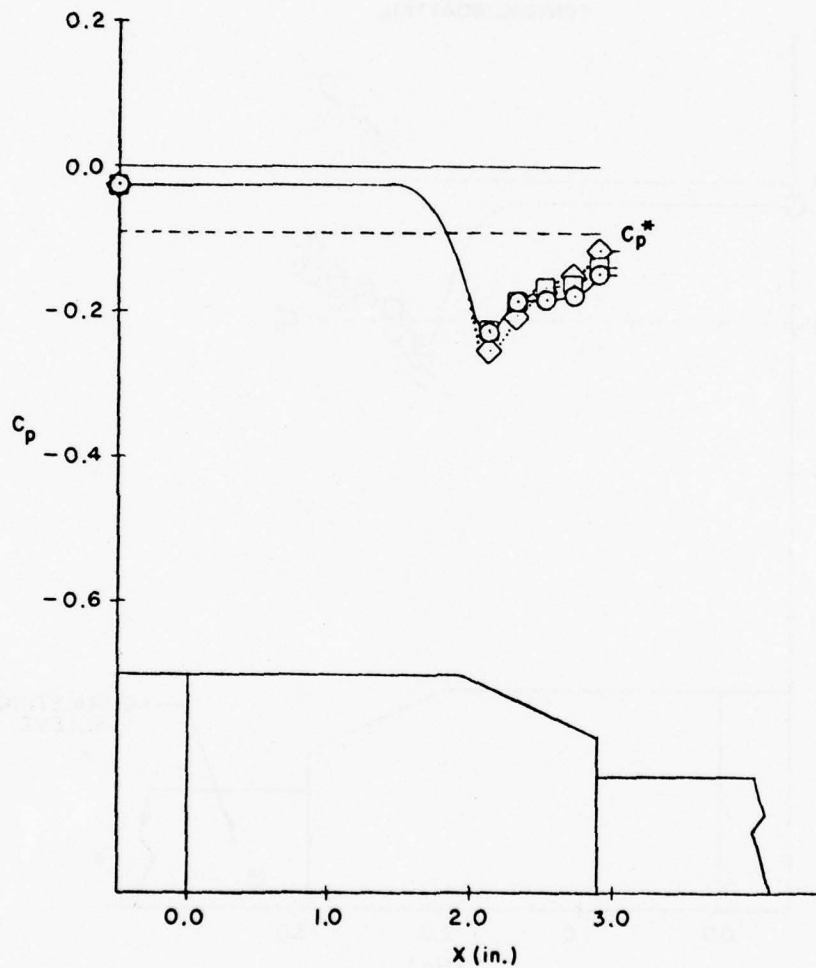


Figure 106. Mass Injection Effect on Boattail and Base Pressure Coefficients for NPR=2, $D_S > 1"$

SYMBOL	NPR	M_∞	p_o (psfa)	Re_L	\dot{m} (lbm/sec)	$C_{D_A,s}$	$C_{D_A,j}$	$\frac{D_j^2}{D_b D_M}$
—○—	2.0	.90	2000	8.7×10^6	0.000	.08241	.09857	0.326
—□—	2.0	.90	2000	8.7×10^6	0.034	.07961	.09438	0.326
...◇...	2.0	.90	2000	8.7×10^6	0.065	.07952	.09036	0.326

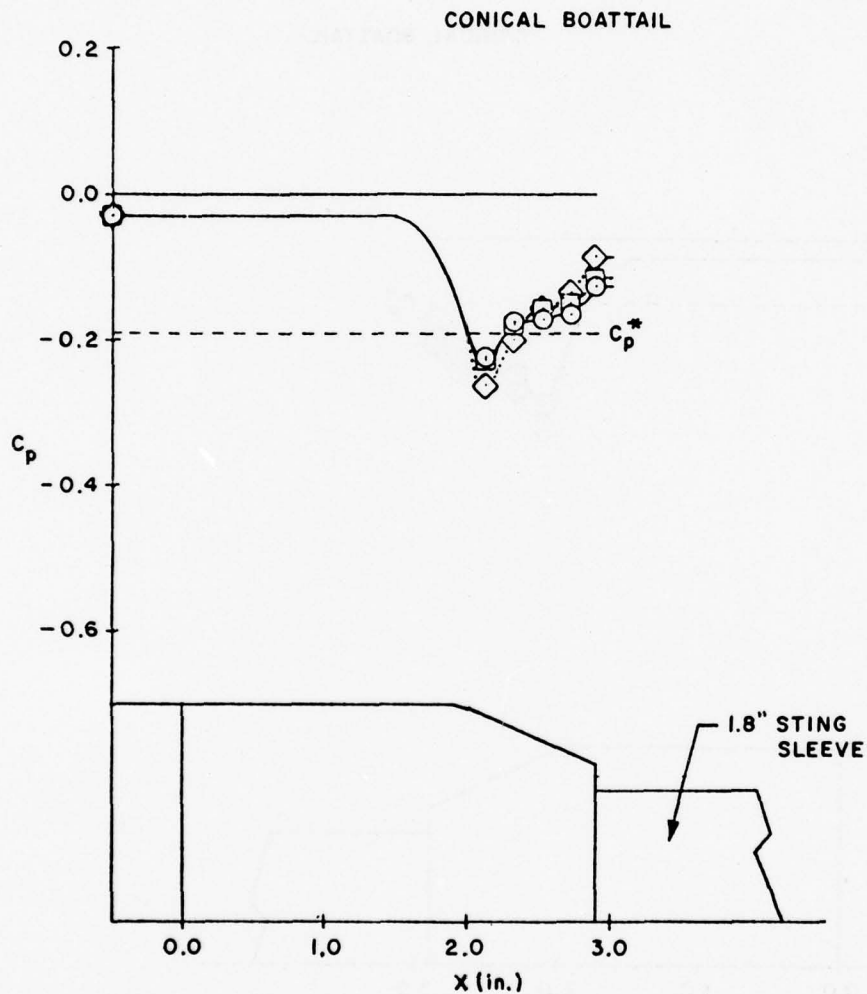


Figure 107. Mass Injection Effect on Boattail and Base Pressure Coefficients for NPR=2, $D_S > 1"$

SYMBOL	NPR	M_∞	p_o (psfa)	Re_L	\dot{m} (lbm/sec)	$C_{DA,s}$	$C_{DA,j}$	$\frac{D_j^2}{D_b D_M}$
—○—	2.0	.95	2000	8.9×10^6	0.000	.09000	.10876	0.326
—□—	2.0	.95	2000	8.9×10^6	0.032	.08589	.10332	0.326
...◇...	2.0	.95	2000	8.9×10^6	0.068	.08696	.10093	0.326

CONICAL BOATTAIL

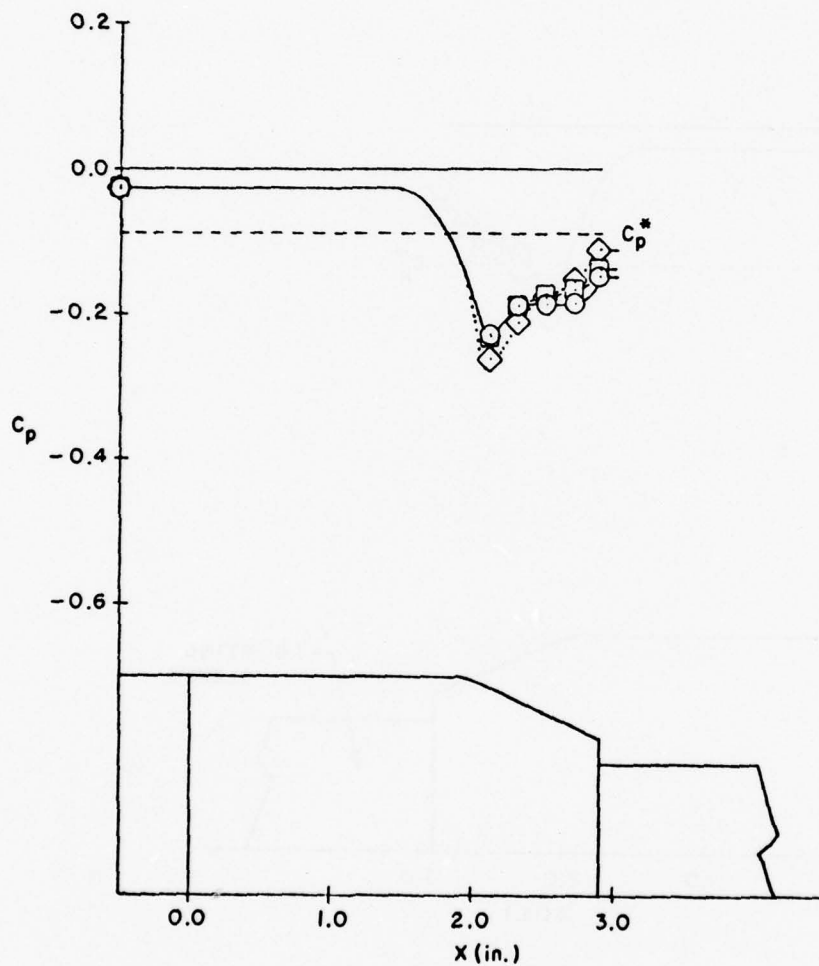


Figure 108. Mass Injection Effect on Boattail and Base Pressure Coefficients for NPR=2, $D_S > 1"$

SYMBOL	NPR	M_∞	p_o (psfa)	Re_L	\dot{m} (lbm/sec)	$C_{DA,s}$	$C_{DA,j}$	$\frac{D_j^2}{D_b D_M}$	$\frac{D_s}{D_b}$
---△---	2.0	.90	2000	8.7×10^6	0.000	.10732	.10300	0.205	.465
—○—	2.0	.90	2000	8.7×10^6	0.000	.09917	.10331	0.258	.651
—□—	2.0	.90	2000	8.7×10^6	0.000	.09236	.10262	0.287	.744
...◇...	2.0	.90	2000	8.7×10^6	0.000	.08241	.09857	0.326	.837

CONICAL BOATTAIL

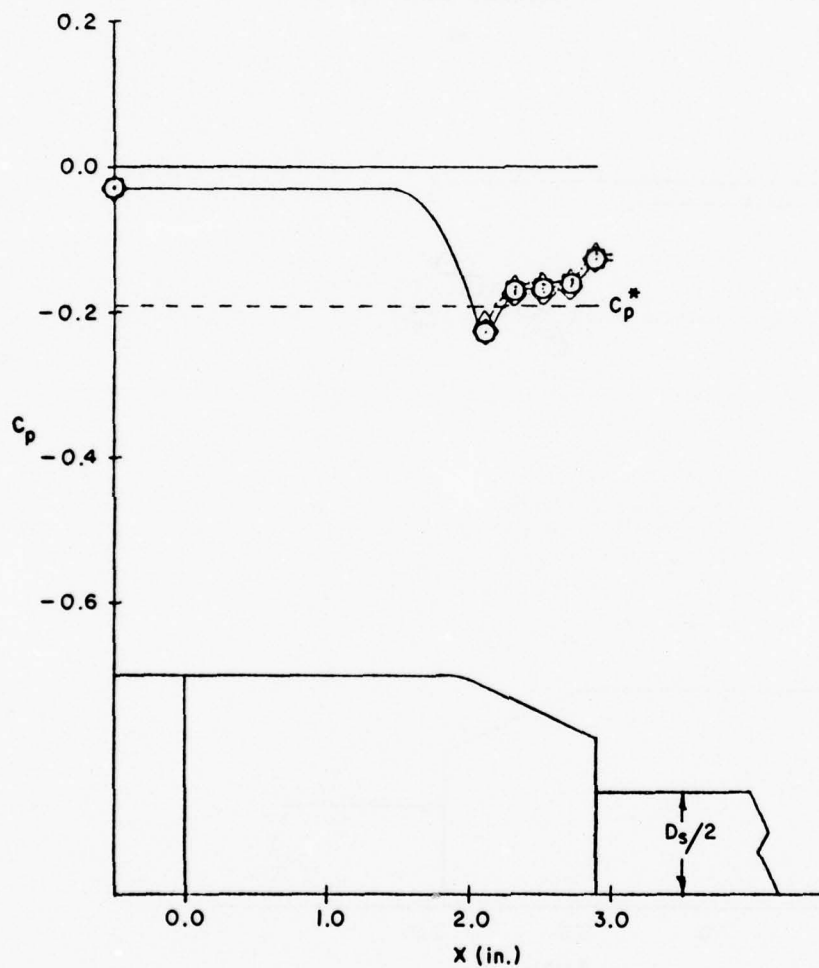


Figure 109. Sting Size Effect on Boattail and Base Pressure Coefficients

SYMBOL	NPR	M_∞	p_o (psfa)	Re_L	\dot{m} (lbm/sec)	$C_{D_A,s}$	$C_{D_A,j}$	$\frac{D_j^2}{D_b D_M}$	$\frac{D_s}{D_b}$
---△---	2.0	.90	2000	8.7×10^6	0.033	.10732	.10300	0.205	.465
---○---	2.0	.90	2000	8.7×10^6	0.034	.09369	.09744	0.258	.651
---□---	2.0	.90	2000	8.7×10^6	0.034	.08693	.09601	0.287	.744
---◇---	2.0	.90	2000	8.7×10^6	0.034	.07961	.09438	0.326	.837

CONICAL BOATTAIL

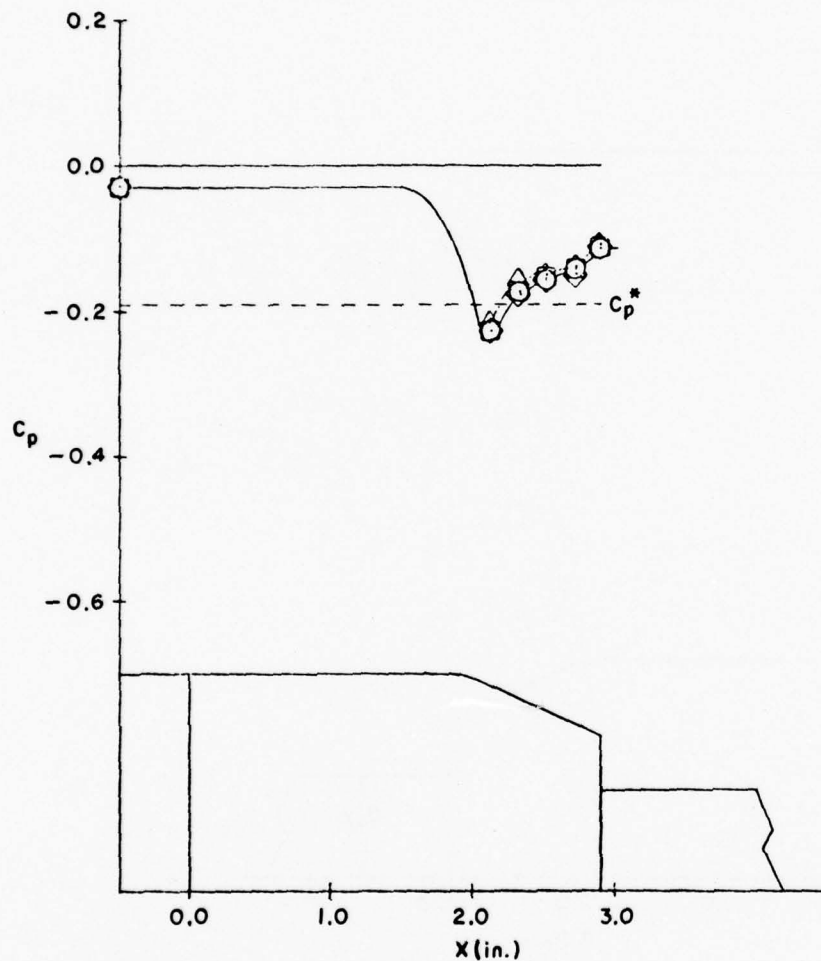


Figure 110. Sting Size Effect on Boattail and Base Pressure Coefficients

SYMBOL	NPR	M_∞	p_o (psfa)	Re_L	\dot{m} (lbm/sec)	$C_{DA,s}$	$C_{DA,j}$	$\frac{D_j^2}{D_b D_M}$	$\frac{D_s}{D_b}$
---△---	2.0	.90	2000	8.9×10^6	0.066	.10732	.10300	0.205	.465
—○—	2.0	.90	2000	8.9×10^6	0.066	.09454	.09099	0.258	.651
—□—	2.0	.90	2000	8.9×10^6	0.066	.08810	.08616	0.287	.744
---◇---	2.0	.90	2000	8.9×10^6	0.065	.07952	.07952	0.326	.837

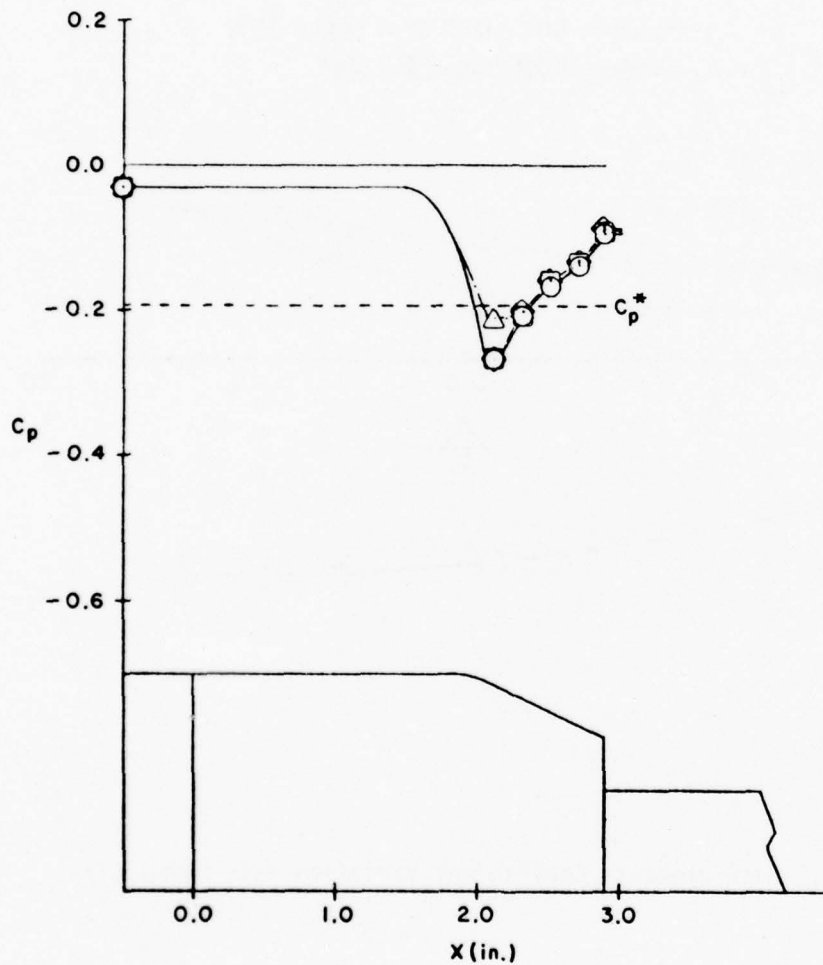


Figure 111. Sting Size Effect on Boattail and Base Pressure Coefficients

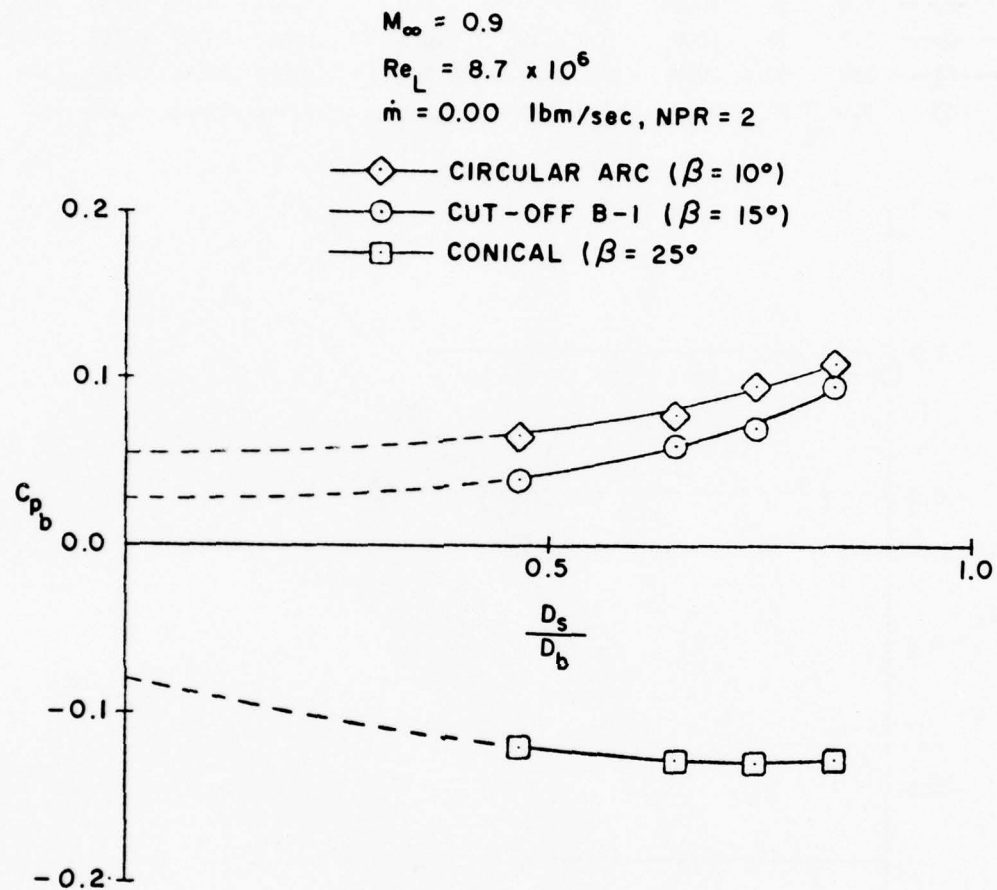


Figure 112. Base Pressure Coefficient Variation With Sting Size

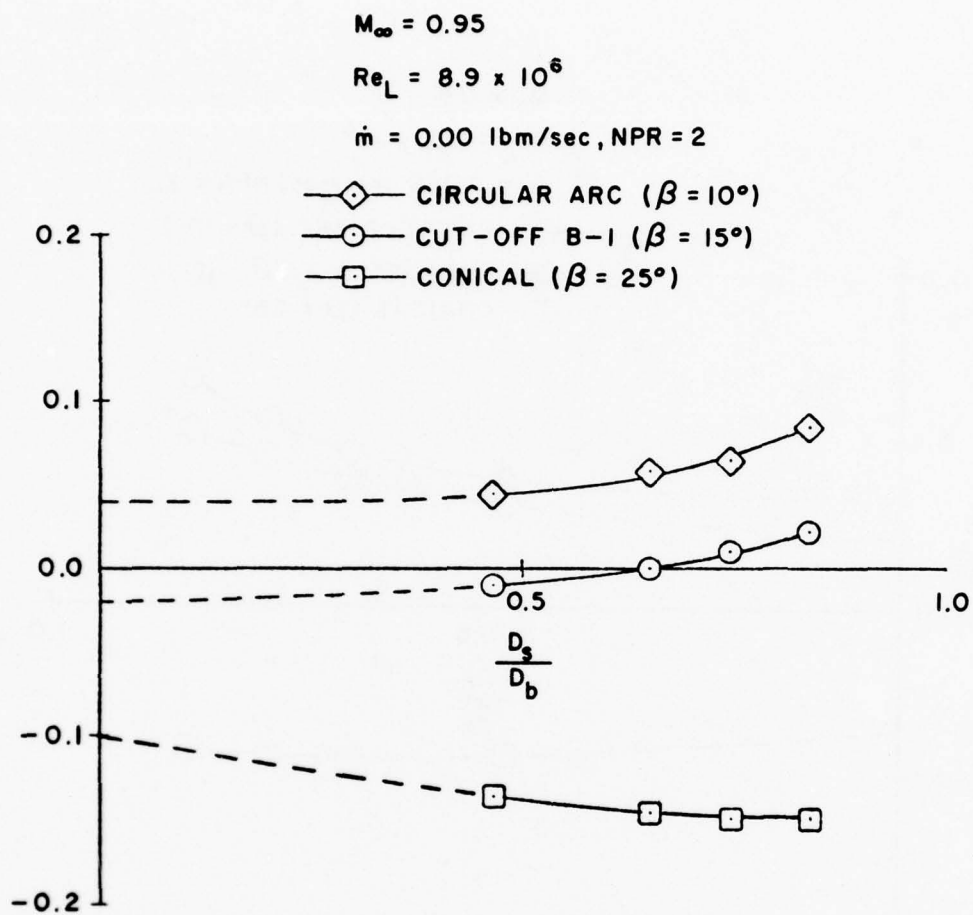


Figure 113. Base Pressure Coefficient Variation With Sting Size

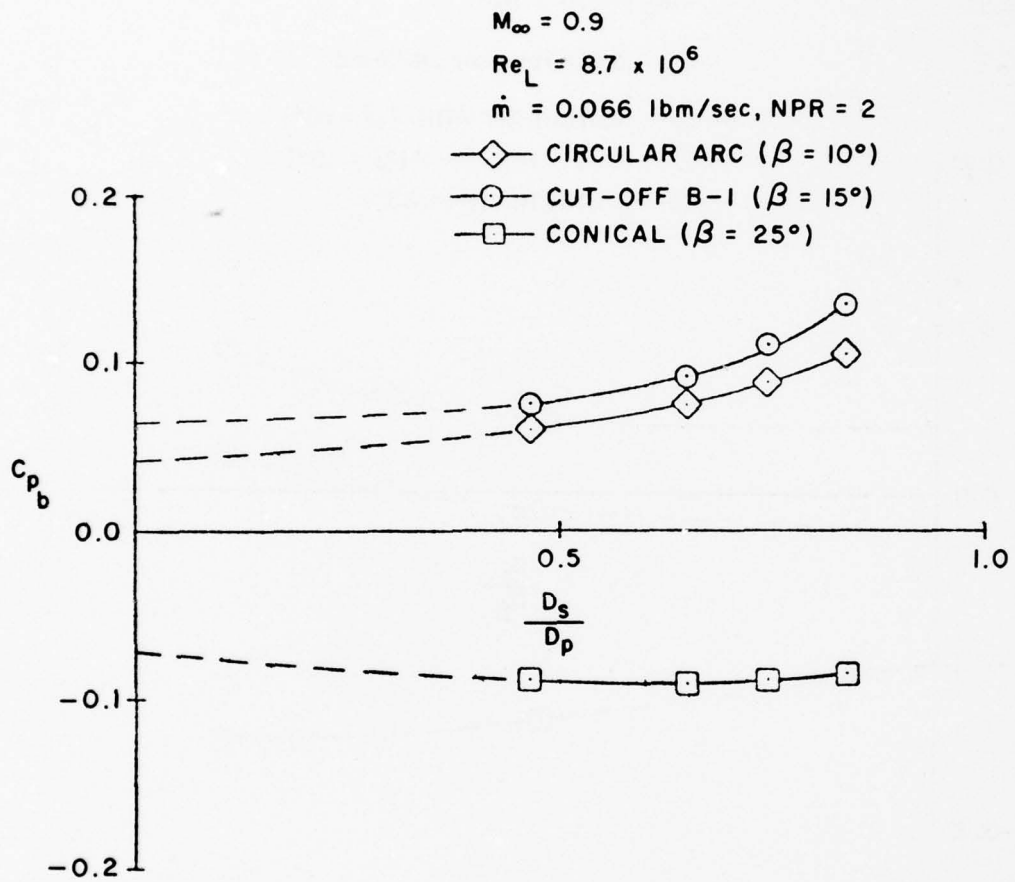


Figure 114. Base Pressure Coefficient Variation With Sting Size

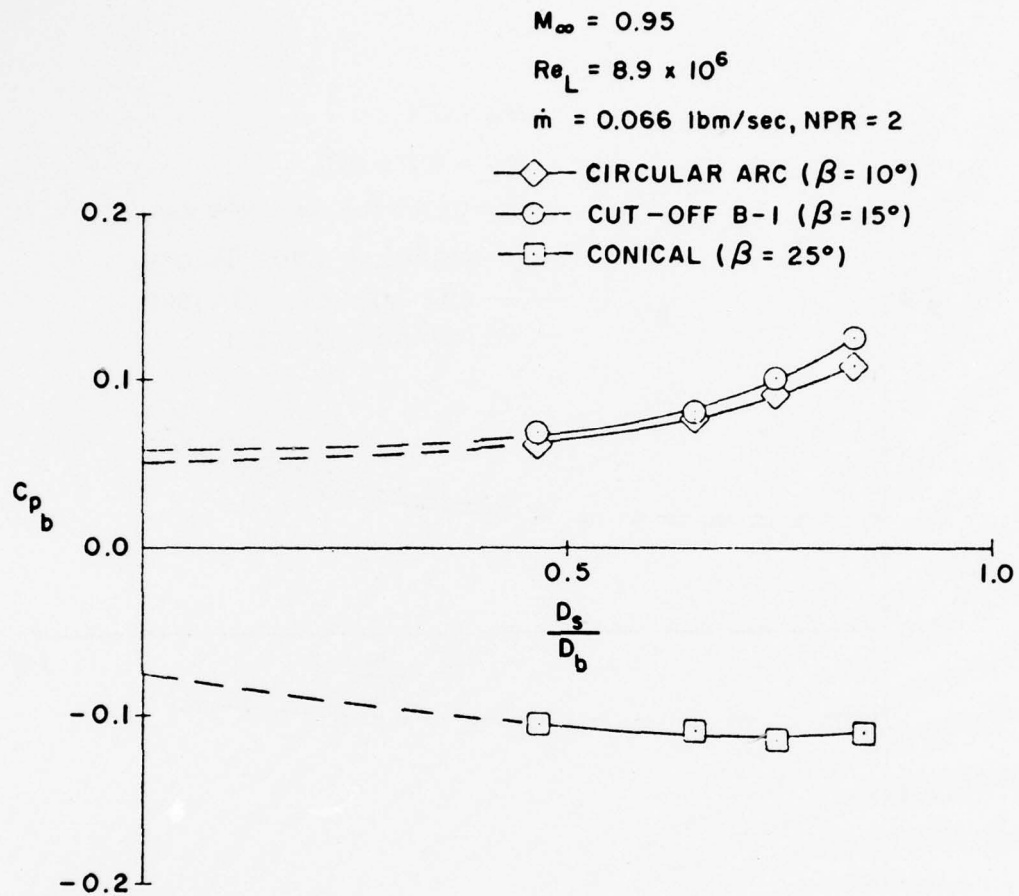


Figure 115. Base Pressure Coefficient Variation With Sting Size

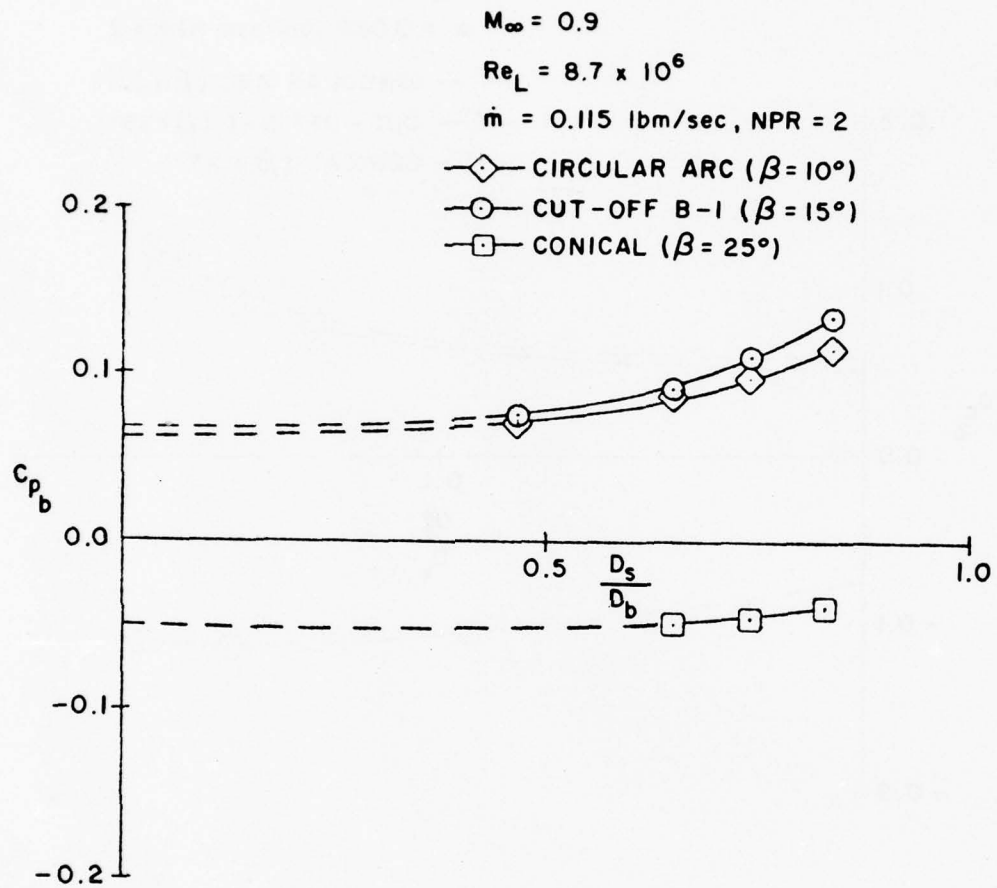


Figure 116. Base Pressure Coefficient Variation With Sting Size

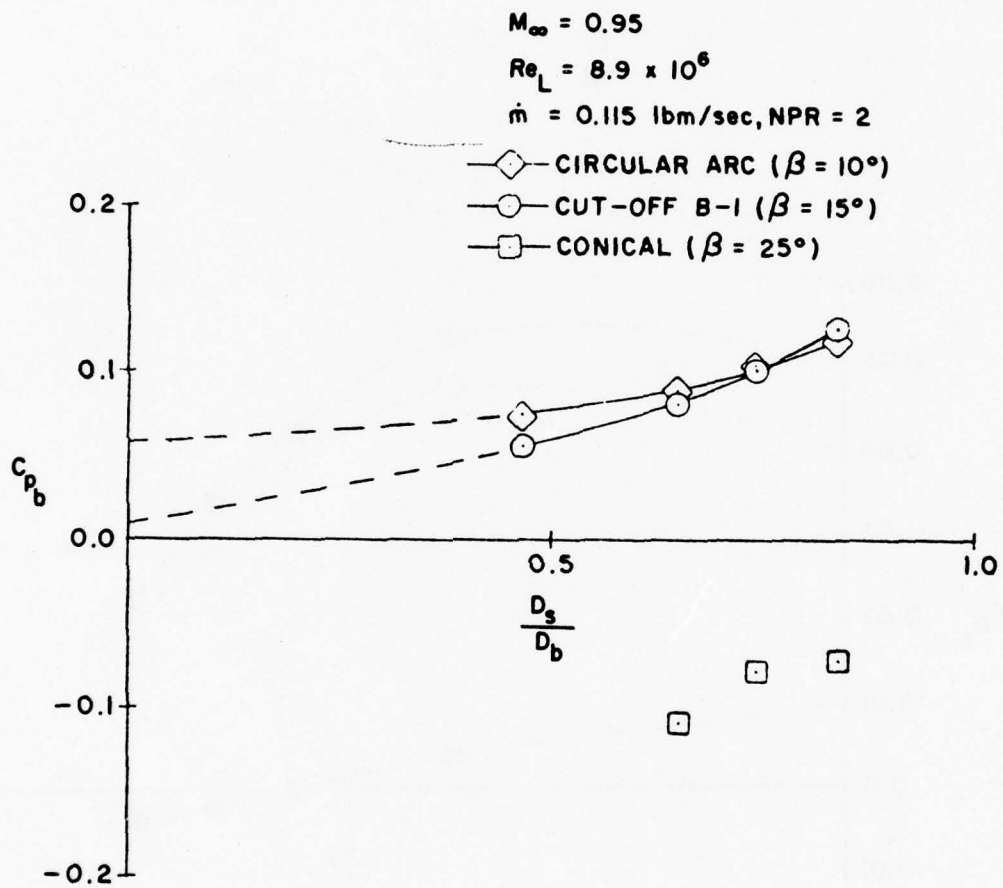


Figure 117. Base Pressure Coefficient Variation With Sting Size

SYMBOL	BOATTAIL	M_∞
◇	CIRCULAR ARC	0.9
◆	"	0.95
○	CUT-OFF B-1	0.9
●	"	0.95
□	CONICAL	0.9
■	"	0.95

$\dot{m} = 0.00$ lbm/sec

$P_o = 2000$ psfa

NPR = 2.0

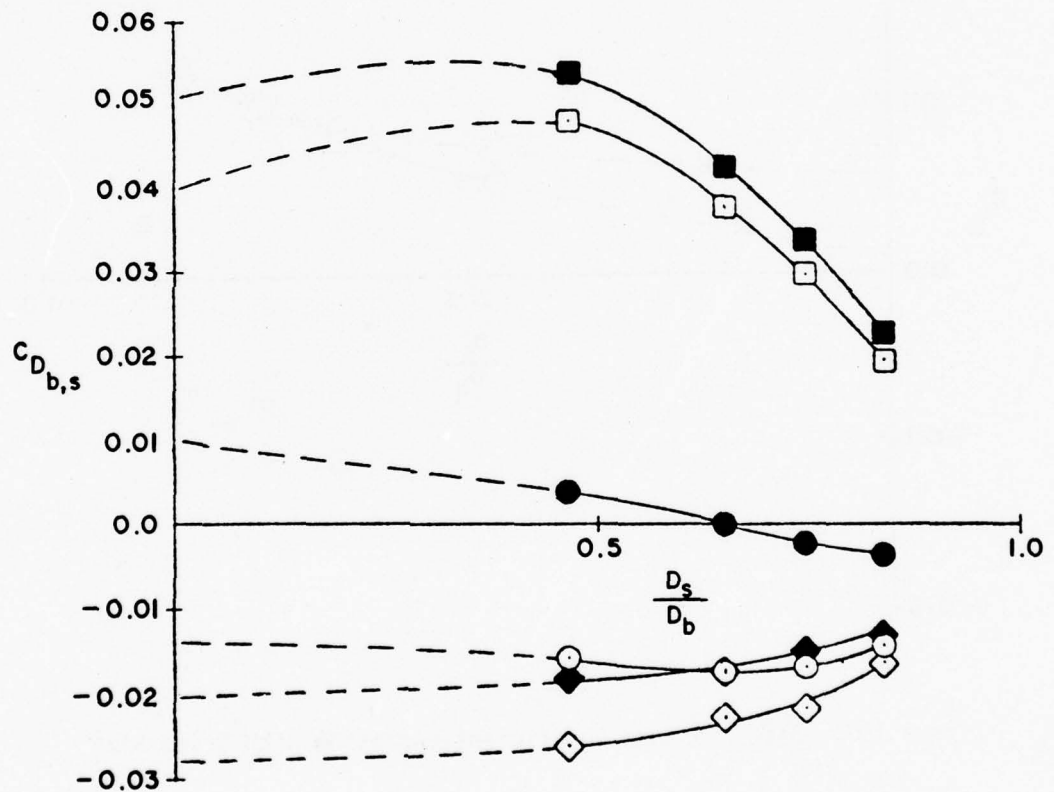


Figure 118. Base Drag Coefficient Variation With Sting Size

SYMBOL	BOATTAIL	M_∞
◇	CIRCULAR ARC	0.9
◆	"	0.95
○	CUT-OFF B-1	0.9
●	"	0.95
□	CONICAL	0.9
■	"	0.95

$\dot{m} = 0.066 \text{ lbm/sec}$

$p_o = 2000 \text{ psfa}$

$\text{NPR} = 2.0$

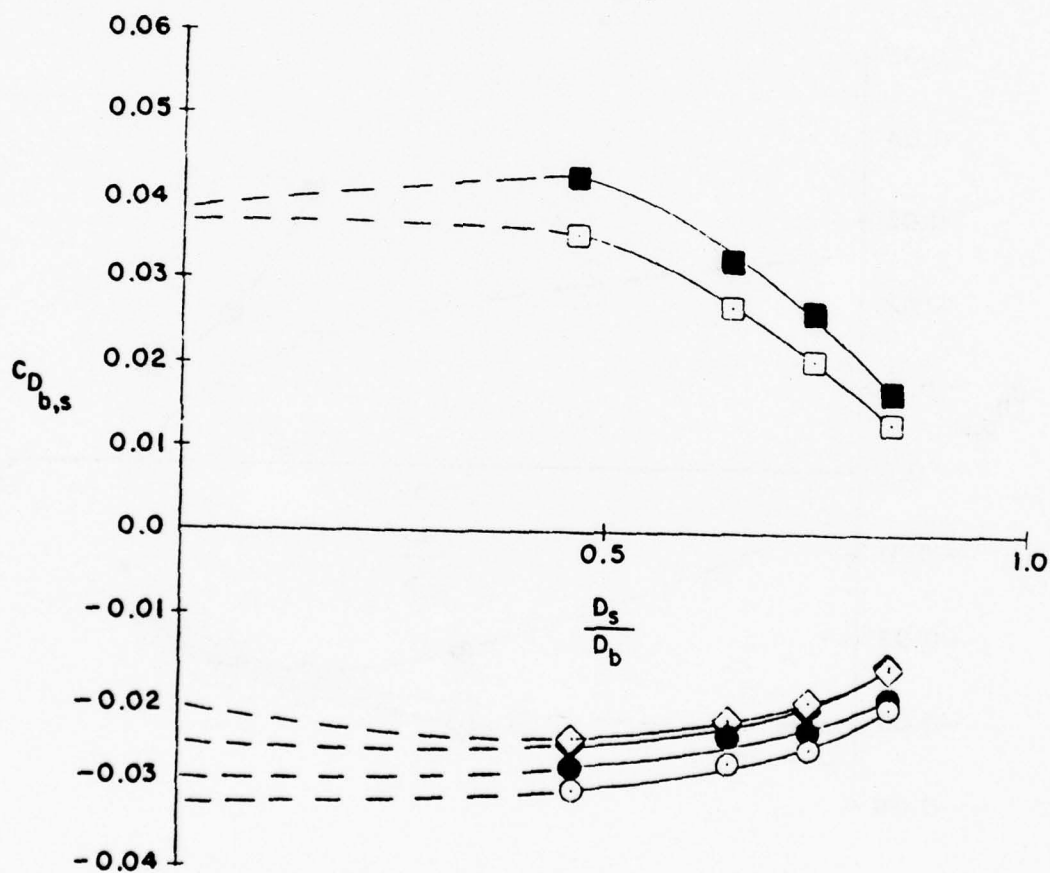


Figure 119. Base Drag Coefficient Variation With Sting Size

SYMBOL	BOATTAIL	M_∞
\diamond	CIRCULAR ARC	0.9
\blacklozenge	"	0.95
\odot	CUT-OFF B-1	0.9
\bullet	"	0.95
\square	CONICAL	0.9
\blacksquare	"	0.95

$\dot{m} = 0.115 \text{ lbm/sec}$

$p_o = 2000 \text{ psfa}$

$NPR = 2.0$

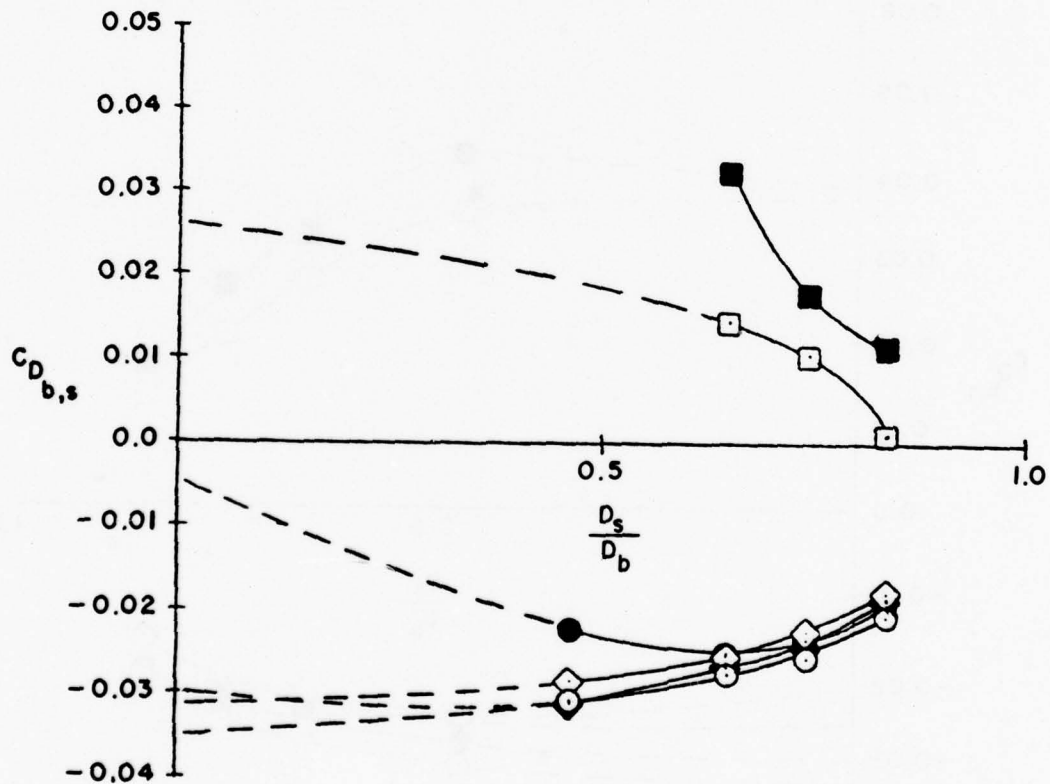


Figure 120. Base Drag Coefficient Variation With Sting Size

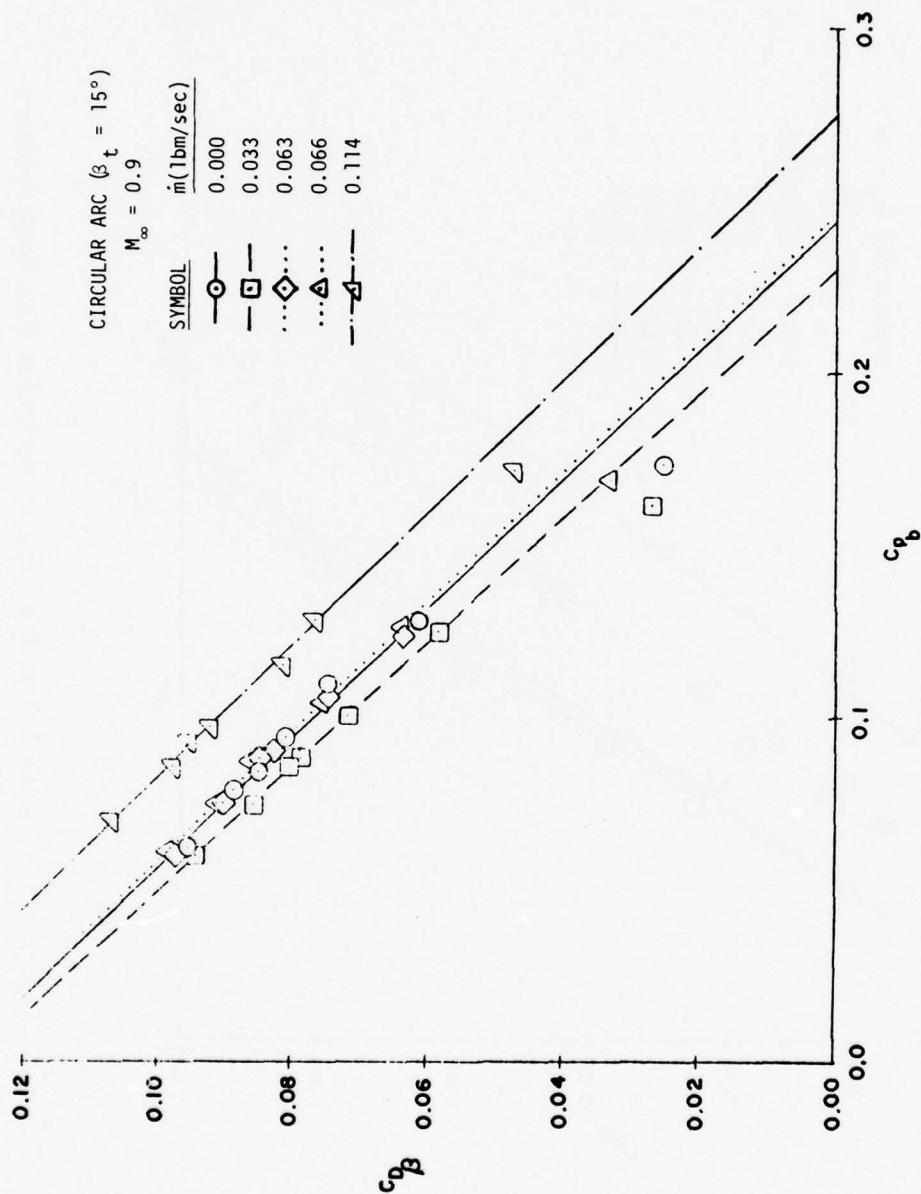


Figure 121. Boattail Drag Coefficient Variation With Base Pressure

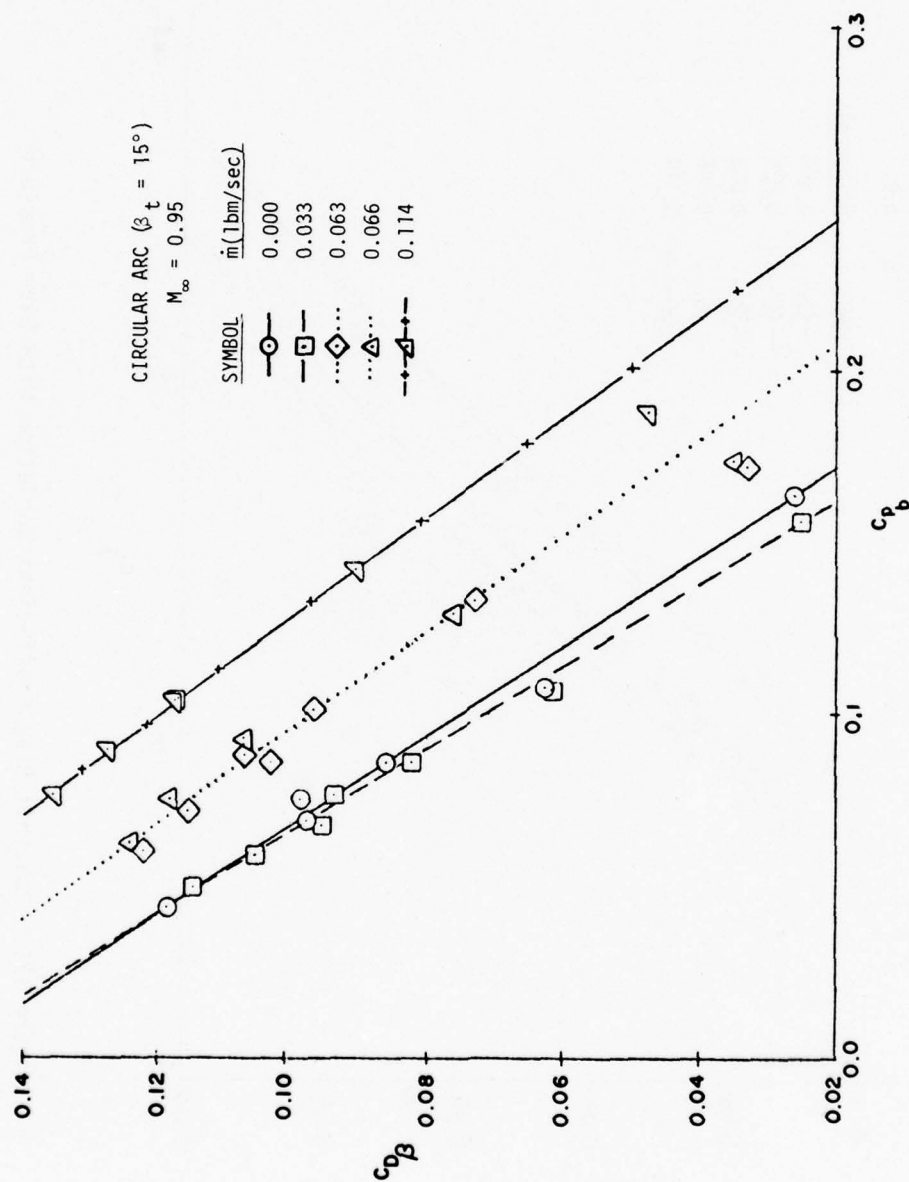


Figure 122. Boattail Drag Coefficient Variation With Base Pressure

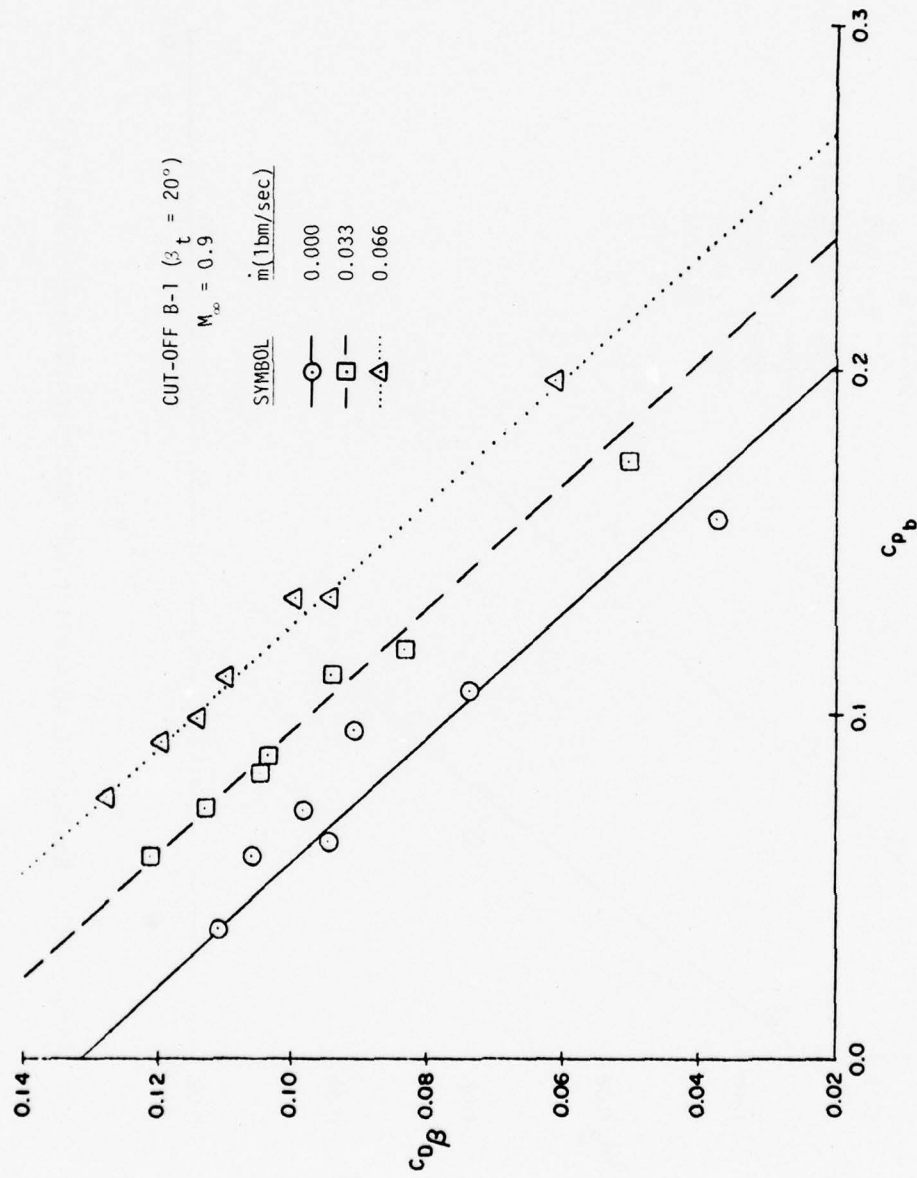


Figure 123. Boattail Drag Coefficient Variation With Base Pressure

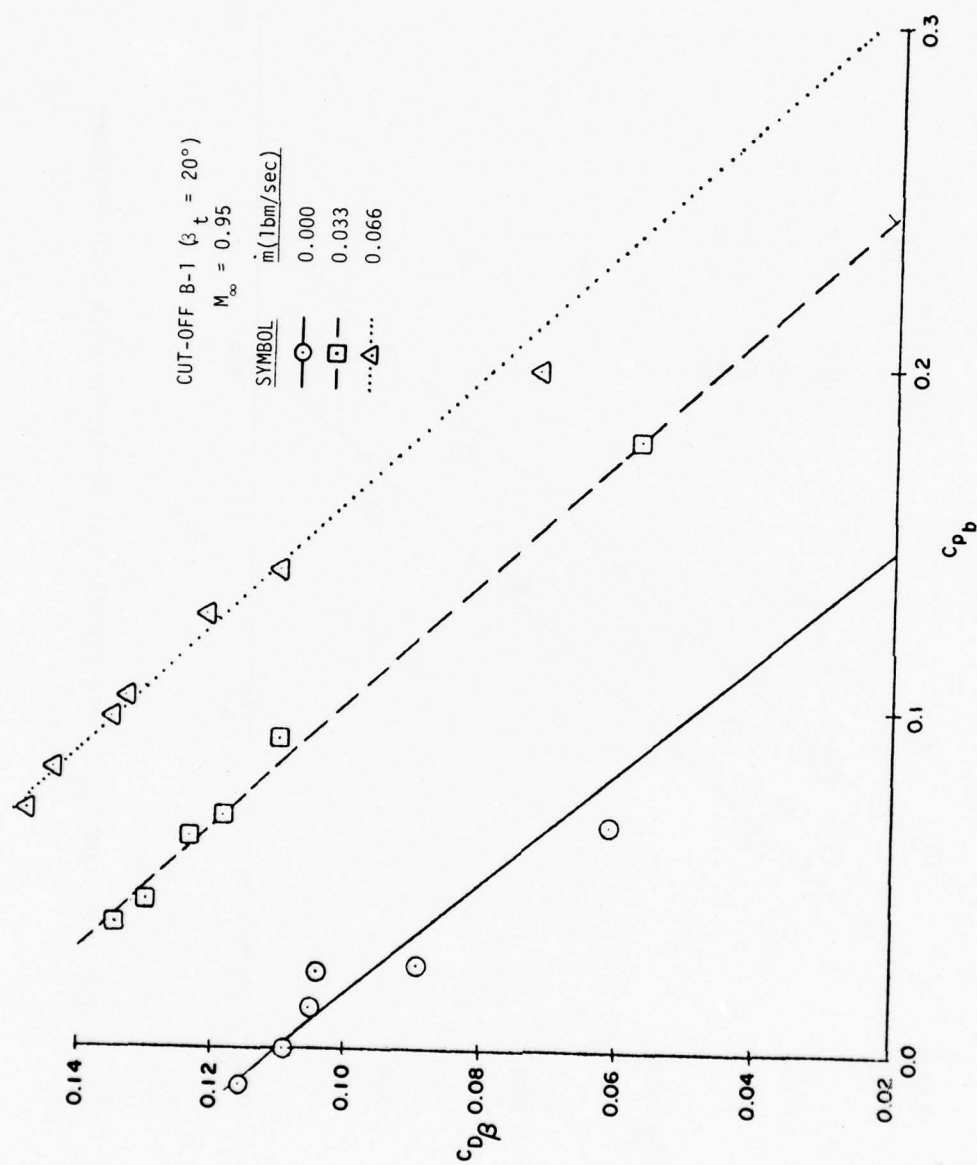


Figure 124. Boattail Drag Coefficient Variation With Base Pressure

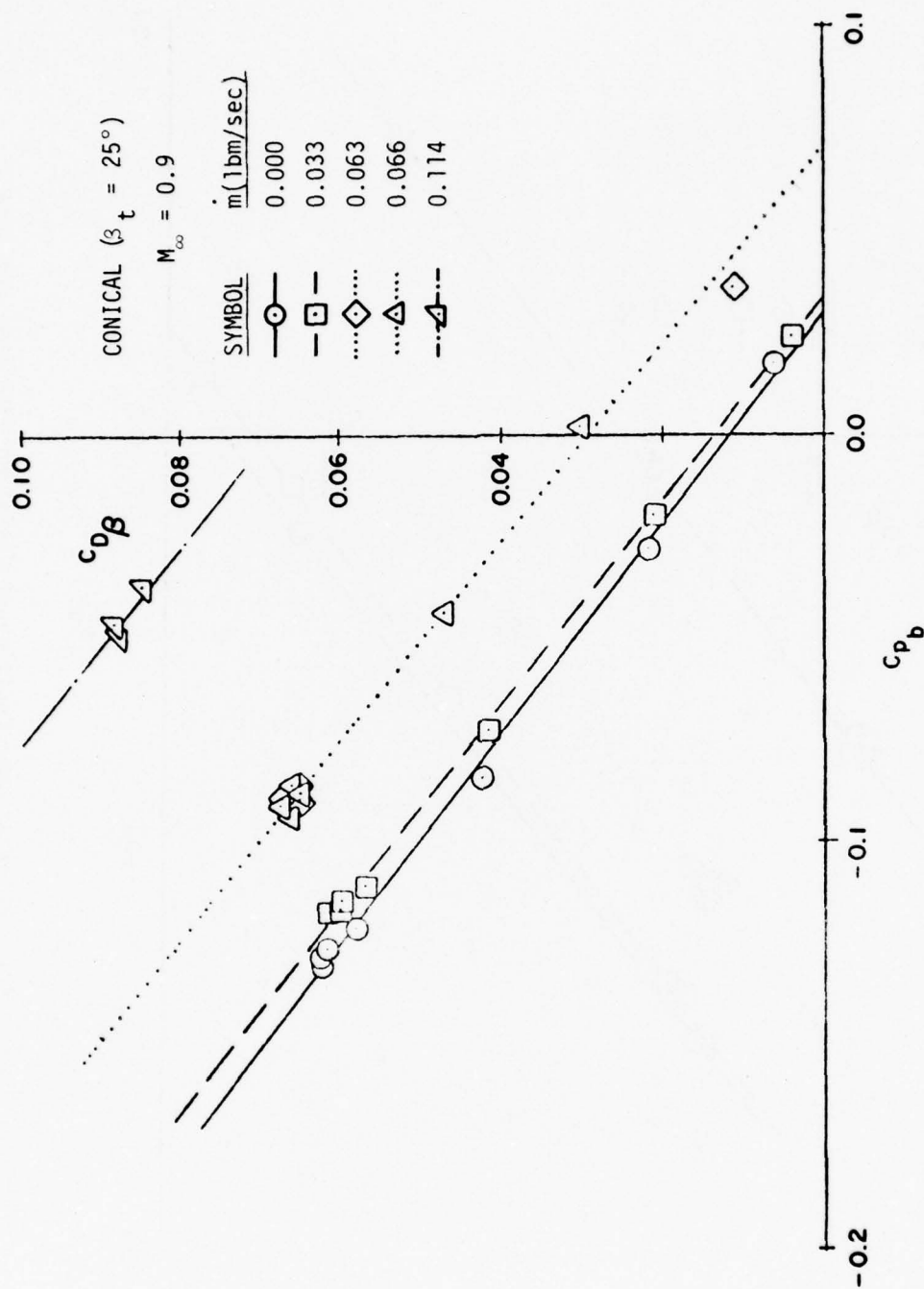


Figure 125. Boattail Drag Coefficient Variation With Base Pressure

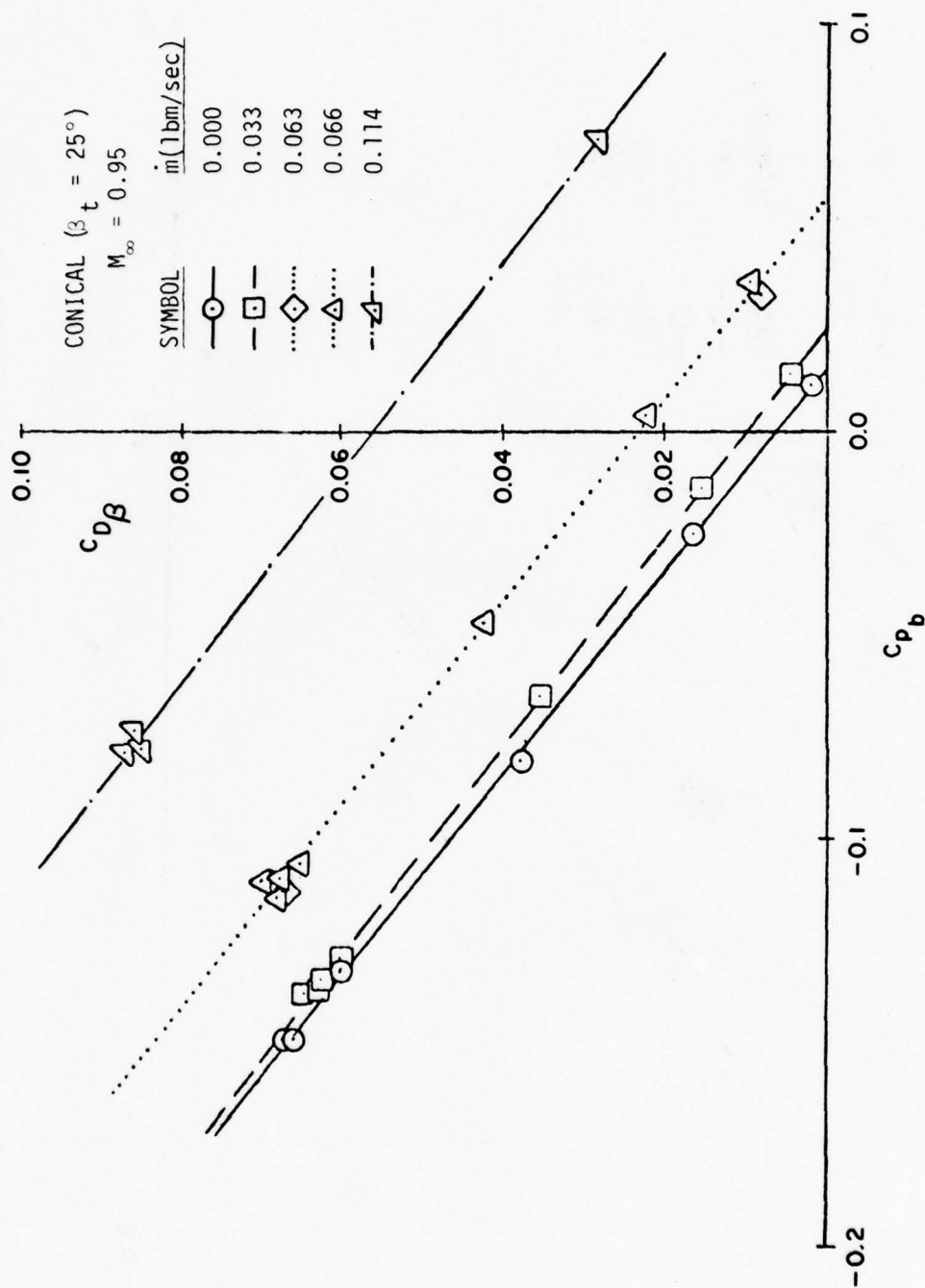


Figure 126. Boattail Drag Coefficient Variation With Base Pressure

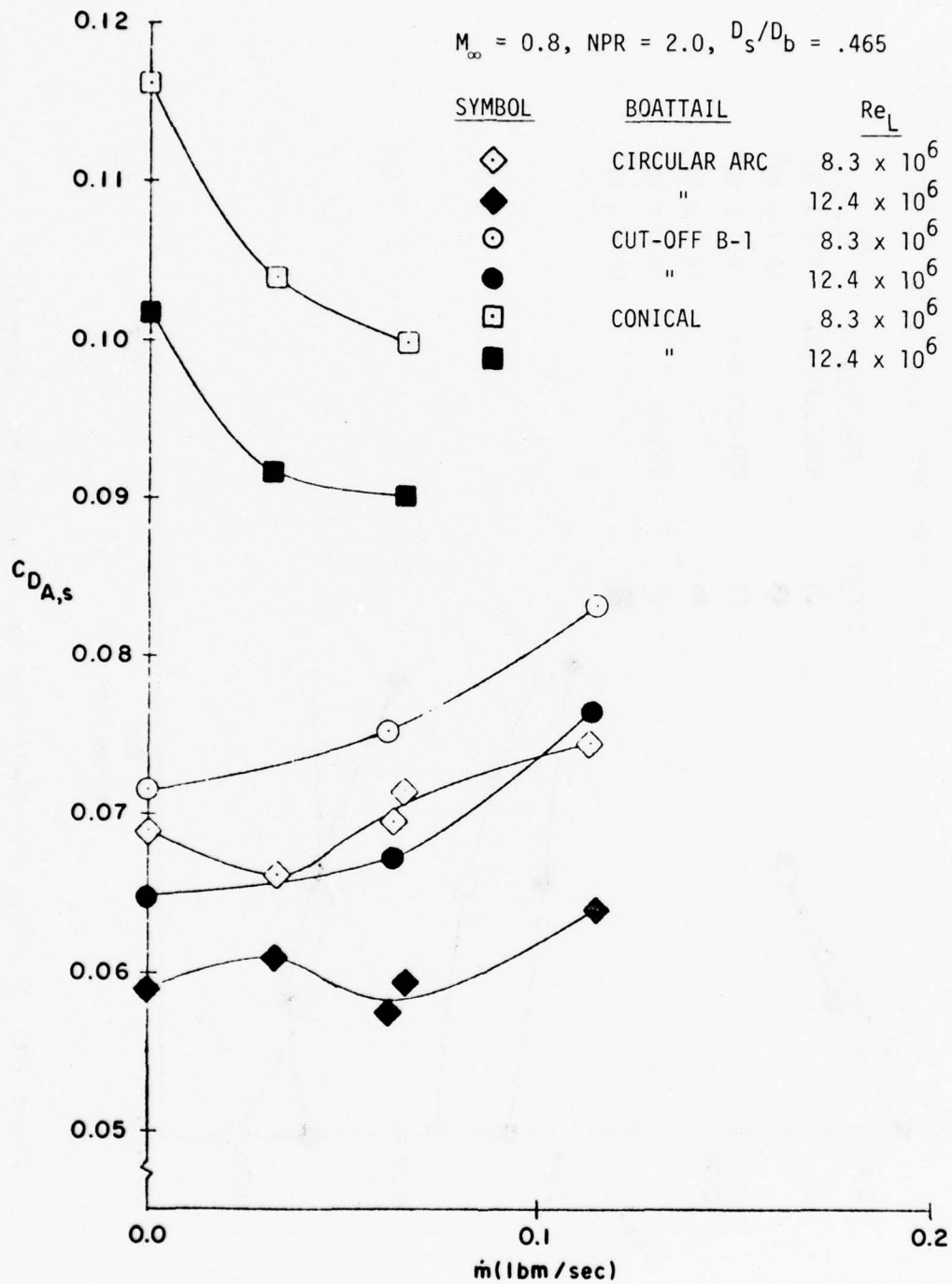


Figure 127. Afterbody Drag Coefficient Variation With Mass Injection for Different Reynolds Numbers, and NPR=2

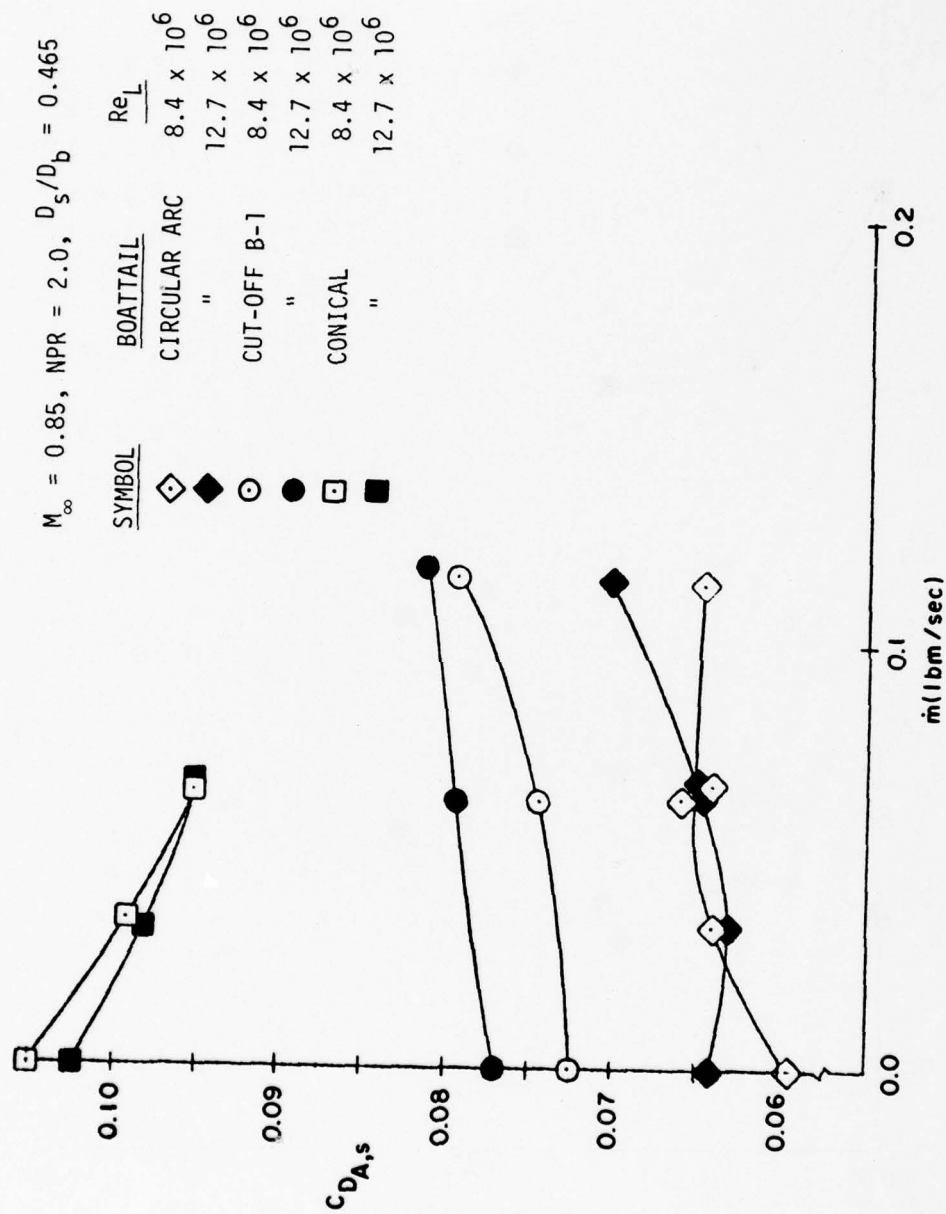


Figure 128. Afterbody Drag Coefficient Variation with Mass Injection for Different Reynolds Numbers, and $NPR=2$

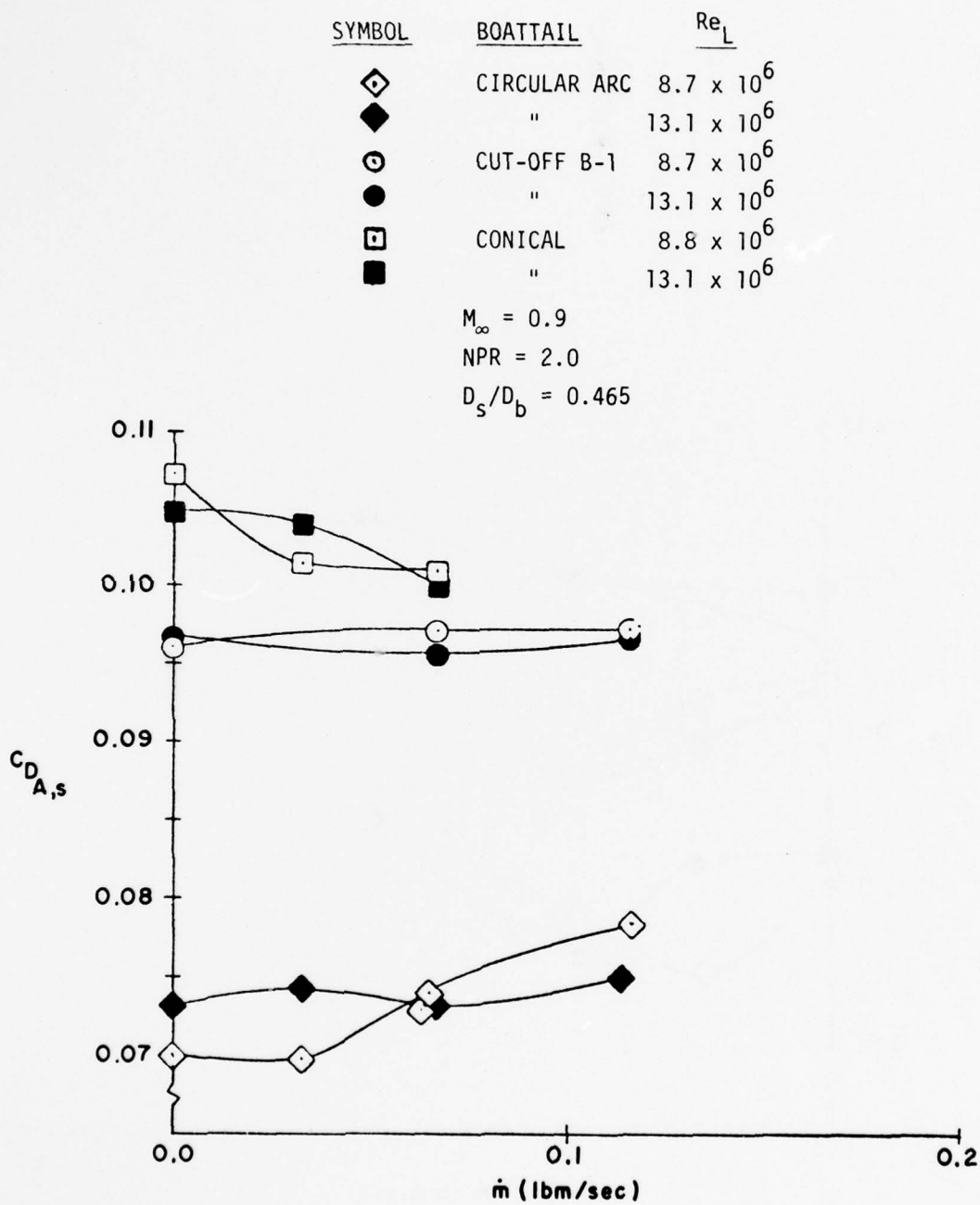


Figure 129. Afterbody Drag Coefficient Variation With Mass Injection for Different Reynolds Numbers, and $NPR=2$

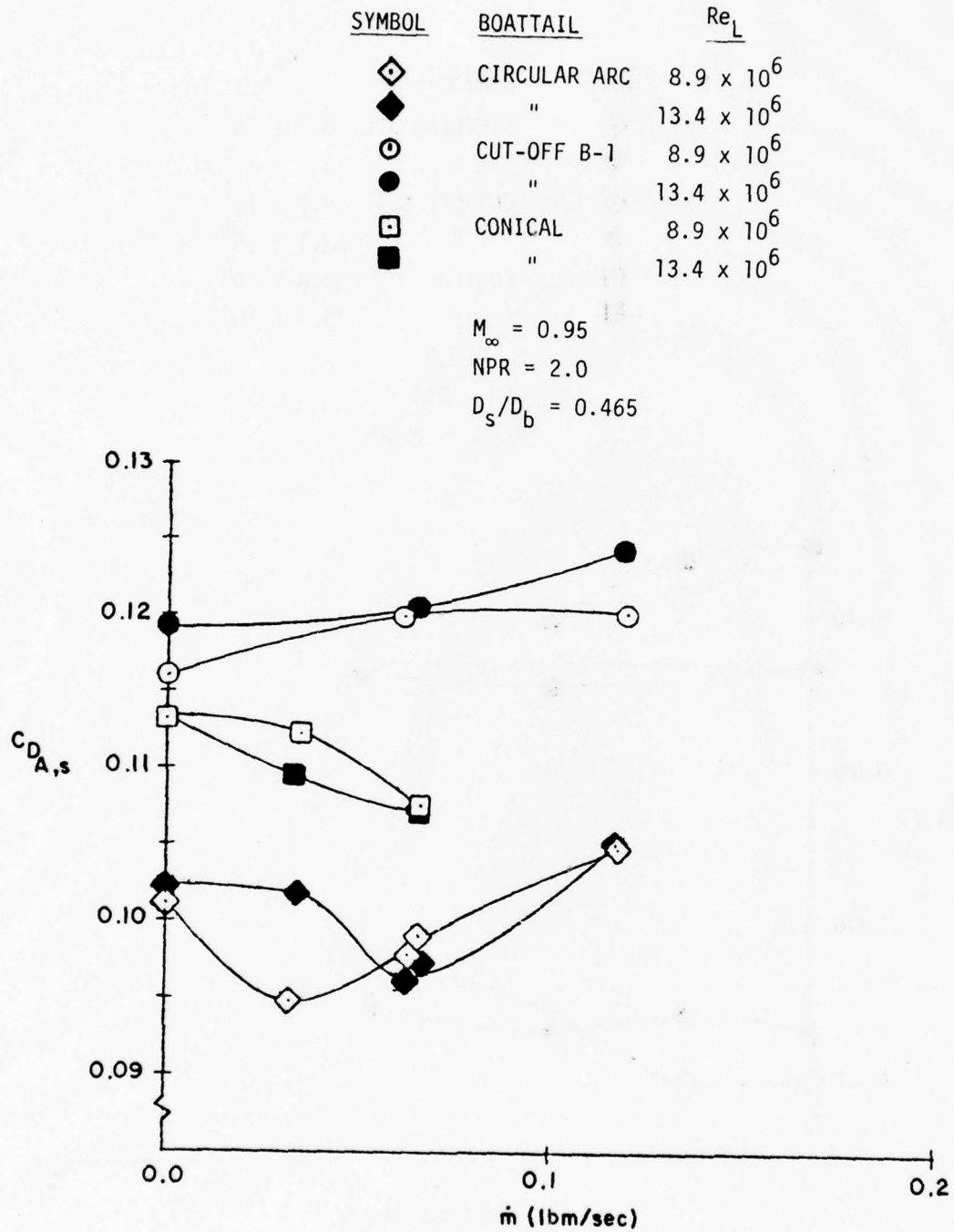


Figure 130. Afterbody Drag Coefficient Variation With Mass Injection for Different Reynolds Numbers, and $NPR=2$

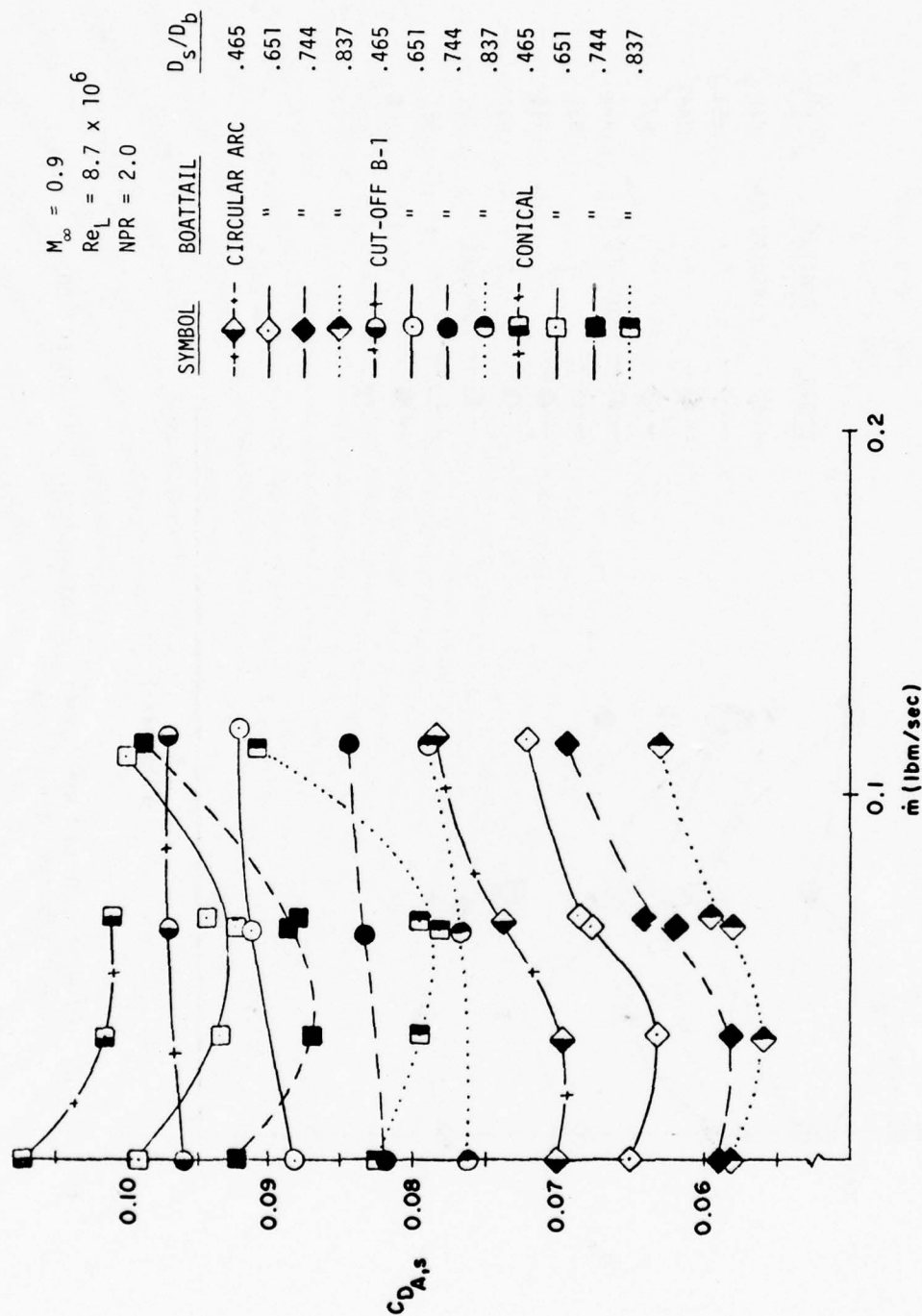


Figure 131. Afterbody Drag Coefficient Variation With Mass Injection for Different Sting Sizes

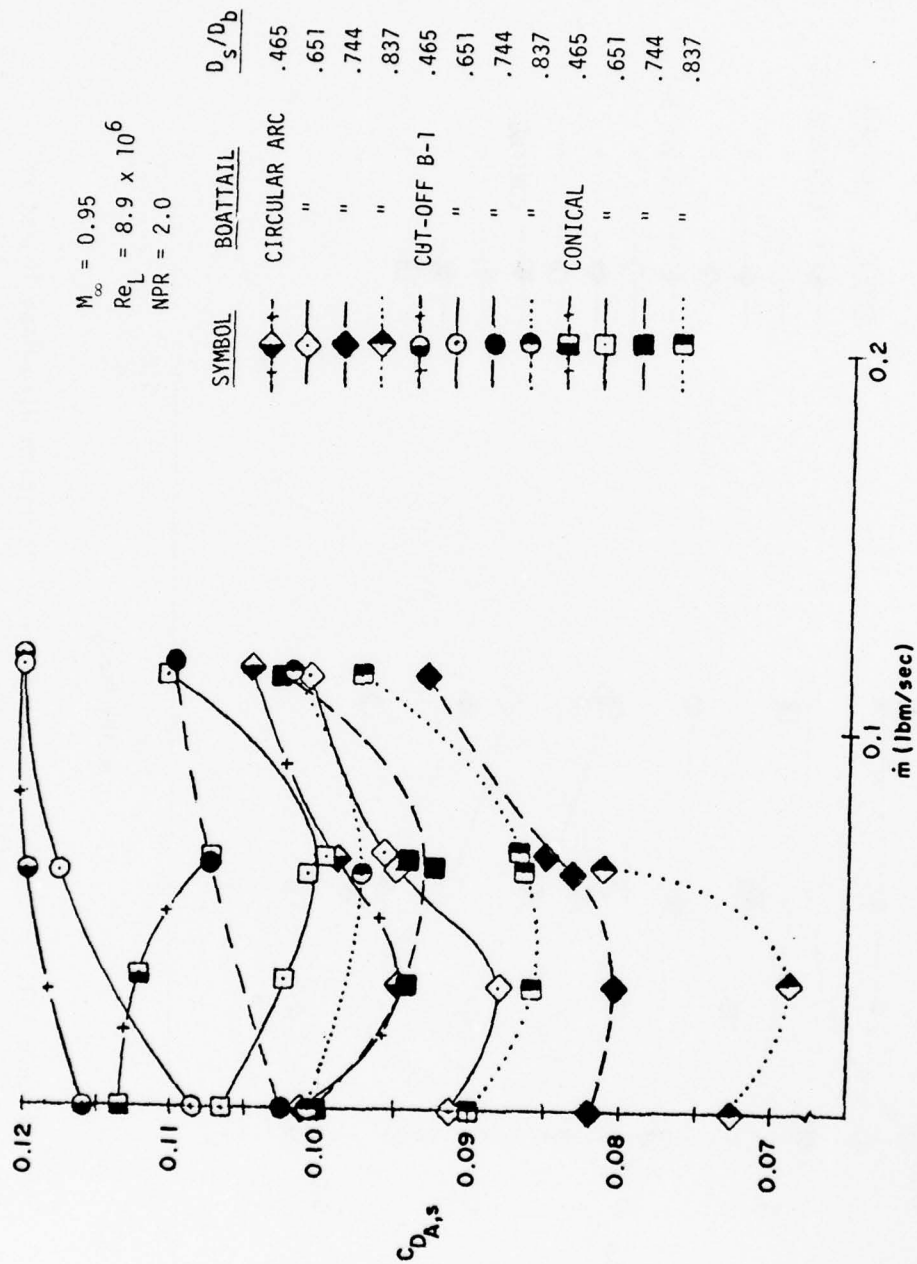


Figure 132. Afterbody Drag Coefficient Variation With Mass Injection for Different Sting Sizes

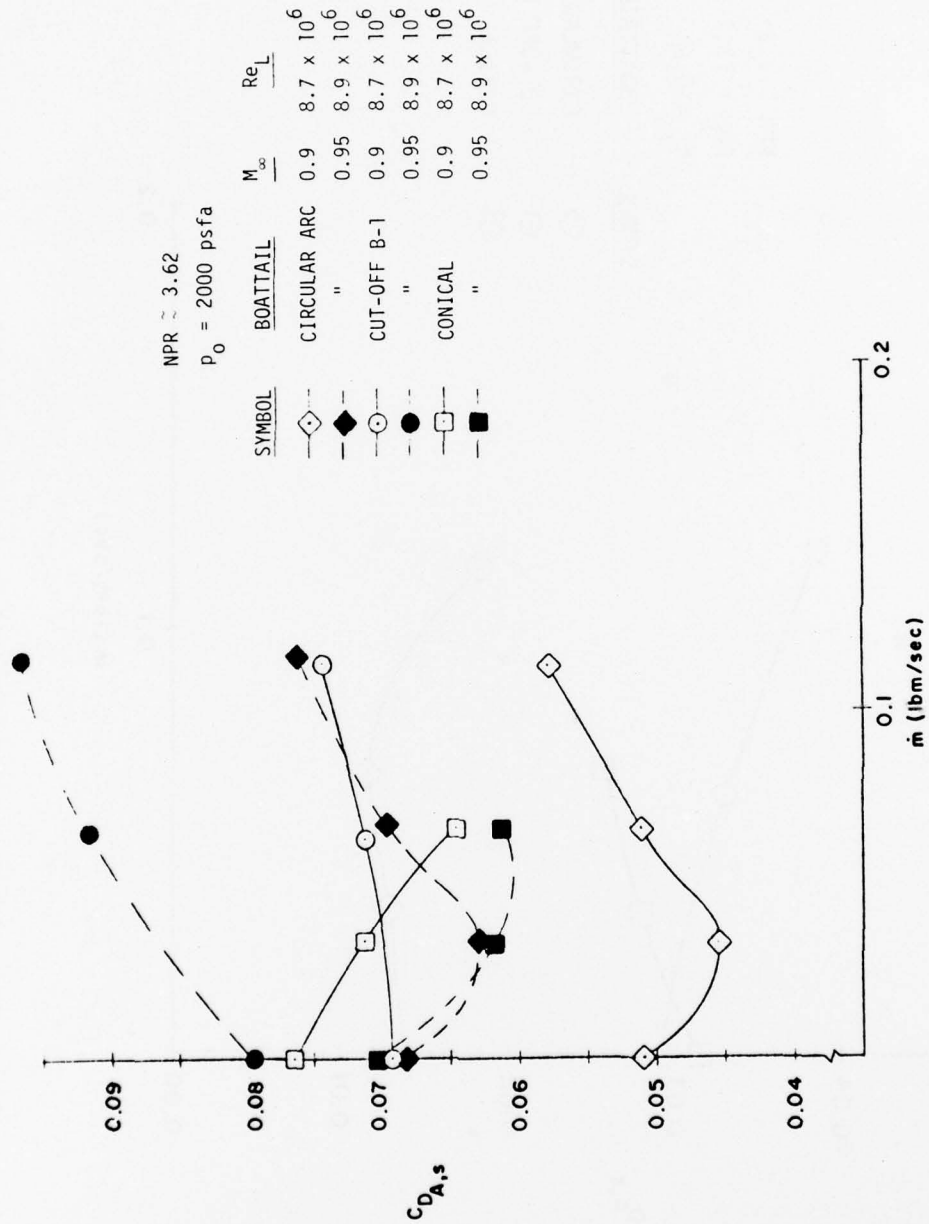


Figure 133. Afterbody Drag Coefficient Variation With Mass Injection for NPR=3.62

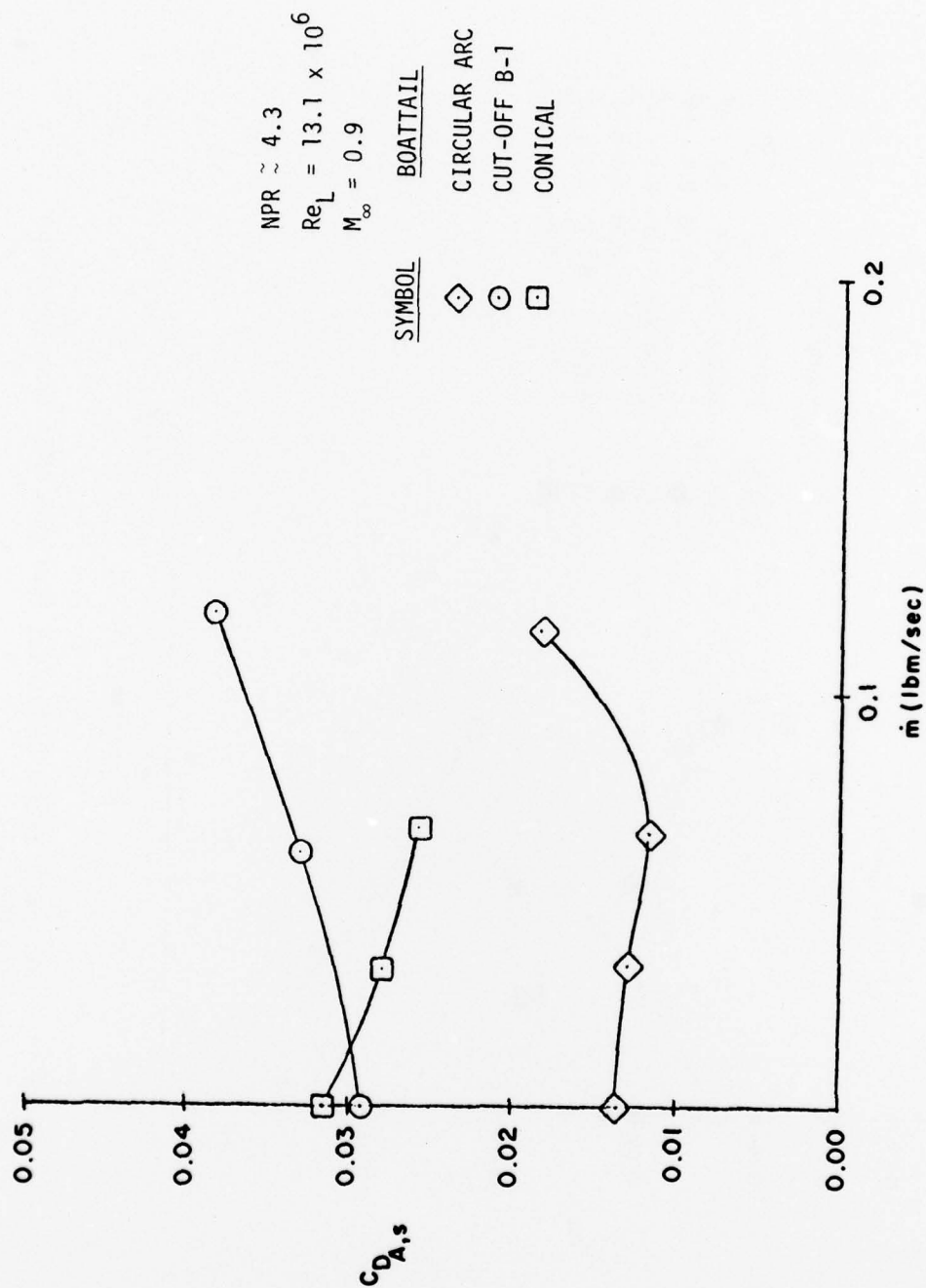


Figure 134. Afterbody Drag Coefficient Variation With Mass Injection for $\text{NPR}=4.3$

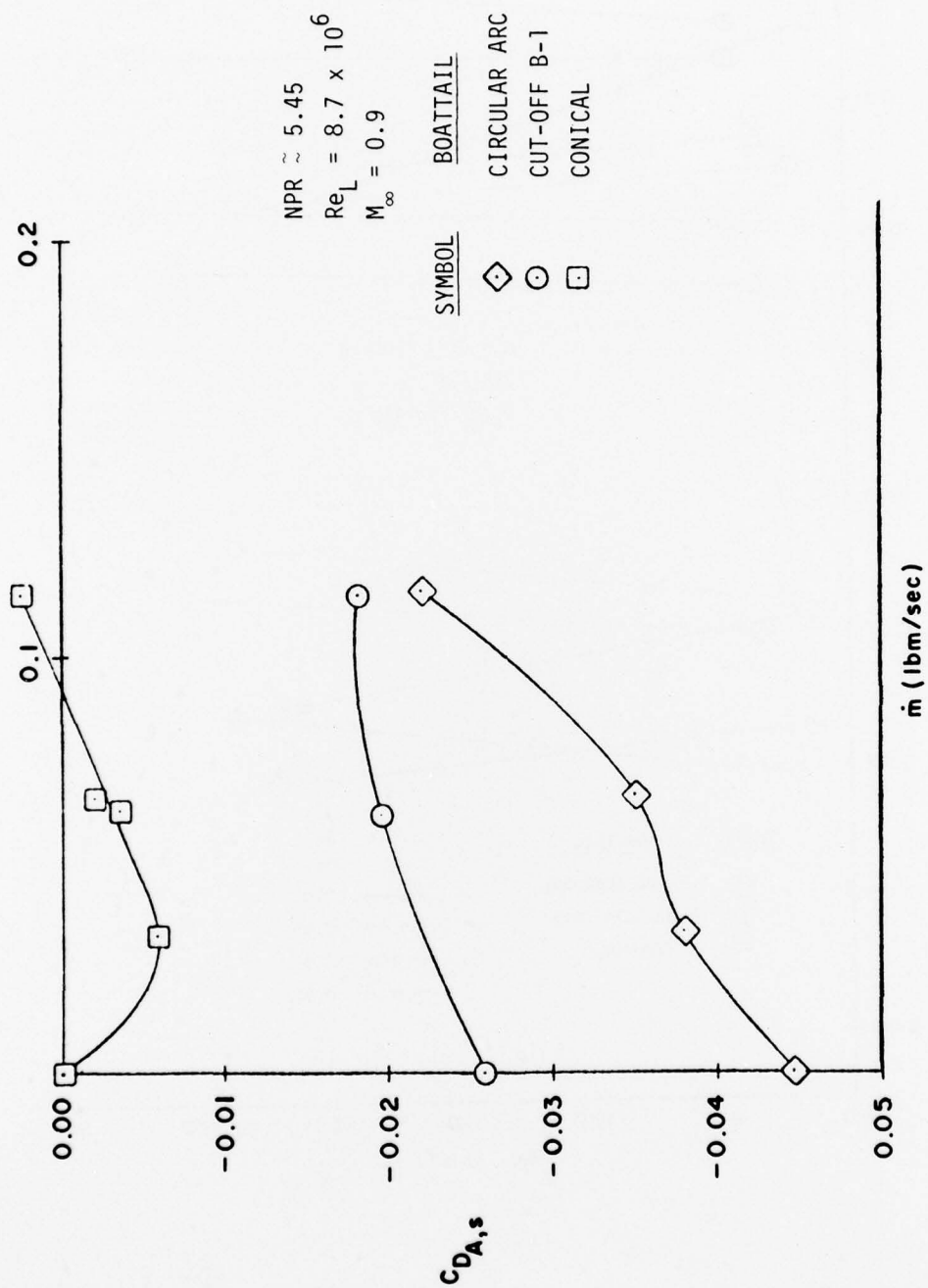


Figure 135. Afterbody Drag Coefficient Variation With Mass Injection for NPR=5.45

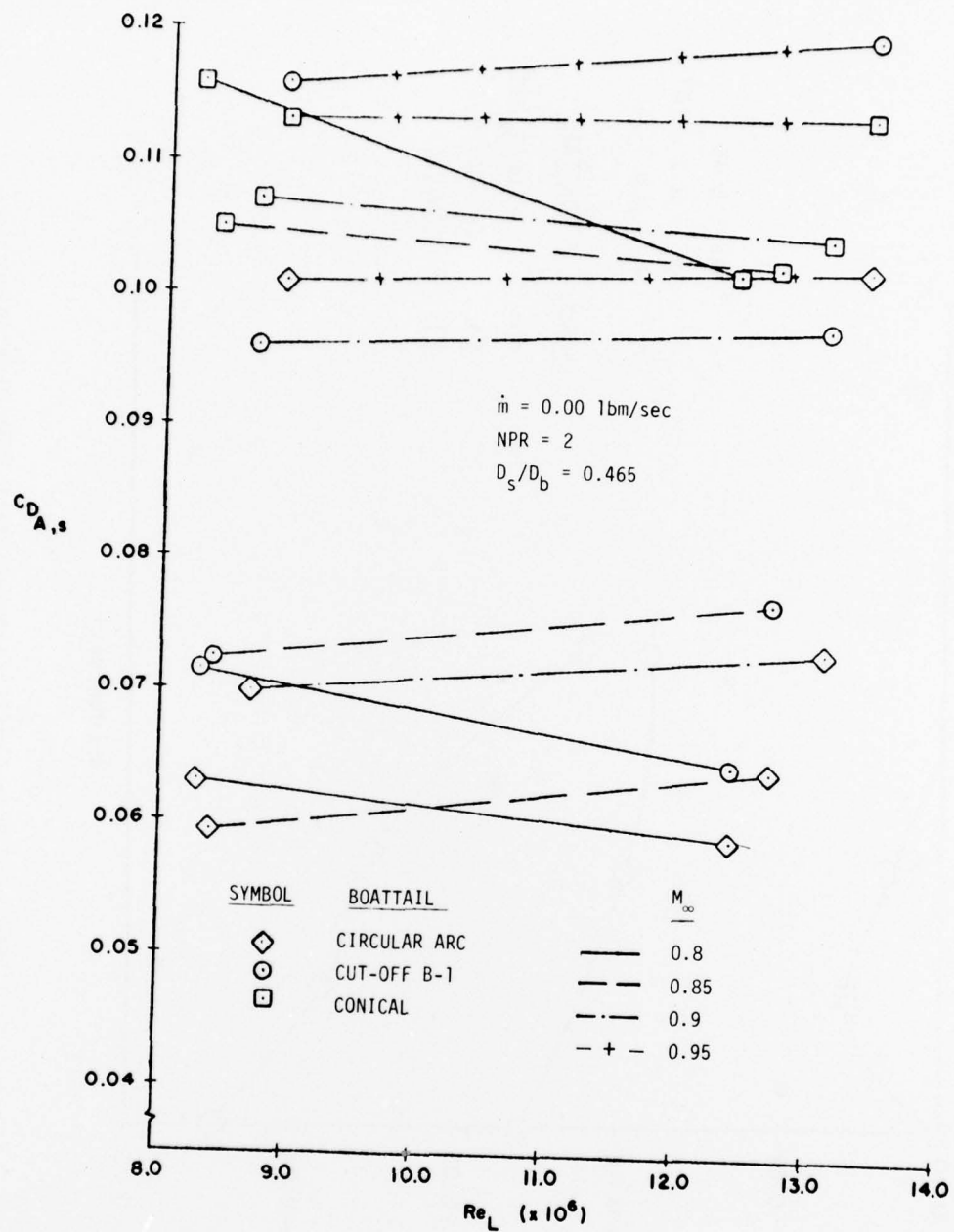


Figure 136. Afterbody Drag Coefficient Variation With Reynolds Number

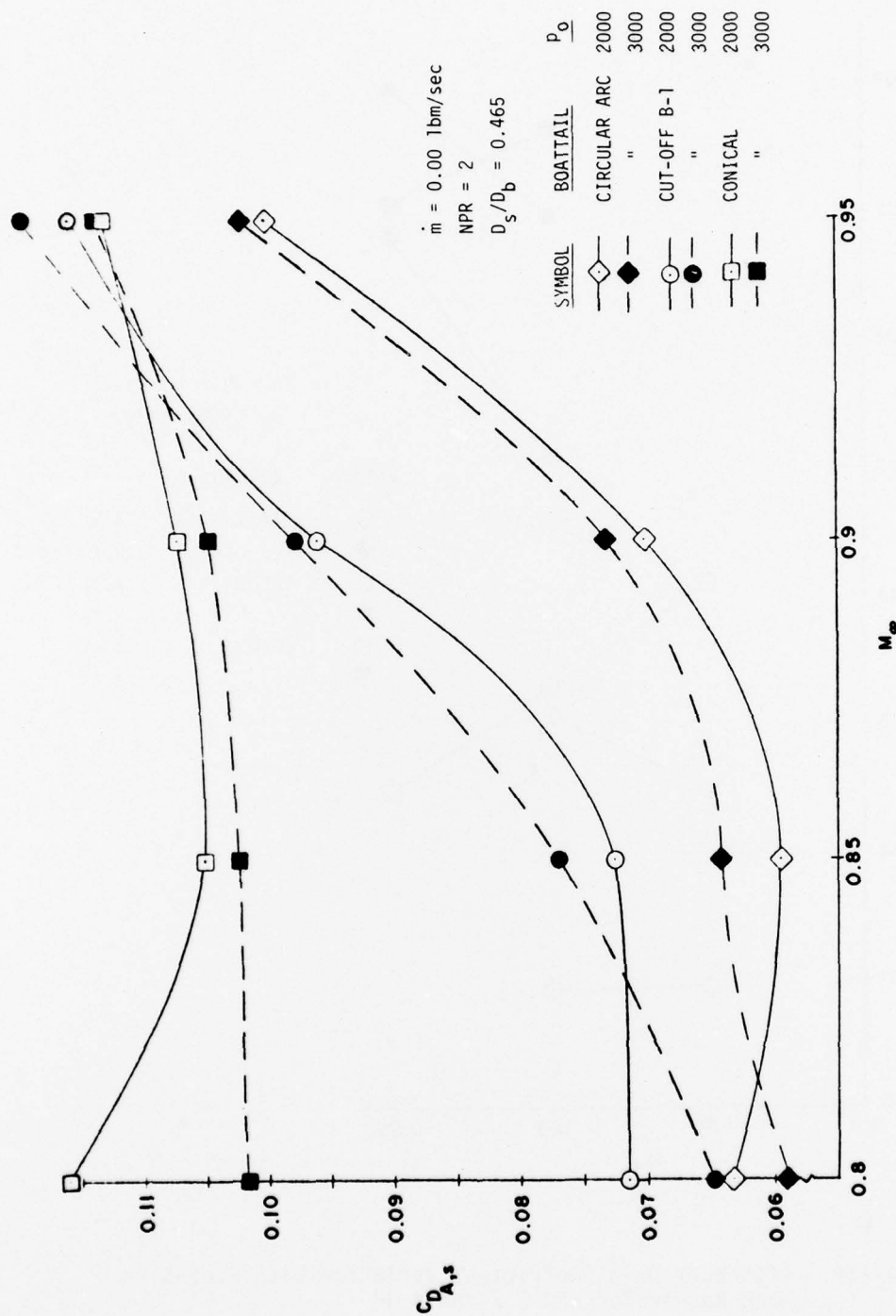


Figure 137. Afterbody Drag Coefficient Variation With Free-Stream Mach Number for NPR=2

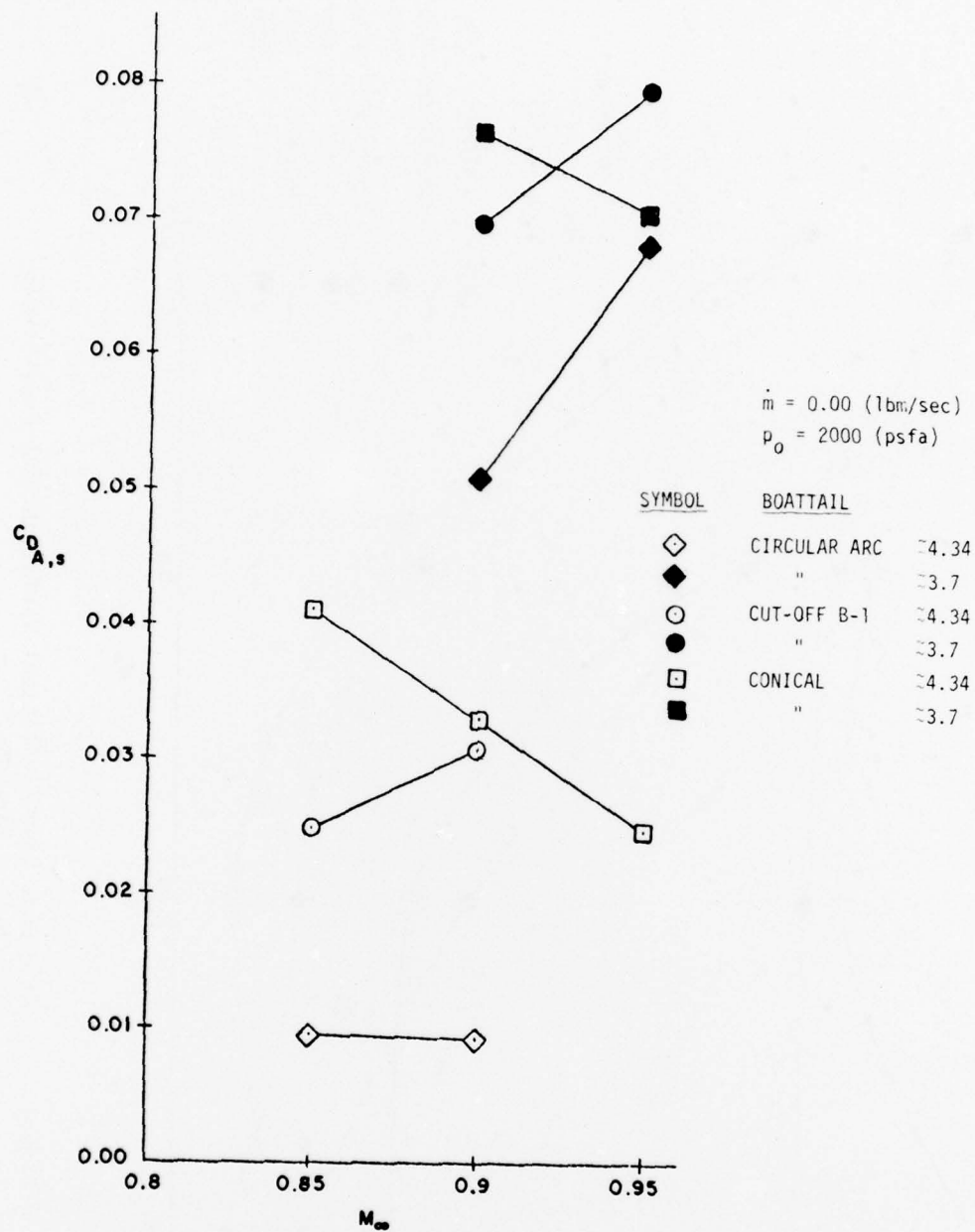


Figure 138. Afterbody Drag Coefficient Variation With Free-Stream Mach Number for NPR=3.7 and 4.34

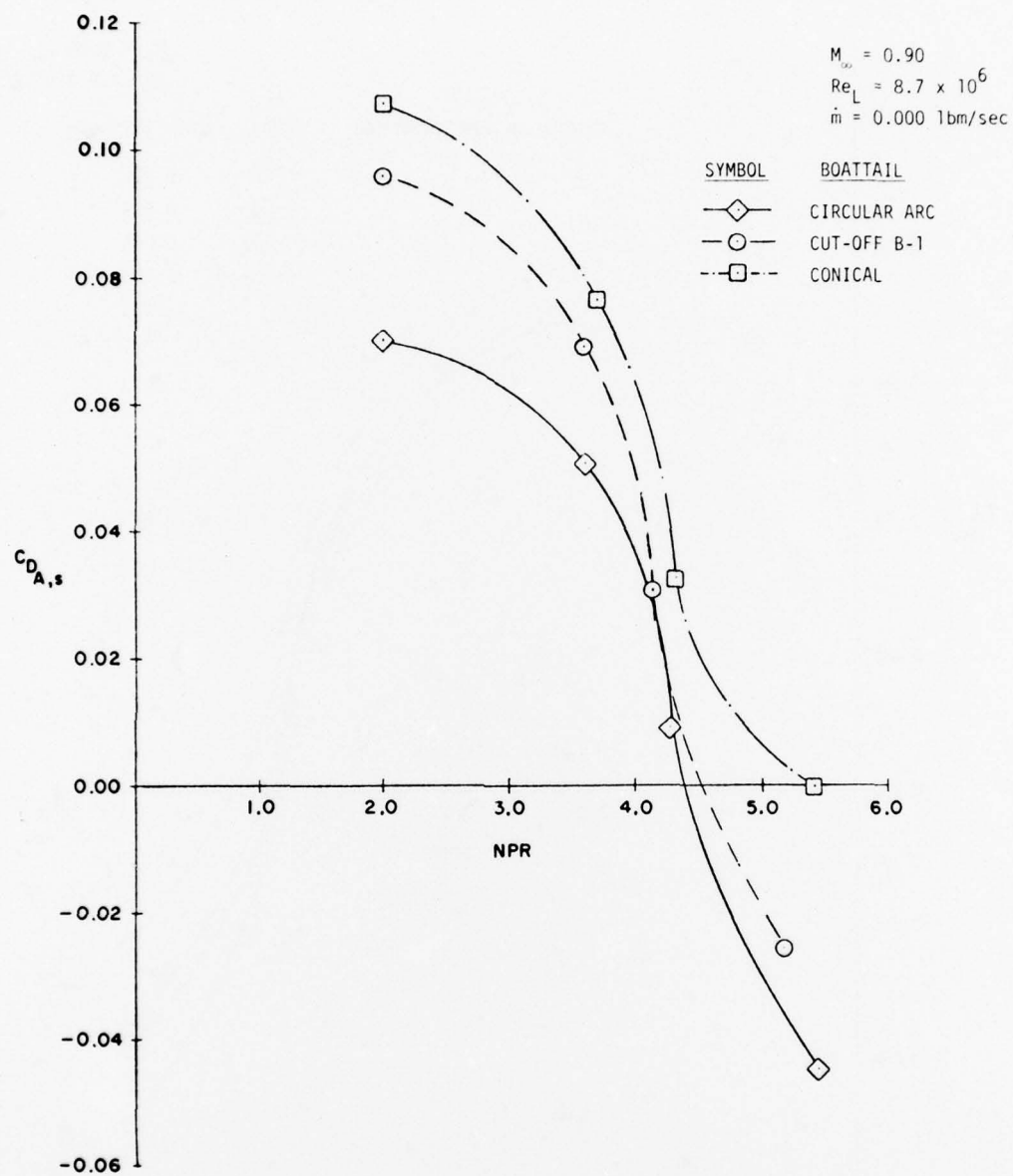


Figure 139. Afterbody Drag Coefficient Variation With Nozzle Pressure Ratio Without Mass Injection

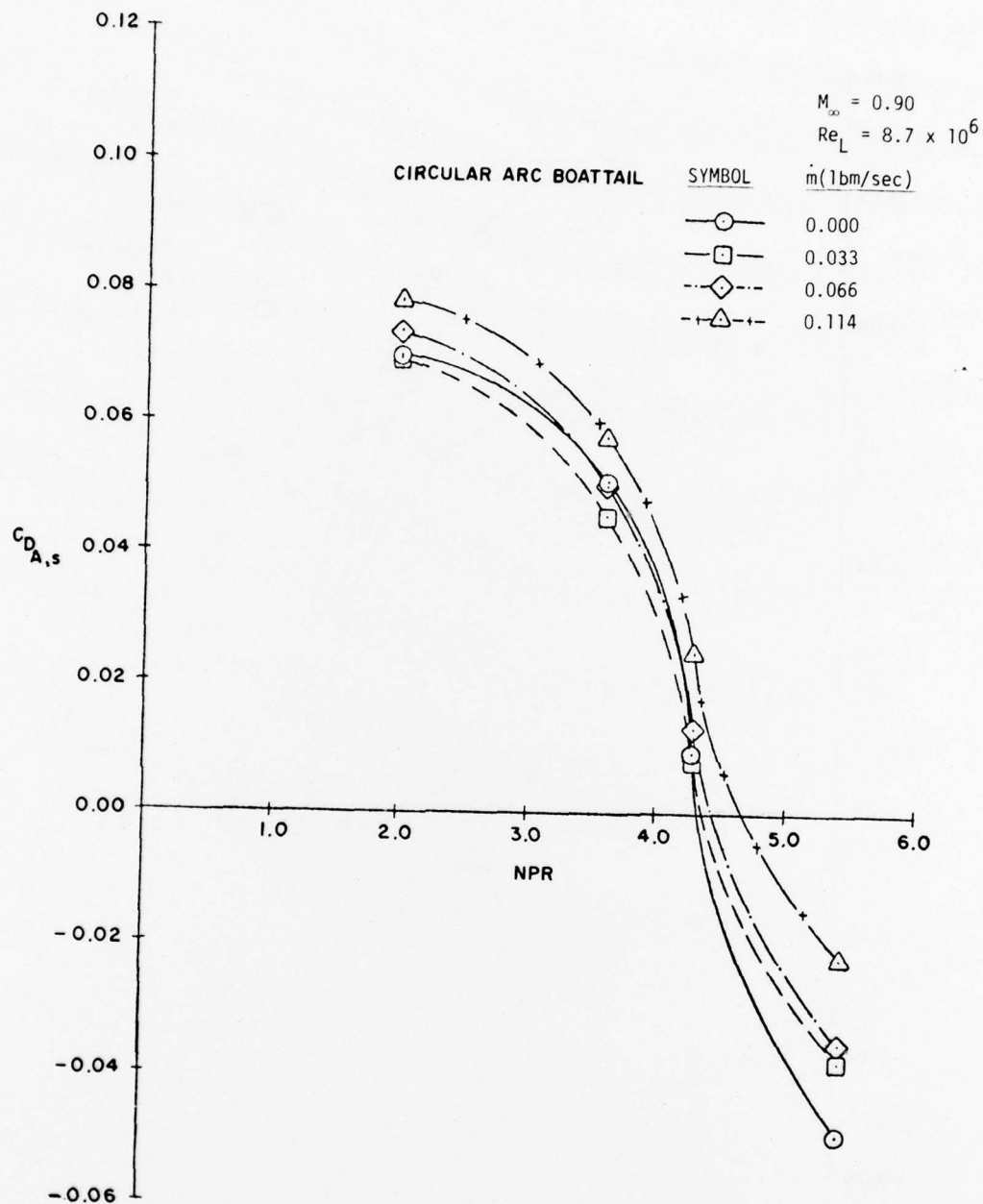


Figure 140. Afterbody Drag Coefficient Variation With Nozzle Pressure Ratio for Different Mass Injection Rates

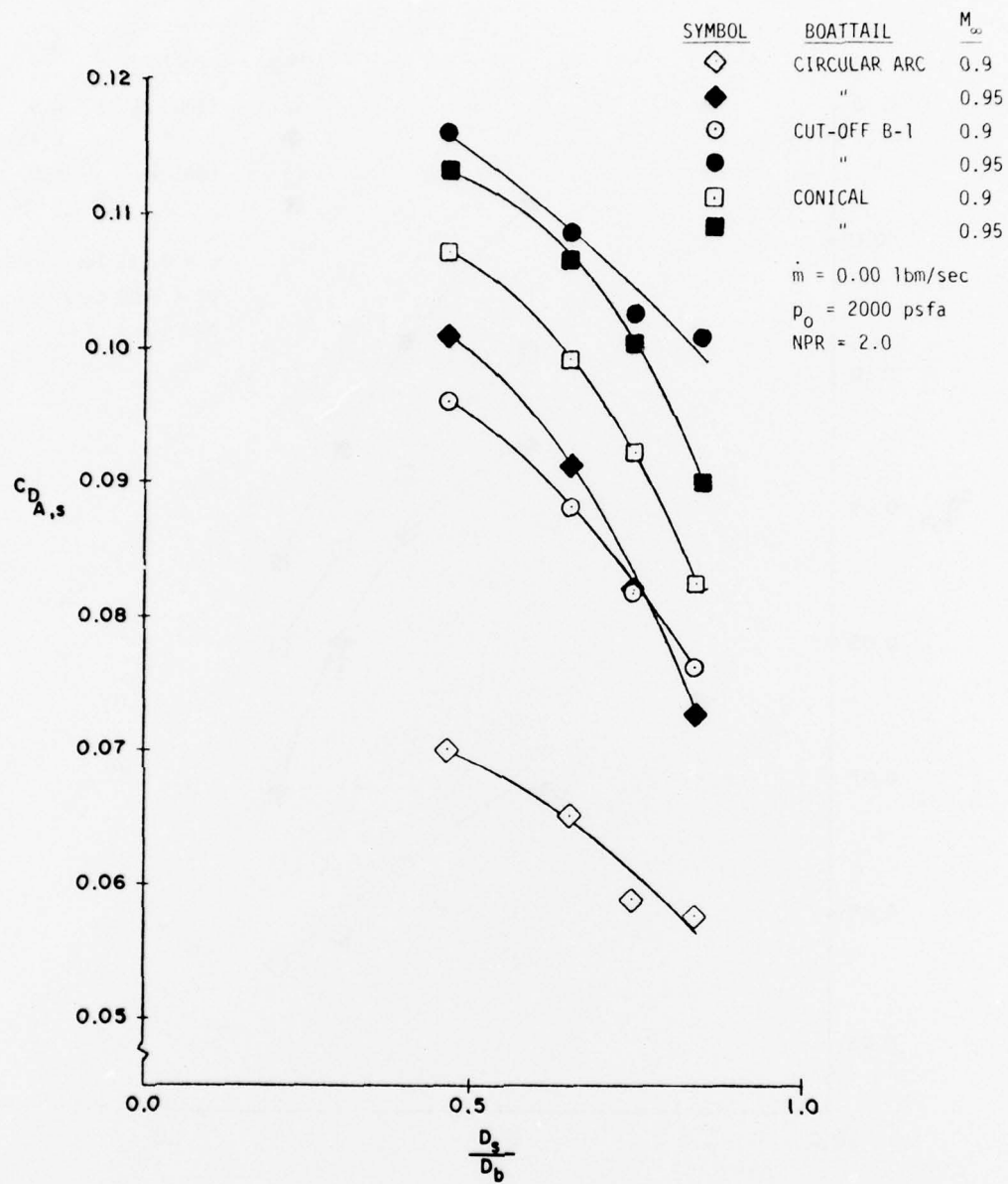


Figure 141. Afterbody Drag Coefficient Variation With Sting Size Without Mass Injection

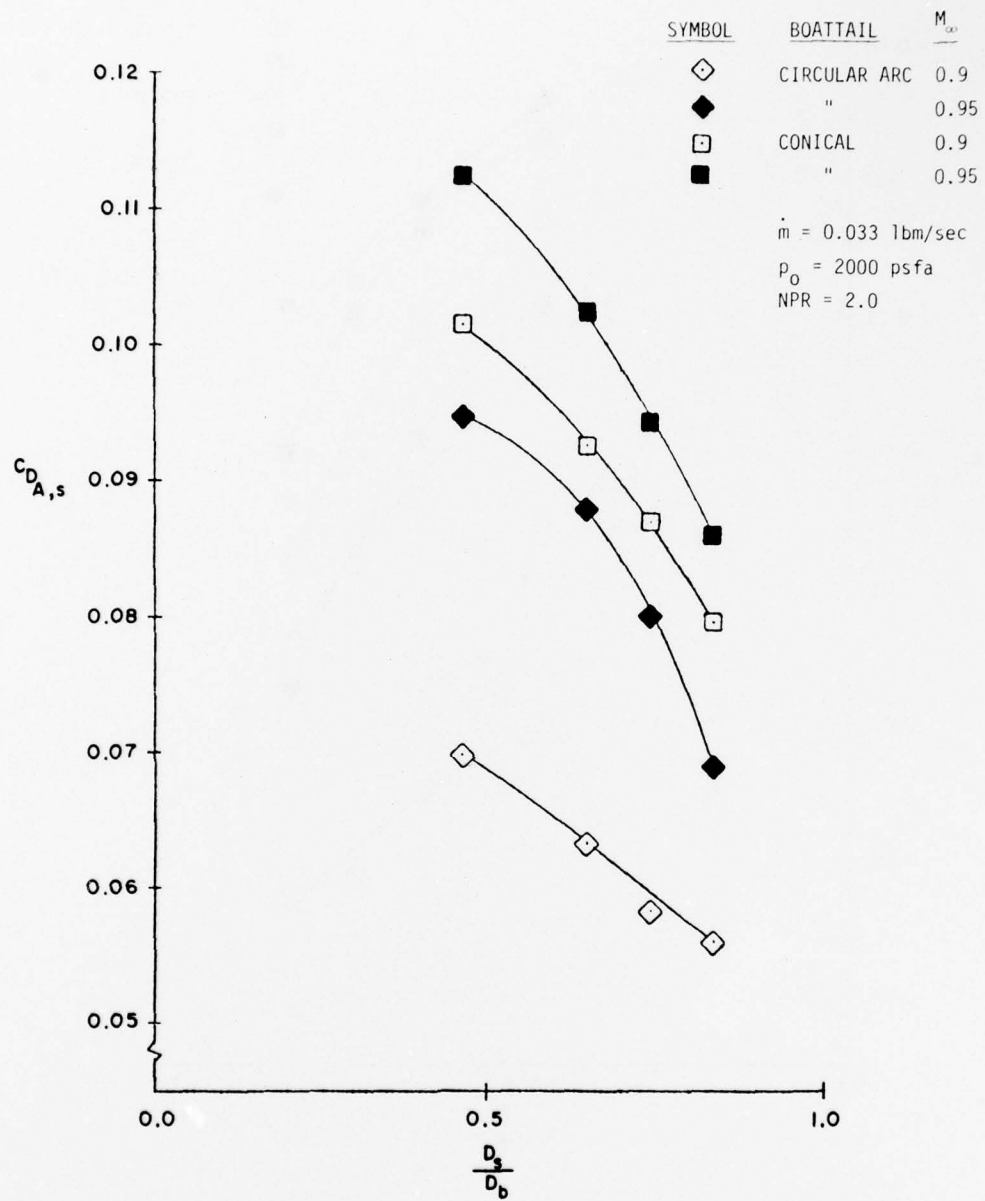


Figure 142. Afterbody Drag Coefficient Variation With Sting Size for $\dot{m}=0.033 \text{ lbm/sec}$

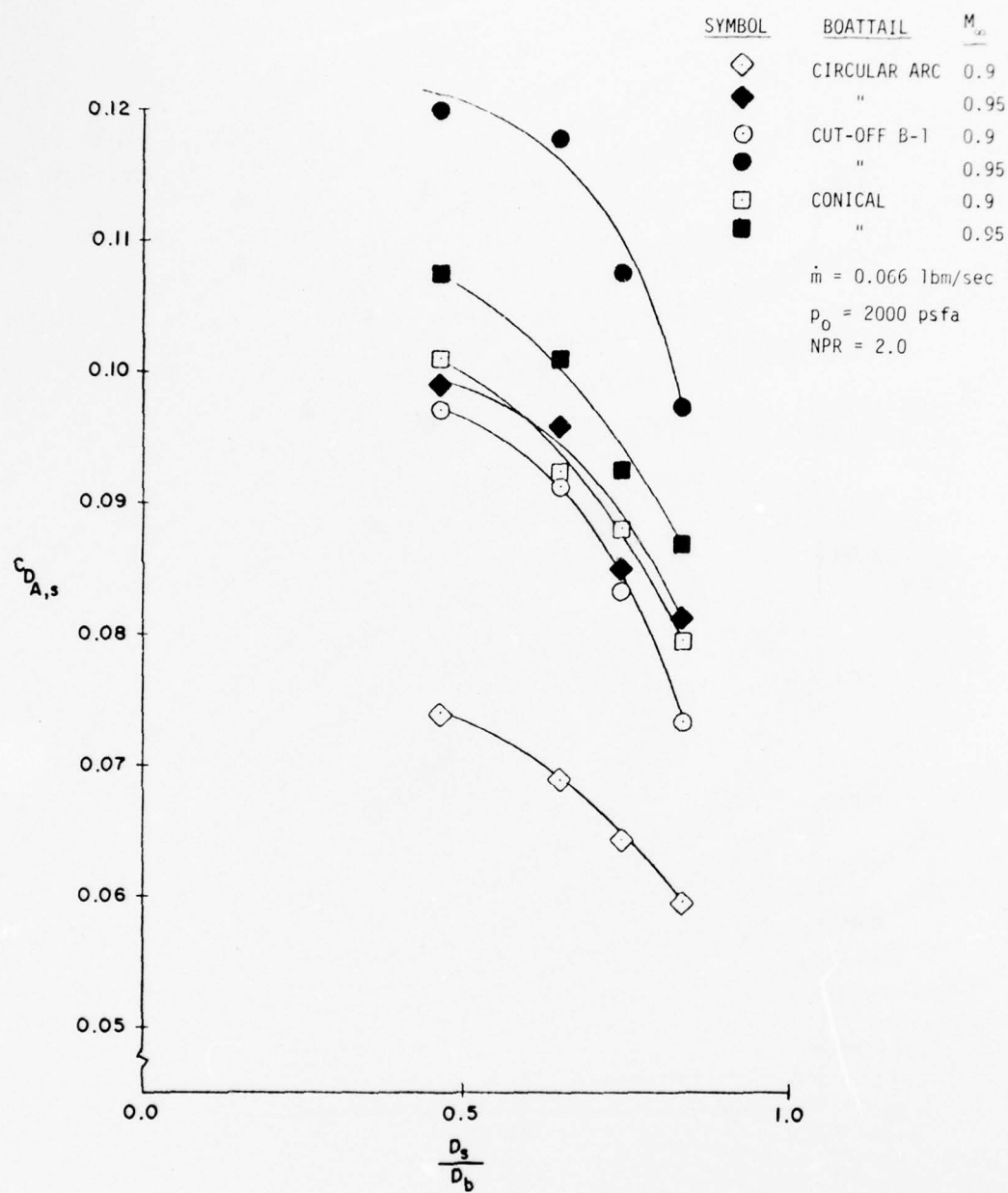


Figure 143. Afterbody Drag Coefficient Variation With Sting Size for $\dot{m}=0.066 \text{ lbm/sec}$

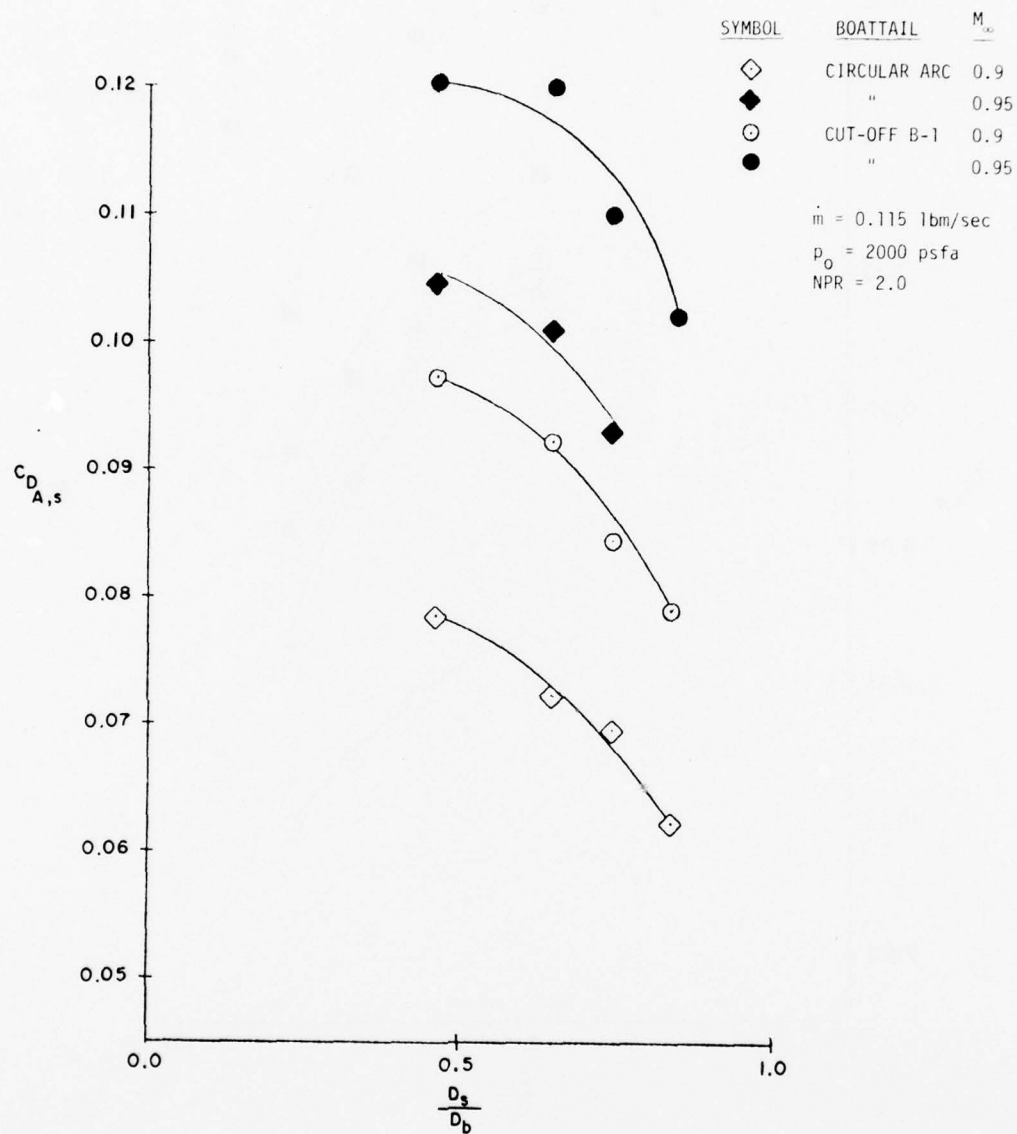


Figure 144. Afterbody Drag Coefficient Variation With Sting Size
 for $\dot{m}=0.115 \text{ lbm/sec}$

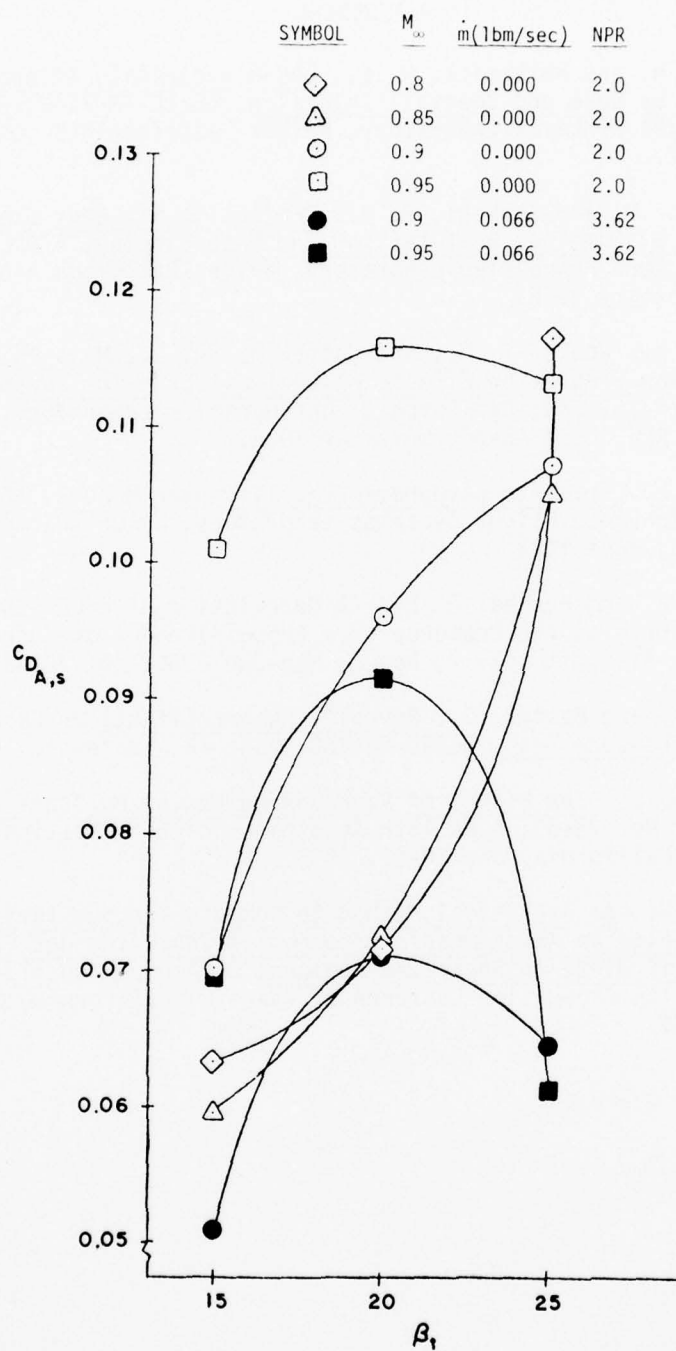


Figure 145. Afterbody Drag Coefficient Variation With Boattail Terminal Angle

REFERENCES

1. Calarese, W. and Walterick, R. E., GAU-8 Projectile Afterbody Drag Reduction by Base and Boattail Injection, AFFDL-TM-77-27-FXM, Air Force Flight Dynamics Laboratory, Wright-Patterson AFB, Ohio 45433, March 1977.
2. Freeman, L. M. and Korkegi, R. H., Projectile Aft-Body Drag Reduction by Combined Boat-tailing and Base Blowing, AFAPL-TR-75-112, Air Force Aero Propulsion Laboratory, Wright-Patterson AFB, Ohio 45433, February 1976.
3. Calarese, W., Weeks, T. M., and Walterick, R. E., Mass Injection and Jet Flow Simulation Effects on Boattail Drag in Transonic Flow, AFFDL-TM-75-161-FXM, Air Force Flight Dynamics Laboratory, Wright-Patterson AFB, Ohio 45433, November 1975.
4. White, H. L., Trisonic Gasdynamic Facility User Manual, AFFDL-TM-73-82-FXM, Air Force Flight Dynamics Laboratory, Wright-Patterson AFB, Ohio 45433, June 1973.
5. McDonald, H. and Hughes, P. F., "A Correlation of High Subsonic Afterbody Drag in the Presence of a Propulsive Jet or Support Sting", J. Aircraft Vol. 2, No. 3, May-Jun 1965, pp. 202-207.
6. Aulehla, F. and Besigk, G., Reynolds Number Effects on Fore and Aft-body Pressure Drag, AGARD-CP-150, page 12, September 1974.
7. Reubush, D. E., The Effect of Reynolds Number on Boattail Drag, AIAA Paper No. 75-63; AIAA 13th Aerospace Sciences Meeting, Pasadena, California, Jan 20-22, 1975.
8. Calarese, W., An Analytical Method to Compute Viscous-Inviscid Transonic Flow on Axisymmetric Afterbodies Including Jet Effects and Boattail Bleed in Separated Regions, AIAA Paper No. 75-1293; AIAA/SAE 11th Propulsion Conference, Anaheim, California, Sep 29 - Oct 1, 1975.